

Cover Page



Universiteit Leiden



The handle <http://hdl.handle.net/1887/29085> holds various files of this Leiden University dissertation

Author: Gaida, Daniel

Title: Dynamic real-time substrate feed optimization of anaerobic co-digestion plants

Issue Date: 2014-10-22

Dynamic Real-Time Substrate Feed Optimization of Anaerobic Co-Digestion Plants

Proefschrift

ter verkrijging van
de graad van Doctor aan de Universiteit Leiden,
op gezag van Rector Magnificus prof. mr. C.J.J.M. Stolker,
volgens besluit van het College voor Promoties
te verdedigen op woensdag 22 oktober 2014
klokke 11:15 uur

door

Daniel Gaida
geboren te Radevormwald, Duitsland
in 1983

Promotiecommissie

Promotor: Prof. Dr. T.H.W. Bäck
Prof. Dr. M. Bongards (Cologne University of Applied Sciences)

Voorzitter: Prof. Dr. J.N. Kok

Overige leden: Prof. Dr. U. Jumar (University of Magdeburg)
Prof. Dr. A. Plaat
Dr. M.T.M. Emmerich
Dr. E.A. Schultes

Cover design: Martin Baljan, B.Sc.

ISBN: 978-94-6259-288-9

Contents

1	Introduction	5
1.1	Aim and Objectives	7
1.2	Main Contributions of this Thesis	8
1.3	Outline of this Thesis	9
I	Dynamic Real-Time Optimization	11
2	Multi-Objective Nonlinear Model Predictive Control	15
2.1	Case I: Number of Objectives $n_o = 1$	17
2.2	Multi-Objective Optimization	21
2.3	Case II: Number of Objectives $n_o > 1$	23
2.4	Summary and Discussion	24
3	Multi-Objective Optimization Algorithms	25
3.1	Hypervolume-based Evolutionary Algorithm	25
3.2	SMS-EGO	29
4	State Estimation	33
4.1	State Estimation using Software Sensors	34
4.2	Hybrid Extended Kalman Filter	38
4.3	Moving Horizon Estimation	40
4.4	Application to an Anaerobic Digestion Process	42
4.5	Summary and Discussion	49
II	Substrate Feed Control for Biogas Plants	51
5	The Anaerobic Digestion Process	55
5.1	Process Description	55
5.2	Important Process Values	56
5.3	Important Definitions and Terms	57
5.4	Typical Reactors	61

6 State of the Art of Biogas Plant Feed Control	65
6.1 Classical Control	67
6.2 Expert Systems	67
6.3 Linearizing Control	68
6.4 Discontinuous Control	69
6.5 Other Advanced Controls	69
6.6 Summary and Discussion	69
6.7 Tables	72
7 Modeling Biogas Plants	85
7.1 The Anaerobic Digestion Model No. 1 (ADM1)	86
7.2 The Substrate Feed	92
7.3 Performance Indicators of Biogas Plants	96
7.4 Model Implementation of an Agricultural Biogas Plant	109
7.5 Model Calibration and Validation	110
7.6 Summary and Discussion	117
III Simulation & Optimization Studies	119
8 State Estimation of the Anaerobic Digestion Process	123
8.1 Introduction	123
8.2 State Estimation using Software Sensors	124
8.3 Summary and Discussion	127
9 Dynamic Real-Time Substrate Feed Optimization of a Biogas Plant	129
9.1 Introduction	129
9.2 Control Structure	130
9.3 Performance Experiments	133
9.4 Summary and Discussion	167
10 Conclusion	173
10.1 Summary	173
10.2 Outlook	176
Bibliography	179
A Anaerobic Digestion Model (Simple)	205
B Biogas Toolbox in MATLAB[®]	209

C ADM1: Petersen Matrix and Model Parameters	213
D Symbols and Abbreviations	219
Samenvatting (Dutch)	231
Curriculum Vitae	233

Chapter 1

Introduction

The European Union (EU) has set a goal that 20 % of the gross final energy consumption in the EU should be produced by renewable energy sources in the year 2020 (Holm-Nielsen et al., 2009). Between the years 2004 and 2011 in the EU this share increased from 8.1 % to 13.0 % (Eurostat, 2013).

In Germany 7.0 % of the gross electrical energy production in 2012 was produced out of biomass (22.6 % of gross electrical energy production was from renewable sources), whereas biogas produced from biomass had the greatest share (FNR, 2013). Biogas mainly consists of methane and carbon dioxide and is produced in so-called biogas plants. In such plants, one of the key components is the digester. In the digesters there is an absence of oxygen, allowing the bacteria to convert the anaerobic degradable biomass in to biogas. Some examples for biomass are manure, grass, energy crops, organic fraction of municipal solid waste (OFMSW), biodegradable wastes from industrial production, wastewater and many more.

Once produced, there are various utilization pathways for biogas. Among them are production of heat (e.g. in third world countries) as well as of electrical and thermal energy while burning it in cogeneration units (also called combined heat and power plants (CHP)) and upgrading biogas to biomethane by removal of carbon dioxide. The latter allowing for the possibilities of either injecting the biomethane into the natural gas grid or utilizing it as vehicle fuel (Holm-Nielsen et al., 2009).

The Renewable Energy Sources Act (EEG) (BMU, 2012a) in Germany fosters the energy production out of renewable energy sources. For the year 2013 FNR (2013) predicts 7,772 biogas plants with an installed electrical power of 3,530 MW. With these numbers Germany has the leading role in the EU regarding biogas production (OBSERV'ER, 2012). In Germany 0.8 million hectares of maize are cultivated for subsequent biogas production (FNR, 2013). This is still “only” one third of the total maize cultivation (FNR, 2013), but it clearly shows that biogas production, as currently carried out in Germany also comes at an ecological cost. To be able to promote and foster biogas under these circumstances as a sustainable energy source, optimal use of

valuable resources is absolutely necessary. This aspect is also considered in the recently announced new 2014 Renewable Energy Sources Act. The first draft suggests that the German government is focusing on the digestion of waste products in the near future, thus trying to reduce ecological costs introduced by the cultivation of maize for energy production.¹

The Netherlands was ranked at the 5th position regarding primary biogas production in the EU in the year 2011 (OBSERV'ER, 2012). In 2013, there was a total of 105 co-digestion plants with an installed electrical power of 129 MW (Agentschap NL, 2013). The current funding scheme for renewable energy in the Netherlands is the Renewable Energy Production Incentive Scheme (SDE+, Dutch: stimuleringsregeling duurzame energieproductie) (Statistics Netherlands, 2012). In 2012 the renewable energy share of gross final energy consumption in the Netherlands was 4.4 % with the 2020 goal being 14 % (Centraal Bureau voor de Statistiek, 2013).

Operation of biogas plants is only economically feasible if they are operated near their optimal operating point. One key aspect for optimization is to choose the most suitable biomasses, called substrates, and their daily throughput. The substrates used strongly effect biogas production, population sizes of different bacteria species in the digesters and digestate quality. Thus, by optimizing the substrate feed, economical, ecological and stability criteria of plant operation can be optimized. At present, most biogas plants in Germany are operated at steady-state, ideally producing sufficient biogas to power an electrical generator at maximum capacity. This allowed biogas plant owners to ensure that they obtained the maximum possible funding (BMU, 2009), until the EEG was amended in 2012. The 2012 amendment introduced the possibility for biogas plants to sell the produced electrical energy directly to an interested customer (BMU, 2012a). Consequently, higher revenues compared to conventional remuneration schemes are possible. Selling energy under the EEG feed-in tariff on EPEX SPOT's Day-Ahead market became an interesting option. EPEX SPOT² is a European power spot market covering France, Germany, Austria and Switzerland. Therefore, there is a need for highly flexible biogas and power production, which in turn requires a closed-loop substrate feed control that is able to track a given setpoint and adjust the substrate mix in an optimal manner.

The current state of control and automation on most full-scale biogas plants is very basic (Wiese and König, 2009). On agricultural biogas plants (ABP) the substrate feed is usually changed on a daily basis based on simple calculations or a rule of thumb (Dewil et al., 2011). Due to a lack of online process instrumentation, it is often not possible to make reliable predictions of expected biogas production and the state of the process. Advances in the development of reliable and robust measurement sensors, as

¹<https://www.clearingstelle-eeg.de/>

²<http://www.epexspot.com/en/>

well as detailed anaerobic digestion (AD) models give hope that these limitations will be lifted in the coming years (Madsen et al., 2011). Nevertheless, it is questionable as to whether biogas plants will ever have adequate instrumentation fitted as standard. Therefore, presently and in the future, control and optimization methods fitted to biogas plants should cope with these limitations. Following this idea in this thesis, the developed real-time feed optimization method requires only very basic instrumentation, so that it will be possible to use it on ordinary full-scale biogas plants.

However, simulation and control of waste digestion is much more challenging than for ABPs. The reason is that feed based on municipal waste will change its composition continuously, requiring continuous adjustment and control of the plant. Nevertheless, the dissemination of the technologies developed in this work will be absorbed by a market that specifically requires these solutions.

1.1 Aim and Objectives

In this thesis a dynamic real-time optimization (RTO) scheme is developed to achieve optimal substrate feed control for biogas plants. RTO continually alters the substrate feed to maximize the economic productivity of the biogas plant while at the same time predefined stability criteria are maintained. In Figure 1.1 the developed dynamic RTO control loop is visualized. An important part of the dynamic RTO scheme is the

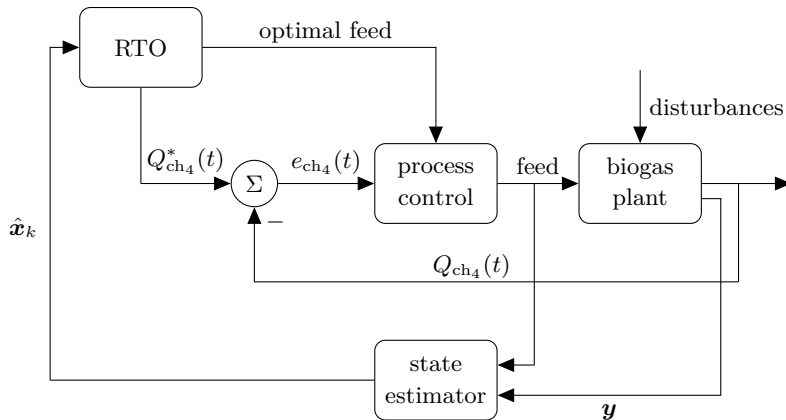


Figure 1.1: Dynamic Real-Time Substrate Feed Optimization. The RTO determines the optimal substrate feed and returns the optimal volumetric methane flow rate $Q^*_{ch4}(t)$. The process control adapts the optimal feed to stabilize the produced methane flow rate $Q_{ch4}(t)$ of the biogas plant around the given setpoint $Q^*_{ch4}(t)$. As a dynamic model is used for prediction, a state estimator is needed that estimates at each time step k the current state estimate \hat{x}_k given the current feed and plant measurements y .

dynamic simulation model of the biogas plant which is used for prediction purposes.

The developed method for the dynamic real-time substrate feed optimization is dedicated to assisting the biogas plant operators in the selection of the optimal substrate feed on a daily basis, ultimately with the goal of autonomously controlling the feed of the plant. The following features are expected from the RTO scheme:

- Determination of optimal substrate mixture for anaerobic co-digestion plants.
- Keeping the plant stable by all means due to prediction.
- Consideration of changing substrate availabilities in the chosen substrate feed.
- Robust stable setpoint tracking.
- Flexibility and extensibility with respect to the optimization goal.

In order to realize a sophisticated real-time feed optimization that is practical to implement, there are multiple objectives that must be achieved.

The first objective is to create a detailed dynamic simulation model for biogas plants. This model is used in the dynamic RTO to continually predict the optimal substrate feed for the controlled plant. Performance and practical usability of RTO is highly dependent upon the underlying model, consequently, a significant amount of effort is necessary to ensure realistic modeling of full-scale biogas plants.

The optimization and prediction method implemented as a part of the RTO scheme, is nonlinear model predictive control (NMPC). Thus, the second objective is to develop and implement NMPC for the substrate feed of biogas plants. NMPC selects a substrate feed trajectory that optimizes an objective function over a prediction horizon. For biogas plants, such an objective function may contain economical, ecological and stability criteria and thus is of a multi-objective nature. Furthermore, it can be highly nonlinear. To solve the nonlinear multi-objective optimization problem, global multi-objective optimization methods such as evolutionary algorithms and efficient global optimization (EGO) are used.

In order to make NMPC predictions with the simulation model, the NMPC must know the current system state of the biogas plant. Therefore, the third objective is to develop a state estimation algorithm that is capable to continually estimate the state of the biogas plant. The challenge to develop a reliable state estimator increases with process model complexity. To achieve this task, supervised machine learning methods are used to estimate the current state given current and past measurement data.

1.2 Main Contributions of this Thesis

To the author's knowledge, dynamic real-time substrate feed optimization has not been applied to anaerobic co-digestion plants before. To achieve this goal, different components from various scientific fields had to be developed, implemented and combined. This is the first main contribution of this thesis.

The heart of the developed RTO scheme is the Anaerobic Digestion Model No. 1 (ADM1) which is the most complex model of the anaerobic digestion process available

at present. There are multiple challenges when attempting to implement this model inside the NMPC. Three of these challenges are that predictions are time consuming, the underlying optimization problem is highly nonlinear and the state estimator must estimate a large state vector of a non observable process. To address the first two challenges, evolution strategies are used that in part use surrogate models to improve speed.

Solving the latter challenge results in the second main contribution of this thesis. This is the development of the state estimation algorithm. Using machine learning methods, a static function is created that maps measured process values to the state vector of the plant and therefore can be used for state estimation. Classical state estimation approaches such as the famous Kalman filter will not be stable because the observability criterion (Simon, 2006) in practice is not satisfied for the ADM1. Therefore, this new state estimation approach is needed.

The last contribution of this thesis to the scientific community is the MATLAB® toolbox for “Simulation, Control & Optimization of Biogas Plants” (Appendix B), which was developed for the purposes of this thesis.

1.3 Outline of this Thesis

This document is structured in five parts.

Part I presents the theoretical foundation to this work. As the proposed real-time optimization scheme uses multi-objective model predictive control, Chapter 2 presents the basics of model predictive control and multi-objective model predictive control. To solve the multi-objective optimization problem formulated in Chapter 2, Chapter 3 reviews multi-objective optimization algorithms which will be used to solve the control problem. They are SMS-EMOA and SMS-EGO which are based on the \mathcal{S} -Metric. For model predictive control a state estimation algorithm is necessary. Therefore, three different state estimation algorithms are described in Chapter 4 which concludes Part I. The state estimation algorithms are the well-known hybrid extended Kalman filter, moving horizon estimation and the newly developed state estimator based on machine learning methods. Using a simple model of an anaerobic digestion process, all three approaches are validated and compared.

Part II applies the concepts introduced in Part I to the application of controlling the substrate feed of biogas plants. It starts with an introduction of the anaerobic digestion process in Chapter 5, which is written for those not familiar with the process. Chapter 6 contains an extensive review of the state of the art of biogas plant feed control revealing the need for feed control particularly for agricultural biogas plants. In Chapter 7, a detailed model for biogas plants is proposed. This model is used within the predictive control algorithm and it is used for validation of the control in the simulation and optimization studies of Part III.

The 3rd part, Part III, starts with Chapter 8 that presents the results obtained with the self-developed state estimator for the biogas plant model of Chapter 7. Chapter 9 outlines the main result of this thesis, the dynamic real-time substrate feed optimization for co-digestion plants. The proposed RTO scheme is validated by means of extensive simulation and optimization studies revealing its performance.

The thesis is concluded by Chapter 10, in which the main results of this thesis and possible future work are summarized.

In the appendices, detailed technical descriptions of the used models are provided. In Part A of the appendix the AD model used in the experiments of Chapter 4 is presented. Part B presents the MATLAB[®] toolbox developed for this thesis in which all simulations and optimization runs are performed. The implementation of the Anaerobic Digestion Model No. 1 used in the biogas plant simulation model developed in Chapter 7 is given in Part C. Finally, all symbols and abbreviations can be reviewed in Part D.

Part I

Dynamic Real-Time Optimization

Introduction

In this first part of the thesis three of the four key ingredients of dynamic real-time optimization (RTO) are discussed in detail:

- Multi-Objective Nonlinear Model Predictive Control (MONMPC) (Chapter 2)
- Multi-Objective Optimization Algorithm (Chapter 3)
- State Estimation Method (Chapter 4)
- Dynamic Process Model (Chapter 7)

The fourth item, namely the dynamic process model, is not dealt with in this part, but in Chapter 7.

In **dynamic real-time optimization** a dynamic simulation model is used to develop a predictive control. In general a RTO system is an upper-level control that provides a setpoint to a lower-level control (Engell, 2007). In the upper-level control the simulation model is used to predict the future economics of the controlled plant, whereas an optimization method generates the setpoint, so that future profits are maximized. The lower-level control holds the controlled variable around the given setpoint. Usually the setpoints are created on a medium time-scale (hours to days) whereas the lower-level control acts on a shorter time-scale such as seconds to minutes, cf. Darby et al. (2011).

Multi-objective nonlinear model predictive control is used in the RTO scheme to continually find optimal substrate feed trajectories over a prediction horizon. The objective function usually comprises terms to maximize the profit, minimize the ecological impact, and to maintain the plant stable at all times. Using the model of the process, different feed trajectories can be evaluated, whereas only the optimal trajectory is applied to the real biogas plant for a much shorter control sampling time. Excellent overviews about nonlinear model predictive control can e.g. be found in Morari and H. Lee (1999), Findeisen et al. (2003), Johansen (2011) and Mayne et al. (2000).

Multi-objective optimization algorithms are used to solve the optimization problem stated by the MONMPC. As the optimization problem is nonlinear, the focus is put on global optimization methods, such as multi-objective evolutionary algorithms (Fleming and Purshouse, 2002).

State estimation methods can be used to estimate the system state of a process, if the state can not be measured directly. As this is the case for a typical biogas plant, a state estimator will be an integral part of the dynamic RTO scheme.

Chapter 2

Multi-Objective Nonlinear Model Predictive Control

Consider a physical, time-dependent, real-world system showing deterministic behavior at any time $t \in \mathbb{R}_0^+$. Assume that the main influence on the system by its environment can be described by a finite number $n_u \in \mathbb{N}_0$ of physical values. They are called the input values of the system. The nominal input values of the system are generated by a function of time $\mathbf{u} : \mathbb{R}_0^+ \rightarrow \mathcal{U}$, which, for each time $t \geq 0$, returns the input of the system at time t symbolized by $\mathbf{u}(t) \in \mathcal{U}$. Each input function u_{i_u} , with $\mathbf{u} := (u_1, \dots, u_{i_u}, \dots, u_{n_u})^T$, returns values out of the set $\mathcal{U}_{i_u} \subseteq \mathbb{R}$, $i_u = 1, \dots, n_u$. The set \mathcal{U} then is defined as $\mathcal{U} := (\mathcal{U}_{i_u})^{n_u} := \mathcal{U}_1 \times \dots \times \mathcal{U}_{n_u}$. Note that the i th input of the system is symbolized by the iterator $i_u \in \{1, \dots, n_u\}$.

Those physical values which are assumed to describe the inherent behavior of the system are put inside the state of the system $\mathbf{x} : \mathbb{R}_0^+ \rightarrow \mathcal{X}$, with the state space $\mathcal{X} \subseteq \mathbb{R}^{n_x}$ and $n_x \in \mathbb{N}_0$ representing the number of physical values in the system state vector $\mathbf{x} \in \mathcal{X}$. The idea of the system state is that if it is known for some time t , then the complete physical system description at that time is known. Examples of state vector components are the position of the system in space, the temperature inside the system or the concentration of fluids or species inside the system.

The sets \mathcal{X} and \mathcal{U} could be generated out of state and input constraints, respectively. If the state (input) constraints are linear, then \mathcal{X} (\mathcal{U}) is a convex set (Boyd and Vandenberghe, 2004).

To be able to predict the future trajectory of the system state \mathbf{x} for a given input trajectory \mathbf{u} the real-world system is described as a system of continuous-time nonlinear stochastic differential equations:

$${}^o\mathbf{x}'(t) = \mathbf{f}({}^o\mathbf{x}(t), \mathbf{u}(t), \boldsymbol{\omega}(t)), \quad {}^o\mathbf{x}(0) = \mathbf{x}(0). \quad (2.1)$$

This future state vector trajectory is symbolized by the vector valued function ${}^o\mathbf{x} : \mathbb{R}_0^+ \rightarrow \mathcal{X}$. As eq. (2.1) is only initialized at time $t = 0$ the calculated state ${}^o\mathbf{x}$ is

called the open loop state, whereas “open” is symbolized by the o in front of \mathbf{x} in $^o\mathbf{x}$. The behavior of the real-world system is approximately modeled using the real-valued smooth vector field $\mathbf{f} : \mathcal{X} \times \mathcal{U} \times \mathbb{R}^{n_\omega} \rightarrow \mathcal{T}\mathcal{X}$, which maps the input space of the function onto the tangent space $\mathcal{T}\mathcal{X} \subseteq \mathbb{R}^{n_x}$. To emphasize that \mathbf{f} is only an approximation of the real system the noise process $\boldsymbol{\omega} : \mathbb{R}_0^+ \rightarrow \mathbb{R}^{n_\omega}$ is introduced as input of the system function \mathbf{f} . This noise process is used to take account for the fact that \mathbf{f} cannot describe exactly what is happening in the real world and for possibly noisy input values \mathbf{u} . This $n_\omega \in \mathbb{N}_0$ dimensional noise process $\boldsymbol{\omega}$ is modeled as a normal distribution with zero-mean and the covariance matrix $\boldsymbol{\Psi}_{\boldsymbol{\omega}} \in \mathbb{R}^{n_\omega \times n_\omega}$, symbolized by $\boldsymbol{\omega}(t) \sim \mathcal{N}(\mathbf{0}, \boldsymbol{\Psi}_{\boldsymbol{\omega}})$. We assume stationary, white noise. That is, $E\langle \boldsymbol{\omega}(t) \cdot \boldsymbol{\omega}^T(\tau) \rangle = \boldsymbol{\Psi}_{\boldsymbol{\omega}} \cdot \delta_D(t - \tau)$, where δ_D is the Dirac delta “function” and $E\langle \cdot \rangle$ denotes the expected value.

Given the initial state of the real system at time $t = 0$, $\mathbf{x}(0)$, for each $t \geq 0$ the approximate state of the system $^o\mathbf{x}(t)$ can be calculated using equation (2.1). As for $t > 0$ there is no further interaction with the real system (thus no feedback) this predictor could be very inaccurate, because it cannot be guaranteed that the predicted state values $^o\mathbf{x}(t)$ track the real state values $\mathbf{x}(t)$ for $t > 0$. The error between the two state vector trajectories is commonly measured by the root-mean-square error (RMSE):

$$\text{RMSE} (^o\mathbf{x}(t), \mathbf{x}(t)) := \left\| (^o\mathbf{x}(t) - \mathbf{x}(t)) \cdot (^o\mathbf{x}(t) - \mathbf{x}(t))^T \right\|_2,$$

whose value must be kept arbitrarily small. Better predictors than eq. (2.1) are presented later in Chapter 4.

The task at hand is to find an optimal input function $\mathbf{u}^* : \mathbb{R}_0^+ \rightarrow \mathcal{U}$, such that an objective function

$$\tilde{\mathbf{J}} : \mathcal{X} \times \mathcal{U} \rightarrow \mathbb{R}^{n_o} \tag{2.2}$$

gets minimized for all $t \in [0, \infty)$, with the number of objectives $n_o \in \mathbb{N}_0$ and the constraint $^o\mathbf{x}(t) \in \mathcal{X} \forall t \in [0, \infty)$. The vector function $\tilde{\mathbf{J}} := (\tilde{J}_1, \dots, \tilde{J}_{n_o})^T$ consists out of n_o scalar-valued objective functions

$$\tilde{J}_{i_o} : \mathcal{X} \times \mathcal{U} \rightarrow \mathbb{R} \tag{2.3}$$

with $i_o = 1, \dots, n_o$. The problem can be formulated as:

$$\begin{aligned} & \text{minimize}_{\mathbf{u}} \tilde{\mathbf{J}} (^o\mathbf{x}(t), \mathbf{u}(t)) \\ \text{subject to } & ^o\mathbf{x}'(t) = \mathbf{f} (^o\mathbf{x}(t), \mathbf{u}(t), \mathbf{0}), & ^o\mathbf{x}(0) = \mathbf{x}(0), \\ & ^o\mathbf{x}(t) \in \mathcal{X}, & \forall t \geq 0, \\ & \mathbf{u} : [0, \infty) \rightarrow \mathcal{U}. \end{aligned} \tag{2.4}$$

The minimum of a vector function is not defined in general, such that it has to be defined what is meant by minimizing the objective function $\tilde{\mathbf{J}}$. To minimize each objective

function \tilde{J}_{i_o} separately is often not well-suited, because most of the time the objective functions are conflicting. Two objective functions are conflicting, if and only if the set of optimal solutions of one objective function does not overlap with the set of optimal solutions of the other objective function. To simplify things, at first the optimal control problem for the case $n_o = 1$ is handled in Section 2.1 before the general case for $n_o > 1$ is solved in Section 2.3. To minimize the objective function $\tilde{\mathbf{J}}$ properly, concepts from multi-objective optimization are used, which are recapped in Section 2.2.

Since minimizing $\tilde{\mathbf{J}}$ in choosing the optimal input \mathbf{u} for all $t \in [0, \infty)$ is in general a hard problem, in practice a heuristic technique named multi-objective nonlinear model predictive control (MONMPC) shall be used that will be introduced in Section 2.1.

2.1 Case I: Number of Objectives $n_o = 1$

For $n_o = 1$ the objective function reduces to the scalar-valued objective function \tilde{J}_1 , defined in equation (2.3), such that the minimum of the objective function is well defined. Thus, for this case problem (2.4) results in the problem formulation:

$$\begin{aligned} \mathbf{u}^* &:= \arg \min_{\mathbf{u}} \tilde{J}_1({}^o\mathbf{x}(t), \mathbf{u}(t)) \\ \text{subject to } {}^o\mathbf{x}'(t) &= \mathbf{f}({}^o\mathbf{x}(t), \mathbf{u}(t), \mathbf{0}), & {}^o\mathbf{x}(0) &= \mathbf{x}(0), \\ {}^o\mathbf{x}(t) &\in \mathcal{X}, & \forall t \geq 0, \\ \mathbf{u} &: [0, \infty) \rightarrow \mathcal{U}. \end{aligned} \quad (2.5)$$

Problem (2.5) states that we try to find the optimal input function \mathbf{u}^* for system (2.1) which for all time $t \geq 0$ minimizes the objective function \tilde{J}_1 .

According to Diehl et al. (2006a) there are three basic approaches to address optimal control problems:

- Dynamic Programming Methods
- Indirect Methods
- Direct Methods

Direct methods can be divided into single shooting, collocation and multiple shooting. The approach followed in this thesis belongs to the method of single shooting. An example of multiple shooting can be found in Diehl et al. (2002, 2003). For collocation see Biegler (1984).

Finding a closed solution for this problem using dynamic programming or indirect methods can be very difficult or even impossible for some systems \mathbf{f} and objective functions \tilde{J}_1 (Findeisen et al., 2003, Diehl et al., 2006a). From a practical viewpoint a closed solution is often not needed, because model mismatch and disturbances acting on the real-world system (both modeled by the noise process $\boldsymbol{\omega}$) will make the solution for $t > t_0 > 0$, with $t_0 \in \mathbb{R}^+$ inaccurate.

Therefore, using nonlinear model predictive control (NMPC), problem (2.5) is only solved over a finite horizon. This finite horizon is called the prediction horizon $T_p \in \mathbb{R}^+$. Having solved problem (2.5) over the prediction horizon $T_p > 0$, the optimal input is applied to the system for a short time period, named (control) sampling time δ . After the sampling time $\delta \in \mathbb{R}^+$ has passed by, problem (2.5) is solved over the prediction horizon again. Therefore T_p is moved forward by time δ and the new solution is applied again for timespan δ and so on. Therefore, problem (2.5) is solved iteratively over the moving horizon T_p , resulting in an approximate solution to problem (2.5).

For $T_p \rightarrow \infty$ and $\delta \rightarrow 0$ the found approximate solution will converge towards the optimal solution \mathbf{u}^* , provided it exists.

The found optimal input functions at each iteration cannot be equal to the input values applied to the system, because they are only defined over the time period T_p . Thus, the found optimal inputs are called open loop input functions. The applied input function to the system is named closed-loop input.

The NMPC approach has at least two justifications:

- As there may be no closed solution to problem (2.5), the approach using NMPC will at least return an approximate solution. The degree of approximation can be defined by the user in choosing appropriate values for the prediction horizon T_p and sampling time δ .
- Because of model mismatch and disturbances a solution has to be calculated repeatedly, anyway. Therefore, there is no need to spend time in solving problem (2.5) over an infinite horizon.

Next to prediction horizon T_p and sampling time δ , the term control horizon $T_c \in \mathbb{R}^+$ with $T_p \geq T_c \geq \delta$ is used as well. Using these terms it can be stated that for each sampling instance $k = 0, 1, 2, \dots$ at time

$$t_k := k \cdot \delta \quad (2.6)$$

NMPC tries to find the optimal open loop input function ${}^o\mathbf{u}_k^* : [t_k, t_k + T_p] \rightarrow \mathcal{U}$ which minimizes the objective function \tilde{J}_1 over the interval $[t_k, t_k + T_p]$, defined by the prediction horizon T_p . Open loop input functions are denoted by ${}^o\mathbf{u} : [t_k, t_k + T_p] \rightarrow \mathcal{U}$. During the time period $[t_k, t_k + T_c]$ the system input ${}^o\mathbf{u}$ may be changed, after that it is kept constant at the value ${}^o\mathbf{u}(t_k + T_c)$, see eq. (2.7). Using these terms, problem

(2.5) can be formulated approximately as:

For each $k = 0, 1, 2, \dots$ set $t_k = k \cdot \delta$ and solve:

$$\begin{aligned} {}^o\mathbf{u}_k^* &:= \arg \min_{{}^o\mathbf{u}} \tilde{J}_1({}^o\mathbf{x}(\tau), {}^o\mathbf{u}(\tau)) \\ \text{subject to } {}^o\mathbf{x}'(\tau) &= \mathbf{f}({}^o\mathbf{x}(\tau), {}^o\mathbf{u}(\tau), \mathbf{0}), & {}^o\mathbf{x}(t_k) &= \mathbf{x}(t_k), \\ {}^o\mathbf{x}(\tau) &\in \mathcal{X}, & \forall \tau \in [t_k, t_k + T_p], \\ {}^o\mathbf{u} &: [t_k, t_k + T_c] \rightarrow \mathcal{U}, \\ {}^o\mathbf{u}(\tau) &= {}^o\mathbf{u}(t_k + T_c), & \forall \tau \in (t_k + T_c, t_k + T_p]. \end{aligned} \quad (2.7)$$

Here it is assumed that for each discrete time t_k the state $\mathbf{x}(t_k)$ of the real system can be observed. As the system state often can not be observed directly, it often has to be estimated for each time t_k , see Chapter 4.

The resulting optimal input ${}^o\mathbf{u}_k^*$ is applied for the interval $[t_k, t_k + \delta]$ to the system:

$$\mathbf{u}(t) = {}^o\mathbf{u}_k^*(t), \quad t \in [t_k, t_k + \delta] \quad (2.8)$$

and the optimization problem in (2.7) is solved again for the next value of k . Note that we assume here that problem (2.7) can be solved in no time. If we would take into account, that a method solving problem (2.7) for one k needs a certain runtime, then the application of the optimal input to the real system according to equation (2.8) will be delayed by the timespan of the runtime.

To simplify the NMPC problem (2.7) further, the open loop input ${}^o\mathbf{u}$ is often restricted to be a piecewise constant function. Therefore, given the open loop input function ${}^o\mathbf{u} := ({}^o u_1, \dots, {}^o u_{i_u}, \dots, {}^o u_{n_u})^T$, each component ${}^o u_{i_u} : \mathbb{R}^+ \rightarrow \mathcal{U}_{i_u}$ is a piecewise constant function. The duration of each constant period of the function ${}^o u_{i_u}$ is given by the sampling time δ . In problem (2.7) it is defined that the open loop input ${}^o\mathbf{u}$ should only be variable over the control horizon T_c . Then, the number of steps of the piecewise constant function over the control horizon T_c is given by $s_c := \frac{T_c}{\delta} \in \mathbb{N}_0$. Thus, each such piecewise constant function ${}^o u_{i_u}$ of the $i_u = 1, \dots, n_u$ inputs can be described by s_c values given in the vector $\mathbf{u}_{i_u} := (u_{i_u,1}, \dots, u_{i_u,s_c})^T \in (\mathcal{U}_{i_u})^{s_c}$ with the $i = 1, \dots, s_c$ amplitudes $u_{i_u,i} \in \mathcal{U}_{i_u}$ as given in equation (2.9). This kind of parametrization is called control vector parametrization (Schlegel et al., 2005). An example of such a piecewise constant input function is depicted in Figure 2.1.

$$\begin{aligned} {}^o u_{i_u}(t_k + \tau) &:= \begin{cases} \sum_{i=1}^{s_c} u_{i_u,i} \cdot \text{rect}(\tau - (i-1) \cdot \delta) & 0 \leq \tau < T_c \\ u_{i_u,s_c} & T_c \leq \tau \leq T_p \end{cases} \\ \text{rect}(\tau) &:= \begin{cases} 1 & 0 \leq \tau < \delta \\ 0 & \text{else} \end{cases} \end{aligned} \quad (2.9)$$

Furthermore, we define

$$\underline{\mathbf{u}} := (\underline{\mathbf{u}}_1^T, \dots, \underline{\mathbf{u}}_{i_u}^T, \dots, \underline{\mathbf{u}}_{n_u}^T)^T \in \mathcal{U}_{\mathcal{F}}, \text{ with} \\ \mathcal{U}_{\mathcal{F}} := (\mathcal{U}_1)^{s_c} \times \dots \times (\mathcal{U}_{i_u})^{s_c} \times \dots \times (\mathcal{U}_{n_u})^{s_c}, \quad (2.10)$$

containing all s_c amplitudes of each of the n_u inputs, which therefore completely describes the piecewise constant open loop input function ${}^o\mathbf{u}$. Using this simplification

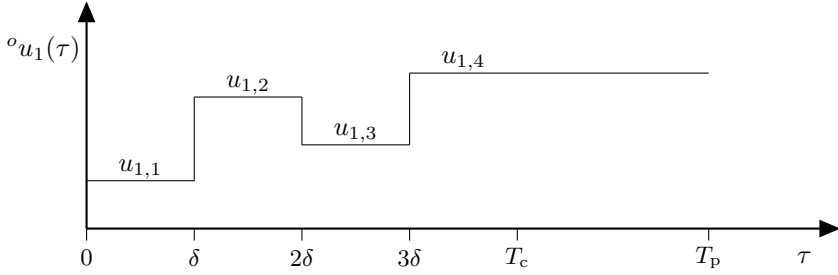


Figure 2.1: Example of a piecewise constant open loop input function ${}^o\mathbf{u}_1$ for $i_u = 1$ and number of steps $s_c = 4$.

the problem in finding a continuous function ${}^o\mathbf{u}$ over the interval $[t_k, t_k + T_c]$ was transformed into the simpler problem of finding a vector $\underline{\mathbf{u}}$ containing only $n_v := s_c \cdot n_u \in \mathbb{N}_0$ components, i.e., the amplitudes of the piecewise constant inputs. This means, that the argument of the objective function $\tilde{\mathbf{J}}$ is changed from a function ${}^o\mathbf{u}$ to a vector $\underline{\mathbf{u}}$ with n_u elements. From now on this vector $\underline{\mathbf{u}}$ is called the vector of optimization or decision variables, containing n_u optimization variables.

The transformation between the vector of optimization variables $\underline{\mathbf{u}}$ and the open loop input function ${}^o\mathbf{u}$ is given by the function

$$\mathbf{f}_{\mathcal{U}} : \mathcal{U}_{\mathcal{F}} \rightarrow \mathcal{U} \quad (2.11)$$

which returns the piecewise constant function

$${}^o\mathbf{u} : [t_k, t_k + T_p] \mapsto \mathbf{f}_{\mathcal{U}}(\underline{\mathbf{u}}) \quad (2.12)$$

given the corresponding vector of optimization variables $\underline{\mathbf{u}}$ using equation (2.9).

To account for this transformation in optimization problem (2.7) a new objective function with a different domain $\mathbf{J} : \mathcal{X} \times \mathcal{U}_{\mathcal{F}} \rightarrow \mathbb{R}^{n_o}$ has to be introduced. Using equation (2.11) the objective function \mathbf{J} is defined by the following equation:

$$\tilde{\mathbf{J}}({}^o\mathbf{x}(\tau), {}^o\mathbf{u}(\tau)) \stackrel{(2.11)}{=} \tilde{\mathbf{J}}({}^o\mathbf{x}(\tau), \mathbf{f}_{\mathcal{U}}(\underline{\mathbf{u}})) =: \mathbf{J}({}^o\mathbf{x}(\tau), \underline{\mathbf{u}}) \quad \forall \tau \in [t_k, t_k + T_p] \quad (2.13)$$

Using the new objective function $\mathbf{J} := (J_1, \dots, J_{n_o})^T$, with $J_{i_o} : \mathcal{X} \times \mathcal{U}_{\mathcal{F}} \rightarrow \mathbb{R}$ and introducing $\underline{\mathbf{u}}_k^* \in \mathcal{U}_{\mathcal{F}}$, with

$${}^o\mathbf{u}_k^* : [t_k, t_k + T_p] \rightarrow \mathbf{f}_{\mathcal{U}}(\underline{\mathbf{u}}_k^*), \quad (2.14)$$

problem (2.7) can be reformulated as:

For each $k = 0, 1, 2, \dots$ set $t_k = k \cdot \delta$ and solve:

$$\begin{aligned} \underline{\mathbf{u}}_k^* &:= \arg \min_{\underline{\mathbf{u}} \in \mathcal{U}_{\mathcal{F}}} J_1({}^o\mathbf{x}(\tau), \underline{\mathbf{u}}) \\ \text{subject to } {}^o\mathbf{x}'(\tau) &= \mathbf{f}({}^o\mathbf{x}(\tau), {}^o\mathbf{u}(\tau), \mathbf{0}), \quad {}^o\mathbf{x}(t_k) = \mathbf{x}(t_k), \quad (2.15) \\ {}^o\mathbf{x}(\tau) &\in \mathcal{X}, \quad \forall \tau \in [t_k, t_k + T_p], \\ {}^o\mathbf{u} : [t_k, t_k + T_p] &\rightarrow \mathbf{f}_{\mathcal{U}}(\underline{\mathbf{u}}). \end{aligned}$$

As ${}^o\mathbf{u}_k^* \stackrel{(2.14)}{=} \mathbf{f}_{\mathcal{U}}(\underline{\mathbf{u}}_k^*)$, equation (2.8) can be applied.

To stress that the open loop input $\underline{\mathbf{u}}$ is the vector of optimization variables, which therefore is the only grip to influence the values of the objective function, if necessary the following notation is used:

$$\mathbf{J}_{\mathbf{x}}(\underline{\mathbf{u}}) := \mathbf{J}({}^o\mathbf{x}(\tau), \underline{\mathbf{u}}). \quad (2.16)$$

The function $\mathbf{J}_{\mathbf{x}} : \mathcal{U}_{\mathcal{F}} \rightarrow \mathbb{R}^{n_o}$, $\mathbf{J}_{\mathbf{x}} := (J_{\mathbf{x},1}, \dots, J_{\mathbf{x},n_o})^T$, will be used in Section 2.2 to simplify the notation, $J_{\mathbf{x},i_o} : \mathcal{U}_{\mathcal{F}} \rightarrow \mathbb{R}$ for $i_o = 1, \dots, n_o$.

2.2 Multi-Objective Optimization

To be able to solve problem (2.4) for $n_o > 1$ the concept of multi-objective optimization is introduced. In multi-objective optimization one tries to solve the following optimization problem:

$$\begin{aligned} &\text{minimize}_{\underline{\mathbf{u}}} \mathbf{J}_{\mathbf{x}}(\underline{\mathbf{u}}) \\ \text{subject to } \underline{\mathbf{u}} &\in \mathcal{U}_{\mathcal{F}} \end{aligned} \quad (2.17)$$

To solve (2.17) a couple of terms are defined to get an idea of how to minimize the vector function $\mathbf{J}_{\mathbf{x}}$.

In Definition 2.1 the notation $\mathbf{J}_{\mathbf{x}}(\underline{\mathbf{u}}_1) \leq \mathbf{J}_{\mathbf{x}}(\underline{\mathbf{u}}_2)$ is used, which is short for $J_{\mathbf{x},i_o}(\underline{\mathbf{u}}_1) \leq J_{\mathbf{x},i_o}(\underline{\mathbf{u}}_2) \forall i_o \in \{1, \dots, n_o\}$, for $\underline{\mathbf{u}}_1, \underline{\mathbf{u}}_2 \in \mathcal{U}_{\mathcal{F}}$.

Definition 2.1 (Custódio et al. (2012)): Given two vectors of optimization variables $\underline{\mathbf{u}}_1, \underline{\mathbf{u}}_2 \in \mathcal{U}_{\mathcal{F}}$, it is said that $\underline{\mathbf{u}}_1$ dominates $\underline{\mathbf{u}}_2$, being represented by $\underline{\mathbf{u}}_1 \prec \underline{\mathbf{u}}_2$, iff $\mathbf{J}_{\mathbf{x}}(\underline{\mathbf{u}}_1) \leq \mathbf{J}_{\mathbf{x}}(\underline{\mathbf{u}}_2)$ and $J_{\mathbf{x},i_o}(\underline{\mathbf{u}}_1) < J_{\mathbf{x},i_o}(\underline{\mathbf{u}}_2) \exists i_o \in \{1, \dots, n_o\}$.

As $\mathbf{J}_{\mathbf{x}}$ shall be minimized, $\underline{\mathbf{u}}_1$ is always preferred over $\underline{\mathbf{u}}_2$, if $\underline{\mathbf{u}}_1 \prec \underline{\mathbf{u}}_2$. Definition 2.1 implies that $\underline{\mathbf{u}}_1 \prec \underline{\mathbf{u}}_2$ if and only if $\mathbf{J}_{\mathbf{x}}(\underline{\mathbf{u}}_1) \leq \mathbf{J}_{\mathbf{x}}(\underline{\mathbf{u}}_2)$ and $\mathbf{J}_{\mathbf{x}}(\underline{\mathbf{u}}_1) \neq \mathbf{J}_{\mathbf{x}}(\underline{\mathbf{u}}_2)$. Some authors define the dominance relation in the space of objective function vectors. In this meaning there exists the following equivalence, which is used in this thesis:

$$\underline{\mathbf{u}}_1 \prec \underline{\mathbf{u}}_2 \equiv \mathbf{J}_{\mathbf{x}}(\underline{\mathbf{u}}_1) \prec \mathbf{J}_{\mathbf{x}}(\underline{\mathbf{u}}_2).$$

Special interest lies in vectors of optimization variables $\underline{\mathbf{u}}$ which are non-dominated within a given set. They are called Pareto optimal points, see Definition 2.2.

Definition 2.2 (Coello Coello (2011)): It is said that a vector of optimization variables $\underline{\mathbf{u}}^* \in \mathcal{U}_{\mathcal{F}}$ is **Pareto optimal** iff there does not exist another $\underline{\mathbf{u}} \in \mathcal{U}_{\mathcal{F}}$ such that $\underline{\mathbf{u}} \prec \underline{\mathbf{u}}^*$.

Pareto optimal points are so-called trade-off solutions. There is no solution which is better (viz. smaller) in all components, but there could be solutions which are at least better in some component(s) and in each case worse in other components.

If, for $\underline{\mathbf{u}}_1, \underline{\mathbf{u}}_2 \in \mathcal{U}_{\mathcal{F}}$, $\underline{\mathbf{u}}_1 \not\prec \underline{\mathbf{u}}_2$ and $\underline{\mathbf{u}}_2 \not\prec \underline{\mathbf{u}}_1$ then $\underline{\mathbf{u}}_1$ and $\underline{\mathbf{u}}_2$ are said to be nondominated points. A subset of $\mathcal{U}_{\mathcal{F}}$ is said to be nondominated when any pair of points in this subset is nondominated (Custódio et al., 2012).

Definition 2.3 (Coello Coello (2011)): The **Pareto optimal set** \mathcal{P}^* is defined by:

$$\mathcal{P}^* := \{\underline{\mathbf{u}} \in \mathcal{U}_{\mathcal{F}} \mid \underline{\mathbf{u}} \text{ is Pareto optimal}\}$$

Out of definition the Pareto optimal set is a nondominated set. The Pareto optimal set contains all Pareto optimal points in the feasible set $\mathcal{U}_{\mathcal{F}}$. As for each vector in the Pareto optimal set, there does not exist a better (in the sense of domination) solution candidate with respect to problem (2.17), each Pareto optimal point will minimize the objective function $\mathbf{J}_{\mathbf{x}}$. In other words, all Pareto optimal points are equally good, thus there is no ranking of Pareto optimal points at the moment. This is why we want to know the Pareto optimal set for the given problem (2.17). A set which contains only a subset of all Pareto optimal points is called approximate Pareto set or just Pareto set. As will be shown later in Chapter 3, it usually is not possible to find the Pareto optimal set but only an approximate Pareto set, because only a finite number of Pareto optimal points can be found.

To the Pareto optimal set there does also exist the corresponding Pareto front, see Figure 2.2, defined as:

Definition 2.4 (Coello Coello (2011)): The **Pareto front** $\mathcal{P}\mathcal{F}^*$ is defined by:

$$\mathcal{P}\mathcal{F}^* := \{\mathbf{J}_{\mathbf{x}}(\underline{\mathbf{u}}) \in \mathbb{R}^{n_o} \mid \underline{\mathbf{u}} \in \mathcal{P}^*\}$$

To each approximate Pareto set there does also exist an approximate Pareto front. So later the question will be to find the best finite set of solutions, which approximates the Pareto front best possibly.

Multi-objective optimization algorithms, see Chapter 3, then have the task to find the Pareto optimal set and therefore the Pareto front. Using both terms the general multi-objective nonlinear model predictive control problem with $n_o > 1$ is studied in Section 2.3.

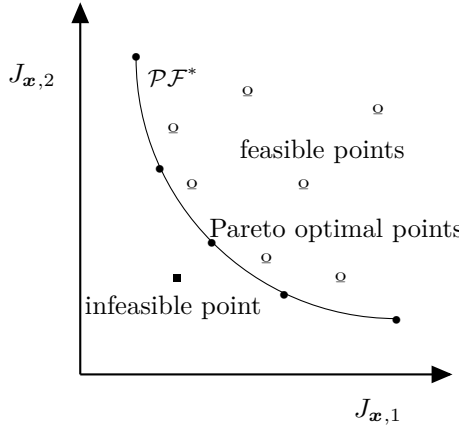


Figure 2.2: Example of a two-dimensional Pareto front. The Pareto front is depicted as a line. Feasible points lie on the right side of the line, infeasible points on the left side. Pareto optimal points are feasible points which lie directly on the Pareto front.

2.3 Case II: Number of Objectives $n_o > 1$

Knowing that the minima of the objective function \mathbf{J} lie on the Pareto front, problem (2.4) is approximately solved by:

For each $k = 0, 1, 2, \dots$ set $t_k = k \cdot \delta$ and solve:

$$\begin{aligned} \mathcal{P}\mathcal{F}_k^* &:= \min_{\underline{\mathbf{u}} \in \mathcal{U}_{\mathcal{F}}} \mathbf{J}({}^o\mathbf{x}(\tau), \underline{\mathbf{u}}) \\ \text{subject to } {}^o\mathbf{x}'(\tau) &= \mathbf{f}({}^o\mathbf{x}(\tau), {}^o\mathbf{u}(\tau), \mathbf{0}), \quad {}^o\mathbf{x}(t_k) = \mathbf{x}(t_k), \quad (2.18) \\ {}^o\mathbf{x}(\tau) &\in \mathcal{X}, \quad \forall \tau \in [t_k, t_k + T_p], \\ {}^o\mathbf{u} : [t_k, t_k + T_p] &\rightarrow \mathbf{f}_{\mathcal{U}}(\underline{\mathbf{u}}). \end{aligned}$$

Let \mathcal{P}_k^* be the corresponding Pareto optimal set to the Pareto front $\mathcal{P}\mathcal{F}_k^*$ for each $k = 0, 1, 2, \dots$. Then the optimal input $\underline{\mathbf{u}}_k^* \in \mathcal{U}_{\mathcal{F}}$ has to be picked out of the solutions inside the Pareto optimal set \mathcal{P}_k^* . One possible approach would be the use of a weighted sum:

$$\underline{\mathbf{u}}_k^* := \arg \min_{\underline{\mathbf{u}} \in \mathcal{P}_k^*} \sum_{i_o=1}^{n_o} \varpi_{i_o} \cdot J_{\mathbf{x}, i_o}(\underline{\mathbf{u}}) \quad (2.19)$$

with $\varpi_{i_o} \in (0, 1)$, $i_o = 1, \dots, n_o$ and $\sum_{i_o=1}^{n_o} \varpi_{i_o} = 1$. The weights ϖ_{i_o} could also be made dependent on the current state of the system $\mathbf{x}(t_k)$.

Other possibilities to determine the optimal input $\underline{\mathbf{u}}_k^*$ out of the Pareto optimal set \mathcal{P}_k^* can be found in Bemporad and Muñoz de la Peña (2009), Valera García et al. (2012) and Flores-Tlacuahuac et al. (2012).

2.4 Summary and Discussion

In this chapter an optimization problem was defined, which states that an objective function $\tilde{\mathbf{J}}$ shall be minimized which depends on state trajectories of a dynamic system ${}^o\mathbf{x}(t)$ and inputs $\mathbf{u}(t)$, eq. (2.4). It was proposed to approximately solve this optimal control problem using multi-objective nonlinear model predictive control. Applying NMPC resulted in the problem formulation (2.18):

For each $k = 0, 1, 2, \dots$ set $t_k = k \cdot \delta$ and solve:

$$\begin{aligned} \mathcal{P}\mathcal{F}_k^* &:= \min_{\underline{\mathbf{u}} \in \mathcal{U}_{\mathcal{F}}} \mathbf{J}({}^o\mathbf{x}(\tau), \underline{\mathbf{u}}) \\ \text{subject to } {}^o\mathbf{x}'(\tau) &= \mathbf{f}({}^o\mathbf{x}(\tau), {}^o\mathbf{u}(\tau), \mathbf{0}), \quad {}^o\mathbf{x}(t_k) = \mathbf{x}(t_k), \quad (2.20) \\ {}^o\mathbf{x}(\tau) &\in \mathcal{X}, \quad \forall \tau \in [t_k, t_k + T_p], \\ {}^o\mathbf{u} : [t_k, t_k + T_p] &\rightarrow \mathcal{f}_{\mathcal{U}}(\underline{\mathbf{u}}). \end{aligned}$$

with the optimal input vector $\underline{\mathbf{u}}_k^*$ in equation (2.19)

$$\underline{\mathbf{u}}_k^* := \arg \min_{\underline{\mathbf{u}} \in \mathcal{P}_k^*} \sum_{i_o=1}^{n_o} \varpi_{i_o} \cdot J_{\mathbf{x}, i_o}(\underline{\mathbf{u}}) \quad (2.21)$$

and application of equation (2.8) which gives the optimal input in the interval $t \in [t_k, t_k + \delta)$

$$\mathbf{u}(t) = {}^o\mathbf{u}_k^*(t) = \mathcal{f}_{\mathcal{U}}(\underline{\mathbf{u}}_k^*), \quad t \in [t_k, t_k + \delta]. \quad (2.22)$$

As open questions remained how to solve the optimization problem in eq. (2.20) and how to get the state of the system at time t_k , $\mathbf{x}(t_k)$, in case it is not directly observable. The first question will be tackled in the next Chapter 3 and the latter question will be answered in Chapter 4.

In model-based control offset-free control in case of plant-model mismatch is an important issue, because there the control error usually is not directly fed back to the control as it is done in conventional control (e.g. Huang et al. (2010), Tian et al. (2012)). There are different approaches to handle this problem. For example it can be solved by introducing a disturbance model that models the plant-model mismatch and persistent disturbances acting on the plant (Maeder et al., 2009, Morari and Maeder, 2012). However, in this thesis it is tackled using RTO, thus a master/slave (or two-layer) approach, whereas the master (upper layer) control is the model-based and the slave (lower layer) is a conventional control. This approach is explained in detail in Chapter 9.

Chapter 3

Multi-Objective Optimization Algorithms

Multi-objective optimization algorithms try to find the Pareto front and the corresponding Pareto optimal set of a multi-objective optimization problem. As in case of continuous function optimization a Pareto front could contain infinite many elements these algorithms in general cannot find the complete Pareto front. Therefore they try to find solutions which approximate the form of the Pareto front best possible.

In this thesis a multi-objective optimization algorithm is used to solve the MONMPC problem stated in Chapter 2. In the simulation and optimization studies in Chapter 9 two multi-objective optimization methods are compared. They are SMS-EMOA (Emmerich et al., 2005, Beume et al., 2007) and SMS-EGO (Wagner et al., 2007, Ponweiser et al., 2008). Both methods are briefly introduced in the following two sections.

Next to the two methods there are also other famous multi-objective optimization methods. Examples are NSGA-II (Deb et al., 2002), SPEA2 (Zitzler et al., 2001), ϵ -MOEA (Deb et al., 2003) and ParEGO (Knowles, 2006). Various publications comparing these different multi-objective optimization methods reveal that both SMS-EMOA and SMS-EGO belong to the best methods of their kind, e.g. (Ponweiser et al., 2008, Wagner et al., 2007, 2010).

3.1 Hypervolume-based Evolutionary Algorithm

An evolutionary algorithm is a stochastic optimization technique inspired by the principles of natural evolution (cf. Alba and Cotta (2006)). It describes a class of different optimization methods which all have the following in common. The key feature of evolutionary algorithms (EAs) is that in each iteration of the algorithm a collection of potential solutions, the so-called population, of the optimization problem is evaluated in parallel. The elements of the population are called individuals. The performance of each

individual is measured by the objective function. In each iteration the population may change, what means that new solutions are created and already existing solutions are discarded from the population to keep the number of individuals inside the population constant. As EAs typically return a set of solutions (the population) in one call, they are especially suited to solve multi-objective optimization problems, compared to methods, which only return one solution at a time.

The purpose of a hypervolume-based EA is to maximize a scalar criterion, which is named the hypervolume indicator (or \mathcal{S} -metric, Zitzler and Thiele (1998)), see Definition 3.1. This criterion is a property of a set and describes the size of a space covered by this set. Below it is shown that the hypervolume indicator of the Pareto front \mathcal{PF}^* is maximal for a given optimization problem. Therefore, by maximizing the hypervolume indicator the algorithm tries to find the best approximation (with a finite number of elements) of the true Pareto front \mathcal{PF}^* . Note that the multi objectives are mapped onto one objective, so that in general each single objective optimization method can be used to solve a multi-objective optimization problem using the hypervolume indicator (Fleischer, 2003, Knowles et al., 2003).

Definition 3.1 (Hypervolume indicator, Custódio et al. (2012)): The hypervolume indicator for some set $\mathcal{A} \subset \mathbb{R}^{n_o}$ and a reference point $\mathbf{r} \in \mathbb{R}^{n_o}$ that is dominated by all the points in \mathcal{A} is defined as:

$$I_H(\mathcal{A}) := Vol \{ \mathbf{b}_{\mathcal{B}} \in \mathbb{R}^{n_o} | \mathbf{b}_{\mathcal{B}} \leq \mathbf{r} \wedge \exists \mathbf{a}_{\mathcal{A}} \in \mathcal{A} : \mathbf{a}_{\mathcal{A}} \leq \mathbf{b}_{\mathcal{B}} \} = Vol \left(\bigcup_{\mathbf{a}_{\mathcal{A}} \in \mathcal{A}} [\mathbf{a}_{\mathcal{A}}, \mathbf{r}] \right)$$

Here Vol denotes the Lebesgue measure of a n_o -dimensional set of points, and $[\mathbf{a}_{\mathcal{A}}, \mathbf{r}]$ denotes the interval box with lower corner $\mathbf{a}_{\mathcal{A}}$ and upper corner \mathbf{r} .

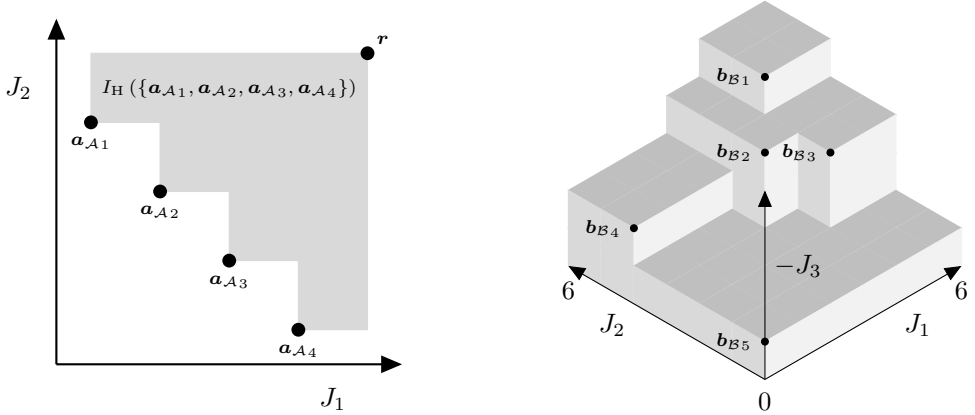
Figure 3.1a shows an example of the hypervolume indicator for a set \mathcal{A} in a two-dimensional and Figure 3.1b in a three-dimensional space. To be able to find the approximation of the Pareto front we first have to be able to compare two different approximate Pareto fronts and to decide which one is better.

Definition 3.2 (Custódio et al. (2012)): Given two nondominated sets \mathcal{A} and \mathcal{B} . \mathcal{A} is better than \mathcal{B} , which is represented by $\mathcal{A} \prec \mathcal{B}$, if and only if

$$\forall \mathbf{b}_{\mathcal{B}} \in \mathcal{B} : \exists \mathbf{a}_{\mathcal{A}} \in \mathcal{A} : \mathbf{a}_{\mathcal{A}} \leq \mathbf{b}_{\mathcal{B}} \text{ and } \exists \mathbf{b}_{\mathcal{B}} \in \mathcal{B} : \exists \mathbf{a}_{\mathcal{A}} \in \mathcal{A} : \mathbf{a}_{\mathcal{A}} \prec \mathbf{b}_{\mathcal{B}}$$

Now the hypervolume indicator is used to compare two Pareto front approximations. In Zitzler et al. (2003) it was shown, that if a certain property holds, the better nondominated set has a higher hypervolume indicator, see Lemma 3.1.

Lemma 3.1 (Custódio et al. (2012), Zitzler et al. (2003)): Let \mathcal{A} and \mathcal{B} be two nondominated sets with the properties $\mathcal{A} \prec \mathcal{B}$ and $\forall \varphi \in \mathcal{A} \cup \mathcal{B} : \varphi \prec \mathbf{r}$, where \mathbf{r}



(a) The hypervolume indicator I_H for the set \mathcal{A} is shaded in grey, cf. Custódio et al. (2012).

(b) The hypervolume indicator I_H for the set \mathcal{B} with $r = (6, 6, 0)^T$, cf. Custódio et al. (2012).

Figure 3.1: Hypervolume indicator for a set $\mathcal{A} := \{\mathbf{a}_{\mathcal{A}1}, \mathbf{a}_{\mathcal{A}2}, \mathbf{a}_{\mathcal{A}3}, \mathbf{a}_{\mathcal{A}4}\} \subset \mathbb{R}^2$ in a two-dimensional space and a set $\mathcal{B} := \{\mathbf{b}_{\mathcal{B}1}, \dots, \mathbf{b}_{\mathcal{B}5}\} \subset \mathbb{R}^3$ in a three-dimensional space.

is the reference point used in the hypervolume computations. Then $I_H(\mathcal{A}) > I_H(\mathcal{B})$.

This means that the hypervolume indicator of the true Pareto front is maximal, because it is always better than or equal to any other possible nondominated set, and therefore $I_H(\mathcal{P}\mathcal{F}^*) \geq I_H(\mathcal{A})$ for any nondominated set \mathcal{A} . Knowing that, it is obviously of interest to maximize the hypervolume indicator, so that the best possible approximation of the Pareto front can be found.

Furthermore in Zitzler et al. (2003) the following Lemma was shown.

Lemma 3.2 (Custódio et al. (2012), Zitzler et al. (2003)): Let \prec be defined as in Definition 3.2, and \mathcal{A} and \mathcal{B} be two nondominated sets with the property $\forall \varphi \in \mathcal{A} \cup \mathcal{B} : \varphi \prec r$, where r is the reference point used in the hypervolume computations. If $I_H(\mathcal{A}) > I_H(\mathcal{B})$ then $\mathcal{B} \not\prec \mathcal{A}$.

This means, that if an algorithm exists, which provably never decreases the hypervolume indicator of the current approximation of the Pareto front, then the approximation will never be worse than the approximation of the previous iteration. The \mathcal{S} metric selection evolutionary multi-objective optimization algorithm (SMS-EMOA) is such a method, which is presented in the following.

3.1.1 SMS-EMOA

SMS-EMOA is initialized with an initial population \mathcal{P}_0 of size μ . In each iteration of the algorithm one solution candidate φ is created out of the current population \mathcal{P}_κ using variation. If the new solution improves the quality of the current population it is kept and another solution is deleted, else it is discarded. The SMS-EMOA algorithm is shown in Algorithm 3.1.

Algorithm 3.1 A SMS-EMOA algorithm (Beume et al., 2008)

Input: $\mathcal{P}_0 \leftarrow \text{init}$

Input: $\kappa \leftarrow 0$

```

1:
2: repeat
3:    $\varphi \leftarrow \text{variation}(\mathcal{P}_\kappa)$ 
4:    $\mathcal{D} \leftarrow \text{dominated\_individuals}(\mathcal{P}_\kappa \cup \{\varphi\})$ 
5:   if  $\mathcal{D} \neq \emptyset$  then
6:      $\phi^* \leftarrow \arg \max_{\phi \in \mathcal{D}} d_n(\phi, \mathcal{P}_\kappa \cup \{\varphi\})$ 
7:   else
8:      $\phi^* \leftarrow \arg \min_{\phi \in (\mathcal{P}_\kappa \cup \{\varphi\})} \Delta I_H(\mathbf{J}_x(\phi), \mathcal{P}\mathcal{F}_\kappa \cup \{\mathbf{J}_x(\varphi)\})$ 
9:   end if
10:   $\mathcal{P}_{\kappa+1} \leftarrow (\mathcal{P}_\kappa \cup \{\varphi\}) \setminus \{\phi^*\}$ 
11:   $\kappa \leftarrow \kappa + 1$ 
12: until some stopping criterion

```

In Algorithm 3.1 the number of dominating points d_n ($\text{card}(\mathcal{A})$) calculates the cardinality of the set \mathcal{A})

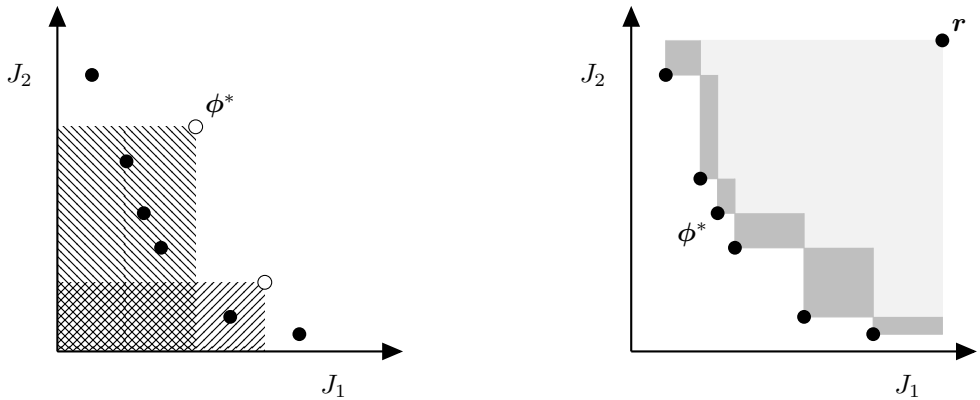
$$d_n(\phi, \mathcal{A}) := \text{card}(\{a_{\mathcal{A}} \in \mathcal{A} \mid a_{\mathcal{A}} \prec \phi\}) \quad (3.1)$$

and the contributing hypervolume ΔI_H

$$\begin{aligned} \Delta I_H(a_{\mathcal{A}}, \mathcal{A}) &:= I_H(\mathcal{A}) - I_H(\mathcal{A} \setminus \{a_{\mathcal{A}}\}) \\ &\text{with } a_{\mathcal{A}} \in \mathcal{A} \end{aligned} \quad (3.2)$$

are used, cf. (Beume et al., 2007). In Algorithm 3.1 all dominated solutions are collected in the set \mathcal{D} which are returned by the function `dominated_individuals`, called in line 4 of the algorithm. The population of solution candidates in iteration κ is symbolized by \mathcal{P}_κ , which is the current approximation of the Pareto optimal set. The corresponding approximation of the Pareto front is given by $\mathcal{P}\mathcal{F}_\kappa$.

In Figure 3.2a the concept of the number of dominating points d_n is visualized. If there are dominated solutions, visualized as the two white circles in Figure 3.2a, then d_n specifies the number of solutions that dominate each dominated solution. One of the solutions with the largest d_n is deleted from the current population, here ϕ^* . If there is no dominated solution, thus all solutions are non-dominated within the population,



(a) The two dominated solutions (white circles) are dominated by solutions which lie in the shaded areas. The point ϕ^* has the higher dominance number, which is three compared to one.

(b) The dark shaded areas visualize ΔI_H of the points, whereas the area of ϕ^* is the smallest.

Figure 3.2: The solutions of a two-dimensional optimization problem are shown. The worst solution ϕ^* will be deleted from the current population, cf. Beume et al. (2008).

then the solution with the smallest contributing hypervolume ΔI_H is deleted, see Figure 3.2b. As by discarding the solution with the smallest contribution always a subset of size μ with largest hypervolume is selected, the hypervolume indicator I_H will never decrease. Either the new solution is directly deleted from the population, which leaves the hypervolume indicator unchanged or the new solution increases the hypervolume indicator.

3.2 SMS-EGO

S -metric selection-based efficient global optimization (SMS-EGO) was first introduced in Ponweiser et al. (2008). SMS-EGO is a multi-objective variant of so called Efficient Global Optimization Algorithms (EGO) (Jones et al., 1998), which were earlier known as Statistical Global Optimization (Cox and John, 1997, Mockus et al., 1978).

In SMS-EGO a meta-model is used to predict objective function evaluations, that are assumed to be expensive. The meta-model is learned from previous exact evaluations. Based on the meta-model it is decided which point is evaluated next using the exact objective function.

The general idea of SMS-EGO is to replace during optimization the original objective function \mathbf{J} with the meta-model generated one $\widehat{\mathbf{J}}$. Thus, an optimization method solves the optimization problem given by $\widehat{\mathbf{J}}$. The returned optimal solution is evaluated by the original objective function \mathbf{J} and this result is used to update the meta-model restarting the optimization process again.

For each component J_{i_o} of the objective function a separate meta-model is created. As meta-model a DACE stochastic process model is used, where DACE is short for 'Design and Analysis of Computer Experiments' (Jones et al., 1998). Each such DACE model returns an estimate of the objective function $\hat{J}_{i_o} \in \mathbb{R}$ and a standard deviation $\hat{s}_{J_{i_o}} \in \mathbb{R}$ representing the uncertainty in the estimation. Both values are collected in the vectors $\hat{\mathbf{J}} := (\hat{J}_1, \dots, \hat{J}_{i_o}, \dots, \hat{J}_{n_o})^T \in \mathbb{R}^{n_o}$ and $\hat{\mathbf{s}}_{\mathbf{J}} := (\hat{s}_{J_1}, \dots, \hat{s}_{J_{i_o}}, \dots, \hat{s}_{J_{n_o}})^T \in \mathbb{R}^{n_o}$.

As the meta-models also return the estimated uncertainty $\hat{\mathbf{s}}_{\mathbf{J}}$ the lower confidence bound $\hat{\mathbf{J}}_{\text{pot}} := \hat{\mathbf{J}} - \alpha_{\text{LCB}} \cdot \hat{\mathbf{s}}_{\mathbf{J}}$, with $\alpha_{\text{LCB}} = -\Phi_{\text{CDF}}^{-1}(0.5 \cdot \sqrt[n]{0.5})$ (Wagner et al., 2010, Emmerich et al., 2006), is used as the objective of some evaluated solution and not just $\hat{\mathbf{J}}$. Here, $\Phi_{\text{CDF}} : \mathbb{R} \rightarrow (0, 1)$ is the cumulative normal distribution function.

Each evaluated $\hat{\mathbf{J}}$ is validated by a measure named additive ϵ -dominance, defined in Def. 3.3.

Definition 3.3 (cf. Zitzler et al. (2003)): Given two vectors of optimization variables $\underline{\mathbf{u}}_1, \underline{\mathbf{u}}_2 \in \mathcal{U}_{\mathcal{F}}$, it is said that $\underline{\mathbf{u}}_1$ ϵ -dominates $\underline{\mathbf{u}}_2$, being represented by $\underline{\mathbf{u}}_1 \preceq_{\epsilon+} \underline{\mathbf{u}}_2$, iff for some $\epsilon \in \mathbb{R}^+$ $\forall i_o \in \{1, \dots, n_o\} : J_{\mathbf{x}, i_o}(\underline{\mathbf{u}}_1) \leq J_{\mathbf{x}, i_o}(\underline{\mathbf{u}}_2) + \epsilon$.

The single-objective function, which tries to find the optimum of $\hat{\mathbf{J}}$ uses additive ϵ -dominance. It distinguishes between two kinds of solution candidates: ϵ -dominated and non- ϵ -dominated solution candidates, see Figure 3.3. Non- ϵ -dominated candidates φ_{pot} yielding $\hat{\mathbf{J}}_{\text{pot}}$ are evaluated based on the negative value of their additional hypervolume contribution: $I_H(\mathcal{P}\mathcal{F}_{\kappa}) - I_H(\mathcal{P}\mathcal{F}_{\kappa} \cup \{\hat{\mathbf{J}}_{\text{pot}}\})$, whereas $\mathcal{P}\mathcal{F}_{\kappa}$ is the current approximation of the Pareto front of \mathbf{J} . However, ϵ -dominated solutions are penalized by a penalty given in equation (3.3), with \mathcal{P}_{κ} being the current approximation of the Pareto optimal set (only containing non-dominated points), (Wagner et al., 2010).

$$p_{\epsilon} := \begin{cases} \max_{\varphi \in \mathcal{P}_{\kappa}} \left[-1 + \prod_{i_o=1}^{n_o} \left(1 + \max \left(\hat{J}_{\text{pot}, i_o} - J_{\mathbf{x}, i_o}(\varphi), 0 \right) \right) \right] & \text{if } \varphi \preceq_{\epsilon+} \varphi_{\text{pot}} \\ 0 & \text{otherwise} \end{cases} \quad (3.3)$$

In equation (3.4) the single-objective function is shown, that is used to find an optimal solution candidate to be evaluated at the original objective function \mathbf{J} .

$$f_{\text{EGO}} := \begin{cases} I_H(\mathcal{P}\mathcal{F}_{\kappa}) - I_H(\mathcal{P}\mathcal{F}_{\kappa} \cup \{\hat{\mathbf{J}}_{\text{pot}}\}) & \text{non-}\epsilon\text{-dominated } \hat{\mathbf{J}}_{\text{pot}} \\ p_{\epsilon} & \epsilon\text{-dominated } \hat{\mathbf{J}}_{\text{pot}} \end{cases} \quad (3.4)$$

In SMS-EGO this objective function is minimized using an interior point method.

The value for ϵ is calculated as in Ponweiser et al. (2008) using $\epsilon = \frac{\Delta \mathcal{P}\mathcal{F}_{\kappa}}{\text{card}(\mathcal{P}\mathcal{F}_{\kappa}) + c \cdot n_{\text{left}}}$.

There, $\Delta\mathcal{P}\mathcal{F}_\kappa := \max(\mathcal{P}\mathcal{F}_\kappa) - \min(\mathcal{P}\mathcal{F}_\kappa)$, where

$$\max(\mathcal{P}\mathcal{F}_\kappa) := \left(\max_{\mathbf{J}_x \in \mathcal{P}\mathcal{F}_\kappa} J_{x,1}, \dots, \max_{\mathbf{J}_x \in \mathcal{P}\mathcal{F}_\kappa} J_{x,i_o}, \dots, \max_{\mathbf{J}_x \in \mathcal{P}\mathcal{F}_\kappa} J_{x,n_o} \right)^T,$$

likewise $\min(\mathcal{P}\mathcal{F}_\kappa)$. Furthermore, $c = 1 - \frac{1}{2^{n_o}}$ is a correction factor and n_{left} is the number of remaining evaluations (Ponweiser et al., 2008).

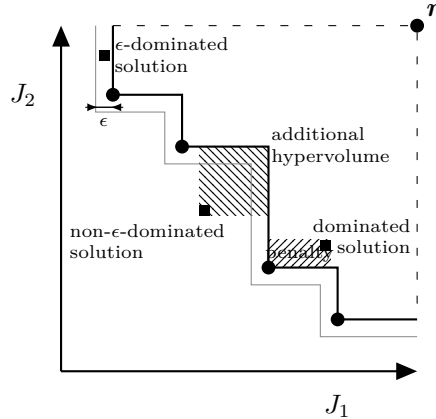


Figure 3.3: Graphical explanation of the concept of ϵ -dominance used in SMS-EGO, cf. Ponweiser et al. (2008).

Chapter 4

State Estimation

Given a real-world system as introduced in the beginning of Chapter 2 it can not be assumed that the state \mathbf{x} of the system is known at each time t . Nevertheless, the NMPC approach in eq. (2.20) assumes, that \mathbf{x} is known at each discrete time t_k , for $k = 0, 1, 2, \dots$ (for the definition of t_k see equation (2.6)). Those $n_y \in \mathbb{N}_0$ process values that can be observed of a system are denoted by the measurement value function $\mathbf{y} : \mathbb{R}^+ \rightarrow \mathcal{Y}$, $\mathcal{Y} \subseteq \mathbb{R}^{n_y}$, and the functional connection of the current measurement values $\mathbf{y}(t)$ and the current state of the system $\mathbf{x}(t)$ is given by:

$$\mathbf{y}(t) = \mathbf{h}(\mathbf{x}(t), \mathbf{v}(t)). \quad (4.1)$$

Inaccuracies in the real-valued measurement function $\mathbf{h} : \mathcal{X} \times \mathbb{R}^{n_v} \rightarrow \mathcal{Y}$ as well as measurement noise, are modeled by the $n_v \in \mathbb{N}_0$ dimensional white Gaussian noise process $\mathbf{v} : \mathbb{R}^+ \rightarrow \mathbb{R}^{n_v}$ with covariance matrix $\mathbf{\Psi}_v \in \mathbb{R}^{n_v \times n_v}$.

The question arises, whether it is possible to estimate the values of the system state \mathbf{x} at each time t_k , given equations (2.1) and (4.1) as well as $\mathbf{u}(\tau)$ and $\mathbf{y}(\tau)$ for each $\tau \in [0, t_k]$. The state vector estimate at time t_k will be symbolized using $\hat{\mathbf{x}}(t_k)$ and the corresponding function is $\hat{\mathbf{x}} : \mathbb{R}^+ \rightarrow \mathcal{X}$. This state estimate $\hat{\mathbf{x}}$ will be used by the NMPC (eq. (2.20)) as an approximation of the real state \mathbf{x} at each time t_k .

Let us assume that there are two different sampling times where the measurement \mathbf{y} and input values \mathbf{u} are acquired. The one for the measurement values is named $\delta_y \in \mathbb{R}^+$ and the one for the input values $\delta_u \in \mathbb{R}^+$. The ratio of the control sampling time δ (see Section 2.1) and both sampling times $\delta_y \leq \delta$ and $\delta_u \leq \delta$ are defined by the symbols:

$$N_{\delta_y} := \frac{\delta}{\delta_y} \in \mathbb{N}_0 \quad \text{and} \quad N_{\delta_u} := \frac{\delta}{\delta_u} \in \mathbb{N}_0. \quad (4.2)$$

In the following three sections (4.1 - 4.3) three different state estimation methods are proposed. Thereafter, they are applied at an anaerobic digestion process in a simulation study in Section 4.4.

4.1 State Estimation using Software Sensors

In this section an approach is developed, that tries to find a function $\mathbf{F}_E : \mathcal{Y}^{N_{\delta_y} \cdot k+1} \times \mathcal{U}^{N_{\delta_u} \cdot k+1} \rightarrow \mathcal{X}$ with the sets

$$\mathcal{Y}^{N_{\delta_y} \cdot k+1} := \{\mathbf{y}(0), \mathbf{y}(\delta_y), \dots, \mathbf{y}(\delta), \mathbf{y}(\delta + \delta_y), \dots, \mathbf{y}(t_k)\} \quad (4.3)$$

and

$$\mathcal{U}^{N_{\delta_u} \cdot k+1} := \{\mathbf{u}(0), \mathbf{u}(\delta_u), \dots, \mathbf{u}(\delta), \mathbf{u}(\delta + \delta_u), \dots, \mathbf{u}(t_k)\} \quad (4.4)$$

estimating the state of the system at time t_k . This function \mathbf{F}_E uses the complete stream of inputs \mathbf{u} and outputs \mathbf{y} of the system recorded from time 0 until time t_k and therefore is a completely data based state estimator. Its returned state estimate $\hat{\mathbf{x}}_{\mathbf{F}_E} : \mathbb{R}^+ \rightarrow \mathcal{X}$ defined as

$$\hat{\mathbf{x}}_{\mathbf{F}_E}(t_k) := \mathbf{F}_E \left(\underbrace{\mathbf{y}(0), \dots, \mathbf{y}(t_k)}_{\in \mathcal{Y}^{N_{\delta_y} \cdot k+1}}, \underbrace{\mathbf{u}(0), \dots, \mathbf{u}(t_k)}_{\in \mathcal{U}^{N_{\delta_u} \cdot k+1}} \right) \in \mathcal{X} \quad (4.5)$$

would be the best state estimate that could be achieved based on the input and output data. Unfortunately the amount of data used in this approach is increasing with time t_k , therefore in practice it will only be possible to find an approximation of this function \mathbf{F}_E , defined as $\tilde{\mathbf{F}}_E : \mathcal{Y}^{N_y+1} \times \mathcal{U}^{N_u+1} \rightarrow \mathcal{X}$. There a constant number of input and output samples is used, which are $N_u + 1 \in \mathbb{N}$ and $N_y + 1 \in \mathbb{N}$ using a sliding window approach. To be able to interpret N_y and N_u some formalism has to be introduced. To make the domain of $\tilde{\mathbf{F}}_E$ sufficiently small, causal moving average filters are used to merge adjacent samples of input and output data to one representative value. A moving average filter for input data $\Lambda_u \in \mathcal{F}_\Lambda$, with the function space of moving average filters \mathcal{F}_Λ and $\Lambda_u : \mathcal{U}^{w_u} \rightarrow \mathcal{U}$, with the window size $w_u \in \mathcal{W}_u \subset \mathbb{N}$ is defined as:

$$\Lambda_u(\mathbf{u}(t_k), \dots, \mathbf{u}(t_k - (w_u - 1) \cdot \delta_u)) := \frac{1}{w_u} \cdot \sum_{i=1}^{w_u} \mathbf{u}(t_k - (i - 1) \cdot \delta_u). \quad (4.6)$$

Note that a moving average filter can be implemented as a tapped delay line with $w_u - 1$ taps.

For the input data N_u moving average filters are used, each with a different window size w_u . Thus, the set of moving average window lengths \mathcal{W}_u has N_u elements and is defined as $\mathcal{W}_u := \{w_{u,1}, \dots, w_{u,N_u}\}$. Then, to each window size $w_{u,i_{\Lambda_u}}$ belongs the moving average filter $\Lambda_{u,i_{\Lambda_u}} \in \mathcal{F}_\Lambda$, returning for each $i_{\Lambda_u} = 1, \dots, N_u$ the moving average value $\bar{\mathbf{u}}_{i_{\Lambda_u}} : \mathbb{R}^+ \rightarrow \mathcal{U}$ defined as:

$$\bar{\mathbf{u}}_{i_{\Lambda_u}}(t_k) := \Lambda_{u,i_{\Lambda_u}}(\mathbf{u}(t_k), \dots, \mathbf{u}(t_k - (w_{u,i_{\Lambda_u}} - 1) \cdot \delta_u)) \in \mathcal{U}. \quad (4.7)$$

We equally define a moving average filter for output data $\Lambda_y \in \mathcal{F}_\Lambda$, $\Lambda_y : \mathcal{Y}^{w_y} \rightarrow \mathcal{Y}$,

with the window size $w_y \in \mathcal{W}_y \subset \mathbb{N}_0$ as

$$\Lambda_y(\mathbf{y}(t_k), \dots, \mathbf{y}(t_k - (w_y - 1) \cdot \delta_y)) := \frac{1}{w_y} \cdot \sum_{i=1}^{w_y} \mathbf{y}(t_k - (i - 1) \cdot \delta_y). \quad (4.8)$$

For the measurement data N_y moving average filters are used, each with a different window size w_y . Thus, the set of moving average window lengths \mathcal{W}_y has N_y elements and is defined as $\mathcal{W}_y := \{w_{y,1}, \dots, w_{y,N_y}\}$. Then, to each window size $w_{y,i_{\Lambda_y}}$ the moving average filter $\Lambda_{y,i_{\Lambda_y}} \in \mathcal{F}_{\Lambda}$ belongs, returning for each $i_{\Lambda_y} = 1, \dots, N_y$ the moving average value $\bar{\mathbf{y}}_{i_{\Lambda_y}} : \mathbb{R}^+ \rightarrow \mathcal{Y}$ defined as:

$$\bar{\mathbf{y}}_{i_{\Lambda_y}}(t_k) := \Lambda_{y,i_{\Lambda_y}} \left(\mathbf{y}(t_k), \dots, \mathbf{y}(t_k - (w_{y,i_{\Lambda_y}} - 1) \cdot \delta_y) \right) \in \mathcal{Y}. \quad (4.9)$$

The vector which is returned by the approximate state estimation function $\tilde{\mathbf{F}}_E$, defined above, is used as state estimate at each time t_k :

$$\hat{\mathbf{x}}(t_k) := \tilde{\mathbf{F}}_E \left(\underbrace{\mathbf{y}(t_k), \bar{\mathbf{y}}_1(t_k), \dots, \bar{\mathbf{y}}_{N_y}(t_k)}_{\in \mathcal{Y}^{N_y+1}}, \underbrace{\mathbf{u}(t_k), \bar{\mathbf{u}}_1(t_k), \dots, \bar{\mathbf{u}}_{N_u}(t_k)}_{\in \mathcal{U}^{N_u+1}} \right). \quad (4.10)$$

Now it is established which values are passed to the estimation function $\tilde{\mathbf{F}}_E$. But, what kind of function $\tilde{\mathbf{F}}_E$ should be is not yet clear. At the moment, and there maybe never will be, an equation which describes for a biogas plant how current and past input and output values let one imply on the current state of the system. Therefore, this function has to be found. In this thesis it was tried to find an approximation for this function using supervised machine learning methods. In supervised learning many matching input and output data samples are presented to the learning method. The method tries to find a general structure in the seen data, which is then generalized to all unseen regions of the data space. In the following subsection this idea is made more clear. Furthermore, three machine learning methods are briefly introduced, which were used to find a model for the state estimation function $\tilde{\mathbf{F}}_E$. These are Random Forests, linear discriminant analysis and generalized discriminant analysis, whereas both discriminant analysis methods are used as data preprocessing methods for a linear classifier. As machine learning methods in general can be highly nonlinear, the state estimator $\tilde{\mathbf{F}}_E$ can be highly nonlinear as well. In contrast to a dynamic state estimation method this one is static. Therefore, issues such as stability and convergence are not applicable. The estimator is always stable. Its estimate does not converge to the real state values, but there remains a data dependent estimation error.

4.1.1 Supervised Machine Learning Methods

To be able to apply machine learning methods training and validation samples are created as follows. Without loss of generalization let us set $\delta_u = \delta_y$. Then the matrices

$$\mathbf{Y} := \begin{pmatrix} \mathbf{y}^T(0), \bar{\mathbf{y}}_1^T(0), \dots, \bar{\mathbf{y}}_{N_y}^T(0), \mathbf{u}^T(0), \bar{\mathbf{u}}_1^T(0), \dots, \bar{\mathbf{u}}_{N_u}^T(0) \\ \mathbf{y}^T(\delta_y), \bar{\mathbf{y}}_1^T(\delta_y), \dots, \bar{\mathbf{y}}_{N_y}^T(\delta_y), \mathbf{u}^T(\delta_y), \bar{\mathbf{u}}_1^T(\delta_y), \dots, \bar{\mathbf{u}}_{N_u}^T(\delta_y) \\ \vdots \\ \mathbf{y}^T(t_k), \bar{\mathbf{y}}_1^T(t_k), \dots, \bar{\mathbf{y}}_{N_y}^T(t_k), \mathbf{u}^T(t_k), \bar{\mathbf{u}}_1^T(t_k), \dots, \bar{\mathbf{u}}_{N_u}^T(t_k) \end{pmatrix}, \quad (4.11)$$

$\mathbf{Y} \in \mathbb{R}^{N \times D}$, $D := n_y \cdot (N_y + 1) + n_u \cdot (N_u + 1)$, $N := k \cdot N_{\delta_y} + 1$, and

$$\mathbf{X} := (\mathbf{x}_{i_x}, \dots, \mathbf{x}_{n_x}) := \begin{pmatrix} \mathbf{x}^T(0) \\ \mathbf{x}^T(\delta_y) \\ \vdots \\ \mathbf{x}^T(t_k) \end{pmatrix} \in \mathbb{R}^{N \times n_x} \quad (4.12)$$

can be defined, with $\mathbf{x}_{i_x} \in \mathbb{R}^N$. Using both matrices \mathbf{X} and \mathbf{Y} , the state estimation problem is to find a mapping $\mathbf{Y} \mapsto \mathbf{x}_{i_x}$ for each state vector component $i_x = 1, \dots, n_x$. As said in the beginning of this chapter it cannot be assumed that the state \mathbf{x} is available at each discrete time t_k . Therefore, the matrix \mathbf{X} is not available. Hence, a calibrated simulation model of the biogas plant at hand is used to generate an approximation of \mathbf{X} , replacing \mathbf{x} with ${}^o\mathbf{x}$ at each simulated time τ . The simulation model consists out of eqs. (2.1) and (4.1). At the same time all vectors \mathbf{y} in \mathbf{Y} are replaced with the values returned by $\mathbf{h}({}^o\mathbf{x}(\tau), \mathbf{v}(\tau))$ at each corresponding time τ . Based on ${}^o\mathbf{x}$ and \mathbf{h} , an approximation of the original problem is solved, assuming that the model emulates the real process with sufficient accuracy.

This estimation problem can be solved using either regression or classification techniques. In this case, classification was used.

To be able to apply discriminant analysis and classification methods on the dataset, the range for each state vector component \mathbf{x}_{i_x} is clustered into $C \in \mathbb{N}_0$ equally distributed classes, $i_x = 1, \dots, n_x$. Thus, vectors are generated containing the class labels corresponding to the simulated values of the state vector components \mathbf{x}_{i_x} , that is, $\boldsymbol{\vartheta}_{i_x} \in \{1, \dots, C\}^N$, $i_x = 1, \dots, n_x$.

Before machine learning methods are applied, the complete dataset \mathbf{Y} is split into a training dataset $\mathbf{Y}_T \in \mathbb{R}^{N_T \times D}$ and a validation dataset $\mathbf{Y}_V \in \mathbb{R}^{N_V \times D}$ with $N_V := N - N_T$, $N_T < N$. In the following, the used machine learning methods are briefly described.

4.1.1.1 Linear Discriminant Analysis (LDA)

Linear discriminant analysis searches for a linear transformation $\mathbf{A}_{\text{LDA}} \in \mathbb{R}^{d \times D}$, $d \leq D$, such that the transformed data $\mathbf{Z} = \mathbf{A}_{\text{LDA}} \cdot \mathbf{Y}_T^T$, $\mathbf{Z} := (\mathbf{z}_1, \dots, \mathbf{z}_{N_T}) \in \mathbb{R}^{d \times N_T}$, can be linearly separated better than the original feature vectors \mathbf{Y}_T^T . The linear transformation \mathbf{A}_{LDA} is determined by solving an optimization problem maximizing the well-known Fisher discriminant criterion:

$$\text{trace} \{ \mathbf{S}_T^{-1} \cdot \mathbf{S}_B \} \quad (4.13)$$

where $\mathbf{S}_T \in \mathbb{R}^{D \times D}$ is total scatter-matrix and $\mathbf{S}_B \in \mathbb{R}^{D \times D}$ is the between-class scatter-matrix for the data (Duda et al., 2000). The LDA and a subsequent linear classifier are both implemented in MATLAB®.

4.1.1.2 Generalized Discriminant Analysis (GerDA) (Stuhlsatz et al., 2012)

LDA is a popular pre-processing and visualization tool used in different pattern recognition applications. Unfortunately, LDA followed by linear classification produces high error rates on many real-world datasets, because a linear mapping \mathbf{A}_{LDA} cannot transform arbitrarily distributed features into independently Gaussian distributed ones. A natural generalization of the classical LDA is to assume a function space \mathcal{F} of nonlinear transformations $\mathbf{f}_{\text{GerDA}} : \mathbb{R}^D \rightarrow \mathbb{R}^d$ and to still rely on having intrinsic features $\mathbf{z}_i := \mathbf{f}_{\text{GerDA}}(\mathbf{y}_i)$, $i = 1, \dots, N_T$, with the same statistical properties as assumed for LDA features. The idea is that a sufficiently large space \mathcal{F} potentially contains a nonlinear feature extractor $\mathbf{f}_{\text{GerDA}}^* \in \mathcal{F}$ that increases the discriminant criterion (4.13) compared with a linear extractor \mathbf{A}_{LDA} . GerDA defines a large space \mathcal{F} using a deep neural network (DNN), and consequently the nonlinear feature extractor $\mathbf{f}_{\text{GerDA}}^* \in \mathcal{F}$ is given by the DNN which is trained with measurements of the data space such that the objective function (4.13) is maximized. Unfortunately, training a DNN with standard methods, like back-propagation, is known to be challenging due to many local optima in the considered objective function. To efficiently train a large DNN with respect to (4.13), in Stuhlsatz et al. (2010a,b) a stochastic pre-optimization has been proposed based on greedily layer-wise trained Restricted Boltzmann Machines (Hinton et al., 2006). After layer-wise pre-optimization all weights \mathbf{W} and biases \mathbf{b} of the GerDA-DNN are appropriately initialized. Nevertheless, pre-optimization is suboptimal in maximizing (4.13), thus a subsequent fine-tuning of the GerDA-DNN is performed using a modified back-propagation of the gradients of (4.13) with respect to the network parameters. In Stuhlsatz et al. (2010a,b) it is shown that stochastic pre-optimization and subsequent fine-tuning yields very good discriminative features and training time is substantially reduced compared with random initialization of large GerDA-DNNs. The GerDA-framework is implemented in MATLAB®.

4.1.1.3 Random Forests

Random Forests consists out of an ensemble of decision trees (Breiman, 2001) and can be used to solve complex classification and regression problems. At each node of such a binary decision tree the dataset at that node is split into two disjoint datasets. At each leaf of the tree the value for the predicted variable is decided. Classification is performed by taking the majority vote of an ensemble of classification trees, where each tree is trained on a bootstrapped sample of the original training dataset. This results in an ensemble of slightly different decision trees leading to improved generalization (Criminisi et al., 2011). The Random Forests algorithm used is from the Random Forests implementation for MATLAB® (and Standalone) (Jaintilal, 2010).

4.2 Hybrid Extended Kalman Filter

Above eq. (4.2) the sampling time for measurement values δ_y was introduced. The hybrid extended Kalman filter proposed in this section will return a state estimate at each time

$$t_j := j \cdot \delta_y \quad (4.14)$$

for $j = 1, 2, 3, \dots$. Setting $t_j = t_k$ with t_k defined in equation (2.6) and using eq. (4.2) it is

$$j = N_{\delta_y} \cdot k. \quad (4.15)$$

Thus, j runs with N_{δ_y} times the frequency of k . At time instant $j = 0$ the filter is started and initialized with the expectation value of the system state at time instant $k = 0$: $E \langle \mathbf{x}(t_0) \rangle$.

To simplify the notation it is generally defined:

$$\mathbf{X}_j := \mathbf{X}(t_j) \quad \text{and} \quad \mathbf{x}_j := \mathbf{x}(t_j) \quad (4.16)$$

as well as

$$\mathbf{X}_k := \mathbf{X}(t_k) \quad \text{and} \quad \mathbf{x}_k := \mathbf{x}(t_k) \quad (4.17)$$

for any matrix $\mathbf{X}(t_j), \mathbf{X}(t_k) \in \mathbb{R}^{m \times n}$ and any vector $\mathbf{x}(t_j), \mathbf{x}(t_k) \in \mathbb{R}^n$, $n, m \in \mathbb{N}$.

A Kalman filter basically can be divided into the two parts prediction and correction. In the prediction step the model equation of the system (eq. (2.1)) is used to predict the current state \mathbf{x}_j of the system given a state estimate from the last iteration $j - 1$. In the correction step the current measurement values \mathbf{y}_j are taken to correct the predicted state estimate. The state estimate at time instant j is named the a priori state estimate, denoted by $\hat{\mathbf{x}}_j^- := \hat{\mathbf{x}}(t_j^-) \in \mathcal{X}$, and the corrected state estimate is the a posteriori state estimate $\hat{\mathbf{x}}_j^+ := \hat{\mathbf{x}}(t_j^+) \in \mathcal{X}$. In Figure 4.1 the idea of both definitions and the meaning of the times t_j^- and t_j^+ are visualized, $t_j^- \lesssim t_j \lesssim t_j^+$.

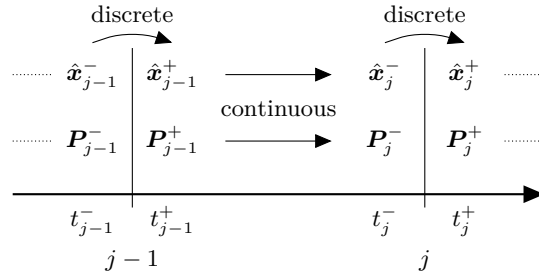


Figure 4.1: Definition of a priori ($\hat{\mathbf{x}}_j^-$, \mathbf{P}_j^-) and a posteriori state estimates and estimation error covariance matrices ($\hat{\mathbf{x}}_j^+$, \mathbf{P}_j^+), respectively (cf. Simon (2006)).

The propagation of the estimation error covariance matrix

$$\mathbf{P}_j := E \left\langle (\mathbf{x}_j - \hat{\mathbf{x}}_j) \cdot (\mathbf{x}_j - \hat{\mathbf{x}}_j)^T \right\rangle \in \mathbb{R}^{n_x \times n_x} \quad (4.18)$$

is visualized in Figure 4.1 as well. The a priori $\mathbf{P}_j^- := \mathbf{P}(t_j^-) \in \mathbb{R}^{n_x \times n_x}$ and a posteriori estimation error covariance matrices $\mathbf{P}_j^+ := \mathbf{P}(t_j^+) \in \mathbb{R}^{n_x \times n_x}$ describe the certainty in the corresponding state estimate at each time t_j^- and t_j^+ , respectively. In the hybrid extended Kalman filter the prediction step is done in continuous-time and the correction step is calculated in discrete time. This filter is dedicated to nonlinear systems that are continuous in nature, but where the measurements \mathbf{y} are measured discretely with a sampling time δ_y .

The algorithm of the hybrid extended Kalman filter can be described as follows (Simon, 2006).

1. The system equations with continuous-time dynamics and discrete-time measurements are given as follows (with the Kronecker delta $\delta_{j_1 j_2}$), (Grewal and Andrews, 2008):

$$\begin{aligned} \text{eq. (2.1)} \quad & {}^\circ \mathbf{x}'(t) = \mathbf{f}({}^\circ \mathbf{x}(t), \mathbf{u}(t), \boldsymbol{\omega}(t)) \\ \text{eq. (4.1)} \quad & \mathbf{y}(t_j) = \mathbf{h}(\mathbf{x}(t_j), \mathbf{v}_j) \\ & \boldsymbol{\omega}(t) \sim \mathcal{N}(\mathbf{0}, \boldsymbol{\Psi}_\omega) \\ & \mathbf{v}_j \sim \mathcal{N}\left(\mathbf{0}, \frac{\boldsymbol{\Psi}_v}{\delta_y}\right) \quad E \langle \mathbf{v}_{j_1} \cdot \mathbf{v}_{j_2}^T \rangle = \delta_{j_1 j_2} \cdot \frac{\boldsymbol{\Psi}_v}{\delta_y} \end{aligned}$$

2. Initialize the filter as follows:

$$\hat{\mathbf{x}}_0^+ = E \langle \mathbf{x}_0 \rangle \quad \mathbf{P}_0^+ = E \left\langle (\mathbf{x}_0 - \hat{\mathbf{x}}_0^+) (\mathbf{x}_0 - \hat{\mathbf{x}}_0^+)^T \right\rangle$$

3. For $j = 1, 2, \dots$ perform the following:

- (a) Integrate the state estimate and its covariance from time t_{j-1}^+ to time t_j^- as

follows:

$$\begin{aligned} {}^o\boldsymbol{x}'(\tau) &= \mathbf{f}({}^o\boldsymbol{x}(\tau), \mathbf{u}(\tau), \mathbf{0}) \\ \mathbf{P}'(\tau) &= \mathbf{A}_j \cdot \mathbf{P}(\tau) + \mathbf{P}(\tau) \cdot \mathbf{A}_j^T + \mathbf{E}_j \cdot \boldsymbol{\Psi}_{\omega} \cdot \mathbf{E}_j^T \\ \tau \in [t_{j-1}^+, t_j^-] &\quad {}^o\boldsymbol{x}(t_{j-1}^+) = \hat{\boldsymbol{x}}_{j-1}^+ \end{aligned}$$

with the linearizations:

$$\begin{aligned} \mathbf{A}_j &:= \frac{\partial \mathbf{f}}{\partial {}^o\boldsymbol{x}}(\hat{\boldsymbol{x}}_{j-1}^+, \mathbf{u}(t_j), \mathbf{0}) & \mathbf{C}_j &:= \frac{\partial \mathbf{h}}{\partial {}^o\boldsymbol{x}}(\hat{\boldsymbol{x}}_{j-1}^+, \mathbf{0}) \\ \mathbf{E}_j &:= \frac{\partial \mathbf{f}}{\partial \boldsymbol{\omega}}(\hat{\boldsymbol{x}}_{j-1}^+, \mathbf{u}(t_j), \mathbf{0}) & \mathbf{F}_j &:= \frac{\partial \mathbf{h}}{\partial \mathbf{v}}(\hat{\boldsymbol{x}}_{j-1}^+, \mathbf{0}) \end{aligned} \quad (4.19)$$

At the end of this integration we set $\hat{\boldsymbol{x}}_j^- = {}^o\boldsymbol{x}(t_j^-)$.

- (b) At time instant j , incorporate the measurement \mathbf{y}_j into the state estimate and estimation covariance as follows ($\mathbf{K}_j^* \in \mathbb{R}^{n_x \times n_y}$ is called optimal Kalman matrix):

$$\begin{aligned} \mathbf{K}_j^* &= \mathbf{P}_j^- \cdot \mathbf{C}_j^T \cdot (\mathbf{C}_j \cdot \mathbf{P}_j^- \cdot \mathbf{C}_j^T + \mathbf{F}_j \cdot \boldsymbol{\Psi}_{\mathbf{v}} \cdot \mathbf{F}_j^T)^{-1} \\ \hat{\boldsymbol{x}}_j^+ &= \hat{\boldsymbol{x}}_j^- + \mathbf{K}_j^* \cdot (\mathbf{y}_j - \mathbf{h}(\hat{\boldsymbol{x}}_j^-, \mathbf{0})) \\ \mathbf{P}_j^+ &= (\mathbf{1}_{n_x} - \mathbf{K}_j^* \cdot \mathbf{C}_j) \cdot \mathbf{P}_j^- \end{aligned} \quad (4.20)$$

The last equation in eq. (4.20) can be replaced by the equivalent expression

$$\mathbf{P}_j^+ = (\mathbf{1}_{n_x} - \mathbf{K}_j^* \cdot \mathbf{C}_j) \mathbf{P}_j^- (\mathbf{1}_{n_x} - \mathbf{K}_j^* \cdot \mathbf{C}_j)^T + \mathbf{K}_j^* \cdot \boldsymbol{\Psi}_{\mathbf{v}} \cdot (\mathbf{K}_j^*)^T$$

which can be shown to be more robust (Simon, 2006).

4.3 Moving Horizon Estimation

Moving horizon state estimation (MHE) estimates the current state \boldsymbol{x}_k out of input and output measurements coming from the system, starting in the past and reaching into present. Therefore, simulations with the plant model (eqs. (2.1) and (4.1)) are started in the past from different initial states $\boldsymbol{x}_o \in \mathcal{X}$ using the given input data \mathbf{u} . The obtained simulation results are compared with the output measurements \mathbf{y} , and the initial state leading to the best agreement of both trajectories (named $\boldsymbol{x}_o^* \in \mathcal{X}$) is used to generate the trajectory of states eventually leading to the current state estimate $\hat{\boldsymbol{x}}(t_k)$. Using the moving window concept, this approach is repeated at every sampling instance k of the control. To put this idea into formalism, the length of the moving horizon $\delta_{\text{MHE}} \in \mathbb{R}^+$ is defined as

$$\delta_{\text{MHE}} := w_{\text{MHE}} \cdot \delta_y \quad (4.21)$$

with the unit-less length of the horizon $w_{\text{MHE}} \in \mathbb{N}$ and the sampling time of the measurement values δ_y , see eq. (4.2). For later use another unit-less length of the

horizon $\tilde{w}_{\text{MHE}} \in \mathbb{N}$ is defined as:

$$\tilde{w}_{\text{MHE}} := \frac{1}{N_{\delta_y}} \cdot w_{\text{MHE}} \stackrel{(4.2)}{=} \frac{\delta_y}{\delta} \cdot w_{\text{MHE}} \stackrel{(4.21)}{=} \frac{\delta_{\text{MHE}}}{\delta}. \quad (4.22)$$

From eq. (4.22) it can be seen that the following relation holds:

$$\frac{\tilde{w}_{\text{MHE}}}{w_{\text{MHE}}} = \frac{\delta_y}{\delta},$$

thus \tilde{w}_{MHE} measures the window-length in the units of δ and w_{MHE} the same in the units of δ_y . Keeping in mind the definitions of t_k and t_j in eqs. (2.6) and (4.14), respectively, and using the system equations (2.1) and (4.1) the moving horizon state estimation problem can be formulated as follows (cf. Busch et al. (2009)):

For each $k = \tilde{w}_{\text{MHE}}, \tilde{w}_{\text{MHE}} + 1, \tilde{w}_{\text{MHE}} + 2, \dots$ solve:

$$\begin{aligned} \mathbf{x}_o^* := \arg \min_{\mathbf{x}_o} & \left[\|\mathbf{x}_o - \tilde{\mathbf{x}}(t_k - \delta_{\text{MHE}})\|_2 + \right. \\ & \left. + \kappa_{\text{MHE}} \cdot \sum_{j=N_{\delta_y} \cdot (k-\tilde{w}_{\text{MHE}})}^{N_{\delta_y} \cdot k} \|\mathbf{y}(t_j) - \mathbf{h}({}^o\mathbf{x}(t_j), \mathbf{v}(t_j))\|_2 \right] \end{aligned} \quad (4.23)$$

$$\begin{aligned} \text{subject to } & {}^o\mathbf{x}'(\tau) = \mathbf{f}({}^o\mathbf{x}(\tau), \mathbf{u}(\tau), \mathbf{0}), & {}^o\mathbf{x}(t_k - \delta_{\text{MHE}}) = \mathbf{x}_o, \\ & {}^o\mathbf{x}(\tau) \in \mathcal{X}, \mathbf{u}(\tau) \in \mathcal{U}, & \forall \tau \in [t_k - \delta_{\text{MHE}}, t_k], \\ & \mathbf{x}_{\text{LB}} \leq \mathbf{x}_o \leq \mathbf{x}_{\text{UB}}. \end{aligned}$$

The state estimate at time t_k , $\hat{\mathbf{x}}(t_k)$, then is given by the final value of the simulation starting at the optimal initial state \mathbf{x}_o^* :

$$\begin{aligned} \hat{\mathbf{x}}(t_k) &= {}^o\mathbf{x}(t_k) & \tilde{\mathbf{x}}_o := {}^o\mathbf{x}(t_{k+1} - \delta_{\text{MHE}}) \in \mathcal{X} \\ {}^o\mathbf{x}'(\tau) = \mathbf{f}({}^o\mathbf{x}(\tau), \mathbf{u}(\tau), \mathbf{0}) & & {}^o\mathbf{x}(t_k - \delta_{\text{MHE}}) = \mathbf{x}_o^* \quad \forall \tau \in [t_k - \delta_{\text{MHE}}, t_k] \end{aligned}$$

In eq. (4.23) $\tilde{\mathbf{x}} : \mathbb{R}^+ \rightarrow \mathcal{X}$ denotes the initial state estimate at the start of the moving window, $\kappa_{\text{MHE}} \in \mathbb{R}^+$ denotes a weighting factor and $\mathbf{x}_{\text{LB}}, \mathbf{x}_{\text{UB}} \in \mathcal{X}$. At the first start of the estimator an initial estimate of $\tilde{\mathbf{x}}(0)$ must be given, all later iterations can generate the initial estimate from the previous optimal simulation. This so called arrival cost can be computed by Kalman filter updates (Busch et al., 2009). Although Diehl et al. (2006b) strictly advises against the very simplified approach of setting $\tilde{\mathbf{x}}(t_k - \delta_{\text{MHE}}) = \tilde{\mathbf{x}}_o$ for each $k = \tilde{w}_{\text{MHE}} + 1, \tilde{w}_{\text{MHE}} + 2, \dots$, this approach is used in the small application given in Section 4.4 to keep things as simple as possible. But, for real systems more sophisticated approaches such as the one in Diehl et al. (2006b) should be used instead. It should be mentioned that the moving horizon state estimation problem can be extended easily with parameter estimation, see Busch et al. (2009).

As the optimization problem stated in eq. (4.23) must be solved for every sampling time t_k , real-time approaches are an important issue. For large-scale and fast systems more sophisticated approaches to solve the optimization problem, especially differential equation (2.1), must be used. Such methods are direct multiple shooting and its real-time implementation (Diehl et al., 2006b,c) as well as approximate solutions (Alessandri et al., 2008, 2010, 2011). Using one of these approaches, very large systems can be solved in real-time, e.g. Busch et al. (2009), Diehl et al. (2006c).

4.4 Application to an Anaerobic Digestion Process

In this section the three proposed state estimation methods are applied to a simple anaerobic digestion model and their performances are compared in a simulation study. The used model was developed by Marsili-Libelli and Beni (1996) and adapted by Shen et al. (2006). Here the implementation and parametrization of the latter is used. An introduction into the anaerobic digestion process is given in Chapter 5. In the following paragraph the applied simulation model is introduced briefly.

The model is a two-population model representing two species of bacteria: acidogenic bacteria (acidogens X_a) and methanogenic bacteria (methanogens X_m). The acidogenic bacteria convert the organic substrate S into acetic acid V_a and carbon dioxide C and the methanogenic bacteria convert the acetic acid V_a into methane Q_{ch_4} and carbon dioxide C as well. The produced gas is transferred between the liquid and gas phase resulting in biogas production Q_{ch_4} and Q_{co_2} . Furthermore, the association and dissociation of acetic acid and sodium bicarbonate as well as the effects of CO_2 and bicarbonate on the liquid phase pH are modelled (Shen et al., 2006). This results in a model containing six ordinary differential equations and two independent inputs S and B_{ic} . Its important variables are given in Table 4.1. All equations and parameters of the model can be found in the appendix of this thesis, Part A. To be able to formulate the

Table 4.1: The most important model variables as in Shen et al. (2006)

Variable	Unit	Description
S	[mg/l]	Organic substrate concentration
X_a	[mg/l]	Acidogenic bacteria concentration
V_a	[mg/l]	Acetic acid concentration
X_m	[mg/l]	Methanogenic bacteria concentration
C	[mg/l]	Carbon dioxide concentration (liquid phase)
P_c	[mg/l]	Carbon dioxide partial pressure (gas phase)
Q_{ch_4}	[l/h]	Methane gas production
Q_{co_2}	[l/h]	Carbon dioxide gas production
S_i	[mg/l]	Influent organic substrate concentration
B_{ic}	[mg/l]	Cation ions concentration introduced by sodium bicarbonate

given model in the standard notation given by equations (2.1) and (4.1), it is defined:

$$\begin{aligned} {}^o\boldsymbol{x} &:= (S, X_a, V_a, X_m, C, P_c)^T & n_x &= 6 \\ \boldsymbol{u} &:= (S_i, B_{ic})^T & n_u &= 2 \\ \boldsymbol{y} &:= (Q_{\text{ch}_4}, Q_{\text{co}_2})^T & n_y &= 2. \end{aligned} \quad (4.24)$$

Note, that methane and carbon dioxide production Q_{ch_4} and Q_{co_2} can be easily measured, so that the such defined measurement vector \boldsymbol{y} can be determined in practice without extraordinary effort. In the following, results for experiments performed for the three state estimation methods are presented.

4.4.1 The Experiments

To compare the three different state estimation methods the following setup is chosen. 30 different simulations from ten different randomly selected initial states with three different input trajectories are performed. The three different input trajectories $\boldsymbol{u}_\alpha := (S_{i,\alpha}, B_{ic,\alpha})^T$, $\alpha = 1, 2, 3$, are visualized in Figure 4.2. The first ten simulations are performed with input \boldsymbol{u}_1 , the next 10 simulations with \boldsymbol{u}_2 and then the last ten simulations with the input trajectory \boldsymbol{u}_3 . The simulation duration for each one is set to 100 days.

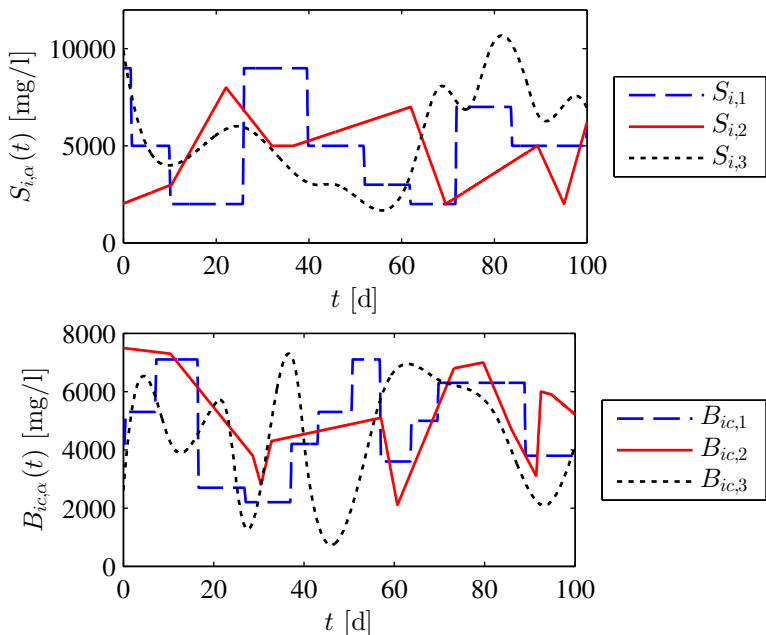


Figure 4.2: Input trajectories $\boldsymbol{u}_\alpha := (S_{i,\alpha}, B_{ic,\alpha})^T$, $\alpha = 1, 2, 3$

The noise processes ω and v are solely modelled as additive input and measurement noise, respectively. Therefore, from eqs. (2.1) and (4.1) it follows:

$$\begin{aligned} {}^o\boldsymbol{x}'(t) &= \boldsymbol{f}({}^o\boldsymbol{x}(t), \boldsymbol{u}(t) + \boldsymbol{\omega}(t), \mathbf{0}) \\ \boldsymbol{y}(t) &= \boldsymbol{h}(\boldsymbol{x}(t), \mathbf{0}) + \boldsymbol{v}(t) \end{aligned} \quad (4.25)$$

The standard deviation of the input noise ω is set to create a signal-to-noise ratio of the input u_α of 26 dB. The measurement noise v is set to the same signal-to-noise ratio for the output values y . The sampling rate of the inputs δ_u as well as for the measurements δ_y is set to one hour. An exception is the Kalman filter, where the sampling rate of the inputs δ_u is set to one minute to achieve more accurate predictions. The prediction results are compared with the simulated values between times t_{k_1} and t_{k_2} with $k_2 > k_1$ and thus following definition (2.6): $t_{k_2} > t_{k_1}$. As the predicted results come with a sampling time δ_y of one hour but the sampling rate of the system δ is one day, the k 's have to be replaced with j 's as defined in eq. (4.14). Let us set $t_{j_1} = t_{k_1}$ and $t_{j_2} = t_{k_2}$ with $j_1 \stackrel{(4.15)}{=} N_{\delta_y} \cdot k_1$ and $j_2 \stackrel{(4.15)}{=} N_{\delta_y} \cdot k_2$. Further, the following notations for each state vector component $i_x = 1, \dots, n_x$ shall be defined:

$$\begin{aligned} \boldsymbol{x}_{i_x,[j_1,j_2]} &:= [x_{i_x}(t_{j_1}), x_{i_x}(t_{j_1} + \delta_y), \dots, x_{i_x}(t_{j_2})]^T \\ &\stackrel{(4.14)}{=} [x_{i_x}(t_{j_1}), x_{i_x}(t_{j_1+1}), \dots, x_{i_x}(t_{j_2})]^T \\ &\stackrel{(4.16)}{=} [x_{i_x,j_1}, x_{i_x,j_1+1}, \dots, x_{i_x,j_2}]^T \end{aligned} \quad (4.26)$$

and

$$\begin{aligned} \boldsymbol{x}_{i_x,[k_1,k_2]} &:= [x_{i_x}(t_{k_1}), x_{i_x}(t_{k_1} + \delta), \dots, x_{i_x}(t_{k_2})]^T \\ &\stackrel{(2.6)}{=} [x_{i_x}(t_{k_1}), x_{i_x}(t_{k_1+1}), \dots, x_{i_x}(t_{k_2})]^T \\ &\stackrel{(4.17)}{=} [x_{i_x,k_1}, x_{i_x,k_1+1}, \dots, x_{i_x,k_2}]^T. \end{aligned} \quad (4.27)$$

To do a fair comparison between all three methods, the estimated and simulated state vector components are compared starting at day $k_1 = 31$ until day $k_2 = 100$. The reason is, that the soft sensor-based method returns its earliest state estimate at day 31 (see Section 4.4.2) whereas the other two methods start at time 0. As $N_{\delta_y} \stackrel{(4.2)}{=} \frac{\delta}{\delta_y} = 24$ it is $j_1 \stackrel{(4.15)}{=} 24 \cdot 31$ and $j_2 \stackrel{(4.15)}{=} 24 \cdot 100$. As performance measure for the i_x th estimated state vector component \hat{x}_{i_x} the root-mean-square error (RMSE) $e_{\hat{x},i_x} \in \mathbb{R}^+$ is used:

$$e_{\hat{x},i_x} := \sqrt{\frac{1}{j_2 - j_1 + 1} (\hat{\boldsymbol{x}}_{i_x,[j_1,j_2]} - \boldsymbol{x}_{i_x,[j_1,j_2]})^T \cdot (\hat{\boldsymbol{x}}_{i_x,[j_1,j_2]} - \boldsymbol{x}_{i_x,[j_1,j_2]})} \quad (4.28)$$

and the total performance measure $e_{\hat{x}} \in \mathbb{R}^+$ is the euclidian mean value of all n_x RMSE

values $e_{\hat{x}, i_x}$:

$$e_{\hat{x}} := \frac{1}{n_x} \cdot \sum_{i_x=1}^{n_x} e_{\hat{x}, i_x} \quad (4.29)$$

4.4.2 State Estimation using Software Sensors

The state estimator is configured as follows. As classification method Random Forests is used with 50 trees and $C = 50$ classes. The training and validation data are generated out of totally 60.000 simulated days. $N_u = 5$ input data filters are used, their window sizes are set to $\mathcal{W}_u = \{12, 24, 3 \cdot 24, 7 \cdot 24, 14 \cdot 24\}$. Remember, that these window sizes $w_{u,i_{\Lambda_u}}$ are measured in the sampling time of the inputs δ_u , see eq. (4.6). As output filters the following $N_y = 7$ are used: $\mathcal{W}_y = \{12, 24, 3 \cdot 24, 7 \cdot 24, 14 \cdot 24, 21 \cdot 24, 31 \cdot 24\}$, eq. (4.8). In Figure 4.3 an example result for the simulation starting at the eighth initial state with the input trajectory u_3 is shown. It can be seen, that the simulated

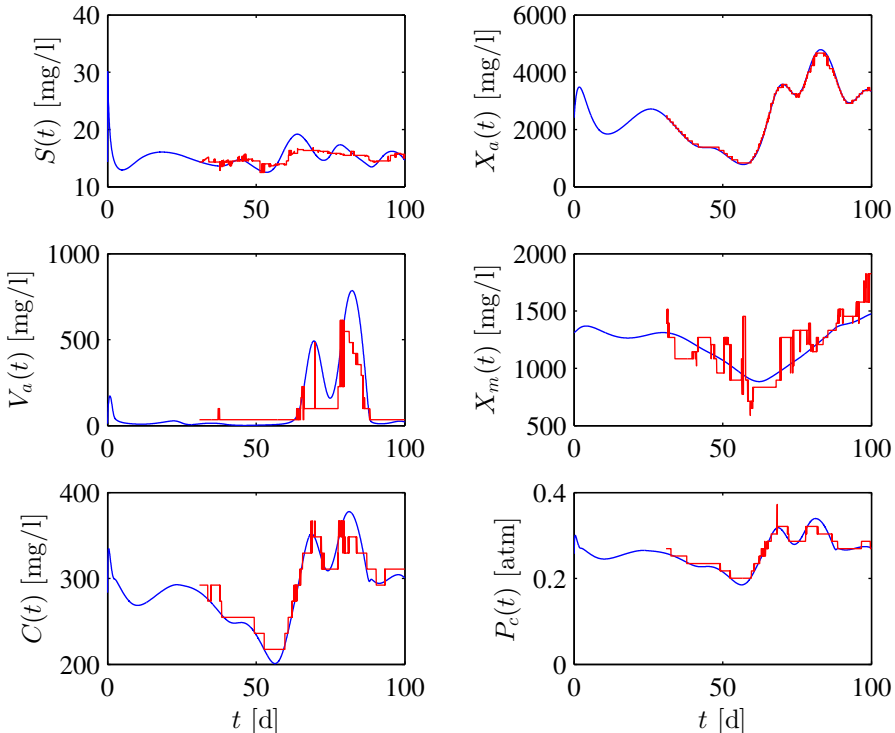


Figure 4.3: Results for state estimation using software sensors for the experiment starting at the eighth initial state with the input trajectory u_3 . The simulation results are coloured in blue and the estimation results in red.

states for some components are estimated quite accurately (e.g. X_a), but others show

a considerable estimation error (e.g. X_m). Nevertheless, in principle, the states are predicted with an almost constant accuracy for all 30 performed experiments as can be seen in the left box plot in Figure 4.6. There, the error measure defined in eq. (4.29) is shown.

4.4.3 Hybrid Extended Kalman Filter

The hybrid extended Kalman filter is initialized as described in Section 4.4.3. Furthermore, the covariance matrix of the process noise Ψ_ω is set to

$$\Psi_\omega = \begin{pmatrix} {\sigma_{\omega_1}}^2 & 0 \\ 0 & {\sigma_{\omega_2}}^2 \end{pmatrix}$$

and the covariance matrix of the measurement noise Ψ_v to

$$\Psi_v = \begin{pmatrix} {\sigma_{v_1}}^2 & 0 \\ 0 & {\sigma_{v_2}}^2 \end{pmatrix}.$$

There, $\sigma_{\omega_{i_u}} \in \mathbb{R}^+$ is the standard deviation of the process noise ω_{i_u} added to input $i_u = 1, 2$ and $\sigma_{v_{i_y}} \in \mathbb{R}^+$ is the standard deviation of the measurement noise v_{i_y} added to output $i_y = 1, 2$. The initial state of the model \mathbf{x}_0 is estimated with three different accuracies: 1 %, 5 % and 10 %, modelled as normal distributed noise. So, in total 90 simulations are performed, 30 for each initial state estimation accuracy. In Figure 4.4 the results of one experiment are shown. As can be seen, the simulated values are estimated with a very high accuracy. Nevertheless, the disadvantage of the Kalman filter is its dependency of an accurate estimate of the initial state (Reif et al., 1999, 2000). This can be seen in Figure 4.6, where the results in dependency of the accuracy of the initial state estimate are shown.

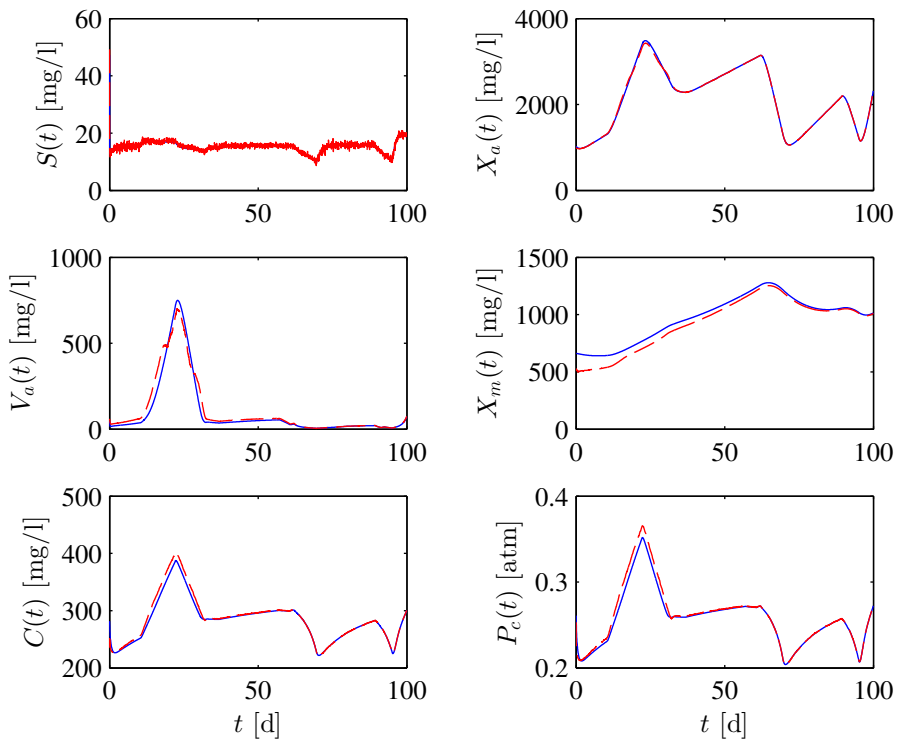


Figure 4.4: Results for state estimation using hybrid EKF. Experiment starting at fourth state, with u_2 as input and 10 % as uncertainty in initial state estimate $\hat{\mathbf{x}}_0^+$. The simulation results are coloured in blue (solid) and the estimation results in red (dashed).

4.4.4 Moving Horizon Estimation

The initial state estimate at the beginning of the 90 simulations $\tilde{\mathbf{x}}(0)$ is known with the same uncertainty as in the case of the Kalman filter, see Section 4.4.3. With the sampling rate δ equal to one day, the window between two iterations is automatically shifted for one day (see eq. (4.23)). The length of the moving horizon \tilde{w}_{MHE} is set to 31, thus equal to the largest window length of the output filters in the software sensor approach, see Section 4.4.2. The optimization problem defined in eq. (4.23) is solved using CMA-ES (Hansen, 2006) with a population size of 20 and four iterations. The lower \mathbf{x}_{LB} and upper bounds \mathbf{x}_{UB} for the optimization variable \mathbf{x}_o are set to $\tilde{\mathbf{x}}(t_k - \delta_{\text{MHE}}) \cdot (1 \pm 0.15)$. In Figure 4.5 the result for one of the estimation experiments is shown. The estimation results are very accurate, but not as accurate as the ones for

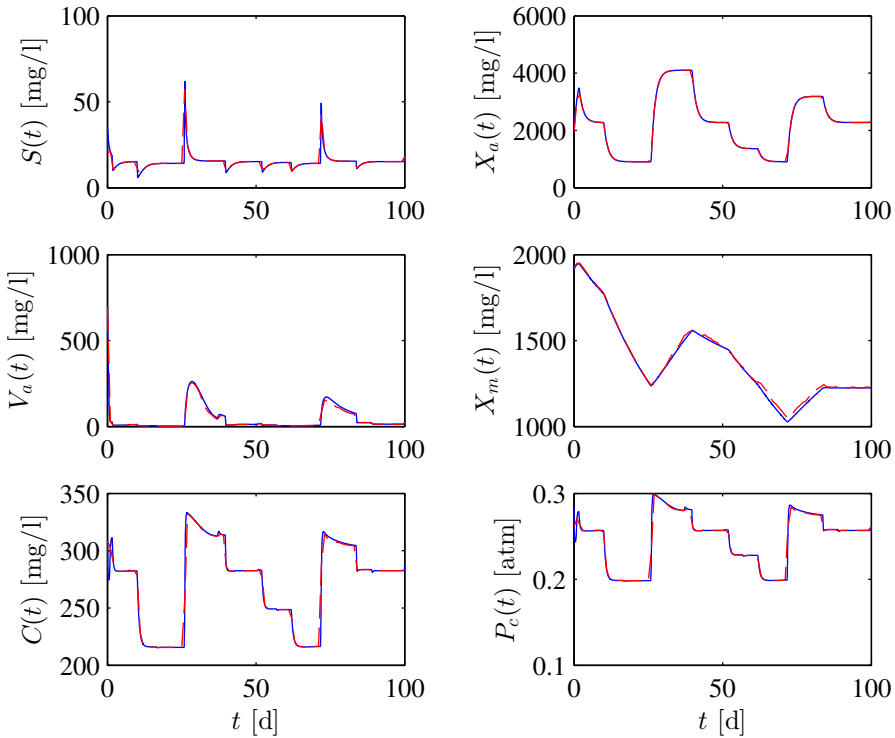


Figure 4.5: Results for state estimation using moving horizon estimation. Experiment starting at first state, with \mathbf{u}_1 as input and 1 % as uncertainty in initial state estimate $\tilde{\mathbf{x}}(0)$. The simulation results are coloured in blue (solid) and the estimation results in red (dashed).

the extended Kalman filter (at least for the configuration used here). Nevertheless, the clear advantage of this approach in comparison to the Kalman filter is its robustness against poor estimates of the initial state $\tilde{\mathbf{x}}(0)$ as can be seen in Figure 4.6, see also

(Haseltine and Rawlings, 2005). It could surely be more robust, for example when the arrival cost in the optimization problem (4.23) is weighted with the inverse covariance matrix of the state estimate as is e.g. done in Busch et al. (2013).

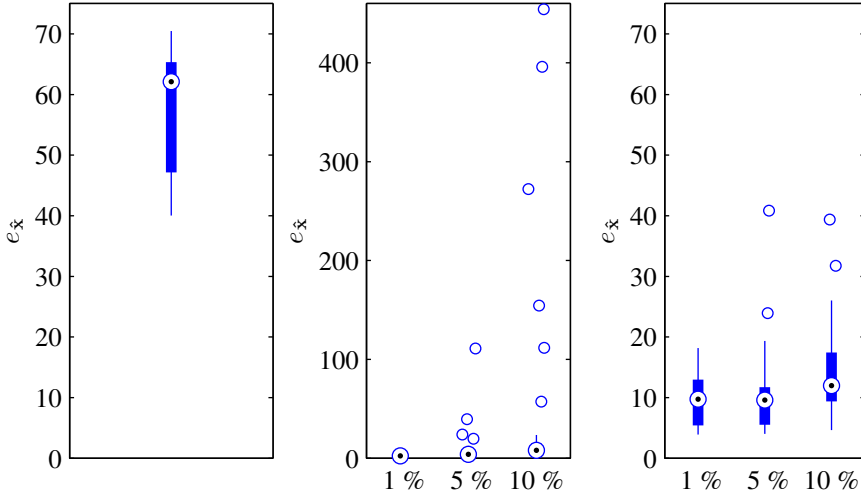


Figure 4.6: Box plots showing the error measure defined in eq. (4.29) evaluated for all 90 (30 for the first approach) simulations for the three methods. Left: Results for the soft sensor state estimation approach, Section 4.4.2. Middle: Dependency of EKF state estimation results on uncertainty in initial state estimate \hat{x}_0^+ with 1 %, 5 % and 10 % normally distributed noise. Right: Results for moving horizon estimation with dependency on uncertainty in initial state estimate as well.

4.5 Summary and Discussion

In this chapter a soft sensor based state estimation method is developed. At hand of a simple anaerobic digestion model it is compared with the hybrid extended Kalman filter and moving horizon estimation.

The main advantage of the soft sensor based state estimation approach compared with conventional state estimation filters (Rawlings and Bakshi, 2006) is that an initial guess of the initial state of the system is not necessary. Furthermore, the state estimator is a static function, such that stability issues and drift are not existent. However, the yield estimation accuracy cannot compete with the approaches extended Kalman filter and moving horizon estimation. Furthermore, the first state estimate in this configuration arrives not before the 31st day of the simulation (see Section 4.4.2). On a real plant this means that measurement data of the last 31 days must be available before this estimator can be used. Before that the plant must be operated by hand. Overall, the hybrid extended Kalman filter yields the best, but also the worst estimation results in dependence of the accuracy of the initial state estimate \hat{x}_0^+ , see Figure 4.6. This and

the problem that the linearized model (eq. (4.19)) is required to be locally observable (Dewil et al., 2011) makes it almost impossible to use for larger anaerobic digestion models such as the ADM1. The reason is, that on biogas plants in practice only a few process values can be measured, such that the plant is not observable.

In conclusion the moving horizon estimation approach is seen as the best tested state estimation candidate for anaerobic digestion processes. Among its advantages are its robustness and explicit incorporation of state constraints and parameter estimation schemes (Rao, 2000, Rao et al., 2003). One challenge of MHE is to implement it for real-time application. The MATLAB® implementation on a standard computer¹ needs for one sample time δ a mean runtime of 1.55 s. In comparison the mean runtime of the hybrid extended Kalman filter is 0.18 s and for the soft sensor approach it is even only 0.03 s. But, these results should only be seen as rough reference values because the implementations were not written for high performance.

As the to be solved optimization problem in MHE (eq. (4.23)) is quite complex and time-consuming in this thesis this approach was not implemented for the ADM1. But, the reader is highly encouraged to spend the effort and to apply moving horizon estimation to the ADM1. How robust the moving horizon estimation approach is against the non-observability of the ADM1 in practice would be interesting to see.

To summarize, in this thesis the self-developed soft sensor based approach is used for state estimation of the ADM1. Results for that can be found in Chapter 8 and its use in a closed-loop control in Chapter 9.

¹Intel® Core™ i7-2600 CPU @ 3.40 GHz, 8.00 GB RAM, Windows 8, 64 bit

Part II

Substrate Feed Control for Biogas Plants

Introduction

In this part of the thesis the fourth component of the developed dynamic real-time substrate feed optimization, introduced in the introduction of Part I, is discussed. This fourth component is the dynamic process model of the controlled biogas plant.

“There is a general agreement in the literature that the application of mathematical models is a prerequisite to improve digester performance” (Dewil et al., 2011). There are various models of the anaerobic digestion process, from very simple ones to very complex models with a lot of equations. So far, only simple models are used for feed control of biogas plants. On the one hand, stability of model-based controls cannot be shown if complex models are used and on the other hand doing simulations with the complex ones in real-time is not yet possible. Furthermore, state and parameter estimation schemes for simple models can be developed more easily. In RTO a complex model may be used, because it has not to be solved in real-time. Therefore, the developed model is a very complex one, such that optimization runs performed in the RTO scheme yield realistic optimal solutions.

To the authors knowledge RTO has not been applied to substrate feed control for biogas plants before. The works of my colleague Christian Wolf (Wolf et al., 2009, Wolf, 2013) and similarly Ziegenhirt et al. (2010) can be seen as predecessors of this works. They focus on feed optimization of biogas plants using methods from evolutionary computation as well. In contrast to this thesis they do not close the loop, but apply the optimal substrate feed in an open loop manner.

Before the model is described in detail in Chapter 7 the anaerobic digestion process is briefly introduced in Chapter 5. An extensive review of published control methods applied to anaerobic digestion processes is given in Chapter 6.

General Remark on Notation

To keep the text readable, in the following the mathematical notation in this part of the thesis is relaxed a little bit. The basic idea is, that all physical, chemical, ... values and parameters x are a product out of a number $\{x\}$ and a unit $[x]$ as given in the following equation (5.0).

$$x := \{x\} \cdot [x] \quad (5.0)$$

Except stated otherwise all numerical values of x are real and positive numbers. Thus, in mathematical notation, all numerical values of x are element of the set of all real and positive numbers, thus $\{x\} \in \mathbb{R}^+$. Often x is dependent on time $t \in \mathbb{R}^+$, then the numbers are generated out of a time-dependent function: $\{x\} : \mathbb{R}^+ \rightarrow \mathbb{R}^+$. Whether x is constant or time-dependent should be clear out of the physical context. Because all such values x are measured in a unit $[x]$ be attentive when plugging the value x into an equation, because it has to be plugged in together with its unit. It is the task of the reader to check whether the units do cancel out. If they do not, appropriate correction terms have to be introduced, e.g. $3600 \frac{\text{s}}{\text{h}}$.

Chapter 5

The Anaerobic Digestion Process

Anaerobic digestion (AD) is the process in which microorganisms break down organic matter in an anaerobic (that means oxygen-free) environment. It is the process which is used to produce biogas in the anaerobic digesters of a biogas plant. As organic matter all kind of biodegradable material can be used such as wastewater, manure, agricultural and food waste, organic fraction of municipal solid waste, microalgae, grass, energy crops and many others (Nallathambi Gunaseelan, 1997).

Biogas is a mixture of different gases containing, in decreasing concentration, methane, carbon dioxide, water vapor, nitrogen, oxygen, hydrogen, ammonia and hydrogen sulphide. As methane is an energy carrier the general idea is to maximize methane production. Its concentration in biogas is usually around 50 % – 75 % (cf. Besgen (2005)).

In this chapter the anaerobic digestion process is described very briefly (see Section 5.1 and 5.2) focusing on those aspects that are important out of the view of process control.

Sections 5.3 and 5.4 are written in the style of glossaries and are dedicated to those which want to familiarize themselves with the most important terms, definitions and reactor configurations used in the field of anaerobic digestion.

For a more complete treatment of the anaerobic digestion process please refer to e.g. Gerardi (2003), Gujer and Zehnder (1983) or Bischofsberger et al. (2005).

5.1 Process Description

The anaerobic degradation (or digestion) process can be separated into four consecutive following steps, which are described in the following four paragraphs.

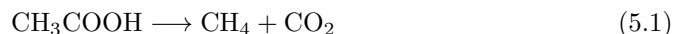
Hydrolysis The anaerobic degradable part of any substrate is seen to be a composite out of carbohydrates, proteins and fats. During the first step, the hydrolysis, the three biomolecules carbohydrate, protein and fat are decomposed into their constituent

parts. All of the three biomolecules are bonds of smaller molecules. Carbohydrates are bonds of monosaccharides, proteins are bonds of proteinogenic amino acids and fats are bonds (so-called esters) of the alcohol glycerol with fatty acids. During hydrolysis these bonds are separated using water, which is available in the digester, and enzymes. The products of the hydrolysis step therefore are monosaccharides, proteinogenic amino acids, glycerol and fatty acids.

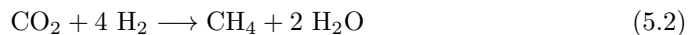
Acidogenesis During the acidogenesis the microorganisms process the products of the hydrolysis mainly to different acids such as propionic, acetic and butyric acid. During these fermentation processes carbon dioxide and hydrogen are produced as well. The acidogenesis of some proteinogenic amino acids also releases the toxic substances ammonia and hydrogen sulphide.

Acetogenesis The acids produced in the acidogenesis step are degraded further to become acetic acid, therefore this step is called acetogenesis. Those fermentation processes are performed by bacteria as well.

Methanogenesis In the last step, the methanogenesis, the methane is produced. There are two path ways of how bacteria produce methane. The first one is the acetoclastic methanogenesis (eq. (5.1)), where acetic acid (CH_3COOH) is converted to methane (CH_4) and carbon dioxide (CO_2)



and the second one is hydrogenotrophic methanogenesis (eq. (5.2)), where carbon dioxide and hydrogen (H_2) is converted to methane as well (Gerardi, 2003).



5.2 Important Process Values

As the anaerobic process is performed by living organisms it must be assured that the environmental conditions in the digester are such that the organisms can survive and reproduce. The participating bacteria have different preferences with respect to pH value, temperature and other environmental factors (Appels et al., 2008). Therefore a compromise has to be found. Most often the environmental conditions are set to the preferences of the methanogenic bacteria, which produce the methane (eqs. (5.1) and (5.2)), Besgen (2005). The reason is, that those are inhibited by the starting material of their performed reactions, thus acetic acid and hydrogen. This has as consequence, that once the methanogens are inhibited the educts in eqs. (5.1) and (5.2) increase, inhibiting the methanogens even more. In the long run, due to the increasing acid

concentration, the pH value drops, that inhibits the methanogens as well (Weiland, 2010), killing them in the end. So, to guarantee a stable process of methanogenesis, it must be assured by all means that this chain reaction never commences.

There are a few more process variables next to pH value, acetic acid and dissolved hydrogen concentrations that affect the well-being of the bacteria. An automatism that stabilizes the pH value around an equilibrium is called a buffer. The buffer in anaerobic digesters mainly depends on the equilibria of ammonia/ammonium, carbon dioxide/bicarbonate and the equilibria of the volatile fatty acids and their salts. A large buffer can compensate an increase of acids, before the pH value and thereby the methanogens are affected. But, as the pH value does not change as long as there is still buffer capacity, based on the pH value no process imbalances can be recognized. Therefore, it is important to monitor the buffer capacity. The most important component of the buffer is the total alkalinity (TA), defined in eq. (7.61), which is a sum of bicarbonate and the salts of the volatile fatty acids. The ratio of volatile fatty acids over total alkalinity (VFA/TA) then is an often used indicator to measure the size of the buffer with respect to the acid concentration in the digester, see Section 7.3.3.8. Ammonia and hydrogen sulphide are important as well, because they are toxic for the microorganisms (Appels et al., 2008, Chen et al., 2008).

5.3 Important Definitions and Terms

This section should be seen as a glossary and only needs to be read if some terms in the field of anaerobic digestion used in this thesis are not familiar to the reader.

5.3.1 Amount of Substance & Molar Mass

The amount of substance is a standards-defined quantity with the unit mol, called mole, that measures the size of a collection of any substance. An amount of 1 mol particles is a number of around $6.02214199(47) \cdot 10^{23}$ of that particles (Avogadro constant) (Tipler and Mosca, 2007). Mole is defined that way, such that 1 mol of the carbon atom ^{12}C weighs 1 g.

Using amount of substance the term molar mass M with the unit $[M] = \frac{\text{g}}{\text{mol}}$ can be introduced. Molar mass defines how much gram (g) an ensemble of 1 mol particles weighs. Given the relative atomic mass (which is defined relative to the mass of the carbon atom ^{12}C) of an element, e.g. oxygen, taken from a periodic table, being $16.00 \frac{\text{mol}_\text{C}}{\text{mol}_\text{O}}$, the molar mass M of oxygen is

$$M_\text{O} = 16.00 \frac{\text{mol}_\text{C}}{\text{mol}_\text{O}} \cdot 1 \frac{\text{g}}{\text{mol}_\text{C}} = 16 \frac{\text{g}}{\text{mol}_\text{O}}.$$

Molar mass M is used in Section 5.3.3 to calculate the chemical oxygen demand of a molecule.

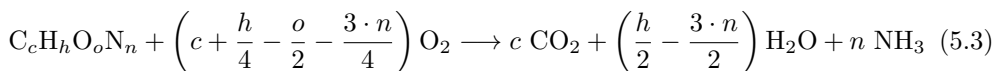
5.3.2 Biomass

As the term biomass has two meanings that are both related to the topic of this thesis, it is specified here which of the two meanings is referred to when we speak about biomass.

On the one hand biomass is a renewable energy source such as organic garbage, wood or plants (McKendry, 2002). On the other hand biomass is used in ecology to specify the mass of living biological organisms. In this thesis, if not stated otherwise, the term biomass is used in the second sense. Therefore, biomass is the mass of bacteria and enzymes living in a digester and being part of the conversion process of substrate to biogas.

5.3.3 Chemical Oxygen Demand

The chemical oxygen demand (COD) of a material defines the amount of oxygen needed to completely oxidize the material. The amount of oxygen O_2 , measured in g, needed to oxidize 1 mol of a biomolecule is defined as $g_{COD} := g O_2$. To calculate the amount of oxygen to oxidize a biomolecule $C_cH_hO_oN_n$ the general combustion equation for biomolecules (eq. (5.3)) can be used (Koch et al., 2010).



Therefore, with the molar mass of oxygen $M_{O_2} = 32.00 \frac{g O_2}{mol_{O_2}}$ (see Section 5.3.1), the COD of one mole of the biomolecule $C_cH_hO_oN_n$ is

$$\begin{aligned} & \left(c + \frac{h - 3 \cdot n}{4} - \frac{o}{2} \right) \frac{mol_{O_2}}{mol_{C_cH_hO_oN_n}} \cdot 32.00 \frac{g O_2}{mol_{O_2}} = \\ & (32 \cdot c + 8 \cdot (h - 3 \cdot n) - 16 \cdot o) \frac{g_{COD}}{mol_{C_cH_hO_oN_n}}. \end{aligned} \quad (5.4)$$

As an example, the COD of 1 mol methane (CH_4) is $(32 + 8 \cdot 4) g_{COD} = 64 g_{COD}$.

In simulation models of the anaerobic digestion process the chemical oxygen demand is a property of conservation and therefore very important, see Section 7.1.

5.3.4 Dilution Rate & Volumetric Flow Rate

Given the volume ΔV of a material passing through a given surface in the time Δt , the volumetric flow rate Q of the material is defined as:

$$Q := \lim_{\Delta t \rightarrow 0} \frac{\Delta V}{\Delta t} = \frac{dV}{dt} \quad [Q] = \frac{m^3}{d}. \quad (5.5)$$

On biogas plants the material could e.g. be a substrate (or substrate mix) or the produced biogas. The volumetric flow rate of substrates is denoted by Q_{IN} and the volumetric flow rate of the produced biogas is symbolized by Q_{gas} , see equation (7.3).

The dilution rate D is defined as the ratio between the volumetric flow rate Q_{IN} of the substrate feed of a digester and the liquid volume of the digester V_{liq} , as given in eq. (5.6).

$$D := \frac{Q_{\text{IN}}}{V_{\text{liq}}} \quad [D] = \frac{1}{\text{d}} \quad (5.6)$$

The dilution rate D is the most often used manipulated variable for substrate feed control (see Chapter 6). On the one hand increasing the dilution rate, increases the amount of substrate fed to the digester and therefore increases biogas production, but on the other hand the biomass is washed out in the rate given by the dilution rate. Therefore, the dilution rate should be smaller than the specific growth rate of the slowest growing biomass, such that the organism can reproduce and survive. Exceptions are high-rate digesters (Section 5.4), where washout of biomass is not directly proportional to the value of the dilution rate.

5.3.5 Fresh Mass

The substrate, as it is fed, is referred to as fresh mass (FM), often but not always referring to the mass of the substrate. To avoid confusion, the initials FM are always (if needed) appended to an unit, when a parameter of the fresh mass substrate is measured. Examples are the mass, measured in kg_{FM} , or the volume, measured in m^3_{FM} , of the fresh mass.

5.3.6 Hydraulic & Sludge Retention Time

In this thesis, the hydraulic retention time HRT of a digester is defined as the ratio of the liquid volume of the digester V_{liq} and the volumetric flow rate of the sludge leaving the digester Q :

$$\text{HRT} := \frac{V_{\text{liq}}}{Q} \quad [\text{HRT}] = \text{d.} \quad (5.7)$$

With the approximation $Q \approx Q_{\text{IN}} \cdot \left(1 - \frac{m_{\text{gas}}}{m_{\text{influent}}}\right)$ the hydraulic retention time can be related to the volumetric flow rate of the substrate feed Q_{IN} . Here, the mass of the biogas leaving the digester is given as m_{gas} and the mass of the influent as m_{influent} . For details see Lübben (2009).

If $Q_{\text{IN}} \approx Q$, then the HRT is equal to the inverse of the dilution rate D , see Section 5.3.4, as it is often given in textbooks, see equation (5.8).

$$\text{HRT} \approx \frac{V_{\text{liq}}}{Q_{\text{IN}} \cdot \left(1 - \frac{m_{\text{gas}}}{m_{\text{influent}}}\right)} \stackrel{m_{\text{gas}} \ll m_{\text{influent}}}{\approx} \frac{V_{\text{liq}}}{Q_{\text{IN}}} \stackrel{(5.6)}{=} \frac{1}{D} \quad (5.8)$$

As said above in Section 5.3.4, for high-rate digesters the washout of the biomass is not related to the dilution rate D . For such digesters the retention time of the biomass

is not equal to the hydraulic retention time, but to the so-called sludge retention time SRT with $SRT \gg HRT$.

5.3.7 Organic Loading Rate

The organic loading rate OLR is defined as:

$$OLR := \frac{Q_{IN} \cdot \rho_{IN} \cdot VS_{IN}}{V_{liq}} \stackrel{(5.8)}{\approx} \frac{\rho_{IN} \cdot VS_{IN}}{HRT} \quad [OLR] = \frac{kg_{VS}}{m^3 \cdot d}. \quad (5.9)$$

In equation (5.9) the raw density ρ_{IN} of the substrate is given in $\frac{kg_{FM}}{m^3}$ and the volatile solids content of the substrate VS_{IN} is given in $\frac{kg_{VS}}{kg_{FM}}$, see Section 5.3.11.

The organic loading rate OLR is the relation between organic mass in the substrate feed, that is $(Q_{IN} \cdot \rho_{IN} \cdot VS_{IN})$, and the liquid volume of the digester V_{liq} . With a rising OLR also biogas production increases, but only until a critical point, where the organically available material inside the digester increases to such an amount that it inhibits the work of the bacteria in the digester. Therefore, the organic loading rate is an indicator for potential process stress, but not a very good one, because it only refers to the substrate feed and not to a process value inside the digester.

5.3.8 Temperature Specifications

Anaerobic digesters are operated in three different temperature regions, with the temperature in the digester T , given as follows (Bischofsberger et al., 2005):

- psychrophilic: $T < 20 \text{ } ^\circ\text{C}$
- mesophilic: $20 \text{ } ^\circ\text{C} \leq T \leq 40 \text{ } ^\circ\text{C}$
- thermophilic: $T > 40 \text{ } ^\circ\text{C}$

Each temperature region has its advantages and disadvantages and each bacteria species has their individual preferred ambient temperature (cf. Besgen (2005)). In general the higher the temperature the faster biochemical reactions occur, on the other hand equilibria are changed, such as the ammonia/ammonium equilibrium which is shifted towards the toxic ammonia, see Section 5.2 (Appels et al., 2008).

5.3.9 Theoretical Oxygen Demand

Bringing the chemical oxygen demand of a substance (COD, Section 5.3.3) in relation to its molar mass (M , Section 5.3.1) results in the theoretical oxygen demand (ThOD), Koch et al. (2010). The ThOD of the biomolecule $C_cH_hO_oN_n$ is thus defined as

$$ThOD := \frac{COD_{C_cH_hO_oN_n}}{M_{C_cH_hO_oN_n}} \stackrel{(5.4)}{=} \frac{32 \cdot c + 8 \cdot (h - 3 \cdot n) - 16 \cdot o}{12 \cdot c + h + 16 \cdot o + 14 \cdot n} \cdot \frac{g_{COD}}{g}, \quad (5.10)$$

where the molar masses of the C, H, O and N atoms were used. The theoretical oxygen demand is used in Section 7.2 to calculate the COD out of the cell content of a substrate.

5.3.10 Total Solids

The total solids (TS) content of a substrate (or a digester probe) is the part of the substrate (or digester probe) which is left over after thermal removal of water. Usually the water is removed by drying for 24 hours at 105 °C or by drying until a constant weight is achieved, VDI (2006). Given the definition of the fresh mass in Section 5.3.5, the water content of a substrate (or a digester probe) is given as the difference of FM and TS. The unit of the TS content is

$$[\text{TS}] = \frac{\text{g}_{\text{TS}}}{\text{kg}_{\text{FM}}} = 0.1 \%_{\text{FM}}.$$

The volatile organic substances which escape together with the water vapour are not measured by this method and have to be determined separately. As an alternative, the TS content can also be corrected by the estimated loss of organics, see Weißbach and Strubelt (2008a,b,c).

To distinguish between the total solids content of a substrate TS_{IN} and the total solids content inside a digester TS the two different symbols are used.

5.3.11 Volatile Solids

The organic dry-weight content, or volatile solids (VS), is the loss of weight of the total solids TS (Section 5.3.10) of a probe, while reducing it to ashes at a temperature of 550 °C, DIN (2001b). This loss of weight is predominantly due to organics, therefore it is called the organic dry-weight content, VDI (2006). The volatile solids is measured in

$$[\text{VS}] = \frac{\text{g}_{\text{VS}}}{\text{kg}_{\text{TS}}} = 0.1 \%_{\text{TS}} \quad \text{or} \quad [\text{VS}] = \frac{\text{g}_{\text{VS}}}{\text{kg}_{\text{FM}}} = 0.1 \%_{\text{FM}}.$$

The organic substances which already escaped during TS determination are not measured by this method and have to be determined separately, see above in Section 5.3.10.

To be able to distinguish between the volatile solids content of a substrate VS_{IN} and the volatile solids content inside a digester VS the two different symbols are used.

5.4 Typical Reactors

In this section a few typical types of anaerobic reactors are described very briefly. The number of different reactor types and their description is by no means complete. Here only those reactors are listed, which are referred to in the control review in Chapter 6. For a more elaborate review please refer to the literature, e.g. Henze and Harremoës (1983), Hickey et al. (1991), Iza et al. (1991) or Skiadas et al. (2003).

5.4.1 Continuous Stirred-Tank Reactor

A continuous stirred-tank reactor (CSTR) is an idealized standard chemical reactor. Its key characteristic is that the concentration values of all substances have the same value all over the reactor. Therefore, a CSTR is often modeled as a perfectly mixed reactor using ordinary differential equations (ODEs). In anaerobic digestion a CSTR has a liquid phase in the bottom and a gas phase in the top with a liquid/gas transfer (Figure 5.1a). The CSTR is the most common reactor employed for wet fermentation (Weiland, 2006).

5.4.2 High-Rate Reactors

High-rate reactors can only be used for the anaerobic treatment of liquids such as wastewater, which flows vertically through the digesters. They are termed high-rate because of their low hydraulic retention time (eq. (5.7)). To avoid washout of biomass the biomass in these reactors is either attached to support material or is fixed in conglomerates of microorganisms (so-called granules) which have a very good settling behavior and therefore are not washed out. Thus, by fixating the biomass the sludge retention time (Section 5.3.6) is decoupled from the hydraulic retention time.

Expanded Granular Sludge Bed / Fluidized Bed Reactor Expanded granular sludge bed (EGSB) and fluidized bed reactors (FBR) are tall and thin reactors, where a high degree of recycle leads to the expansion (fluidization) of the sludge bed, Chou et al. (2011). Therefore, the wastewater to sludge contact is improved by enlarging the active surface of the sludge (Seghezzo et al., 1998). In FBR the biomass is attached to inert support media, such as sand or gravel (Figure 5.1c) (Henze and Harremoës, 1983) and in EGSB the biomass is granular, see UASB below. Furthermore, both digesters are distinguished from each other based on the degree of bed expansion (Iza et al., 1991).

Fixed Bed Reactor Key characteristic of anaerobic fixed bed reactors (AFB) (also called anaerobic filters (Zaher, 2005)) is the fixed support media inside the digester where the microorganisms are attached to (see Figure 5.1b). In general, AFBs are operated without recycle (Henze and Harremoës, 1983).

Upflow Anaerobic Sludge Blanket Reactor In upflow anaerobic sludge blanket (UASB) reactors (Lettinga et al., 1980) aggregations of microorganisms are formed, which are termed granules. Granules have very good settling behavior, such that UASB reactors can be operated with low hydraulic retention times without being concerned with washout of biomass. Different models exist about anaerobic granulation, a review is given in Liu et al. (2003).

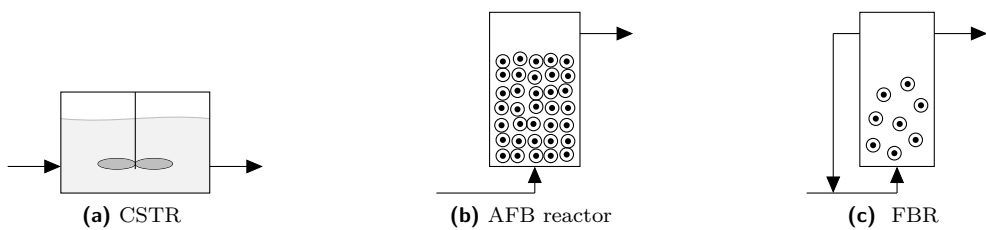


Figure 5.1: Schematics of CSTR, AFB reactor and FBR, cf. Henze and Harremoës (1983).

Upflow Anaerobic Sludge Blanket-Anaerobic Filter Reactor The upflow anaerobic sludge blanket-anaerobic filter (UASB-AF) reactor is a combination of an upflow anaerobic sludge blanket (UASB) reactor, located in the lower part, and an anaerobic filter (AF), located in the upper part. The UASB-AF combines the advantages of both single reactors and diminishes their disadvantages, Rajesh Banu and Kaliappan (2007). The filter in the upper part protects for sudden washout of biomass in extreme cases as it can happen in UASB reactors, Ramakrishnan and Surampalli (2012).

Chapter 6

State of the Art of Biogas Plant Feed Control

The anaerobic digestion process is used for a wide range of applications (Olsson et al., 2007). Depending on the application the main objectives for process control vary. Whereas the goal of agricultural biogas plants (ABP) is renewable energy production, anaerobic wastewater treatment aims for minimization of the pollution (measured as COD) in the effluent while maximizing the throughput. Therefore, control objectives and properties of potential feed control algorithms must be adapted to match the needs of the application. Although the primary goal of ABP is energy production a control also needs to assure safe and stable process conditions. At the same time profit has to be maximized and ecological criteria have to be met. But, most control methods proposed so far are only capable of satisfying one or two of these criteria at the same time. **The most often encountered ones are:**

- maximization or set-point tracking of methane production rate (economical criteria)
- minimization or set-point tracking of COD in the digester effluent (ecological criteria)
- control of stability criteria, such as VFA, VFA/TA, propionate or dissolved hydrogen

An important difference between ABP and anaerobic waste treatment plants is that in the latter application the operator often cannot choose between different feeds, because there often is only one mixed feedstream available, e.g. wastewater. Given a limited storage capacity for the input, the scope of feed control is restricted. This is in contrast to ABP, where a range of different feeds is used. These are all separately stored and solely used for energy production.

To investigate whether control methods exist, which optimally control either an ABP or a waste treatment process, respectively, a definition of optimal control for both

applications is necessary. This definition is given in Definitions 6.1 and 6.2.

Definition 6.1: A substrate feed control for an ABP is said to be optimal if it is a robustly stable setpoint control for the produced volumetric flow rate of methane, while maximizing the economical benefit, minimizing the ecological footprint and maximizing process stability.

Definition 6.2: A substrate feed control for an anaerobic waste treatment process is said to be optimal if it is a robustly stable setpoint control for effluent COD, while maximizing the throughput as well as economical benefit, minimizing the ecological footprint and maximizing process stability. Instead of a COD setpoint control, minimizing the effluent COD is possible as well.

Most of the published control methods are applied to anaerobic wastewater treatment systems, only very few are focused on controlling dry (total solids content $TS > 20\%_{FM}$) or semi-dry ($8\%_{FM} < TS < 15\%_{FM}$) digestion processes. Due to that most controls are only capable to control the feed of one substrate, mostly the wastewater. Therefore, the dilution rate of the feed is very often used as the manipulated variable. Depending on the application control variables such as methane flow rate or COD in the effluent as well as stability parameters such as VFA/TA, bicarbonate (Rozzi et al., 1985), propionate or dissolved hydrogen are used (see also Molina et al. (2009), Boe et al. (2010)). In low-buffered systems pH can also be an indicator for process stability (Björnsson et al., 2000).

The following extensive review of control methods proposed for biogas plant control is presented to give an overview of the state of the art of AD control. The review includes 146 publications focusing on the development of algorithms for substrate feed control for anaerobic digestion processes. Only those anaerobic digestion processes are included, that produce biogas, thus excluding dark fermentation and processes producing acids only. The control methods range from simple on/off and PID controllers over fuzzy and neural network control up to linearizing and other advanced approaches such as adaptive, robust and model-based control methods.

Excellent reviews on monitoring and control of anaerobic digesters can be found in Ols-son et al. (2007) and Pind et al. (2003). The experience of 15 years in instrumentation, control and automation in anaerobic digesters is summarized in Steyer et al. (2006). In Batstone and Steyer (2007) and Strömberg et al. (2012) comparisons of different control approaches are performed in simulation studies using the Anaerobic Digestion Model No. 1 (ADM1) (see Section 7.1, Batstone et al. (2002a)). They are two of the very few objective control comparisons of three, respectively four control methods. However, a broad comparison of the high number of existing control methods has not yet been performed. Thus, the need for further objective performance evaluation and

comparison of control strategies at full-scale AD plants is high.

6.1 Classical Control

To classical control methods belong the well known PID controllers and on/off control. Applications of these control methodologies are listed in the Tables 6.1, 6.2 and 6.3. For the convenience of the user all tables are shifted to the end of this chapter, see Section 6.7.

In the 70s the first control methods were proposed (Table 6.1), which are mainly on/off controls, that set the manipulated variable to a binary value depending on predefined threshold values. They were followed by PID controls including P, PI, and PID cascade controls, which are listed in Tables 6.2 and 6.3. PID cascade controls are a simple but effective approach for feed control such that they are nowadays still developed and published with good results. Their advantages are that two possibly conflictive setpoints can be simultaneously controlled while the setpoint of the master loop can be set by an expert system. As previously noted, most approaches are dedicated to control anaerobic wastewater treatment processes, such that almost all listed methods use the dilution rate as the manipulated variable.

Approaches such as Liu et al. (2004a), Alferes et al. (2008), Alferes and Irizar (2010) are dedicated to control biogas production at a setpoint, or to operate the digester at high organic load, respectively. Therefore they try to maximize the economical benefit of the digester, whereas the setpoint is set accordingly to not overload the digester. But they do not use direct measurements such as VFA, COD, dissolved hydrogen or bicarbonate which are able to signalize whether the digester is currently overloaded. This is done by Zhou et al. (2012), where the methane flow rate setpoint is set based on measurements of VFA and VFA/TA.

Another approach is to minimize COD in the effluent or the VFA content inside the digester as is e.g. done by Alvarez-Ramirez et al. (2002), Batstone and Steyer (2007), Mu et al. (2007). Their goal is to stabilize the digester and maximize the degradation of COD. In contrast to them the approach in García-Díéguez et al. (2011) is able to maximize the methane flow rate, while tracking a setpoint for VFA in the digester effluent. However, as the setpoint for methane depends on the VFA concentration in the digester, this control is not suited to control agricultural biogas plants, which are in need of a user-defined methane setpoint. Together with Boe and Angelidaki (2012) it is the only approach that was applied at pilot-scale, the others were applied at lab-scale, none was applied at full-scale.

6.2 Expert Systems

Expert systems are rule-based systems (Table 6.4), fuzzy systems (Table 6.5) and systems extended with a surrogate model such as an artificial neural network (Table

6.6). As biogas plants are nonlinear processes, applying nonlinear control methods comes quite natural. Such expert systems are quite popular for controlling anaerobic digesters because of their intuitive design based on rules and their non-linearity coping with the non-linearity of the plant. The first approach is performed by rule-based systems such as the well-known fuzzy controls and the latter one by the use of neural networks. Furthermore, expert systems can incorporate all measured variables easily and are easily extensible if an additional process value is measured in the future.

Because of their non-linearity their disadvantage is that it can not be proofed whether the closed-loop control is stable. Furthermore, surrogate models need proper data to train them otherwise these models can be very bad representatives of the real process. Especially for full-scale plants obtaining data representing the full range of operation very often is not possible, such that those models actually only will work on lab- and pilot-scale where a dynamic operation is more easily.

Approaches not listed in the tables, because not really fitting but related to this topic are Flores et al. (2000a) and Kottas et al. (2006).

6.3 Linearizing Control

Conventional linear controls have a disadvantage controlling a nonlinear process because the closed loop is nonlinear (see Figure 6.1). Linearizing controls are designed so that the closed loop is linear. Linear means, that the time t dependent dynamics of the control error signal $e(t)$ can be described by the first order differential equation $\frac{d}{dt}e(t) + C(t) \cdot e(t) = 0$, with the damping factor $C(t) > 0$, assuming $\frac{d}{dt}C(t) \approx 0$. As a consequence the control error converges exponentially to zero with increasing time t : $e(t) = \exp(-C(t)) \cdot e(0)$. As a result linearizing controls can be highly nonlinear, which means that they are not per default robust against uncertainties such as noise or model mismatch. **Using interval observers, they can be made robust against uncertainties in the process input and initial states.** Furthermore, model parameters can be properly estimated using adaptive schemes. Linearizing controls can have different kind of properties from model-based, adaptive to robust, which is why there are many different philosophies and approaches on how to develop linearizing controls. Linearizing controls are popular for a stabilizing feed control of anaerobic digestion processes and the dilution rate is mostly used as manipulated variable. The approaches found in the literature are listed in the Tables 6.7 and 6.8.

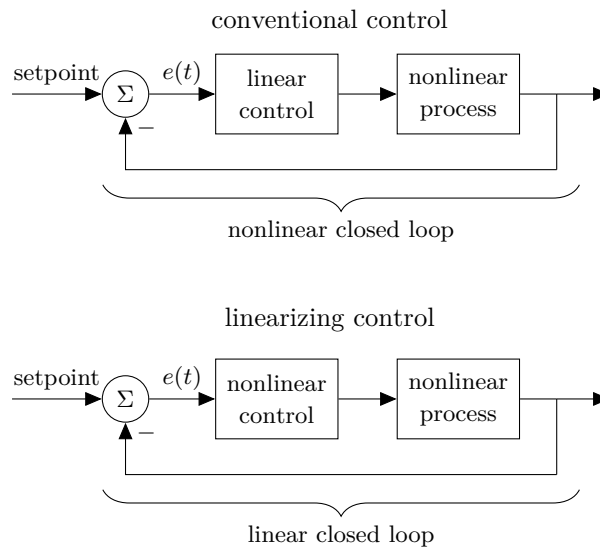


Figure 6.1: Comparison between conventional and linearizing control (cf. Bastin and Dochain (1990)).

6.4 Discontinuous Control

Discontinuous controls come from optimal control theory solving Pontryagin's maximum principle (see Table 6.9). As they switch from a minimal to a maximal dilution rate in one instant they have a bang-bang behavior. This behavior does not seem to be practical for full-scale ABP, because, although theoretically impossible, such a huge instantaneous change in the dilution rate might lead to process imbalances.

6.5 Other Advanced Controls

Other advanced control approaches are not further subdivided into different groups and contain model-based, robust, adaptive and other approaches. They are listed in Tables 6.10, 6.11 and 6.12.

6.6 Summary and Discussion

In this chapter an extensive review on feed control of the anaerobic digestion process is given. Despite the vast amount of publications in this field, none was found focusing on dynamic real-time feed optimization of co-digestion plants. The two key features of dynamic RTO are an arbitrary optimization criterion to be defined by the user and a dynamic model that is used for prediction. In most proposed control algorithms the optimization criterion is restricted to be either to maximize or control methane production or to minimize or control the COD concentration in the effluent. Furthermore, no model based feed control was found that uses the Anaerobic Digestion

Model No. 1 as prediction model. As a result, this review revealed a lack in research on dynamic real-time feed optimization whereas this thesis is trying to make a contribution to this field.

In the following paragraphs the main results of the review are examined.

Manipulated Variable By far the most developed controls use the dilution rate as manipulated variable (see Figure 6.2a). Examples for other manipulated variables are recirculation rates and the addition of bases to stabilize the process. In case of a co-digestion plant only one substrate or a constant substrate mix can be controlled using the dilution rate as manipulated variable. The other substrates then must be calculated based on boundary conditions such as hydraulic retention time, organic loading rate or restrictions defined by funding schemes (Zhou et al., 2012). For German ABP some funding schemes are linked to a required minimal amount of manure and a maximal allowable amount of maize in the feed (BMU, 2012a).

Scale of the Digester Looking at the scale of the digesters where the control methods were applied to, it can be observed that most of the evaluations were performed at lab-scale or pilot-scale plants (Figure 6.2b). However, a clear distinction between lab and pilot-scale is difficult. Therefore, digesters with a volume from 500 l to 10 m³ are considered to be pilot-scale, while smaller digesters are lab-scale and larger ones full-scale. The largest part of all proposed controllers are applied to simulation models only. If controls are evaluated at simulation models, nowadays complex models (such as Batstone et al. (2002b), Siegrist et al. (2002)) should be used to make the evaluation as realistic as possible. As stability of controls can only be proved for simple models exhaustive simulations can show the performance and stability of the control empirically. Figure 6.2b clearly shows, that feed control of the anaerobic digestion process has not yet reached full-scale application. The main reasons are a lack of measurement devices and missing advanced diagnosis schemes, that are needed for process monitoring (Batstone et al., 2004, Alcaraz-González et al., 2012). Whereas control approaches for waste treatment processes, which come very close to the optimal control defined in Definition 6.2, do exist (e.g. García-Diéguéz et al. (2011), Dimitrova and Krastanov (2009)), an optimal control for agricultural biogas plants as defined in Definition 6.1 has not yet been developed. Although robustly stable methane setpoint controls are available (e.g. Hilgert et al. (2000)), wrongly chosen setpoints might easily lead to process imbalances that strongly affect process stability. Therefore, the key is to set the setpoint properly, so that the process is stable at all times.

Substrates Looking at the substrates it can be observed, that the vast majority of controls are applied to wastewater treating plants (see Figure 6.2c). Wastewater

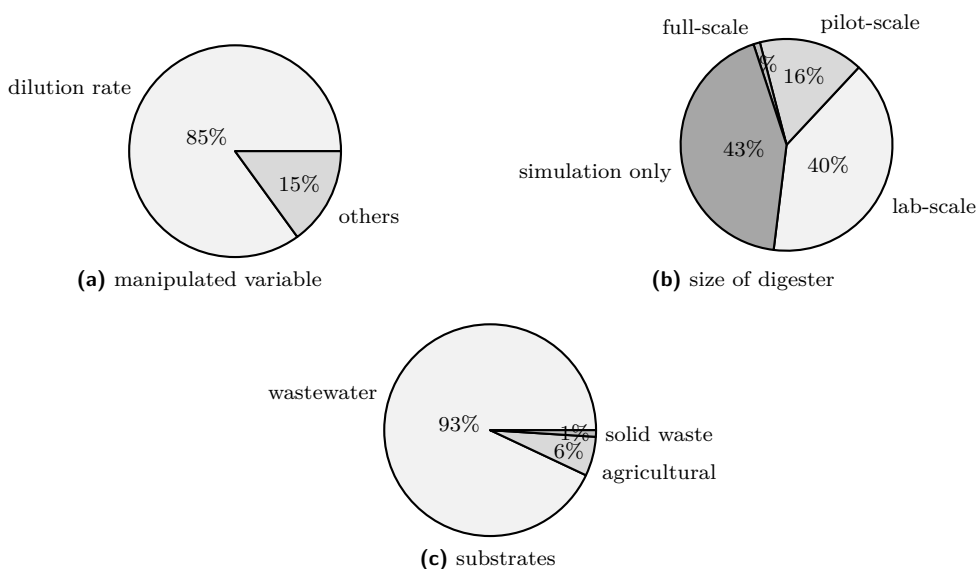


Figure 6.2: Percentage distribution of manipulated variable (121 publications), size of digester (134 publications) and substrates (109 publications) of the reviewed publications.

includes different streams from municipal treatment plants and industry. Agricultural substrates are energy crops, grass and manure. Solid waste is the organic fraction of municipal solid waste as well as biowaste. For the latter two substrates only a very few feed controls were developed in the past. Treating wastewater in high-rate reactors offers the opportunity to operate with very low hydraulic retention times requiring a control with a low sampling rate.

Concluding Remarks Substrate feed control for anaerobic wastewater treatment has come very far in the last decades. Control algorithms yielding a good performance are available and ready to be used in practice. But, feed controllers for ABP and solid waste digesting plants are still lacking. The key difficulty with ABP is a lack of a methane setpoint control which offers an economically profitable operation and at the same time guaranteeing stable operation. Before such a control can be applied, robust measurement devices must be installed or soft sensor approaches should be used to estimate key process values. In solid waste digestion the main problem seems to lie in the lack of sufficiently, mechanically robust measurement devices. Because of the solids content such measurement devices are under very high mechanical stress, which makes them more expensive than those developed for wastewater treatment plants. High solid contents also lead to bad miscibility inside the digester. It is astonishing how few full-scale applications are published in the literature. And the question remains

how well advanced control methods applied to small-scale plants or simulation models do perform in the real world at full-scale biogas plants.

To get a better overview over the vast amount of feed controllers the author thinks that more objective comparisons of different controls should be published. Today it is not that difficult to compare them at hand of advanced simulation models such as the ADM1 (see Section 7.1) (Batstone et al., 2002a). For anaerobic wastewater treatment the benchmark model BSM2 (Jeppsson et al., 2007) can be used, but to the author's knowledge no benchmark model for agricultural biogas plants exists.

6.7 Tables

In the following all tables created in this review are listed.

They are:

- Classical Control of Biogas Plants
 - Table 6.1: on/off controls
 - Table 6.2: PID controls
 - Table 6.3: adaptive PID and PID cascade controls
- Expert Systems Control of Biogas Plants
 - Table 6.4: expert systems
 - Table 6.5: fuzzy controls
 - Table 6.6: neural networks and special fuzzy systems
- Linearizing Control of Biogas Plants
 - Table 6.7: Part I
 - Table 6.8: Part II
- Discontinuous Control of Biogas Plants
 - Table 6.9
- Other Advanced Controls for Biogas Plants
 - Table 6.10: Part I
 - Table 6.11: Part II
 - Table 6.12: Part III

Table 6.1: Classical Control of Biogas Plants: on/off controls

Control type	Author	Description	Manipulated variable	Control variable
on/off	Podruzny and van den Berg (1984)	"on" time proportional-integral to reference error measured biogas flow rate Q_{gas} application: lab-scale AFB, synthetic wastewater	dilution rate	biogas flow rate
on/off	Denac et al. (1988)	"off" time proportional to surplus above threshold application: lab-scale FBR, wastewater	dilution rate	effluent VFA
on/off	Rozzi (1984)	proposal of three controllers (1, 2, 3) purpose of stabilization application: simulation only	alkaline solution	1) pH 2) bicarbonate 3) pH, pCO_2
on/off	Whitmore and Lloyd (1986)	membrane inlet mass spectrometry measures dissolved H_2 application: lab-scale CSTR, wastewater, thermophilic	dilution rate	dissolved H_2
on/off	Whitmore et al. (1987)	as in Whitmore and Lloyd (1986), except: mesophilic	dilution rate	dissolved H_2
on/off	Andrews (1974)	application: CSTR, simulation only, wastewater	recirculation	CH_4 flow rate
on/off	Pretorius (1994)	pH is measured in an unbuffered region based on biogas stripping application: lab-scale UASB, synthetic wastewater, mesophilic	dilution rate	pH
on/off	Romli et al. (1994)	2-stage (CSTR, FBR), recirculation is changed to find optimum: min. addition of caustic soda/max. biogas flow rate application: lab-scale CSTR, wastewater, mesophilic	caustic soda	pH
on/off + P	Graef (1972), Graef and Andrews (1974)	proposal of three controllers: 1, 2) on/off, 3) P in 1) the scrubbed gas (CO_2) is recirculated to the digester application: CSTR, simulation only	1) gas scrubbing 2) base addition 3) sludge recycle	1, 2) pH 3) CH_4 flow rate

Table 6.2: Classical Control of Biogas Plants: PID controls

Control type	Author	Description	Manipulated variable	Control variable
P	Cord-Ruwisch et al. (1997)	setpoint control; purpose: high OLR and stability application: lab-scale CSTR, wastewater, mesophilic	dilution rate	dissolved H ₂
P	Andrews (1974)	application: CSTR, simulation only, wastewater	base addition	pH
P	Franke et al. (2008)	as in Cord-Ruwisch et al. (1997) application: lab-scale CSTR, agricultural, mesophilic	dilution rate	dissolved H ₂
P deadband	Denac et al. (1990)	based on alkaline consumption application: lab-scale FBR, wastewater	- dilution rate - alkali addition	- effluent VFA - pH
I deadband	Feitkenhauer et al. (2002)	application to an acidic phase reactor, goal: max. VFA application: lab-scale CSTR, wastewater	dilution rate	VFA
PI	von Sachs et al. (2003)	application: two-phase AD system, lab-scale FBR (2nd phase), wastewater, mesophilic expert system overrules control in special user-defined cases	dilution rate	biogas flow rate
PI	Batstone and Steyer (2007)	proposal of two controls (1, 2) application: simulation only (ADM1), wastewater	dilution rate	1) VFA 2) alkalinity
PI	Mu et al. (2007)	decision system switches between both manipulated variables application: simulation only, lab-scale UASB (ADM1d), wastewater	- recirculation-to-influent ratio - dilution rate	effluent COD
PI + PID	Ryhiner et al. (1993), Heinzel et al. (1993)	proposal of four controllers (1 PI, 2 PID, 3 PI, 4 PID) application: lab-scale FBR, whey, mesophilic	dilution rate	1),2) pH 3) dissolved H ₂ 4) organic acids
PI + PID	Simeonov (1994)	four different gas setpoints according to a performance index application: simulation only; taken from Pind et al. (2003)	dilution rate	biogas flow rate
PID	Marsili-Libelli and Beni (1996)	purpose: stabilization application: simulation only	bicarbonate addition	bicarbonate alkalinity

Table 6.3: Classical Control of Biogas Plants: adaptive PID and PID cascade control

Control type	Author	Description	Manipulated variable	Control variable
adaptive PI	Perrier and Do-chain (1993)	proposal of three controllers (1, 2, 3) application: simulation only	dilution rate	1) effluent COD 2) dissolved H ₂ 3) propionate
adaptive PID	Zhou et al. (2012)	CH ₄ setpoint set by VFA and VFA/TA application: simulation only (ADM1), CSTR, manure and corn	dilution rate	CH ₄ flow rate
cascade P	Liu et al. (2004a,b)	inner loop: pH; outer loop: gas flow rate setpoint of outer loop given by rule-based supervisory system lab-scale AFB reactor, wastewater, mesophilic	dilution rate	OLR
cascade P	Boe and Angelidaki (2012)	inner loop: VFA; outer loop: gas flow rate rule-based system as in Liu et al. (2004a) application: pilot-scale CSTR, manure, thermophilic	dilution rate	CH ₄ flow rate
cascade P	Liu et al. (2006)	same as Liu et al. (2004a) inner loop pH control is rule-based variable-gain P control with rules defined by state machine lab-scale AFB reactor, wastewater, mesophilic	dilution rate	OLR
cascade P	Alferes et al. (2008)	same as Liu et al. (2004a) includes fill level of an upstream equalization tank application: simulation only (ADM1), UASB-AF, wastewater	dilution rate	- OLR - fill level
cascade P	Alferes and Irizar (2010)	same as Alferes et al. (2008) rule-based supervisory system implemented by a fuzzy module application: simulation only (ADM1), UASB-AF, wastewater	dilution rate	- OLR - fill level
cascade PI	Alvarez-Ramirez et al. (2002)	inner loop: VFA; outer loop: COD application: lab-scale UASB, wastewater	dilution rate	effluent COD
cascade PID	García-Díéguez et al. (2011)	inner loop: methane flow rate; outer loop: VFA application: pilot-scale UASB-AF, wastewater, mesophilic	dilution rate	- CH ₄ flow rate - effluent VFA

Table 6.4: Expert Systems Control of Biogas Plants: expert systems

Control type	Author	Description	Manipulated variable	Control variable
expert system	Boe (2006), Boe et al. (2008)	if propionate ..., then in-/decrease feed high fluctuations in biogas flow rate, because propionate is too persistent application: lab-scale CSTR, cow manure, thermophilic	dilution rate	propionate
expert system	Barnett and Andrews (1992)	rules implemented with fuzzy logic inputs: a lot; output: a few next to dilution rate application: simulation only	dilution rate	normal operation
expert system	Chynoweth et al. (1994)	rules based on CH_4 flow rate, its derivative, dilution rate and its derivative able to distinguish between overloading, underloading and inhibition application: lab-scale CSTR, wastewater, mesophilic	dilution rate	CH_4 flow rate
expert system	Moletta et al. (1994)	inputs: pH, biogas flow rate, H_2 content of biogas application: lab- and pilot-scale FBR, wastewater, mesophilic	dilution rate	normal operation
expert system	Ehlinger et al. (1994)	decision tree: pH, gas and H_2 flow rate application: lab-scale FBR, mesophilic, wastewater	dilution rate	normal operation
expert system	Flores et al. (2000b)	application: start-up of pilot-scale UASB-AF reactor, wastewater	dilution rate	normal operation
expert system	Pullammanappallil et al. (1991, 1998)	bumpless switch between four different control strategies based on a t-test: 1) set-point control, 2) constant yield control 3) batch operation, 4) constant dilution rate application: lab-scale CSTR, wastewater, mesophilic	dilution rate	CH_4 flow rate
expert fuzzy system	Müller et al. (1997)	H_2 and CH_4 flow rate; uses Fuzzy C-Means Clustering of Marsili-Libelli and Müller (1996) application: lab-scale FBR, wastewater, mesophilic	- bypass - storage - dilution	normal, overload, inhibition, toxicity
expert fuzzy system	Puñal et al. (2001, 2002), Carrasco (2002)	many input variables application: pilot-scale UASB-AF, wastewater	flow rates	over-, underload recovery

Table 6.5: Expert Systems Control of Biogas Plants: fuzzy controls

Control type	Author	Description	Manipulated variable	Control variable
fuzzy P	Bernard et al. (2001b)	inputs: TA, VFA/TA application: pilot-scale FBR, wastewater	dilution rate	VFA/TA
fuzzy P	Scherer et al. (2008, 2009)	inputs: pH value, CH ₄ content and specific gas flow rate application: lab-/pilot-scale CSTR, agricultural, meso-/thermophilic	dilution rate	OLR
fuzzy I	Boscolo et al. (1993)	inputs: nine variables application: pilot-scale CSTR, OFMSW, thermophilic	- feed rate - TS of feed - recycling rates	normal operation
fuzzy P + PI	Murnleitner (2001), Murnleitner et al. (2002), Grepmeier (2002)	inputs: H ₂ , CH ₄ , biogas flow rate, pH, filling level application: lab-scale FBR, two-stage, wastewater, mesophilic	- different flows (PI) - pH (P) - temperature (P)	overload avoidance
fuzzy PI	Estaben et al. (1997)	inputs: error to setpoints of gas flow rate and pH value and the derivatives of the errors; output: change of feed rate application: lab-scale FBR, wastewater	dilution rate	- gas flow rate - pH value
fuzzy PI	Puñal et al. (2003)	inputs: error of VFA to its setpoint and its derivative output: change of feed rate application: pilot-scale AFB, wastewater	dilution rate	effluent VFA
fuzzy PI	Garcia et al. (2007)	inputs: CH ₄ flow rate; H ₂ content of gas; VFA/TA output: change of feed rate application: ADM1, lab-scale UASB-AF, wastewater	dilution rate	OLR
fuzzy PI	Wolfsberger (2008)	eight different fuzzy controls application: lab-scale, agricultural, meso-/thermophilic	dilution rate	OLR
fuzzy PI cascade	Martinez-Sibaja et al. (2007)	- inner loop (conventional PI): pH - outer loop (fuzzy PI): gas flow rate application: simulation only	dilution rate	- gas flow rate - pH value

Table 6.6: Expert Systems Control of Biogas Plants: neural networks and special fuzzy systems

Control type	Author	Description	Manipulated variable	Control variable
hierarchical fuzzy	Steyer et al. (1997)	inputs: control error of pH, T and biogas flow rate for a small rule-set a hierarchical fuzzy structure is chosen application: lab-scale FBR, wastewater, mesophilic	dilution rate	VFA
neural network	Holubar et al. (2002, 2003)	ANN models for: pH, VFA, biogas production and composition optimal COD loading rate is solution of max. CH_4 flow rate and COD degradation; application: lab-scale CSTR, primary sludge	COD loading rate	CH_4 flow rate
neural	Wilcox et al. (1995), Guwy et al. (1997)	ANN model for bicarbonate alkalinity (BA) out of past BA values application: lab-scale FBR, ice-cream and baker's yeast WW	BA dosing pump	bicarbonate alkalinity
neural network	Emmanouilides and Petrou (1996)	adaptive on-line trained neural networks application: simulation only	dilution rate	- CH_4 flow rate - effluent COD
neural-fuzzy	Yordanova et al. (2004)	fuzzy PI, fuzzy tuning control application: simulation only, wastewater	dilution rate	biogas flow rate
neural-fuzzy	Waewsak et al. (2010)	ANN models for: pH, TA and VFA, predicted out of past values application: lab-scale UASB-AF, synthetic WW, mesophilic	dilution rate	- high performance - stability
fuzzy supervision	Carlos-Hernandez et al. (2007)	Takagi-Sugeno supervisor switches between: 1) open loop, 2) base addition (fuzzy PI), 3) dilution rate (fuzzy PI) application: FBR, wastewater, simulation only	- base addition - dilution rate	high performance
fuzzy supervision	Carlos-Hernandez et al. (2010a)	as in Carlos-Hernandez et al. (2007) PCA and Takagi-Sugeno estimate biomass and substrate application: CSTR, wastewater, simulation only	- base addition - dilution rate	CH_4 flow rate
fuzzy supervision	Gurubel et al. (2013)	as in Carlos-Hernandez et al. (2010a), additional using PSO to improve setpoint tracking	- base addition - dilution rate	CH_4 flow rate
neural-fuzzy	Carlos-Hernandez et al. (2010b)	as in Carlos-Hernandez et al. (2007) neural observer trained by EKF estimates methanogenic biomass application: FBR, abattoir wastewater, simulation only	- base addition - dilution rate	high performance

Table 6.7: Linearizing Control of Biogas Plants: Part I

Control type	Author	Description	Manipulated variable	Control variable
linearizing	Alvarez-Ramirez et al. (1996), Monroy et al. (1996)	adaptive, no need for measuring biogas flow rate application: lab-scale UASB, wastewater, mesophilic	dilution rate	effluent COD
linearizing	Petre et al. (2007)	adaptive, asymptotic state observer application: simulation only	dilution rate	effluent COD
feedback linearization	Angulo et al. (2007)	derivation using AM1 (Bernard et al., 2001a), model-based application: simulation only, AFB reactor, wastewater	dilution rate	effluent VFA
external linearization	Renard et al. (1988)	adaptive control, influent COD needs to be measured application: lab-scale CSTR, WW (citric acid), mesophilic	dilution rate	effluent COD
external linearization	Johnson et al. (1995)	Renard et al. (1988) approach used application: lab-scale AFB, wastewater, mesophilic	dilution rate	effluent COD
external linearization	Renard et al. (1991)	adaptive control, influent COD needs to be measured application: lab-scale CSTR, WW (citric acid), mesophilic	dilution rate	propionate
linearizing	Dochain and Perrier (1993)	direct adaptive linearizing application: CSTR, simulation only	dilution rate	propionate
linearizing	Dochain et al. (1991)	nonlinear adaptive, model-based application: CSTR, simulation only	dilution rate	dissolved H ₂
linearizing	Bernard et al. (2001b)	adaptive control, influent COD estimated by soft sensor application: pilot-scale FBR, wastewater	- dilution rate - alkalinity	VFA/TA
linearizing	Rincon et al. (2009)	adaptive control, normal form of fold bifurcation application: simulation only, wastewater	dilution rate	effluent VFA
linearizing	Simeonov and Queinnec (2006)	model-based, organic wastes and acetate application: simulation only, CSTR, mesophilic	acetate addition	biogas flow rate

Table 6.8: Linearizing Control of Biogas Plants: Part II

Control type	Author	Description	Manipulated variable	Control variable
robust linearizing	Rapaport and Harmand (2002)	interval observer application: simulation only, CSTR	dilution rate	effluent COD
geometric	Méndez-Acosta et al. (2003, 2004, 2005)	to avoid overshooting fuzzy-based gain-scheduling and anti-windup scheme are used, high-gain observer application: simulation only, AFB, wastewater	dilution rate	effluent COD
geometric robust	Méndez-Acosta et al. (2007a, 2008)	model-based: extended Luenberger observer application: pilot-scale AFB, wastewater	dilution rate	effluent VFA
geometric robust	Méndez-Acosta et al. (2007b)	model-based: extended Luenberger observer; proposal of two controls (1, 2); TOC: total organic carbon application: pilot-scale AFB, wastewater, mesophilic	dilution rate	1) VFA 2) TOC
geometric robust	Méndez-Acosta et al. (2010)	model-based: extended Luenberger observer, antiwindup structure application: simulation only, wastewater	- dilution rate - alkali solution	- VFA - TA
linearizing	Dochain and Bastin (1985)	nonlinear adaptive application: CSTR, simulation only	dilution rate	effluent VFA
Generic Model Control	Costello et al. (1989)	improvement of Dochain and Bastin (1985) application: CSTR, simulation only, wastewater	dilution rate	effluent COD
linearizing	Petre et al. (2013)	three controls: 1) adaptive (asymptotic observer), 2) robust, 3) robust-adaptive (interval observer, both) application: CSTR, simulation only, wastewater	dilution rate	effluent COD
VSM	Tartakovsky et al. (2002, 2005)	variable structure model (VSM) containing three linear submodels, for each submodel one linearizing control application: lab-scale UASB, synthetic wastewater, mesophilic	influent COD	effluent COD
decoupled linearizing	Aguilar-Garnica et al. (2007, 2009)	two-phase AD system, modeled by PDE, observer-based estimator application: simulation only, two AFBs, wastewater	recycle flow rates	- effluent VFA - effluent COD

Table 6.9: Discontinuous Control of Biogas Plants

Control type	Author	Description	Manipulated variable	Control variable
singular control	Stamatelatou et al. (1997)	optimal is model-based (bang-bang), suboptimal is P control application: CSTR, simulation only	dilution rate	CH ₄ flow rate
switching control policy	Sbarciog et al. (2011, 2012a), Sbarciog and Vande Wouwer (2012)	bang-bang control maximizes CH ₄ flow rate application: CSTR, simulation only, wastewater	dilution rate	CH ₄ flow rate
switching control policy	Sbarciog et al. (2012b)	as Sbarciog et al. (2011) and others, but biogas measured only application: CSTR, simulation only, wastewater	dilution rate	CH ₄ flow rate
piecewise continuous	Chamroo et al. (2008)	two controls (1, 2) application: simulation only	dilution rate	1) effluent COD 2) CH ₄ flow rate
sliding mode	Tabrizi et al. (2010)	application: AFB, simulation only, wastewater	dilution rate	effluent COD
sliding mode	Kravaris and Savoglidis (2012)	application: CSTR, simulation only	dilution rate	CH ₄ flow rate

Table 6.10: Other Advanced Controls for Biogas Plants: Part I

Control type	Author	Description	Manipulated variable	Control variable
disturbance monitoring	Steyer et al. (1999)	increased biogas yield caused by an impulse in feed is compared with expected. Overloading/inhibition reflected by an unsatisfactory gas yield. application: lab-scale FBR, wastewater, mesophilic	dilution rate	biogas flow rate
disturbance accommodating	Harmand et al. (2000)	ARMAX model with bias estimation application: lab-scale FBR, wastewater	dilution rate	biogas flow rate
nonlinear adaptive	Polihronakis et al. (1993)	proposal of three controls: 1), 2) and combination of both combination switches between both control objectives application: full-scale, wastewater	dilution rate	1) effluent COD 2) CH ₄ flow rate
adaptive robust	Hilgert et al. (2000)	ARMAX model with uncertain part, estimated by kernel estimator application: lab-scale FBR, wastewater, mesophilic	dilution rate	biogas flow rate
adaptive	Harmon et al. (1993)	taken from Pind et al. (2003) application: lab-scale CSTR, glucose	temperature	CH ₄ flow rate
nonlinear	Harmon et al. (1990)	constant reactor yield control application: lab-scale CSTR, synthetic WW, thermophilic	dilution rate	CH ₄ flow rate
sampled delayed control	García-Sandoval et al. (2007)	nonlinear, robust, delayed measurements application: simulation only, wastewater	dilution rate	effluent COD
sampled delayed control	Méndez-Acosta et al. (2011)	same as in García-Sandoval et al. (2007), COD measured daily application: lab-scale AFB, wastewater, mesophilic	dilution rate	effluent COD
robust output feedback	Antonelli et al. (2002, 2003)	nonlinear; only measured variable: CH ₄ flow rate application: pilot-scale AFB, wastewater, mesophilic	dilution rate	CH ₄ flow rate
robust output feedback	Mailleret and Bernard (2001), Mailleret et al. (2003)	CH ₄ flow rate and input COD needed application: pilot-scale AFB, wastewater	dilution rate	effluent COD

Table 6.11: Other Advanced Controls for Biogas Plants: Part II

Control type	Author	Description	Manipulated variable	Control variable
nonlinear adaptive	Mailleret et al. (2004)	CH ₄ flow rate needed application: pilot-scale AFB, wastewater	dilution rate	effluent COD
nonlinear adaptive	Dimitrova and Krastanov (2009)	extremum seeking algorithm to maximize CH ₄ production application: simulation only	dilution rate	- effluent COD - CH ₄ flow rate
adaptive	Seok (2003)	recursive system identification, convex optimization problem application: lab-scale FBR, wastewater, mesophilic	dilution rate	propionate
extremum seeking	Marcos et al. (2004a,b)	adaptive; substrate concentration kept at setpoint application: CSTR, AFB, simulation only	dilution rate	CH ₄ flow rate
extremum seeking	Simeonov et al. (2007), Simeonov and Stoyanov (2011)	application: CSTR, simulation only, mesophilic	dilution rate	CH ₄ flow rate
LQT	Mu et al. (2008)	linear quadratic tracking (LQT) and error integral action application: simulation only, lab-scale UASB, distributed model, wastewater	- recirculation-to-feed ratio - bypass-to-feed ratio	effluent COD
NMPC	Aceves-Lara et al. (2010)	asymptotic observer estimates influent, effluent and some product concentrations; dark fermentation application: lab-scale CSTR, diluted molasses, mesophilic	dilution rate	H ₂ flow rate
EPSAC-MPC	Ordace et al. (2012)	Extended Prediction Self-Adaptive Control (EPSAC) application: simulation only (ADM1), wastewater sludge	feed flow rates	CH ₄ flow rate

Table 6.12: Other Advanced Controls for Biogas Plants: Part III

Control type	Author	Description	Manipulated variable	Control variable
variable-gain	Rodríguez et al. (2006)	indirect COD control by controlling H ₂ in gas phase application: pilot-scale UASB-AF, wastewater	dilution rate	effluent COD
composed	Wang et al. (2011, 2013)	algebraic differential estimator, adaptive (Wang et al., 2011); model-free (Wang et al., 2013) application: CSTR, simulation only, agricultural, mesophilic	dilution rate	CH ₄ flow rate
adaptive optimization	Ryhiner et al. (1992)	steepest descent finds optimal operating point application: FBR, wastewater	dilution rate	- CH ₄ flow rate - VFA
saturated proportional	Grognard and Bernard (2006)	no input COD measurement needed; attracts to a region application: simulation only, wastewater	dilution rate	effluent COD
H_∞	Flores-Estrella et al. (2013)	application: simulation only, wastewater	dilution rate	effluent COD
dynamic compensator	Simeonov and Stoyanov (2003)	linear model with interval parameters; proposes two controls (1, 2) application: simulation only	dilution rate	1) biogas flow rate 2) effluent COD
robust adaptive	Rincón et al. (2012)	Lyapunov-like function application: simulation only, wastewater	dilution rate	effluent VFA
robust set-valued	Alcaraz-González et al. (2000)	interval observers, nonlinear application: simulation only, AFB, wastewater	dilution rate	- effluent VFA - effluent COD
robust interval	Alcaraz-González et al. (2001, 2005)	interval observers application: pilot-scale AFB, wastewater	dilution rate	effluent COD

Chapter 7

Modeling Biogas Plants

In this chapter the simulation model of the biogas plant used inside the model predictive control (Chapter 2) and used for performance evaluation of the control using simulations (chapters 8 and 9) is presented. The most important part of a biogas plant model is the model of the anaerobic digestion process. In this thesis the Anaerobic Digestion Model No. 1 (ADM1) is used for that purpose (Section 7.1). The ADM1 is the nowadays most often used and most complex simulation model of the AD process. The complexity of the ADM1 allows a very detailed characterization of the substrate feed, which is very important for a realistic model representation of the real world (Section 7.2). A biogas plant is a system where energy is produced (in case the produced biogas is burned in combined heat and power plants (CHPs): electrical and thermal energy) and where energy is consumed. Typical energy sinks are pumps, stirrers and the heat losses through the digester insulation. The produced energy is usually sold, such that economic issues must be included in the model as well. As all such aspects determine how well a biogas plant is operated those criteria are performance indicators, whose models are described in Section 7.3.

In Section 7.4 the implementation of a model of a full-scale biogas plant, developed in MATLAB[®], is shown. The calibration and validation of that model on real data is discussed in Section 7.5.

Next to the ADM1 there are many other models of the anaerobic digestion process, all started with the model of Andrews (1968). As there are a lot of excellent reviews on such models in this thesis the author does without a review, but refers to the reviews in Appels et al. (2008), Dewil et al. (2011), Donoso-Bravo et al. (2011), Gavala et al. (2003), Gerber and Span (2008), Gerber (2009), Lauwers et al. (2013), Lübken et al. (2010), Saravanan and Sreekrishnan (2006), Tomei et al. (2009) and Wolf (2013).

General Remark on Notation To avoid tedious formalism all definitions and equations in this chapter assume that the biogas plant only contains one anaerobic digester which is fed with one single substrate and the biogas is burned in one combined

heat and power plant. Nevertheless all definitions can easily be generalized for a biogas plant with more than one digester, substrate and CHP. In this generalized manner the algorithms, modeling each biogas plant, are implemented (see Part B of the appendix). Here, this simplification is only done to clean up the notation.

7.1 The Anaerobic Digestion Model No. 1 (ADM1)

The Anaerobic Digestion Model No. 1 was published by a Task Group of the International Water Association in 2002, (Batstone et al., 2002a,b). It can be seen as a merger of all previously published AD models and is since then established as the standard model for the AD process.

The ADM1 models the anaerobic digestion process in 19 biochemical processes, six acid/base equilibria, three liquid/gas transfer processes and one for the pressure in the gas phase. The 19 biochemical processes include the main chemical reactions of the four steps of anaerobic digestion described in Section 5.1. They are preceded by a disintegration step, which models the physical breakup of the substrates into their biomolecules. For a CSTR (Section 5.4.1) the ADM1 can be modeled as an ordinary differential equation (ODE) system as given in equation (7.1) with the definitions of the ADM1 state vector ${}^o\mathbf{x}_{AD} : \mathbb{R}^+ \rightarrow \mathbb{R}^{37}$ and the ADM1 input vector ${}^o\mathbf{u}_{AD} : \mathbb{R}^+ \rightarrow \mathbb{R}^{34}$ in eq. (7.2).

$${}^o\mathbf{x}_{AD}'(\tau) = \mathbf{D}_u(\tau) \cdot {}^o\mathbf{u}_{AD}(\tau) - \mathbf{D}_x(\tau) \cdot {}^o\mathbf{x}_{AD}(\tau) + \mathbf{V}({}^o\mathbf{x}_{AD})^T \cdot \boldsymbol{\rho}({}^o\mathbf{x}_{AD}) \quad (7.1)$$

The 37 components of the ADM1 state vector ${}^o\mathbf{x}_{AD}$ are listed in Table 7.1. The first 33 components of the input ${}^o\mathbf{u}_{AD}$ are in the same order as in the state vector ${}^o\mathbf{x}_{AD}$, such that in eq. (7.2) the missing input components are abbreviated with dots. The input vector ${}^o\mathbf{u}_{AD}$ is modeled in Section 7.2. Please note that, because in the considered case the biogas plant only contains one digester which is fed with one substrate, the state vector \mathbf{x} and the input vector \mathbf{u} , both defined in Chapter 2, are identical to ${}^o\mathbf{x}_{AD}$ and ${}^o\mathbf{u}_{AD}$, respectively.

$$\begin{aligned} {}^o\mathbf{x}_{AD} &:= ({}^o x_{AD,1}, {}^o x_{AD,2}, \dots, {}^o x_{AD,i}, \dots, {}^o x_{AD,37})^T \\ {}^o\mathbf{u}_{AD} &:= \left(S_{su,IN}, S_{aa,IN}, S_{fa,IN}, S_{va,IN}, \dots, S_{ac,IN}^-, S_{hco3,IN}^-, S_{nh3,IN}, Q_{IN} \right)^T \end{aligned} \quad (7.2)$$

In eq. (7.1) the linear matrix function $\mathbf{V} : \mathbb{R}^{37} \rightarrow \mathbb{R}^{29 \times 37}$ is the stoichiometric matrix and the nonlinear vector function $\boldsymbol{\rho} : \mathbb{R}^{37} \rightarrow \mathbb{R}^{29}$ is the vector of the process rates. The input $\mathbf{D}_u : \mathbb{R}^+ \rightarrow \mathbb{R}^{37 \times 34}$ and state transition matrix $\mathbf{D}_x : \mathbb{R}^+ \rightarrow \mathbb{R}^{37 \times 37}$ are diagonal matrices with the dilution rate D on their main diagonal. The vector of process rates $\boldsymbol{\rho} := (\rho_1, \dots, \rho_j, \dots, \rho_{29})^T$ is affected by the available substrate and biomass but is also affected negatively by inhibiting process values such as ammonia, pH and hydrogen. $\mathbf{V}, \boldsymbol{\rho}, \mathbf{D}_u$ and \mathbf{D}_x are defined in the appendix, see Part C.

Using the liquid/gas transfers, biogas production is calculated. The ADM1, in its standard implementation, models biogas as a mixture of the three gases hydrogen (H_2), methane (CH_4) and carbon dioxide (CO_2). Their volumetric flow rates are defined as Q_{h_2} , Q_{ch_4} , Q_{co_2} , respectively, and are measured in $\frac{m^3}{d}$. The volumetric flow rate of total produced biogas Q_{gas} is defined as the sum of the biogas components, as given in equation (7.3).

$$Q_{gas} := \sum_{i \in \{h_2, ch_4, co_2\}} Q_i = Q_{h_2} + Q_{ch_4} + Q_{co_2} \quad [Q_{gas}] = \frac{m^3}{d} \quad (7.3)$$

The relative content r_i of each biogas component $i \in \{h_2, ch_4, co_2\}$ is defined in equation (7.4).

$$r_i := \frac{Q_i}{Q_{gas}}, \quad i \in \{h_2, ch_4, co_2\} \quad [r_i] = 100 \% \quad (7.4)$$

7.1.1 Extensions of the Anaerobic Digestion Model No. 1

Over the last decade quite a lot of extensions to the ADM1 have been proposed and successfully implemented. Figure 7.1 visualizes the percentage distribution of five different categories of extensions. In total 73 publications have been found in the literature.

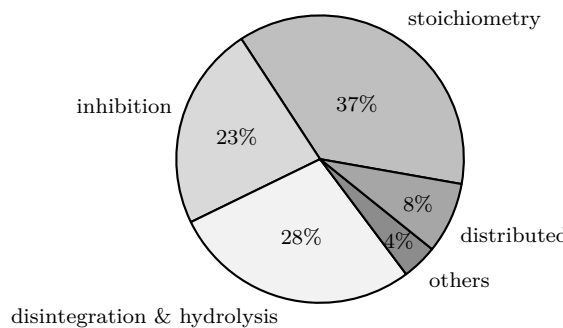


Figure 7.1: Percentage distribution of ADM1 extensions (73 publications).

The **disintegration & hydrolysis** steps are extended to account for different rates of degradability of different substrates and substrate components. The effects of particle size, TS content, thermal and ultrasound pretreatment, start-up behavior and others on the degradation behaviour of substrates were studied.

Process inhibition due to some substances inside the digester is modeled in the ADM1 by continuous **inhibition** functions $I : \mathbb{R}^{37} \rightarrow [0, 1]$. They are multiplied with the reaction rate ρ_j of the affected reaction $j \in \{1, \dots, 19\}$ and return 1, when no inhibition is active. A few more inhibition functions next to the ones already implemented

in the ADM1 were proposed over the last years. Examples are inhibition by total volatile fatty acids, sodium, long chain fatty acids (LCFAs), phenolic compounds and pharmaceuticals.

Extensions affecting the **stoichiometry** of the ADM1 are those that include more processes or make the stoichiometry variable. Examples are precipitation reactions, sulphate and nitrate reduction, inclusion of phenolic compounds, ethanol and lactic acid, variable stoichiometry, microbial storage, acetate oxidation and multi-species models.

On the one hand **distributed** models can be used to model different layers in the reactor (1d-models) and on the other hand they can be used to analyze the interaction between different types of biomass species in sludge granules (2d- and 3d-models).

7.1.2 Applications of the Anaerobic Digestion Model No. 1

The ADM1 was applied to many different substrate feeds in liquid as well as in solid form. In Figure 7.2a the percentage distribution of four different types of substrates can be seen. To the class of liquid wastes belong substrates with a low total solids content. Examples are sewage sludge from wastewater treatment plants and olive pulp. To the wastewater type belong winery, black, paper mill as well as synthetic wastewater. Agricultural substrates are those mainly fed on agricultural biogas plants. Examples are grass silage, different crops and all sorts of manure. Finally, solid wastes are the organic fraction of municipal solid wastes (OFMSW) as well as vegetable/kitchen waste.

The digestion temperature most of the time is in the mesophilic temperature region as is visualized in Figure 7.2b. Most reactors are continuously stirred (CSTR) as is

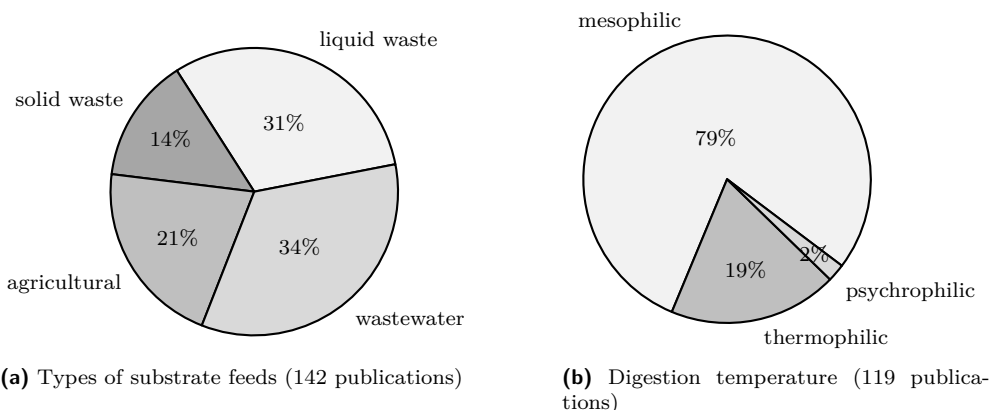


Figure 7.2: Applications of the ADM1: Part I

depicted in Figure 7.3a. To them also all lab experiments performed in e.g. bottles or

vessels belong. The ADM1 most of the time is calibrated to lab-scale experiments, but pilot- as well as full-scale applications have a fair share of all applications as well, see Figure 7.3b.

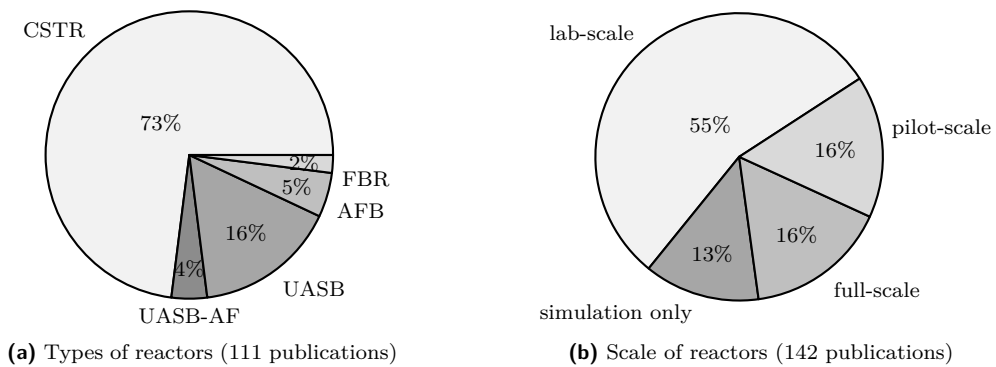


Figure 7.3: Applications of the ADM1: Part II

In all these applications different implementations of the Anaerobic Digestion Model No. 1 were used and also the substrate characteristics were modeled differently. But, so far, it seems that all these applications could be modeled with some ADM1 implementation with sufficient accuracy. At the moment a best practice guide on how to model a biogas plant properly using the ADM1 with different types of substrates (liquid, solid) is not there yet.

The references to all publications used to create the charts in this and the previous subsection can be found here¹.

7.1.3 Implementation of the ADM1 in this Work

In this thesis basically the ADM1 implementation of Simba 6.4, Tschepeetzki and Ogurek (2010), is used. This is an implementation of the ADM1 as system of ODEs with the extension proposed in Wett et al. (2006). The following further extensions were added to the model.

To account for the loss of mass, which is released with the produced biogas, the volumetric flow rate of the substrate feed is reduced by the mass loss of the expected biogas production as suggested in Koch (2010). To not change the substrate feed parameters the input concentrations in \mathbf{u}_{AD} are multiplied with the inverse of the mass reduction factor. Using this change it is possible to model the fill-level of the digester. Koch (2010) furthermore suggests a TS dependent hydrolysis (affecting the

¹<http://www.mendeley.com/groups/3709301/anaerobic-digestion-model-no-1/>

process rates ρ_j with $j = 2, 3, 4$) using equation (7.5), which is implemented as well. In eq. (7.5) the bijection $j_S : \{2, 3, 4\} \rightarrow \{\text{ch}, \text{pr}, \text{li}\}$ is used.

$$\underbrace{\rho_j = k_{\text{hyd},j_S(j)} \cdot X_{j_S(j)}}_{\text{original ADM1 eq.}} \cdot \frac{1}{1 + \left(\frac{\text{TS}}{K_{\text{hyd}}}\right)^{n_{\text{hyd}}}} \quad (7.5)$$

There the inhibition constant of hydrolysis K_{hyd} , $[K_{\text{hyd}}] = \%_{\text{FM}}$, and the inhibition index of hydrolysis n_{hyd} , $[n_{\text{hyd}}] = 100\%$, are used.

Table 7.1: State vector components ${}^o x_{AD,i}$ of the ADM1 (Tschepeetzki and Ogurek, 2010)

i	${}^o x_{AD,i}$	Description	Unit
1	S_{su}	monosaccharides	$\text{kg}_{\text{COD}} \cdot \text{m}^{-3}$
2	S_{aa}	amino acids	$\text{kg}_{\text{COD}} \cdot \text{m}^{-3}$
3	S_{fa}	total long chain fatty acids (LCFA)	$\text{kg}_{\text{COD}} \cdot \text{m}^{-3}$
4	S_{va}	valeric acid S_{hva} + valerate; $S_{hva} := S_{va} - S_{va}^-$	$\text{kg}_{\text{COD}} \cdot \text{m}^{-3}$
5	S_{bu}	butyric acid S_{hbu} + butyrate; $S_{hbu} := S_{bu} - S_{bu}^-$	$\text{kg}_{\text{COD}} \cdot \text{m}^{-3}$
6	S_{pro}	propionic acid S_{hpro} + propionate; $S_{hpro} := S_{pro} - S_{pro}^-$	$\text{kg}_{\text{COD}} \cdot \text{m}^{-3}$
7	S_{ac}	acetic acid S_{hac} + acetate; $S_{hac} := S_{ac} - S_{ac}^-$	$\text{kg}_{\text{COD}} \cdot \text{m}^{-3}$
8	S_{h2}	hydrogen	$\text{kg}_{\text{COD}} \cdot \text{m}^{-3}$
9	S_{ch4}	methane	$\text{kg}_{\text{COD}} \cdot \text{m}^{-3}$
10	S_{co2}	carbon dioxide	$\text{kmol} \cdot \text{m}^{-3}$
11	S_{nh4}^+	ammonium	$\text{kmol} \cdot \text{m}^{-3}$
12	S_I	soluble inert	$\text{kg}_{\text{COD}} \cdot \text{m}^{-3}$
13	X_c	composite	$\text{kg}_{\text{COD}} \cdot \text{m}^{-3}$
14	X_{ch}	carbohydrates	$\text{kg}_{\text{COD}} \cdot \text{m}^{-3}$
15	X_{pr}	proteins	$\text{kg}_{\text{COD}} \cdot \text{m}^{-3}$
16	X_{li}	lipids	$\text{kg}_{\text{COD}} \cdot \text{m}^{-3}$
17	X_{su}	biomass of sugar degraders	$\text{kg}_{\text{COD}} \cdot \text{m}^{-3}$
18	X_{aa}	biomass of amino acids degraders	$\text{kg}_{\text{COD}} \cdot \text{m}^{-3}$
19	X_{fa}	biomass of LCFA degraders	$\text{kg}_{\text{COD}} \cdot \text{m}^{-3}$
20	X_{c4}	biomass of valerate + butyrate degraders	$\text{kg}_{\text{COD}} \cdot \text{m}^{-3}$
21	X_{pro}	biomass of propionate degraders	$\text{kg}_{\text{COD}} \cdot \text{m}^{-3}$
22	X_{ac}	biomass of acetate degraders	$\text{kg}_{\text{COD}} \cdot \text{m}^{-3}$
23	X_{h2}	biomass of hydrogen degraders	$\text{kg}_{\text{COD}} \cdot \text{m}^{-3}$
24	X_I	particulate inert	$\text{kg}_{\text{COD}} \cdot \text{m}^{-3}$
25	X_p	particulate products arising from biomass decay	$\text{kg}_{\text{COD}} \cdot \text{m}^{-3}$
26	S_{cat}^+	cations	$\text{kmol} \cdot \text{m}^{-3}$
27	S_{an}^-	anions	$\text{kmol} \cdot \text{m}^{-3}$
28	S_{va}^-	valerate	$\text{kg}_{\text{COD}} \cdot \text{m}^{-3}$
29	S_{bu}^-	butyrate	$\text{kg}_{\text{COD}} \cdot \text{m}^{-3}$
30	S_{pro}^-	propionate	$\text{kg}_{\text{COD}} \cdot \text{m}^{-3}$
31	S_{ac}^-	acetate	$\text{kg}_{\text{COD}} \cdot \text{m}^{-3}$
32	S_{hco3}^-	bicarbonate	$\text{kmol} \cdot \text{m}^{-3}$
33	S_{nh3}	ammonia	$\text{kmol} \cdot \text{m}^{-3}$
34	p_{iSh2}	partial pressure of S_{h2}	bar
35	p_{iSch4}	partial pressure of S_{ch4}	bar
36	p_{iSc02}	partial pressure of S_{co2}	bar
37	p_{total}	sum of all partial pressures	bar

7.2 The Substrate Feed

The substrate feed of the biogas plant is modeled as the input vector ${}^o\mathbf{u}_{AD}$ defined in equation (7.2). If the biogas plant is fed with more than one substrate, ${}^o\mathbf{u}_{AD}$ contains a weighted sum of the substrates concentrations, weighted by the fed amount of each substrate. Most components of the input vector ${}^o\mathbf{u}_{AD}$ are measured as COD (Section 5.3.3) concentrations, which is a very common measurement in wastewater treatment. For agricultural substrates measuring the chemical oxygen demand is not that usual. In agriculture it is more common to analyze the cell content of the substrate by the extended Weender analysis (Van Soest et al., 1991), see Table 7.2. Using the approach in Koch et al. (2010) the particulate COD of the substrate can be calculated out of the cell components, see Subsection 7.2.1. In Table 7.3 all measurement values used for the full substrate characterization are listed.

Table 7.2: In the extended Weender analysis the substrate is determined by the depicted components (cf. Schuldt and Dinse (2010), Koch et al. (2010)).

		fresh mass FM			
		total solids TS _{IN}			
		volatile solids VS _{IN}			
H ₂ O	ash	RP	RL	carbohydrates	
				nitrogen free extract NFE := VS _{IN} - RF - RP - RL	RF
				non fiber carbohydrates	neutral detergent fiber NDF
				NFC := RF + NFE - NDF	
				hemicellulose	ADF
				cellulose	ADL
		cell content		cell wall	

7.2.1 COD containing Input Variables

The total chemical oxygen demand in the substrate COD_{total} exists as soluble COD and particulate chemical oxygen demand COD_X, all measured in $\frac{\text{kg}_{COD}}{\text{m}^3}$. The particulate COD of the substrate COD_X is approximated using equation (7.6) as suggested in Koch (2010). ThOD_i, $i \in \{\text{pr}, \text{li}, \text{l}, \text{ch}\}$, denote the theoretical oxygen demand of protein, lipids, lignin and carbohydrates, respectively (Section 5.3.9).

$$\text{COD}_X \approx \rho_{IN} \cdot \text{TS}_{IN} \cdot \underbrace{\left(RP \cdot \text{ThOD}_{\text{pr}} + RL \cdot \text{ThOD}_{\text{li}} + ADL \cdot \text{ThOD}_{\text{l}} + (RF + NFE - ADL) \cdot \text{ThOD}_{\text{ch}} \right)}_{=: \overline{\text{VS}_{IN} \cdot \text{ThOD}}} \quad (7.6)$$

$=: \overline{\text{VS}_{IN} \cdot \text{ThOD}}$ used later in eq. (7.57)

In equation (7.6) the density of the substrate ρ_{IN} is needed, which is modeled in equation (7.7). Values for the needed single densities $\rho_{\text{pr}}, \rho_{\text{li}}, \dots$ to calculate the density

Table 7.3: Measured parameters for substrate feed characterization

Symbol	Description (... of/in substrate)	Unit	Method
TS _{IN}	total solids (Section 5.3.10)	% _{FM}	DIN EN 12880, DIN (2001a)
VS _{IN}	volatile solids (Section 5.3.11)	% _{TS}	DIN EN 12879, DIN (2001b)
RP	raw protein	% _{TS}	VDLUFA (1997) III 4.1.1
RL	raw lipids	% _{TS}	VDLUFA (1997) III 5.1.1
NDF	neutral detergent fiber	% _{TS}	VDLUFA (1997) III 6.5.1
ADF	acid detergent fiber	% _{TS}	VDLUFA (1997) III 6.5.2
ADL	acid detergent lignin	% _{TS}	VDLUFA (1997) III 6.5.3
pH _{IN} ∈ ℝ ⁺	pH value	—	DIN EN 12176, DIN (1998)
S _{nh4,IN} ⁺	ammonium value	mol _l ⁻¹	DIN 38406-5, DIN (1983)
TA _{IN}	total alkalinity	mmol _l ⁻¹	DIN 38409-7, DIN (2005)
T _{IN}	temperature	°C	DIN 38404-4, DIN (1976)
S _{va,IN}	valeric acid	g _l ⁻¹	gas chromatography (GC)
S _{bu,IN}	butyric acid	g _l ⁻¹	GC, BMU (2012b)
S _{pro,IN}	propionic acid	g _l ⁻¹	GC, BMU (2012b)
S _{ac,IN}	acetic acid	g _l ⁻¹	GC, BMU (2012b)
D _{VS} ∈ [0, 1]	degradation level	100 %	Koch et al. (2009)
k _{dis}	disintegration rate	1 _d ⁻¹	difficult to determine,
k _{hyd,ch}	hydrolysis rate carbohydrates	1 _d ⁻¹	see discussion in
k _{hyd,pr}	hydrolysis rate protein	1 _d ⁻¹	Astals et al. (2013) (k _{dis})
k _{hyd,li}	hydrolysis rate lipids	1 _d ⁻¹	and Batstone et al. (2009)
COD _{filtrate}	total COD of filtrate	kg _{COD} _m ³	DIN ISO 15705, DIN (2003)
S _{I,IN}	soluble inerts	kg _{COD} _m ³	Ince et al. (1998)
p _{IN}	substrate costs	€ _t ⁻¹	—

of the substrate ρ_{IN} , $[\rho_{IN}] = \frac{\text{kg}_{\text{FM}}}{\text{m}^3}$, can be found in Gerber (2009).

$$\rho_{IN} = TS_{IN} \cdot \left(RP \cdot \rho_{pr} + RL \cdot \rho_{li} + (RF + NfE) \cdot \rho_{ch} + \dots + (1 - VS_{IN}) \cdot \rho_{ash} \right) + (1 - TS_{IN}) \cdot \rho_{H_2O} \quad (7.7)$$

The raw fiber content RF of the substrate is not needed in this approach, because in all equations (e.g. eqs. (7.6) and (7.11)) only the sum RF + NfE is needed, which per definition (Table 7.2) is equal to VS_{IN} – RP – RL and thus can be calculated.

As Figure 7.4 visualizes, the total chemical oxygen demand COD_{total} of the substrate is split into disintegrated and non-disintegrated COD. The disintegrated chemical oxygen demand is approximated by the COD of the filtrate COD_{filtrate}, which contains the soluble COD as well. Soluble COD in the substrate is solely assumed to be existent in the form of the short chain fatty acids (SCFAs) S_{va,IN}, S_{bu,IN}, S_{pro,IN} and S_{ac,IN} as well as soluble inerts S_{I,IN}, which all have to be measured, see Table 7.3. The other soluble

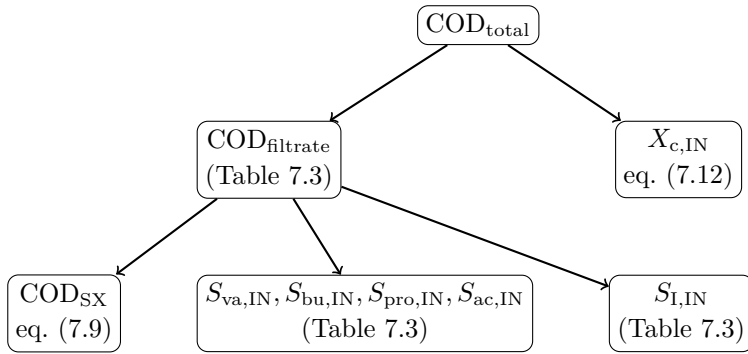


Figure 7.4: Fragmentation of total COD of substrate COD_{total}.

COD components are assumed to be zero, see equation (7.8).

$$S_{su,IN} = S_{aa,IN} = S_{fa,IN} = S_{h2,IN} = S_{ch4,IN} = 0 \frac{\text{kg}_{\text{COD}}}{\text{m}^3} \quad (7.8)$$

The disintegrated particulate COD, which is the disintegrated COD excluding the soluble COD, is symbolized by COD_{SX}, [COD_{SX}] = $\frac{\text{kg}_{\text{COD}}}{\text{m}^3}$, and given as

$$\text{COD}_{\text{SX}} \approx \text{COD}_{\text{filtrate}} - S_{va,IN} - S_{bu,IN} - S_{pro,IN} - S_{ac,IN} - S_{I,IN}. \quad (7.9)$$

COD_{SX} is used in equation (7.10) to calculate the COD fractions of carbohydrates, proteins and lipids.

$$\begin{aligned} X_{ch,IN} &= \frac{\text{COD}_{\text{SX}}}{f_{ch,Xc} + f_{pr,Xc} + f_{li,Xc}} \cdot (f_{ch,Xc} + f_{li,Xc} \cdot (1 - f_{fa,li})) \\ X_{pr,IN} &= \frac{\text{COD}_{\text{SX}}}{f_{ch,Xc} + f_{pr,Xc} + f_{li,Xc}} \cdot f_{pr,Xc} \\ X_{li,IN} &= \frac{\text{COD}_{\text{SX}}}{f_{ch,Xc} + f_{pr,Xc} + f_{li,Xc}} \cdot f_{li,Xc} \cdot f_{fa,li} \end{aligned} \quad (7.10)$$

In equation (7.10) the fractions given in equation (7.11)

$$\begin{aligned} f_{pr,Xc} &:= \frac{RP}{VS_{IN}} \in [0, 1] \\ f_{li,Xc} &:= \frac{RL}{VS_{IN}} \in [0, 1] \\ f_{ch,Xc} &:= \frac{(RF + NfE - NDF) + (NDF - ADL) \cdot d}{VS_{IN}} \in [0, 1] \\ f_{xi,Xc} &:= \frac{ADL + (NDF - ADL) \cdot (1 - d)}{VS_{IN}} \in [0, 1], \end{aligned} \quad (7.11)$$

$f_{fa,li} = 0.95$, $d = \frac{NDF - VS_{IN} \cdot (1 - D_{VS})}{NDF - ADL} \in [0, 1]$ and $f_{pr,Xc} + f_{li,Xc} + f_{ch,Xc} + f_{xi,Xc} = 1$ are used, Koch et al. (2010). The non-disintegrated part of the particulate chemical oxygen demand COD_X is modeled as the ADM1 input component $X_{c,IN}$ and is given

in equation (7.12).

$$X_{c,IN} = COD_X - COD_{SX} \quad (7.12)$$

The following particulate inputs are set to zero:

$$X_{I,IN} = X_{p,IN} = 0 \frac{\text{kg}_{\text{COD}}}{\text{m}^3}.$$

If the substrate is some sort of manure the biomass in the substrate is calculated as suggested in Lübken et al. (2007b) and subtracted from $X_{c,IN}$. The biomasses $X_{su,IN}$, $X_{aa,IN}$, $X_{fa,IN}$, $X_{c4,IN}$, $X_{pro,IN}$, $X_{ac,IN}$ and $X_{h2,IN}$ are set to equal ratios of the calculated values in Lübken et al. (2007b). If the substrate is not manure, then all mentioned biomass fractions are set to $0 \frac{\text{kg}_{\text{COD}}}{\text{m}^3}$.

The ionized SCFAs are set in eq. (7.13) by the acid/base equilibria using the measured acid concentrations and the dissociation constants $pK_{S_{va}}$, $pK_{S_{bu}}$, $pK_{S_{pro}}$ and $pK_{S_{ac}} \in \mathbb{R}^+$.

$$\begin{aligned} S_{va,IN}^- &= \frac{S_{va,IN}}{1 + 10^{pK_{S_{va}} - pH_{IN}}} & [S_{va,IN}^-] &= \frac{\text{kg}_{\text{COD}}}{\text{m}^3} \\ S_{bu,IN}^- &= \frac{S_{bu,IN}}{1 + 10^{pK_{S_{bu}} - pH_{IN}}} & [S_{bu,IN}^-] &= \frac{\text{kg}_{\text{COD}}}{\text{m}^3} \\ S_{pro,IN}^- &= \frac{S_{pro,IN}}{1 + 10^{pK_{S_{pro}} - pH_{IN}}} & [S_{pro,IN}^-] &= \frac{\text{kg}_{\text{COD}}}{\text{m}^3} \\ S_{ac,IN}^- &= \frac{S_{ac,IN}}{1 + 10^{pK_{S_{ac}} - pH_{IN}}} & [S_{ac,IN}^-] &= \frac{\text{kg}_{\text{COD}}}{\text{m}^3} \end{aligned} \quad (7.13)$$

7.2.2 Other Input Variables

The components of the input vector ${}^o\mathbf{u}_{AD}$ that are not measured in COD concentrations are modeled as follows. The input concentration of bicarbonate $S_{hco3,IN}^-$, $[S_{hco3,IN}^-] = \frac{\text{kmol}}{\text{m}^3}$, is calculated out of the measured total alkalinity value TA_{IN} according to equation (7.14), which comes directly out of the definition of the TA value in equation (7.61).

$$S_{hco3,IN}^- = TA_{IN} - S_{an,IN}^- - S_{ac,IN}^- - S_{pro,IN}^- - S_{bu,IN}^- - S_{va,IN}^- + S_{cat,IN}^+ \quad (7.14)$$

The soluble CO₂ concentration $S_{co2,IN}$ is calculated out of the acid/base equilibrium in equation (7.15), Berg et al. (2007).

$$S_{co2,IN} = 10^{6.3 - pH_{IN}} \cdot S_{hco3,IN}^- \quad [S_{co2,IN}] = \frac{\text{kmol}}{\text{m}^3} \quad (7.15)$$

The ammonia concentration $S_{nh3,IN}$ is calculated out of the measured ammonium value $S_{nh4,IN}^+$ using the ammonia/ammonium equilibrium, eq. (7.16) (Karlson et al., 2005).

$$S_{nh3,IN} = 10^{pH_{IN} - 9.25} \cdot S_{nh4,IN}^+ \quad [S_{nh3,IN}] = \frac{\text{kmol}}{\text{m}^3} \quad (7.16)$$

Finally, the input variables $S_{\text{cat,IN}}^+$ and $S_{\text{an,IN}}^-$ are set such that the pH value calculated from the input stream ${}^o\mathbf{u}_{\text{AD}}$ (see Section 7.3.3.3) is equal to the measured pH value pH_{IN} of the substrate (Kleerebezem and Van Loosdrecht, 2006).

7.3 Performance Indicators of Biogas Plants

Apart from the anaerobic digestion process, which is modeled by the ADM1, also energy related components such as CHPs and stirrer (Section 7.3.1), financial issues (Section 7.3.2) as well as other physical and chemical models (Section 7.3.3) are included in the biogas plant model. They are described in this section.

7.3.1 Energy

7.3.1.1 Electrical and Thermal Energy Production

The produced electrical P_{el} and thermal power P_{th} of a combined heat and power plant are modeled using the following two equations (7.17) and (7.18), respectively (cf. Gerber (2009)).

$$P_{\text{el}} = \eta_{\text{el}} \cdot h_{v,h} \cdot Q_{\text{gas}} \quad [P_{\text{el}}] = \frac{\text{kWh}}{\text{d}} \quad (7.17)$$

$$P_{\text{th}} = \eta_{\text{th}} \cdot h_{v,h} \cdot Q_{\text{gas}} \quad [P_{\text{th}}] = \frac{\text{kWh}}{\text{d}} \quad (7.18)$$

Values for the electrical η_{el} and thermal degree of efficiency η_{th} are found in data sheets of combined heat and power plants; $[\eta_{\text{el}}] = [\eta_{\text{th}}] = 100\%$. Both values must be given with respect to the higher heating value $h_{v,h}$, otherwise the lower heating value must be used in eqs. (7.17) and (7.18) instead. The volumetric flow rate of the produced biogas Q_{gas} is returned by the ADM1 (eq. (7.3)).

The higher heating value $h_{v,h}$ of the produced biogas is defined as the weighted sum of the higher heating values $h_{v,h,i}$ of the $i \in \{\text{h}_2, \text{ch}_4, \text{co}_2\}$ biogas components (eq. (7.19)) (DIN, 1997). The weights are given by the gas concentrations r_i (eq. (7.4)) of the i gas components.

$$h_{v,h} := \sum_{i \in \{\text{h}_2, \text{ch}_4, \text{co}_2\}} r_i \cdot h_{v,h,i} \quad [h_{v,h}] = \frac{\text{kWh}}{\text{m}^3}, \quad [r_i] \stackrel{!}{=} 100\% \quad (7.19)$$

7.3.1.2 Electrical Energy Consumption of Agitator

The mechanical power of an agitator P_{mix} needed to mix the content of a digester is calculated in equation (7.20) (Gerber, 2009). The agitator has a diameter d_{mix} , a rotation speed n_{mix} , $[n_{\text{mix}}] = \frac{1}{\text{s}}$, and the density of the sludge inside the digester is approximated by $\rho_{\text{digester}} \approx 1000 \frac{\text{kg}}{\text{m}^3}$.

$$P_{\text{mix}} = N_p \cdot \rho_{\text{digester}} \cdot n_{\text{mix}}^3 \cdot d_{\text{mix}}^5 \quad [P_{\text{mix}}] = \text{W} \quad (7.20)$$

There is a relation between the Newton (or power) number N_p and the Reynolds number Re , which can be determined using the characteristic curve of the agitator. For a stirred vessel the Reynolds number Re is defined in equation (7.21) with the effective viscosity η_{eff} (Gerber, 2009).

$$Re := \frac{\rho_{\text{digester}} \cdot n_{\text{mix}} \cdot d_{\text{mix}}^2}{\eta_{\text{eff}}} \quad [Re] = 100 \text{ \%} \quad (7.21)$$

For a total solids content TS inside the digester of 3 %_{FM} or higher the effective viscosity η_{eff} can be calculated using equation (7.22) (Gerber, 2009), $[n_{\text{mix}}] \stackrel{!}{=} \text{s}^{-1}$.

$$\eta_{\text{eff}} = \alpha_T \cdot K_c \cdot \left(\frac{11}{2 \cdot \pi} \cdot n_{\text{mix}} \right)^{n_{\text{flow}}-1} \cdot \left(\frac{3 \cdot n_{\text{flow}} + 1}{4 \cdot n_{\text{flow}}} \right)^{n_{\text{flow}}} \quad [\eta_{\text{eff}}] = \text{mPa} \cdot \text{s} \quad (7.22)$$

The consistency coefficient K_c , flow index n_{flow} and temperature correction α_T are given in equations (7.23) to (7.25) (Gerber, 2009). In these equations the TS content (see eq. (7.57)) and the temperature T inside the digester are used. The units in the three equations must be $[\text{TS}] \stackrel{!}{=} \%_{\text{FM}}$ and $[T] \stackrel{!}{=} {}^\circ\text{C}$.

$$K_c := C_{K_c,1} \cdot \exp(C_{K_c,2} \cdot \{\text{TS}\}) \quad [K_c] = \text{Pa} \cdot \text{s} \quad (7.23)$$

$$n_{\text{flow}} := C_{n_{\text{flow}},1} \cdot \exp(-C_{n_{\text{flow}},2} \cdot \{\text{TS}\}) \quad [n_{\text{flow}}] = 100 \text{ \%} \quad (7.24)$$

$$\alpha_T := C_{T,1} \cdot \exp(-C_{T,2} \cdot \{T\}) \quad [\alpha_T] = 100 \text{ \%} \quad (7.25)$$

Values for the substrate dependent coefficients $C_{K_c,1}, C_{K_c,2}, C_{n_{\text{flow}},1}, C_{n_{\text{flow}},2}, C_{T,1}$ and $C_{T,2}$ can be found in Türk (1994) and Gerber (2009).

If no characteristic curve for the given agitator is available, the Newton number N_p can also be calculated approximately out of the Reynolds number Re . According to Plank (1988) the following relations hold for the submersible agitator

$$N_p \approx \begin{cases} \frac{50}{Re} & 1 \leq Re < 3.1 \\ \frac{4}{[\log_{10}(Re)]^2} & 3.1 \leq Re \leq 2 \cdot 10^4 \end{cases} \quad [N_p] = 100 \text{ \%} \quad (7.26)$$

and the central mixer, both for using a baffle only,

$$N_p \approx \begin{cases} \frac{80}{Re} & 1 \leq Re < 40 \\ 2 & 40 \leq Re \leq 10^5 \end{cases} \quad [N_p] = 100 \text{ \%} \quad (7.27)$$

With the mechanical power P_{mix} of the agitator calculated in equation (7.20), the electrical power input of the stirrer P_{MIX} is then given by

$$P_{\text{MIX}} := \frac{P_{\text{mix}}}{\eta_{\text{mix}}} \cdot \tau_{\text{mix}} \quad [P_{\text{MIX}}] = \frac{\text{kWh}}{\text{d}} \quad (7.28)$$

with the electrical degree of efficiency for the stirrer η_{mix} , measured in 100 % and the runtime of the stirrer τ_{mix} , $[\tau_{\text{mix}}] = \frac{\text{h}}{\text{d}}$.

7.3.1.3 Dissipation Agitator

The power P_{diss} , which is dissipated by the stirrer inside the digester, is assumed to be equal to the mechanical power of the stirrer needed to mix the sludge inside the digester P_{mix} (eq. (7.20)), Gerber (2009).

$$P_{\text{diss}} = P_{\text{mix}} \cdot \tau_{\text{mix}} \quad [P_{\text{diss}}] = \frac{\text{kWh}}{\text{d}} \quad (7.29)$$

7.3.1.4 Electrical Energy Consumption of Substrate and Sludge Transport

Pumps The electrical power P_{pump} needed to pump a volumetric flow rate Q of liquid substrate or sludge is calculated in equation (7.30) (Gerber, 2009). There, the energy needed to lift the material by the geodetic head of the pump Δh_{geo} , $[\Delta h_{\text{geo}}] = \text{m}$, and to transport it by a distance l_{pipe} is calculated, assuming an electrical degree of efficiency of the pump η_{pump} , $[\eta_{\text{pump}}] = 100\%$. The density ρ of substrates is calculated as in equation (7.7) and the density of sludge is approximated with $\rho \approx 1000 \frac{\text{kg}}{\text{m}^3}$. g is the gravitational acceleration with $g \approx 9.81 \frac{\text{m}}{\text{s}^2}$.

$$P_{\text{pump}} = \frac{Q \cdot \rho}{\eta_{\text{pump}}} \cdot g \cdot \Delta h_{\text{geo}} + \frac{Q}{\eta_{\text{pump}}} \cdot \Delta p_{\text{L}} \quad [P_{\text{pump}}] = \frac{\text{kWh}}{\text{d}} \quad (7.30)$$

The pressure loss Δp_{L} in the pipe, with diameter d_{pipe} and length l_{pipe} , is calculated using the Darcy-Weisbach equation

$$\Delta p_{\text{L}} = \frac{\lambda_{\text{pipe}} \cdot \rho \cdot v_{\text{pipe}}^2 \cdot l_{\text{pipe}}}{2 \cdot d_{\text{pipe}}} \quad [\Delta p_{\text{L}}] = \text{Pa.} \quad (7.31)$$

The velocity of the medium in the pipe v_{pipe} is defined in equation (7.32) (Gerber, 2009).

$$v_{\text{pipe}} := \frac{4 \cdot Q}{\pi \cdot d_{\text{pipe}}^2} \quad [v_{\text{pipe}}] = \frac{\text{m}}{\text{s}} \quad (7.32)$$

The calculation of the pressure loss coefficient λ_{pipe} , $[\lambda_{\text{pipe}}] = 100\%$, depends on the Reynolds number Re_{pipe} , which for a stream in a pipe is defined in equation (7.33) using the effective viscosity of the medium in the pipe $\eta_{\text{eff,pipe}}$, eq. (7.35) (Gerber, 2009).

$$Re_{\text{pipe}} := \frac{v_{\text{pipe}} \cdot d_{\text{pipe}} \cdot \rho}{\eta_{\text{eff,pipe}}} \quad [Re_{\text{pipe}}] = 100\% \quad (7.33)$$

Using definition (7.33) and introducing the pipe roughness k_{pipe} , $[k_{\text{pipe}}] = \text{mm}$, the

pressure loss coefficient λ_{pipe} can be calculated in equation (7.34) (Türk, 1994).

$$\lambda_{\text{pipe}} \approx \begin{cases} \frac{64}{Re_{\text{pipe}}} & Re_{\text{pipe}} \leq 2300 \\ \left[\frac{0.25}{\log_{10} \left(\frac{Re_{\text{pipe}}^{15}}{Re_{\text{pipe}}} + 0.2692 \cdot \frac{k_{\text{pipe}}}{d_{\text{pipe}}} \right)} \right]^2 & 2300 < Re_{\text{pipe}} < 10^3 \cdot \frac{d_{\text{pipe}}}{k_{\text{pipe}}} \\ \left[\frac{0.25}{\log_{10} \left(3.715 \cdot \frac{d_{\text{pipe}}}{k_{\text{pipe}}} \right)} \right]^2 & Re_{\text{pipe}} \geq 10^3 \cdot \frac{d_{\text{pipe}}}{k_{\text{pipe}}} \end{cases} \quad (7.34)$$

The effective viscosity of the medium in the pipe $\eta_{\text{eff,pipe}}$, $[\eta_{\text{eff,pipe}}] = \text{Pa} \cdot \text{s}$, is approximated using equation (7.35) (Türk, 1994), $[\text{TS}] \stackrel{!}{=} \%_{\text{FM}}$, $[\dot{\gamma}] \stackrel{!}{=} \text{s}^{-1}$.

$$\eta_{\text{eff,pipe}} \approx \begin{cases} \eta_w + C_{\text{visc}} \cdot \{\text{TS}\} & \text{TS} < 3 \%_{\text{FM}} \\ K_c \cdot \left(\frac{3 \cdot n_{\text{flow}} + 1}{4 \cdot n_{\text{flow}}} \right)^{n_{\text{flow}}} \cdot \{\dot{\gamma}\}^{n_{\text{flow}} - 1} & 3 \%_{\text{FM}} \leq \text{TS} \leq 8 \%_{\text{FM}} \\ \frac{4 \cdot \tau_{\text{pipe}}}{\pi \cdot \dot{\gamma}} + K_c \cdot \left(\frac{\pi}{4} \cdot \{\dot{\gamma}\} \right)^{n_{\text{flow}} - 1} & \text{TS} > 8 \%_{\text{FM}} \end{cases} \quad (7.35)$$

The viscosity of water η_w , $[\eta_w] = \text{Pa} \cdot \text{s}$, is calculated as in Gerber (2009) using a polynom of fifth order, shear rate $\dot{\gamma}$ and shear stress τ_{pipe} are given in equation (7.36) and (7.37), respectively.

$$\dot{\gamma} := \frac{8 \cdot v_{\text{pipe}}}{d_{\text{pipe}}} \stackrel{(7.32)}{=} \frac{32 \cdot Q}{\pi \cdot d_{\text{pipe}}^3} \quad [\dot{\gamma}] = \frac{1}{\text{s}} \quad (7.36)$$

$$\tau_{\text{pipe}} := C_{\tau,1} \cdot \exp(C_{\tau,2} \cdot \{\text{TS}\}) \quad [\tau_{\text{pipe}}] = \text{Pa}, \quad [\text{TS}] \stackrel{!}{=} \%_{\text{FM}} \quad (7.37)$$

The equations to calculate K_c and n_{flow} are (7.23) and (7.24), respectively. Parameter values for C_{visc} , $C_{K_c,1}$, $C_{K_c,2}$, $C_{n_{\text{flow}},1}$, $C_{n_{\text{flow}},2}$, $C_{\tau,1}$ and $C_{\tau,2}$ for different substrates can be found in Türk (1994) and Gerber (2009).

Solids Supply The power P_{solids} needed to feed the biogas plant with solid substrates is calculated in equation (7.38) using the specific energy value p_{char} given in $\frac{\text{kWh}}{\text{t}}$, the volumetric flow rate of the solid substrates Q_{IN} and the density of the substrates ρ_{IN} , eq. (7.7).

$$P_{\text{solids}} = p_{\text{char}} \cdot Q_{\text{IN}} \cdot \rho_{\text{IN}} \quad [P_{\text{solids}}] = \frac{\text{kWh}}{\text{d}} \quad (7.38)$$

Values for the specific energy value p_{char} for typical solid supply units are given in Gerber (2009).

7.3.1.5 Heat Flux due to Substrate Feed

The volumetric flow rate of the substrate feed Q_{IN} with a temperature T_{IN} introduces a heat sink or source, depending on the digesters temperature T . In this thesis the simple approach, e.g. taken in Lübben et al. (2007b), is used to calculate the needed

(i.e. $T > T_{IN}$, respectively released) power $P_{substrate}$ in equation (7.39).

$$P_{substrate} = Q_{IN} \cdot \rho_{IN} \cdot c_{substrate} \cdot (T - T_{IN}) \quad [P_{substrate}] = \frac{\text{kWh}}{\text{d}} \quad (7.39)$$

The specific heat capacity of the substrates $c_{substrate}$ is calculated as in Gerber (2009), whose approach is of the same type as in eq. (7.7), $[c_{substrate}] = \frac{\text{kJ}}{\text{kg}\cdot\text{K}}$.

A more detailed approach is taken in Gerber (2009), which also incorporates the heat flux induced by the produced biogas and digestate leaving the digester.

7.3.1.6 Heat Loss through Digester Wall, Roof and Ground

The heat loss through the digester wall, roof and ground is calculated using three separate equations. The approach is similar to the approaches of Lindorfer et al. (2006), Lübken et al. (2007b) and the complex one in Gerber (2009). The radiation of the heat through the digester wall P_{wall} is calculated in equation (7.40) with the surface area of the cylindrical digester $A_{wall} = \pi \cdot d_{dig} \cdot h_{dig}$. Here d_{dig} and h_{dig} are the digester diameter and wall height, respectively, see Fig. 7.5.

$$P_{wall} = A_{wall} \cdot k_{wall} \cdot (T - T_{ambient}) \quad [P_{wall}] = \frac{\text{kWh}}{\text{d}} \quad (7.40)$$

In equation (7.40) the heat transfer coefficient of the wall k_{wall} and the ambient temperature $T_{ambient}$ are used.

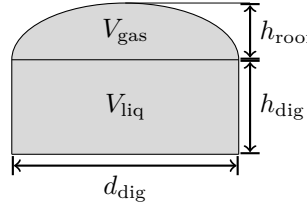


Figure 7.5: Schematic of a typical agricultural digester. h_{dig} and h_{roof} can be calculated using equations $V_{liq} = \pi \cdot \frac{d_{dig}^2}{4} \cdot h_{dig}$ and $V_{gas} = \frac{\pi}{6} \cdot h_{roof} \cdot (\frac{3}{4}d_{dig}^2 + h_{roof}^2)$, respectively.

The heat loss through the roof P_{roof} is calculated in equation (7.41), assuming a roof surface $A_{roof} = \pi \cdot \left(\frac{d_{dig}^2}{4} + h_{roof}^2 \right)$ (see Fig. 7.5) and the heat transfer coefficient of the roof k_{roof} .

$$P_{roof} = A_{roof} \cdot k_{roof} \cdot (T - T_{ambient}) \quad [P_{roof}] = \frac{\text{kWh}}{\text{d}} \quad (7.41)$$

The heat loss through the ground P_{ground} is calculated in equation (7.42) with the ground surface $A_{ground} = \pi \cdot \frac{d_{dig}^2}{4}$, the heat transfer coefficient of the ground k_{ground} and the ground temperature T_{ground} .

$$P_{ground} = A_{ground} \cdot k_{ground} \cdot (T - T_{ground}) \quad [P_{ground}] = \frac{\text{kWh}}{\text{d}} \quad (7.42)$$

Values for all heat transfer coefficients, measured in $\frac{\text{W}}{\text{m}^2 \cdot \text{K}}$, can be found in Gerber (2009).

7.3.1.7 Thermal Energy Production due to Microbial Activity

The thermal energy production $P_{\text{mic_heat}}$ due to microbial activity inside the anaerobic digester is calculated in equation (7.43) using the parameters in Tables 7.4 and 7.5, Lübken et al. (2007b).

$$P_{\text{mic_heat}} = \sum_{j=5}^{12} \Delta E_j \cdot f_j \cdot \rho_j \cdot V_{\text{liq}} \quad [P_{\text{mic_heat}}] = \frac{\text{kWh}}{\text{d}} \quad (7.43)$$

Table 7.4: Calculation of thermal energy production due to microbial activity

Symbol	Description	Unit
f_j^{-1}	g _{COD} of 1 mol of the educt of process j	$\frac{\text{g}_{\text{COD}}}{\text{mol}}$
ρ_j	kinetic rate of process j of ADM1, Section 7.1	$\frac{\text{kg}_{\text{COD}}}{\text{m}^3 \cdot \text{d}}$
V_{liq}	digester volume of liquid phase	m^3

Table 7.5: Values for energy released due to microbial activity ΔE_j (Lübken et al., 2007b)

j	Process	released energy ΔE_j , $[\Delta E_j] = \frac{\text{kJ}}{\text{mol}}$
5	uptake of sugars	-117.36
6	uptake of amino acids	-36.46
7	uptake of LCFA	494.88
8	uptake of valerate	89.99
9	uptake of butyrate	83.67
10	uptake of propionate	90.87
11	uptake of acetate	-27.34
12	uptake of hydrogen	-18.86

7.3.1.8 Others

The heat energy released to the digester by biological desulphurisation to reduce hydrogen sulphide in the gas phase by addition of fresh air is calculated in Lindorfer et al. (2006). Furthermore, oxygen, reacting in an exothermic reaction, is also fed to the digester together with the solid substrates, which is modeled in Lindorfer et al. (2006) as well. In Gebremedhin et al. (2005) solar radiation and in Wu and Bibeau (2006) a 3-d heat transfer model for an anaerobic digester are developed. Axaopoulos et al. (2001) combines solar collectors with an anaerobic digester.

7.3.1.9 Summary

To summarize the energy part 7.3.1 now follows what is done with the produced and consumed energy values.

The produced electrical energy per day P_{el} (eq. (7.17)) is injected into the local electricity grid, which is benefited financially on a kWh basis, see the next section on finance Section 7.3.2.

The consumed electrical energy per day

$$P_{\text{el,consume}} := P_{\text{MIX}} + P_{\text{pump}} + P_{\text{solids}} \quad [P_{\text{el,consume}}] = \frac{\text{kWh}}{\text{d}} \quad (7.44)$$

must be bought from the local energy provider (eqs. (7.28), (7.30) and (7.38)).

The daily thermal energy balance of a biogas plant ΔP_{th} , $[\Delta P_{\text{th}}] = \frac{\text{kWh}}{\text{d}}$, is calculated as follows (using eqs. (7.18), (7.29), (7.39), (7.40), (7.41), (7.42) and (7.43))

$$\Delta P_{\text{th}} := P_{\text{th}} + P_{\text{diss}} + P_{\text{mic_heat}} - P_{\text{substrate}} - (P_{\text{wall}} + P_{\text{roof}} + P_{\text{ground}}). \quad (7.45)$$

If ΔP_{th} is negative, then the remaining thermal energy must be produced by a heating with an efficiency η_{heat} , $[\eta_{\text{heat}}] = 100\%$. This is for example the case when the biogas plant has no CHP. If ΔP_{th} is positive, then the surplus thermal energy is assumed to be used externally for heating. This part of thermal energy gets either a real or a virtual financial value, such that it can be balanced with the financial value of the electrical energy and the substrate costs, see Section 7.3.2.

7.3.2 Finance

The profit obtained selling the produced electrical and thermal energy in Germany is determined by the Renewable Energy Sources Act - EEG, BMU (2012a). In the year 2000 the first version of the EEG came into force, with reissues in the years 2004, 2009 and 2012. Both EEG versions of 2009 and 2012 are implemented in the developed MATLAB® toolbox, see appendix Part B. They both have in common, that a basic remuneration for each produced kWh electric is paid. The value of the remuneration depends on the total electrical power of the plant and the year of construction. On top of the basic remuneration further payments are possible, which depend on criteria the biogas plant has to meet.

EEG 2009 In the EEG 2009 a bonus system defines the additional remuneration. The payment per electrical kWh is for example increased if the produced thermal energy is used as well, substrates taken from the preservation of the countryside are used and if at least thirty mass percent of the substrate feed is manure (manure bonus). For each fulfilled bonus the total remuneration is increased.

EEG 2012 In the EEG 2012 all bonuses were dropped, except for the bonus of gas preparation, which existed already in the EEG 2009. Instead of the bonuses, the additional remuneration became dependent on the fed substrates directly. All possible substrates are classified into three categories, whereas the categories are remunerated differently. If substrates from different substrate classes are used, then the proportionally produced amount of methane of each substrate defines the height of the remuneration. The EEG 2012 defines as precursor a minimal thermal energy usage of 35 %.

Profit The total profit of the produced electrical and thermal energy E_{plant} , $[E_{\text{plant}}] = \text{€}$, is calculated in the following simplified manner. The remuneration for the produced electrical energy (as calculated in EEG 2009 or 2012) is symbolized by r_{EEG} and costs for electrical energy by p_{el} , $[r_{\text{EEG}}] = [p_{\text{el}}] = \frac{\text{€}}{\text{kWh}_{\text{el}}}$. The virtual or real revenue of the produced thermal energy is denoted by r_{th} . If thermal energy is consumed instead, thus $\Delta P_{\text{th}} < 0$, the costs for producing the needed thermal energy shall be given by p_{th} , $[r_{\text{th}}] = [p_{\text{th}}] = \frac{\text{€}}{\text{kWh}_{\text{th}}}$. In the toolbox the financial profit is calculated as given in eq. (7.46) using eqs. (7.17), (7.44) and (7.45).

$$E_{\text{plant}} := \begin{cases} P_{\text{el}} \cdot r_{\text{EEG}} - P_{\text{el,consume}} \cdot p_{\text{el}} + \Delta P_{\text{th}} \cdot r_{\text{th}} - p_{\text{IN}} & \Delta P_{\text{th}} \geq 0 \\ P_{\text{el}} \cdot r_{\text{EEG}} - P_{\text{el,consume}} \cdot p_{\text{el}} + \Delta P_{\text{th}} \cdot \eta_{\text{heat}} \cdot p_{\text{th}} - p_{\text{IN}} & \Delta P_{\text{th}} < 0 \end{cases} \quad (7.46)$$

If more than one substrate is fed to the biogas plant the total substrate costs is a sum over all single substrate costs p_{IN} and has to be inserted in the equation instead. In the calculation of the profit all other costs such as man hours, credit rates, etc. are neglected, because they are seen as fix costs, which are independent of the substrate feed.

Although not explicitly stated, the profit E_{plant} is a function of the plant's state and substrate feed. So, in mathematical terms, $E_{\text{plant}} : \mathcal{X} \times \mathcal{U} \rightarrow \mathbb{R}$. The reason is, that e.g. the produced electrical power P_{el} depends on the state of the biogas plant, because the produced biogas Q_{gas} does (see eqs. (7.3) and (7.17)). Furthermore, the substrate costs p_{IN} are directly linked to the substrate feed. The profit E_{plant} is used in the definition of the objective function in Section 7.3.4.

7.3.3 Physics and Chemistry

7.3.3.1 COD Degradation Rate

The degradation rate of the COD, which is fed with the substrate (see Section 7.2), is a criteria used in the objective function. Both, total soluble COD and total particulate COD are investigated.

The total soluble COD concentration $SS_{COD,IN}$ fed to the digester is defined in equation (7.47). The components of the input vector ${}^o\mathbf{u}_{AD} := ({}^o u_{AD,1}, \dots, {}^o u_{AD,i}, \dots, {}^o u_{AD,34})^T$ are defined in equation (7.2).

$$SS_{COD,IN} := \sum_{i=1}^9 {}^o u_{AD,i} + S_{I,IN} \quad [SS_{COD,IN}] = \frac{\text{kg}_{COD}}{\text{m}^3} \quad (7.47)$$

The total soluble COD concentration flowing out of the digester and into the final storage tank is symbolized by $SS_{COD,FST}$, defined in equation (7.48) using the ADM1 state variables defined in eq. (7.2).

$$SS_{COD,FST} := \sum_{i=1}^9 {}^o x_{AD,i} + S_I \quad [SS_{COD,FST}] = \frac{\text{kg}_{COD}}{\text{m}^3} \quad (7.48)$$

The degradation rate of soluble COD is defined in equation (7.49) using the volumetric flow rate of the substrate feed Q_{IN} and the volumetric flow rate of the sludge flowing into the final storage tank Q_{FST} , both measured in $\frac{\text{m}^3}{\text{d}}$.

$$COD_{SS,degrade} := \frac{SS_{COD,FST} \cdot Q_{FST}}{SS_{COD,IN} \cdot Q_{IN}} \in [0, 1] \quad (7.49)$$

The total particulate COD of the substrate feed $VS_{COD,IN}$ is defined in eq. (7.50) and the particulate COD leaving the digester $VS_{COD,FST}$ is defined in eq. (7.51).

$$VS_{COD,IN} := \sum_{i=13}^{25} {}^o u_{AD,i} \quad [VS_{COD,IN}] = \frac{\text{kg}_{COD}}{\text{m}^3} \quad (7.50)$$

$$VS_{COD,FST} := \sum_{i=13}^{25} {}^o x_{AD,i} \quad [VS_{COD,FST}] = \frac{\text{kg}_{COD}}{\text{m}^3} \quad (7.51)$$

Again, the degradation rate of total particulate COD is defined in equation (7.52).

$$COD_{VS,degrade} := \frac{VS_{COD,FST} \cdot Q_{FST}}{VS_{COD,IN} \cdot Q_{IN}} \in [0, 1] \quad (7.52)$$

7.3.3.2 Faecal Bacteria Removal Capacity

In Lübken (2009), Lübken et al. (2007a) the removal capacity of anaerobic digestion for faecal bacteria is studied. Two models for two bacteria are proposed using multiple regression. In eq. (7.53) the removal capacity for intestinal enterococci η_{IE} and in eq. (7.54) the one for faecal coliforms η_{FC} is given.

$$\eta_{IE} = 98.29 - 2.2 \cdot \left(\frac{1}{\{HRT\}} \right)^2 + 0.031 \cdot \{T\} \quad [\eta_{IE}] = \% \quad (7.53)$$

$$\eta_{FC} = 98.29 - 1.0 \cdot \left(\frac{1}{\{HRT\}} \right)^2 + 0.031 \cdot \{T\} \quad [\eta_{FC}] = \% \quad (7.54)$$

As parameters the digester temperature T , $[T] \stackrel{!}{=} {}^{\circ}\text{C}$, and the hydraulic retention time HRT, $[\text{HRT}] \stackrel{!}{=} d$, are used.

7.3.3.3 The pH Value

The pH value is defined as the negative value of the common logarithm of the activity of hydrogen ions (Nielsen et al., 2008). Nevertheless, in ADM1 it is assumed, that the ion activity can be approximated with the concentration of the hydrogen ion $c(\text{H}^+)$, thus pH is calculated as:

$$\text{pH} \approx -\log_{10}(c(\text{H}^+)).$$

For a discussion on the validity of this assumption see Nielsen et al. (2008). Inside the digester (likewise in the substrate) the concentration of the hydrogen ion is calculated in equation (7.55) using the dissociation constant of water $K_w \in \mathbb{R}^+$ and the total alkalinity value TA defined in eq. (7.61) (Tschepeetzki and Oigurek, 2010). To calculate the pH value of the substrate the values TA_{IN} and $S_{\text{nh4,IN}}^+$ are used instead of TA and S_{nh4}^+ , respectively; $[\text{TA}] \stackrel{!}{=} [S_{\text{nh4}}^+] \stackrel{!}{=} \frac{\text{mol}}{1}$.

$$c(\text{H}^+) = \frac{\{\text{TA}\} - \{S_{\text{nh4}}^+\} + \sqrt{(-\{\text{TA}\} + \{S_{\text{nh4}}^+\})^2 + 4 \cdot K_w}}{2} \quad (7.55)$$

7.3.3.4 Propionic to Acetic Acid Concentration

There are indications, that the ratio of propionic to acetic acid in the digester is a good indicator to determine process instability (Hill et al., 1987, Marchaim and Krause, 1993). But there are also results that show that it is possible to have a stable process with high values of that ratio (Ahring et al., 1995, Pullammanappallil et al., 2001). Nevertheless, this criterion is included in the model and implemented as:

$$P/A := \frac{S_{\text{pro}}}{S_{\text{ac}}} \quad [S_{\text{pro}}] \stackrel{!}{=} [S_{\text{ac}}] \stackrel{!}{=} \frac{\text{mol}}{1} \quad (7.56)$$

7.3.3.5 Total Solids in Digester

Given the relation between the TS content TS_{IN} and the particulate chemical oxygen demand COD_X of a substrate in equation (7.6) the total solids content TS in the digester is approximated using equation (7.57). For the description of all parameters see Section 7.2.

$$\text{TS} \approx \text{ash} + \frac{\text{VS}_{\text{IN}}}{\rho_{\text{IN}}} \cdot \frac{1}{\text{VS}_{\text{IN}} \cdot \overline{\text{ThOD}}} \cdot \underbrace{\sum_{i=13}^{25} o_x_{\text{AD},i}}_{\stackrel{(7.51)}{=} \text{VS}_{\text{COD,FST}}} \quad [\text{TS}] = \%_{\text{FM}} \quad (7.57)$$

As for the estimation of the TS inside the digester substrate parameters are used, this clearly is only an approximation. To avoid confusion it should be claimed, that here the particulate COD inside the digester and not inside the final storage tank must be used. For the plant configuration assumed here, consisting out of only one digester, both values are the same.

7.3.3.6 Volatile Solids in Digester

The volatile solids content VS inside a digester is calculated out of the estimated TS content in the digester (see above, eq. (7.57)) and the ash content of the substrate feed. Assuming that the ash content inside the digester is the same as the one of the substrate feed, the volatile solids content VS inside the digester is given as in equation (7.58).

$$\{\text{VS}\} := 1 - \frac{\{\text{ash}\}}{\{\text{TS}\}} \quad [\text{ash}] \stackrel{!}{=} [\text{TS}] \stackrel{!}{=} \%_{\text{FM}}, \quad [\text{VS}] = 100 \%_{\text{TS}} \quad (7.58)$$

7.3.3.7 Volatile Solids Degradation Rate

The degradation rate of volatile solids during anaerobic digestion is calculated in equation (7.59), Koch (2010).

$$\text{VS}_{\text{degrade}} := 1 - \frac{\text{VS}_{\text{FST}} \cdot (1 - \{\text{VS}_{\text{IN}}\})}{(1 - \{\text{VS}_{\text{FST}}\}) \cdot \text{VS}_{\text{IN}}} \in [0, 1] \quad [\text{VS}_{\text{IN}}] \stackrel{!}{=} [\text{VS}_{\text{FST}}] \stackrel{!}{=} 100 \%_{\text{TS}} \quad (7.59)$$

The volatile solids content of the substrate feed VS_{IN} is measured in 100 %_{TS} as well as the volatile solids content entering the final storage tank VS_{FST}. In this scenario the latter is equal to the volatile solids content inside the digester as calculated in eq. (7.58).

7.3.3.8 VFA/TA Value

As proposed in Schoen et al. (2009) the VFA/TA value is modeled using the volatile fatty acids concentration VFA calculated in equation (7.60)

$$\text{VFA} := S_{\text{ac}} + S_{\text{pro}} + S_{\text{bu}} + S_{\text{va}} \quad [\text{VFA}] = \frac{\text{gHAc}_{\text{eq}}}{1} \quad (7.60)$$

and the total alkalinity value TA as calculated in eq. (7.61). The process values used in both calculations are defined in Table 7.1.

$$\text{TA} := S_{\text{an}}^- + S_{\text{hco}_3}^- + S_{\text{ac}}^- + S_{\text{pro}}^- + S_{\text{bu}}^- + S_{\text{va}}^- - S_{\text{cat}}^+ \quad [\text{TA}] = \frac{\text{gCaCO}_{3\text{eq}}}{1} \quad (7.61)$$

The VFA/TA := $\frac{\text{VFA}}{\text{TA}}$ is measured in $\frac{\text{gHAc}_{\text{eq}}}{\text{gCaCO}_{3\text{eq}}}$. The VFA/TA value is an important stability indicator for a biogas plant, which should be around $(0.15 - 0.45) \frac{\text{gHAc}_{\text{eq}}}{\text{gCaCO}_{3\text{eq}}}$ (Voßet al., 2009).

7.3.4 Objective Function

The objective function, once defined in equation (2.13), in this thesis is implemented as a two-dimensional function: $\mathbf{J} := (J_1, J_2)^T$, thus the number of objectives is $n_o = 2$. The objective function \mathbf{J} contains out of an integral over the stage cost $\mathbf{F} := (F_1, F_2)^T$ plus a terminal cost (also called terminal penalty term) $\mathbf{T}_{\text{penalty}} := (T_{\text{penalty},1}, T_{\text{penalty},2})^T$, e.g. see eq. (7.62).

The first component of the objective function J_1 ,

$$J_1 := \frac{1}{T_p} \cdot \int_{t_k}^{t_k + T_p} F_1(\tau) d\tau + T_{\text{penalty},1}, \quad (7.62)$$

is defined as the average of the negative financial profit E_{plant} (defined in eq. (7.46)) obtained by operating the biogas plant over the prediction horizon T_p , with

$$F_1(\tau) := -E_{\text{plant}}(^o\mathbf{x}(\tau), ^o\mathbf{u}(\tau)) \quad [F_1] = \frac{\epsilon}{1000}. \quad (7.63)$$

The minus sign in eq. (7.63) is added because the optimization problem in eq. (2.18) is formulated as a minimization problem. In eq. (7.62) the first component of the terminal cost $T_{\text{penalty},1}$ is used, which is defined as:

$$T_{\text{penalty},1} := \kappa_{T,1} \cdot F_1(t_k + T_p), \quad (7.64)$$

with the weighting factor $\kappa_{T,1} \in \mathbb{R}^+$.

The second component of the objective function J_2 ,

$$J_2 := \frac{1}{T_p} \cdot \int_{t_k}^{t_k + T_p} F_2(\tau) d\tau + \int_{t_k}^{t_k + T_p} \|{}^o\mathbf{u}'(\tau)\|_2^2 d\tau + T_{\text{penalty},2}, \quad (7.65)$$

contains a weighted sum of all $n_c \in \mathbb{N}_0$ constraints that are active over the prediction horizon, defined in the second component of the stage cost F_2 :

$$F_2(\tau) := \sum_{i_c=1}^{n_c} \kappa_{i_c} \cdot \text{constraint}_{i_c}({}^o\mathbf{x}(\tau), {}^o\mathbf{u}(\tau)) \quad [F_2] = 1. \quad (7.66)$$

Furthermore J_2 contains the integral over the change of the open loop control input ${}^o\mathbf{u}$ and the terminal penalty term $T_{\text{penalty},2}$ with the weighting factor $\kappa_{T,2} \in \mathbb{R}^+$:

$$T_{\text{penalty},2} := \kappa_{T,2} \cdot F_2(t_k + T_p) \quad (7.67)$$

In eq. (7.66) the weights $\kappa_{i_c} \in \mathbb{R}^+$ are normalized, $\sum_{i_c}^{n_c} \kappa_{i_c} = 1$, and the constraints are defined as:

$$\text{constraint}_{i_c} : \mathcal{X} \times \mathcal{U} \rightarrow \begin{cases} 0 & \text{if inactive} \\ 0 < \dots \leq 1 \text{ or } \frac{4.6851^2}{6} & \text{if active.} \end{cases} \quad (7.68)$$

Such that all constraints are smooth, some of the them are implemented using the Tukey biweight function $\rho_{\text{Ty}} : \mathbb{R} \rightarrow \mathbb{R}^+$, which is defined as, with $C_{\text{Ty}} := 4.6851$

(Comport et al., 2006):

$$\rho_{\text{Ty}}(u_{\text{Ty}}) := \begin{cases} \frac{C_{\text{Ty}}^2}{6} \left[1 - \left(1 - \left(\frac{u_{\text{Ty}}}{C_{\text{Ty}}} \right)^2 \right)^3 \right] & |u_{\text{Ty}}| \leq C_{\text{Ty}} \\ \frac{C_{\text{Ty}}^2}{6} & \text{else.} \end{cases} \quad (7.69)$$

In eq. (7.69) $u_{\text{Ty}} \in \mathbb{R}$ must be replaced by the difference between the constrained value and its constraint. An alternative to Tukey's biweight function could be to use Harrington's desirability function (Wagner and Trautmann, 2010). For all entries mentioned in Section 7.3.3 there exist one or two constraint definitions. The following list gives an overview:

- COD degradation rate: eqs. (7.49) and (7.52) are normalized soft constraints
- Faecal Bacteria Removal Capacity: using eqs. (7.53) and (7.54) normalized soft constraints can be stated
- pH value: lower and upper boundary as normalized hard constraint
- propionic to acetic acid concentration: upper boundary for equation (7.56) using equation (7.69)
- total solids in digester: upper boundary for eq. (7.57) using eq. (7.69)
- volatile solids degradation rate: lower boundary for equation (7.59) (not yet implemented)
- VFA/TA value: upper boundary using eq. (7.69)
- VFA: lower and upper boundary for eq. (7.60) using eq. (7.69)
- TA: lower boundary for eq. (7.61) using eq. (7.69)
- OLR: upper boundary for eq. (5.9) using eq. (7.69)
- HRT: lower and upper boundary for eq. (5.7) using eq. (7.69)
- sum of ammonia S_{nh_3} and ammonium $S_{\text{nh}_4}^+$: upper boundary using eq. (7.69)
- methane concentration in biogas: lower boundary using eq. (7.69)
- excess biogas: lost profit in 1000 €/d
- degree of utilization of CHPs: normalized soft constraint

As defined in eq. (2.19) the optimal substrate feed is determined by the minimum value of the scalar objective function, which is also called fitness,

$$J_{1D} := \sum_{i_o=1}^{n_o} \varpi_{i_o} \cdot J_{i_o} \stackrel{n_o=2}{=} \varpi_1 \cdot J_1 + \varpi_2 \cdot J_2. \quad (7.70)$$

In Chapter 9 also the one-dimensional stage cost F_{1D} will be needed:

$$F_{1D} := \sum_{i_o=1}^{n_o} \varpi_{i_o} \cdot F_{i_o} \stackrel{n_o=2}{=} \varpi_1 \cdot F_1 + \varpi_2 \cdot F_2. \quad (7.71)$$

In this thesis ecological criteria are not yet integrated in the objective function. Ecology of biogas plants is discussed in life cycle assessment (LCA), see e.g. (Berglund and

Börjesson, 2006, Cherubini and Strømman, 2011, Patterson et al., 2011).

7.4 Model Implementation of an Agricultural Biogas Plant

In the simulation experiments performed in Chapter 8 and Chapter 9 a model of a biogas plant is used. This model and the real plant are described here. The modeled biogas plant is a full-scale agricultural biogas plant with an electrical power of 500 kW, located in Germany. The plant is configured as a two-stage system with a primary (1st) ($V_{liq} = 1977 \text{ m}^3$) and a secondary (or post) digester ($V_{liq} = 4182 \text{ m}^3$), whereas the secondary digester also serves as final storage tank. A pumping station offers the possibility of interchanging sludge between both digesters. The first digester is mainly fed with maize silage, swine and cattle manure as well as varying substrates such as grass silage, corn-cob-mix (CCM) and whole crop silage (German: Ganzpflanzensilage - GPS). The secondary digester is not fed. The produced biogas is burned in two CHPs with an electrical power of 250 kW each. The produced power P_{el} is injected into the local grid, which is enumerated by the EEG 2009 (Section 7.3.2). Both digesters are heated with the thermal energy produced by the CHPs and are operated at about $T = 40 \text{ }^\circ\text{C}$ in the mesophilic temperature region. The biogas plant is fed based on the observed vs. the expected biogas production, but in an open loop fashion. The main target is to run the CHPs at full capacity. The produced biogas is analyzed online by a gas analysator, which measures CH_4 , CO_2 and H_2 .

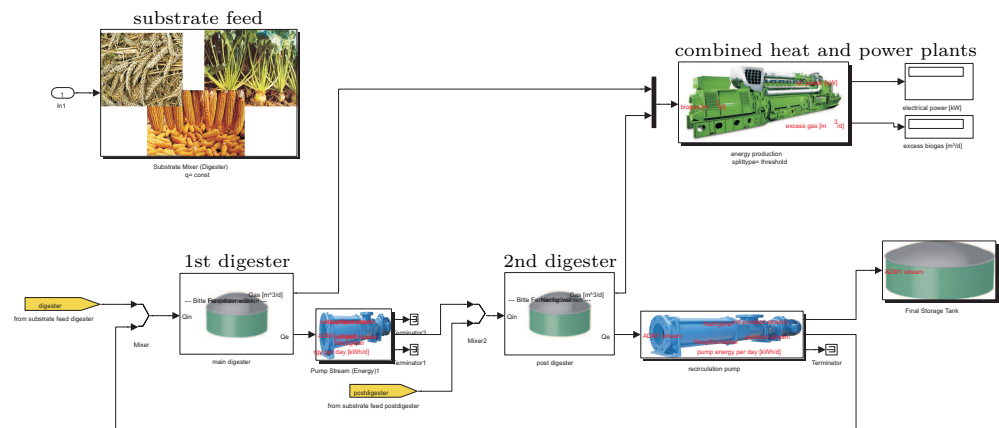


Figure 7.6: Model implementation of the agricultural biogas plant in Simulink[®].

The simulation model is implemented in MATLAB[®] in a self-developed toolbox which is used for all performed simulation experiments in this thesis. For more details about the toolbox see Part B of the appendix. The implementation of the biogas plant model

is depicted in Figure 7.6. One can see the two digesters, two pumps, one block for mixing the substrates and a block representing the two combined heat and power plants. The secondary digester is implemented by two separate blocks: the post digester block and the final storage tank block. All aspects that were discussed in this chapter are implemented in this model.

7.5 Model Calibration and Validation

To achieve reliable simulation results for the modeled biogas plant the most sensitive parameters of the ADM1 have to be calibrated. However, (Ogurek and Alex, 2013) points out that before calibration of parameters the model structure should be checked. E.g., if a large CSTR reactor is modeled it might be very valuable to model this reactor with more than one CSTR model, which are stacked vertically to model different layers in the real digester. To reduce complexity and computation time, in this thesis only one CSTR is used to model the real digester.

Sensitivity analyses for the ADM1 have been performed a lot, e.g. Jeong et al. (2005), Lee et al. (2009), Wichern et al. (2008) and Wolfsberger (2008). Model calibration can be done manually or be stated as an optimization problem as is e.g. done in Wenzel (2008) and Wichern et al. (2009). For a review see Donoso-Bravo et al. (2011).

The above described biogas plant model is calibrated manually based on offline and online measurements. Due to a limited budget the cost intensive offline measurements could not be taken into account for the validation period as well, so that validation was only possible based on online measurements. The calibration period ran from 22/11/2011 until 22/01/2012 followed by the validation period until 21/04/2012. At that time the plant was fed with maize silage, swine manure and partly corn-cob-mix and grass silage, see Figure 7.7. The parameters of these four substrates as is defined in Table 7.3 are listed in Table 7.6. The given parameter values are either determined by repetitive measurement of different substrate probes or estimated by using typical values for each individual substrate.

Model calibration was based on model parameters which either were connected to the substrates or associated with the digesters. The disintegration rate k_{dis} and the maximum uptake rates $k_{m,c4}$, $k_{m,pro}$, $k_{m,ac}$ and $k_{m,h2}$ are modeled to be substrate dependent and the half saturation coefficient for ammonia $K_{I,NH3}$ is linked to the digesters directly. All other ADM1 parameters are set to default values as given in Tschepetzki and Ogurek (2010), which can be found in Part C of the appendix. The maximum uptake rates were attached to the substrates because of their wide spectrum of values for an agricultural feedstock reported in the literature, e.g. Gehring et al. (2009), Girault et al. (2011), Koch et al. (2010), Wichern et al. (2007, 2008, 2009) and Wolfsberger (2008). Although a dependency of these parameters on the biogas plant's

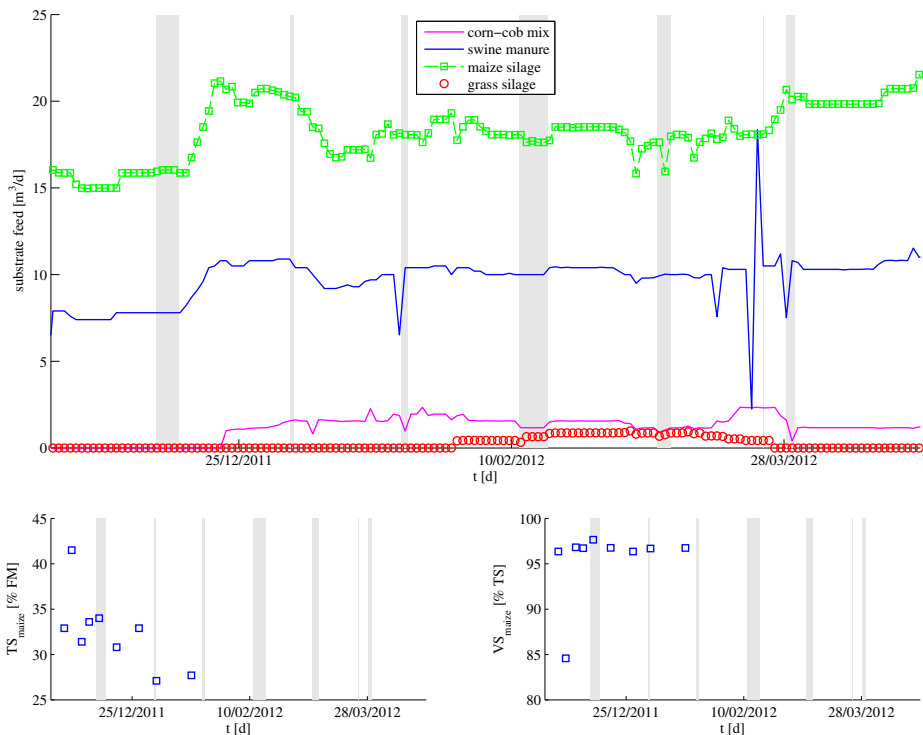


Figure 7.7: Top: Substrate feed of the full-scale biogas plant during calibration and validation. Bottom: Total solids (left) and volatile solids (right) of maize silage measured during the calibration period. Periods highlighted by the gray colored vertical bars symbolize times where no online data could be recorded.

state is more likely, without a model for this dependency the parameters can only be related to the substrates which on the other hand influence the digester's state. The calibrated values for the substrate dependent parameters are given in Table 7.7 and the value for the parameter K_{I,NH_3} was set to $0.0020 \frac{\text{kmolN}}{\text{m}^3}$ for the first digester and to $0.0011 \frac{\text{kmolN}}{\text{m}^3}$ for the second digester (default: $0.0018 \frac{\text{kmolN}}{\text{m}^3}$).

Calibration and validation results are depicted in Figure 7.8 for online measured variables and in Figure 7.9 for offline measured variables.

As can be seen in Figure 7.8 biogas and electrical energy production can be modeled quite reasonably. The reference signal for the biogas flow rate is not measured directly but calculated out of the differential of stored biogas in the gas chamber and consumed biogas in the CHPs. Therefore, the reference signal is quite noisy and error prone. The simulated electrical energy assumed a continuous operation of the CHPs. But, as can be seen in the reference signal of the electrical power, there are quite a lot of negative peaks in the data that signalize down times of either one of the two CHPs, e.g. due to maintenance.

Table 7.6: Measured parameters for substrate feed characterization.

parameter	maize silage	swine manure	corn-cob-mix	grass silage	unit
TS _{IN}	Fig. 7.7	6.1	67.6	34.1	%FM
VS _{IN}	Fig. 7.7	71.6	93.5	84.6	%TS
RP	8.69	16.31	10.54	17.5	%TS
RL	3.68	4.55	5.3	6.6	%TS
NDF	43.64	50.64	43.64	47.5	%TS
ADF	21.86	35.86	21.86	29.8	%TS
ADL	2.15	3.15	4.01	5.3	%TS
pH _{IN}	3.93	7.1	4.0	4.1	—
S _{nh4,IN} ⁺	0.66	4	0.55	1.5	g l ⁻¹
TA _{IN}	6	212.22	5.69	7.01	mmol l ⁻¹
T _{IN}	13	16.37	10	10	°C
S _{va,IN}	0	0	0	0	g l ⁻¹
S _{bu,IN}	0	0	0	0	g l ⁻¹
S _{pro,IN}	0	0.8	0.6	0	g l ⁻¹
S _{ac,IN}	1.18	12.43	3.5	1.53	g l ⁻¹
D _{VS}	0.8	0.95	0.95	0.75	100 %
k _{hyd,ch}	10	10	10	10	l d ⁻¹
k _{hyd,pr}	10	10	10	10	l d ⁻¹
k _{hyd,li}	10	10	10	10	l d ⁻¹
COD _{filtrate}	15.97	20	46.3	27.89	kg _{COD} m ⁻³
S _{I,IN}	13.03	7.3	35.3	22.89	kg _{COD} m ⁻³
p _{IN}	40	4	135	25	€ t ⁻¹

The measured methane content in the produced biogas is very noisy. Furthermore, the sensor seems not to be calibrated well. Although on 11/02/2012 the sensor was recalibrated, the simulated biogas and methane content shortly after that date cannot produce as much electrical power as was measured.

The level of hydrogen in the produced biogas can basically be modeled, but not their dynamics which often signalize process disturbances. E.g. the peak on 05/01/2012 was due to contaminated manure. As the contamination was not modeled the peak could not be represented in the simulation results.

The offline measured variables can essentially be modeled (see Figure 7.9). As the offline measurements are done in single probes taken out of the large digesters, it must be questioned whether the measured values are really of ground truth. Therefore, during calibration it is not tried to pay attention to each individual measurement, but more to

Table 7.7: Calibrated values of the substrate dependent ADM1 parameters. At the bottom of the table the default value (Tschepetzki and Oigurek, 2010) and a range of values found in the literature are given.

Substrate	k_{dis}	$k_{m,c4}$	$k_{m,\text{pro}}$	$k_{m,\text{ac}}$	$k_{m,h2}$
maize silage	0.14	20	3.8	4.8	35.9
swine manure	0.27	20	3.8	6.8	36.1
corn-cob mix	0.06	20	4	4.2	35.9
grass silage	0.04	20	8	4.9	35.6
default	0.5	20	13	8	35
range in literature	0.05 - 1.74	13.7 - 35	3.8 - 23.3	3.6 - 17.9	5 - 35

the general trend. In the beginning of the calibration period the VFA concentration in the post digester was quite high, even higher as in the first digester. This was due to the butyric acid concentration in the probe, which could not be modeled accurately in the beginning of the calibration period. The total alkalinity in the first digester was a little under-predicted and in the secondary digester a little over-predicted. Furthermore, the total solids content in the secondary digester is over-predicted. The measured pH values in both digesters are a bit higher as simulated.

In Figures 7.10 and 7.11 4-plot analyses (Fortuna et al., 2007) of the model residuals for biogas volumetric flow rate Q_{gas} and methane concentration r_{ch_4} are visualized. In the plots one can see whether the assumption is true that the obtained residuals are roughly normal, with a mean of 0 and some constant variance, and independently distributed². In the top left of a 4-plot analysis a run sequence plot is shown. In the plot it can be observed whether a time dependency does exist. In the run sequence plot of Figure 7.10 a shift in the lowest frequency can be seen. In the beginning it is much higher as in the end. In Figure 7.11 from around sample 190 onwards a shift and slow drift in location can be observed. The shift comes with the recalibration of the sensor. If the lag plot, top right, is structureless, then the randomness assumption holds. Especially in Figure 7.10 the lag plot shows a slightly linear structure, thus the randomness assumption does not hold here. In the histogram, bottom left, the distribution of the residuals can be studied. In both figures a normal distribution may be assumed, where as the one in Figure 7.10 has a too long tail in the direction of high residual values. In the right bottom corner of a 4-plot analysis a normal probability plot is shown. If all residuals lie on the visualized line, then they are normally distributed. This is especially true for the residuals in Figure 7.11.

Based on the presented validation results it can be seen how difficult it is to calibrate such a complex model to a full-scale biogas plant. The quality, amount and domain

²<http://www.itl.nist.gov/div898/handbook>

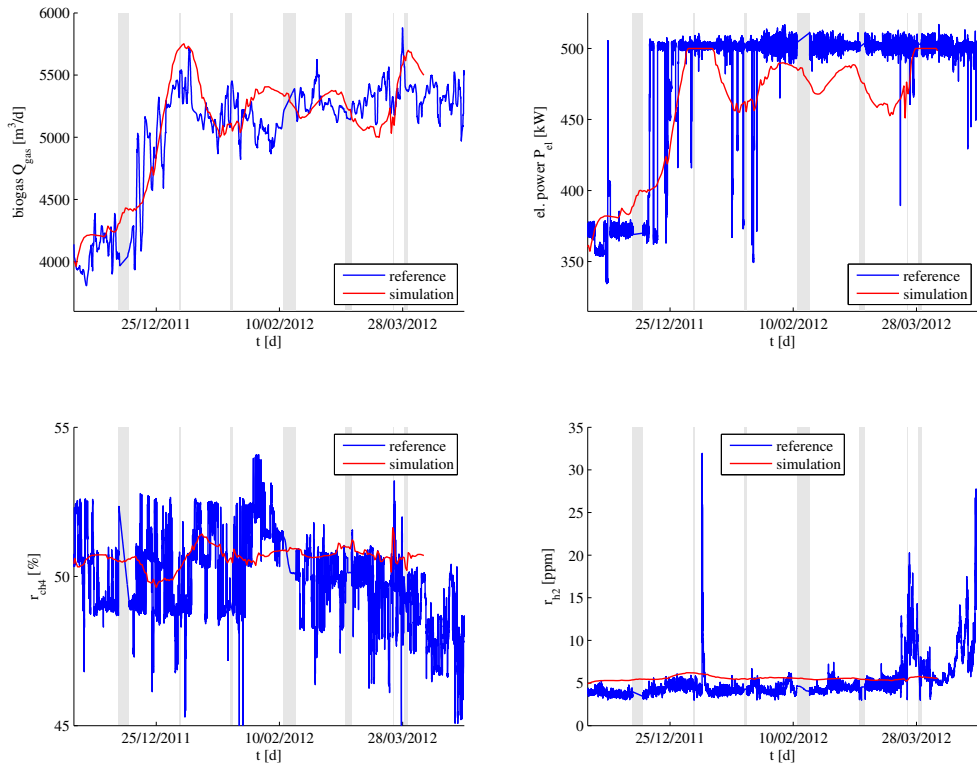


Figure 7.8: Calibration and validation results for the full-scale biogas plant: Online measurements. Top left: Biogas production Q_{gas} , top right: electrical power production P_{el} , bottom left: methane content r_{ch_4} in the produced biogas, bottom right: hydrogen content r_{h_2} in the produced biogas.

of the available online measurement data is often poor and probes not representative for the complete digester content. But there is no alternative to a complex gray box model. A simpler gray box model (created by omitting some equations) would be easier to calibrate, but would provide less information and a black box model would suffer even more from the insufficient data.

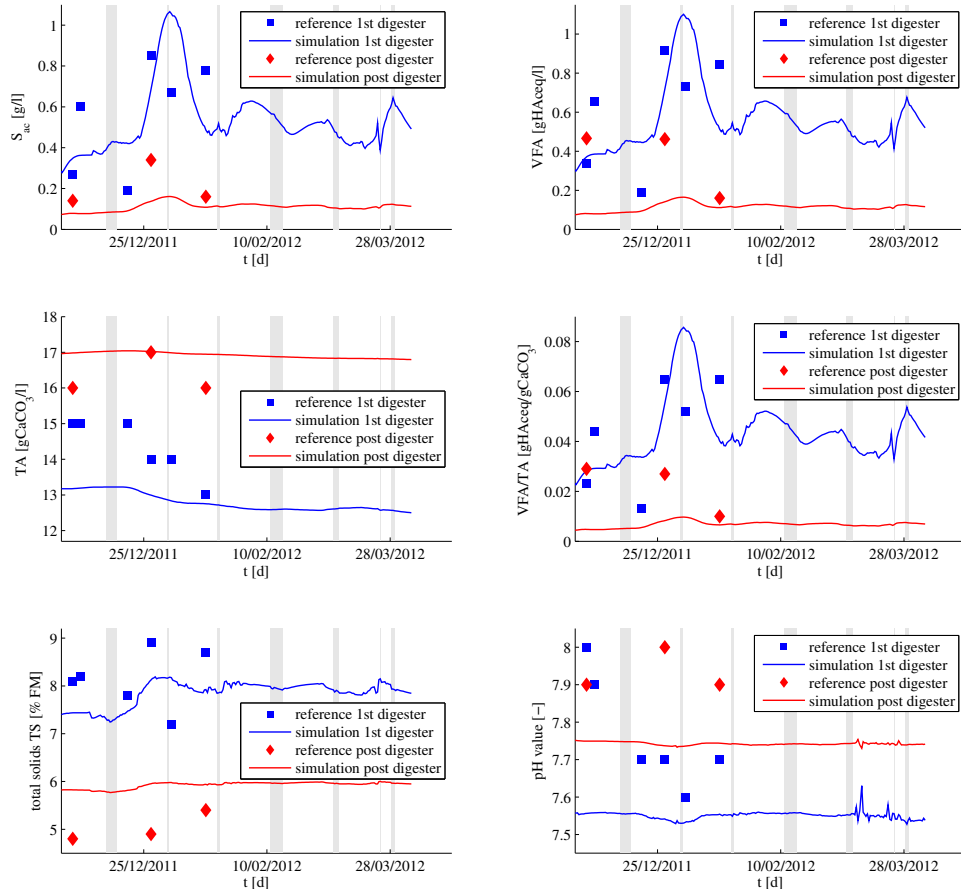


Figure 7.9: Calibration and validation results for the full-scale biogas plant: Offline measurements. Top left: acetic acid concentration S_{ac} , top right: volatile fatty acids VFA, middle left: total alkalinity TA, middle right: ratio of VFA to TA: VFA/TA, bottom left: total solids TS and bottom right: pH value

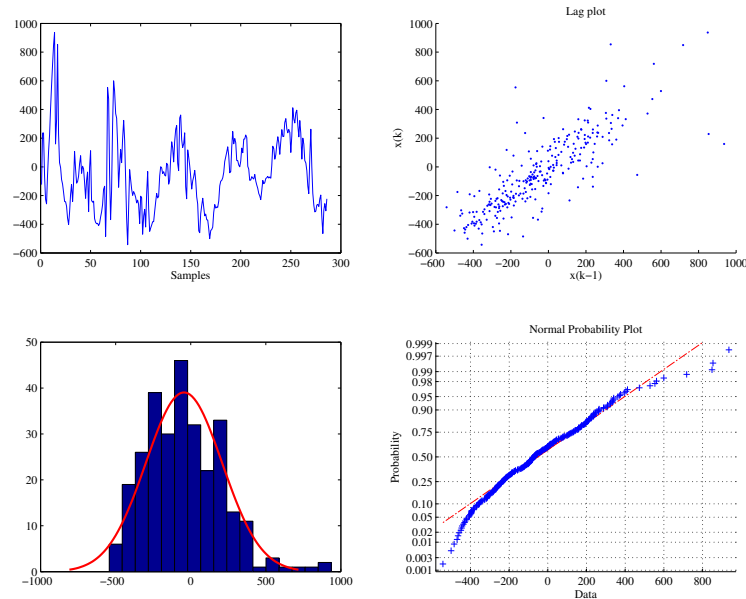


Figure 7.10: 4-plot analysis of model residuals for biogas flow rate Q_{gas} . In the lag plot $x(k)$ stands for the residual of the k th measurement.

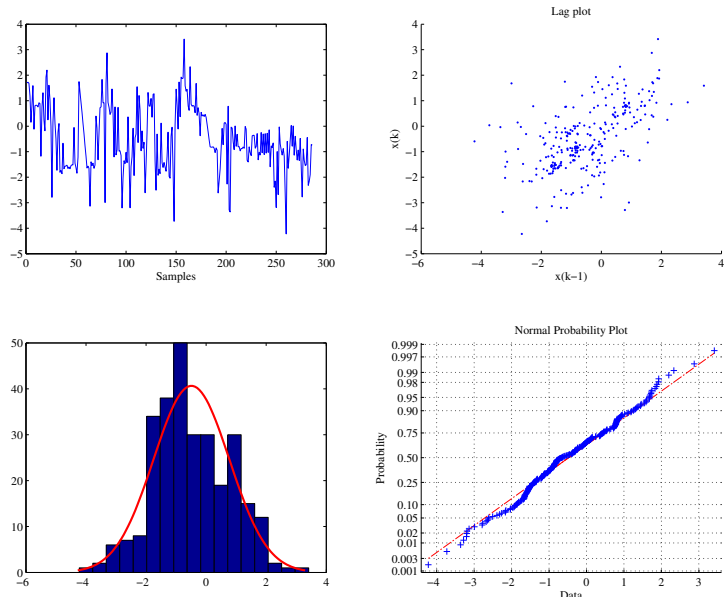


Figure 7.11: 4-plot analysis of model residuals for methane content $r_{\text{ch}4}$. In the lag plot $x(k)$ stands for the residual of the k th measurement.

7.6 Summary and Discussion

In this chapter the simulation model of the biogas plant was proposed. Regarding the different models of the anaerobic digestion process here a pretty standard implementation of the ADM1 was used. The review in Section 7.1.1 revealed that there are much more sophisticated modeling approaches that use the ADM1 as well. As the focus of this thesis is on model predictive control and not on model development, this standard solution was used. Nevertheless, in the context of this thesis all other advanced model approaches could be used as well. This also includes models for different reactor types such as the UASB reactor. Especially the approach in Zaher et al. (2009) seems to be very well suited when the plant is fed with different substrates.

Also other parts of the model could be extended. For example a model for a gas storage tank or for the ensilage process could be added to make the model more real.

Compared with the complexity of full-scale biogas plants the ADM1 with all its extensions still is only a very crude approximation. Examples of influences on the biogas production process that are not modeled but certainly have an impact are:

- The concentration of all substances inside the digesters is far from equally distributed as is assumed by the ADM1.
- Environmental parameters such as pressure, temperature and gas transfer are assumed to be constant in the digester. Stacking a few ADM1 blocks vertically with sludge recirculation between these layers gradients of these parameters can be modeled, see (Ogurek and Alex, 2013). That way also floating layers can be simulated which could be modeled reducing the gas transfer rate. In (Ogurek and Alex, 2013) it was shown that these parameters have a significant influence on parameters such as VFA/TA, pH and CO₂ concentration.
- The presence or absence of trace elements that are needed by the biomass in the digesters is neglected.
- Adaptation of biomass to environmental changes such as seasonal influences are not handled here, but will be important in the future, when waste as dominating feed substance will be used.
- Non-ideal mixing of substrates. Here, the substrates are modeled as ideally mixed. In practice they are not, because liquid and solid substrates are often fed separately. In Zaher et al. (2009) all fed substrates are hydrolyzed independently which might be a more realistic modeling approach. In (Ogurek and Alex, 2013) the disintegration step is modeled separately for each substrate.

All this makes it very difficult to calibrate the model reliably at hand of the available measurements. Based on the noisy data it is often difficult to see whether there is a certain modeled cause changing the data or if the cause is not modeled. In the latter case it appears to the observer that the measured effects might be generated by stochastic

variations.

This model is used in Part III of this thesis. On the one hand it is used to create and validate the state estimator in Chapter 8 and on the other hand it is used to evaluate the developed RTO scheme in Chapter 9.

Part III

Simulation & Optimization Studies

Introduction

In this part the main achievements of this thesis are presented. They are the dynamic real-time substrate feed optimization scheme for biogas plants and the state estimation method, which is a necessary part of the former.

As the dynamic real-time substrate feed optimization scheme uses the biogas plant simulation model presented in Section 7.4 for prediction, it needs the state vector of the biogas plant in each control sampling time. Unfortunately most of the state vector components of this model cannot be or are not measured on full-scale biogas plants.³ Therefore, the state estimator is needed, which estimates the state of the plant given past and present measurement data, see Section 4.1.

The developed dynamic real-time optimization scheme has a two-layer architecture (Adetola and Guay, 2010, Würth et al., 2011). The upper layer solves the optimization problem and proposes an optimal setpoint that the lower layer has to track. This structure has traditionally been used for economic optimization of chemical processes (Ellis and Christofides, 2014). Next to the two-layer architecture also an one-layer (De Souza et al., 2010) and a three-layer layout (Alves et al., 2010) are used for process optimization. The main advantage of the two-layer approach is that the real-time optimization problem and the setpoint tracking task can be solved in different time-scales. This allows to use very large models in the RTO and furthermore a two-layer architecture is more transparent for the plant operators, cf. Würth et al. (2011). A disadvantage of the two-layer approach is that the upper and lower layer often do not use the same model (here, the lower layer does not use a model at all) and therefore inconsistencies may arise (De Souza et al., 2010).

This third part of the thesis contains two chapters. In Chapter 8 estimation results of the state estimator developed in Chapter 4 applied to the simulation model out of Section 7.4 are presented.

In Chapter 9 numerous simulation and optimization experiments are performed for the dynamic RTO scheme. In these experiments the biogas plant model of Section 7.4 is optimally controlled. In some tests the state estimator from Chapter 8 is used. In all others an ideal state estimator is used instead.

³See Table 7.1 for the definition of the state vector of the ADM1.

Chapter 8

State Estimation of the Anaerobic Digestion Process

8.1 Introduction

The anaerobic digestion process depends on the population and vitality of different biomass species. Therefore, almost all dynamic models define the concentration of at least one biomass population in their state vector (at least all dynamic models reviewed in Gerber (2009) and Wolf (2013)). Although there are approaches to measure biomass concentration (Davey et al., 1993, Ferreira et al., 2005) on biogas plants it usually is not measured online yet. Therefore it has to be estimated. More complex models such as the ADM1 define many more state vector components (see Table 7.1) where most of them cannot be measured online as well or where measuring them on- or offline is too expensive, cf. Spanjers and van Lier (2006).

In this chapter (Sec. 8.2) the state estimator introduced in Section 4.1 is applied to the simulation model developed in Section 7.4. Similar results were also published in Gaida et al. (2012b) in the course of this thesis. The developed state estimator is needed in the optimal feed control introduced in Chapter 9. Simulation results of the control using the state estimator can be found in Section 9.3.6.

In the past various different state estimation methods were applied to anaerobic digestion processes. Among them are an observer based estimator based on a variable structure model (Morel et al., 2006a,b), a mass balance based estimator (Bernard et al., 2000), extended Kalman filter (Jones et al., 1989, 1992, Polster, 2009), robust interval observer (Montiel-Escobar et al., 2012), fuzzy estimator (Polit et al., 2001, Carlos-Hernandez et al., 2009), adaptive observer (Rodriguez et al., 2011) and recurrent neural networks observer (Urrego-Patarroyo et al., 2008). In Alcaraz-González and González-Álvarez (2007) an excellent review on observer design for anaerobic digestion processes is given.

8.2 State Estimation using Software Sensors

The state estimation approach introduced in Section 4.1, proposed to only use input values \mathbf{u} and output values \mathbf{y} of the anaerobic digestion process to estimate its state $\hat{\mathbf{x}}$ (see eq. (4.10)). Here, the time t dependent input vector function \mathbf{u} is defined by the volumetric flow rates $Q_{\text{substrate}}$ of the $n_u = 4$ available substrates, which are measured in $\frac{\text{m}^3}{\text{d}}$, that is

$$\mathbf{u} := (Q_{\text{maize}}, Q_{\text{manure}}, Q_{\text{grass}}, Q_{\text{ccm}})^T \quad (8.1)$$

It shall be assumed that the volumetric flow rates of these substrates are measured with a sampling rate of $\delta_u = 6$ h. The physical and chemical parameters of the substrates are assumed to be constant, so that the developed estimator only yields reliable results for substrate characteristics the estimator has learned during training.

The output vector function \mathbf{y} is composed of the simulated pH values inside the two digesters (pH_1, pH_2), the produced biogas volumetric flow rates ($Q_{\text{gas},1}, Q_{\text{gas},2}$) and the relative amount of methane and carbon dioxide ($r_{\text{ch}_4,1}, r_{\text{co}_2,1}, r_{\text{ch}_4,2}, r_{\text{co}_2,2}$) in the produced biogas (eq. (7.4)). Thus, in total there are $n_y = 8$ measurement variables, four for each digester:

$$\mathbf{y} := \left(\underbrace{\text{pH}_1, Q_{\text{gas},1}, r_{\text{ch}_4,1}, r_{\text{co}_2,1}}_{\text{primary digester}}, \underbrace{\text{pH}_2, Q_{\text{gas},2}, r_{\text{ch}_4,2}, r_{\text{co}_2,2}}_{\text{secondary digester}} \right)^T \quad (8.2)$$

These measurements are assumed to be measured with a sampling rate of $\delta_y = 6$ h as well.

It is important to note that output vector function \mathbf{y} and input vector function \mathbf{u} were chosen deliberately so that they contain process parameters, which are measured in practice on almost every biogas plant.

The current state estimate $\hat{\mathbf{x}}(t_k)$ is calculated out of the current input and output values as well as their moving averages, see eq. (4.10). The settings for the moving average filters are summarized in Table 8.1. It can be seen that $N_u = 5$ moving average filters for the inputs are used and $N_y = 7$ for the outputs.

Table 8.1: Settings of moving average filters for input and output values. For the definitions of the moving average filters see eqs. (4.6) and (4.8).

$N_u = 5$	$i_{\Lambda_u} = 1, \dots, N_u$	1	2	3	4	5	
	$w_{u,i_{\Lambda_u}}$	12 h	1 d	3 d	7 d	14 d	
$N_y = 7$	$i_{\Lambda_y} = 1, \dots, N_y$	1	2	3	4	5	6
	$w_{y,i_{\Lambda_y}}$	12 h	1 d	3 d	7 d	14 d	21 d
							31 d

To create the measurement matrix \mathbf{Y} in total 120 simulations each lasting 950 days

were performed with randomly varying substrate mixtures (defined by \mathbf{u}), leading to $N = 456,000$ samples (see eq. (4.11)). With the above defined numbers for N_u and N_y the second dimension of the matrix \mathbf{Y} is given as $D = 88$, see eq. (4.11).

The values of each substrate flow were restricted to remain between a lower and an upper bound as can be seen in the left part of Table 8.2. In the right section of Table 8.2 the resulting ranges of the measurement values \mathbf{y} are shown.

Table 8.2: Range of the measurement matrix \mathbf{Y} .

component	min	max	unit	component	min	max	unit
Q_{maize}	5.00	30.00	$\frac{\text{m}^3}{\text{d}}$	pH_1	7.28	7.72	—
Q_{manure}	5.00	40.00	$\frac{\text{m}^3}{\text{d}}$	$Q_{\text{gas},1}$	1,486.38	9,390.72	$\frac{\text{m}^3}{\text{d}}$
Q_{grass}	0.00	5.00	$\frac{\text{m}^3}{\text{d}}$	$r_{\text{ch}_4,1}$	45.67	56.59	%
Q_{ccm}	0.00	5.00	$\frac{\text{m}^3}{\text{d}}$	$r_{\text{co}_2,1}$	43.41	54.33	%
				pH_2	7.64	7.89	—
				$Q_{\text{gas},2}$	72.85	2,796.08	$\frac{\text{m}^3}{\text{d}}$
				$r_{\text{ch}_4,2}$	48.63	63.14	%
				$r_{\text{co}_2,2}$	36.86	51.37	%

To train and validate the supervised machine learning methods (see Section 4.1.1) in total five training and five validation datasets are created using 5-fold cross-validation. Each training dataset contains the data from 24 selected simulations and thus each validation dataset contains the data from the remaining 96 simulations.

As explained in Section 4.1.1 the estimation task is solved as classification problem. Therefore, the simulated state vectors \mathbf{X} are divided into $C = 10$ classes, see eq. (4.12). To measure the performance of the classification methods on the validation datasets the misclassification rate (MCR) is used as a performance measure. This measure is defined as:

$$\begin{aligned} \text{MCR} &:= 100 \cdot \left(1 - \frac{1}{N_V} \cdot \sum_{i=1}^{N_V} \Gamma(\mathbf{y}_i) \right), \quad \mathbf{Y}_V := (\mathbf{y}_1, \dots, \mathbf{y}_i, \dots, \mathbf{y}_{N_V})^T \\ \Gamma(\mathbf{y}_i) &:= \begin{cases} 1 & \text{if } \mathbf{y}_i \text{ classified correctly} \\ 0 & \text{otherwise} \end{cases} \end{aligned} \tag{8.3}$$

For this application in this thesis the two methods LDA and Random Forests are used (see Subsection 4.1.1.1 and Subsection 4.1.1.3). In the publication Gaida et al. (2012b) also the method GerDA (see Subsection 4.1.1.2) was used with very good results. Out of time and resource issues the method was not applied this time.

For LDA only the dimension of the projected feature space d has to be specified,

see Section 4.1.1.1. Here, an LDA transformation into a feature space of $d = C - 1$ dimensions led to the best subsequent linear classification results.

Random Forests was configured with 20 decision trees. Further parameters are set to default values as are given in the implementation of Jaintilal (2010).

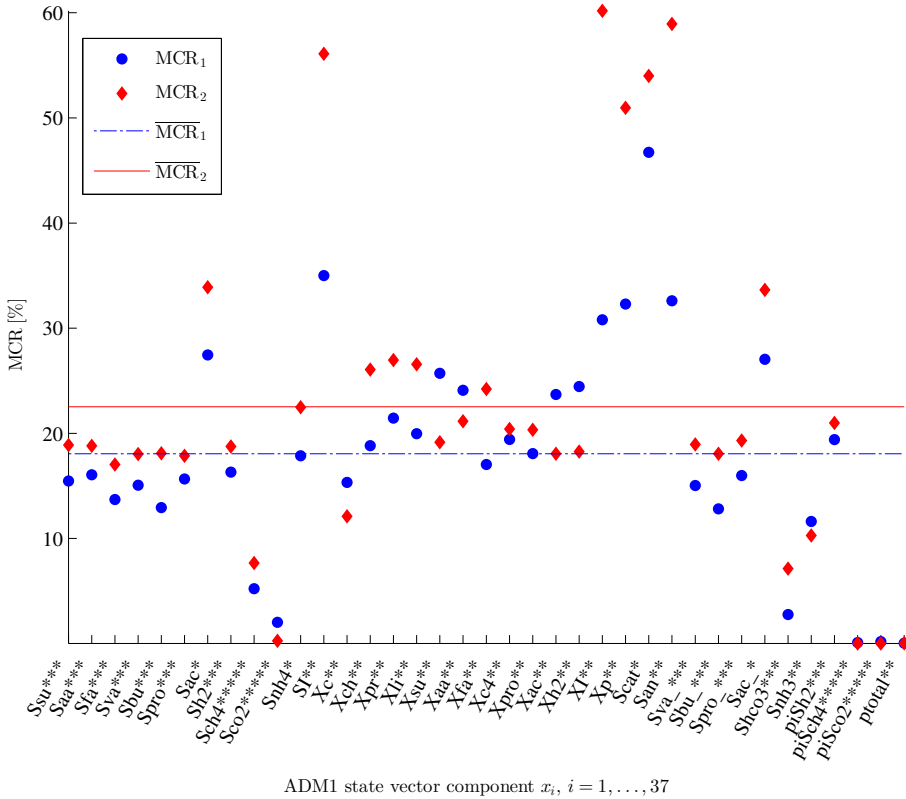


Figure 8.1: Comparison of the MCR of the state estimators for the two digesters using RF. The n_* stars (*) next to the x-axis labels signifies that for these state vector components only a $C - n_*$ classification problem was solved, due to insufficient data support for some of the classes. This was addressed by merging such classes with their neighbor class.

In Figure 8.1 the mean MCR obtained during the 5-fold cross-validation for both digesters is shown. Next to the results for each state vector component also the mean performance over all state vector components are visualized as straight lines. The state vector of the ADM1 is defined in Table 7.1. The symbols of the state vector components shown in Figure 8.1 are not exactly visualized the same way as they are in Table 7.1. But, as the state vector components are given in the same order the meaning of each symbol can be deduced.

A mean misclassification rate $\overline{\text{MCR}}$ of around 20 % as is visualized in Figure 8.1 is not

really satisfying. In Gaida et al. (2012b) better results could be obtained. The reason for the decrease in performance could be because in this thesis a more complex model is used as was used in Gaida et al. (2012b). Especially the connection of some kinetic parameters to the substrates (see Section 7.5) might lead to more severe non-linearities and worse predictability. Nevertheless, this accuracy is seen as good enough for its purpose. As will be seen in the next Chapter 9 it is recommended to perform predictions over 100 days or longer. The obtained state after 100 days depends largely on the substrate feed and only very loosely on the initial state. Therefore, the exact value of the initial state is not that important if one operates with large prediction horizons. As most biogas plants are operated in steady state, to work with a long prediction horizon is good practice. If a biogas plant is operated dynamically as it will be more often the case in the future the initial state becomes more important again. In that case, the question will be whether the state estimator's accuracy will be sufficient for dynamic plant operation. This question will not be answered in this thesis.

The average results for both methods LDA and Random Forests are given in Table 8.3. It can be seen that LDA yields very bad results, therefore it is not used any further for the state estimation task in this thesis. Applying LDA to the first 25 principal components, determined using principal component analysis (PCA), better results can be achieved, see Table 8.3. The application of Random Forests to the first 25 principal components yields worse results than using Random Forests directly on the raw data.

Table 8.3: Performance comparison of the state estimators on the investigated methods. MCR and $\bar{\sigma}_{\hat{x}}$ are the mean MCR (standard deviation, respectively) over all state vector components.

method	MCR ₁ ($\pm \bar{\sigma}_{\hat{x},1}$) [%]	MCR ₂ ($\pm \bar{\sigma}_{\hat{x},2}$) [%]
LDA	71.68 (± 13.53)	70.13 (± 19.33)
LDA & PCA	24.94 (± 12.56)	31.35 (± 17.54)
Random Forests	18.06 (± 10.31)	22.53 (± 15.76)

In Gaida et al. (2012b) further experiments were performed regarding number of moving average filters and estimator performance using noisy data.

8.3 Summary and Discussion

In this chapter it could be shown that the state estimation approach originally proposed in Section 4.1 is capable to estimate the state vector of the ADM1 with moderate accuracy. Whether the accuracy is sufficient will be investigated in the simulation studies in Section 9.3.6 of the next chapter. However, it should be mentioned that for practical use of this state estimator two challenges have to be dealt with. On the one hand, the state estimator depends on the simulation model of the biogas plant and on the other hand it depends on the characteristics of the fed substrates.

As the anaerobic digestion process changes and usually the substrates do not have constant parameters as well, the state estimator has to be retrained throughout. If the model is changed or recalibrated, also the machine learning method, here Random Forests, must be learned anew. To avoid spending the time for the full training process online learning methods that update the surrogate model based on new data might be an option. For Random Forests there are algorithms called online Random Forests, e.g. see (Osman, 2008, Saffari et al., 2009, Denil et al., 2013).

As measuring substrate parameters frequently is costly and elaborate, to estimate them instead or additionally is an interesting alternative. Especially for biogas plants operating on the OFMSW the input changes constantly so that substrate parameters must either be measured online or be estimated. There are a couple of publications focusing on input estimation for the anaerobic digestion process, e.g. see (Theilliol et al., 2003, Jáuregui-Medina et al., 2009).

Alternatives to state-based controls are controllers that use directly measurable variables with or without a data-driven model. In this case it is important to measure a combination of process values that lets the control identify the “state” of the process. Examples of that approach can e.g. be found in Boe et al. (2010), Castellano et al. (2007) and Molina et al. (2009).

Chapter 9

Dynamic Real-Time Substrate Feed Optimization of a Biogas Plant

9.1 Introduction

In Chapter 2 the MONMPC optimization problem was stated (eqs. (2.20) - (2.22)), whose eqs. are repeated here for convenience:

For each $k = 0, 1, 2, \dots$ set $t_k = k \cdot \delta$ and solve:

$$\begin{aligned} \mathcal{P}\mathcal{F}_k^* &:= \min_{\underline{\mathbf{u}} \in \mathcal{U}_{\mathcal{F}}} \mathbf{J}({}^o\mathbf{x}(\tau), \underline{\mathbf{u}}) \\ \text{subject to } {}^o\mathbf{x}'(\tau) &= \mathbf{f}({}^o\mathbf{x}(\tau), {}^o\mathbf{u}(\tau), \mathbf{0}), \quad {}^o\mathbf{x}(t_k) = \mathbf{x}(t_k), \quad (9.1) \\ {}^o\mathbf{x}(\tau) &\in \mathcal{X}, \quad \forall \tau \in [t_k, t_k + T_p], \\ {}^o\mathbf{u} : [t_k, t_k + T_p] &\rightarrow \mathcal{f}_{\mathcal{U}}(\underline{\mathbf{u}}), \end{aligned}$$

with equation (2.21)

$$\underline{\mathbf{u}}_k^* := \arg \min_{\forall \underline{\mathbf{u}} \in \mathcal{P}_k^*} \sum_{i_o=1}^{n_o} \varpi_{i_o} \cdot J_{\mathbf{x}, i_o}(\underline{\mathbf{u}}) \quad (9.2)$$

and application of equation (2.22)

$$\mathbf{u}(t) = {}^o\mathbf{u}_k^*(t) = \mathcal{f}_{\mathcal{U}}(\underline{\mathbf{u}}_k^*), \quad t \in [t_k, t_k + \delta]. \quad (9.3)$$

In this chapter MONMPC is applied to the simulation model of the biogas plant introduced in Section 7.4 in four performance experiments (I - IV), each containing various tests. The same simulation model is used as model \mathbf{f} inside the NMPC formulation. To take into account plant-model mismatch, measurement noise and errors is important during evaluation of the control. Therefore, for the controlled simulation model these effects are additionally implemented in some tests, see Section 9.3.2.

As objective function \mathbf{J} in eq. (9.1) the one defined in Section 7.3.4 is used. In experiment II and III this objective function is extended by an additional setpoint

control term, which is described in the according sections 9.3.4 and 9.3.5.

In all but the last experiment (IV, Section 9.3.6) the current state vector $\mathbf{x}(t_k)$ is directly taken out of the controlled simulation model. Thus, in experiments I to III a perfect state estimator is used. Only in experiment IV a real state estimation algorithm is used. There, some of the previous tests are repeated to see the deterioration of the quality of the results introduced by the state estimator out of Chapter 8.

Each input variable $u_{i_u,i}$, $i_u = 1, \dots, n_u$ and $i = 1, \dots, s_c$ (see eq. (2.9)) represents the volumetric flow rate of a substrate, measured in $\frac{m^3}{d}$. The i_u th input variable, $i_u = 1, \dots, n_u$, is bound between constant lower $LB_{i_u} \in \mathcal{U}_{i_u}$ and upper $UB_{i_u} \in \mathcal{U}_{i_u}$ boundaries, thus $LB_{i_u} \leq u_{i_u,i} \leq UB_{i_u}$ or equally $\mathcal{U}_{i_u} := [LB_{i_u}, UB_{i_u}]$. In experiment II both boundary vectors $\mathbf{LB} := (LB_1, \dots, LB_{i_u}, \dots, LB_{n_u})^T \in \mathcal{U}$ and $\mathbf{UB} := (UB_1, \dots, UB_{i_u}, \dots, UB_{n_u})^T \in \mathcal{U}$ depend on the available dynamically changing feed stock, see Section 9.3.4, in all other experiments they are constant.

9.2 Control Structure

In Figure 9.1 the complete control loop developed in this thesis is shown. It is dedicated to optimally control the substrate feed of anaerobic co-digestion plants. In this section the functionality and structure of the control loop is explained.

As pointed out in the summary of Chapter 2 (Section 2.4) offset-free control using model-based control does not come naturally. In case of plant-model mismatch there can be a steady-state offset because the control error is not directly minimized by the model-based control. To avoid such an offset a cascading control is developed, where the MONMPC is the master and a simpler setpoint control is the slave control. The slave control should track a directly measurable process value. Depending on the application this might be the produced volumetric methane flow rate Q_{ch_4} (for ABP) or the effluent VFA or COD (for anaerobic waste treatment plants), cf. Definitions 6.1 and 6.2 in Chapter 6. Note that online-measurement of effluent COD is expensive but possible using UV/Vis spectroscopy (Langergraber et al., 2004, Brito et al., 2013).

The setpoint (here it is assumed the methane setpoint $Q_{ch_4}^*(t)$) is set by the master loop containing the MONMPC, which is performing the real-time optimization. As process control a methane setpoint control can be used (e.g. (Hilgert et al., 2000, Antonelli et al., 2003)), which controls the dilution rate $D(t)$. The solution of the MONMPC optimization problem at time t_k is the optimal methane setpoint $Q_{ch_4}^*(t)$ as well as the corresponding optimal substrate feed ${}^o\mathbf{u}_k^*[t_k, t_k + \delta]$. Both are passed to the process control, see Figure 9.1. The process control changes the dilution rate $D(t)$ based on the given control error

$$e_{ch_4}(t) := Q_{ch_4}^*(t) - Q_{ch_4}(t). \quad (9.4)$$

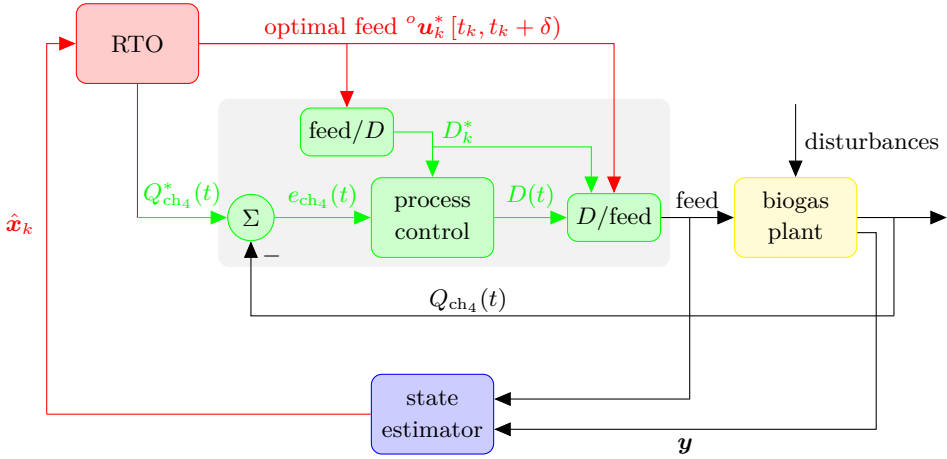


Figure 9.1: Real-Time Substrate Feed Optimization. The background colours of the blocks visualize where they are implemented. The green and yellow blocks are implemented in Simulink® for evaluation purposes. When the control should be applied to the real biogas plant, then the green blocks must be implemented in the PLC (programmable logic controller). The red block is always implemented in MATLAB® and the blue block is implemented in MATLAB® with optional usage of Simulink®.

Here the dilution rate $D(t)$ can be seen as a scaling factor which is only altered by the process control in case of model inaccuracies or process disturbances. The scaling is done in the “ D/feed ” block in Figure 9.1 where the given optimal substrate feed ${}^o\mathbf{u}_k^* [t_k, t_k + \delta]$ is scaled by $\frac{D(t)}{D_k^*}$, with the optimal dilution rate calculated in the “ feed/D ” block

$$D_k^* := \frac{\sum_{i_u=1}^{n_u} {}^o\mathbf{u}_{i_u,k}^* [t_k, t_k + \delta]}{V_{\text{liq}}}. \quad (9.5)$$

Then, the feed applied to the biogas plant \mathbf{u}_{ctrl} is given by:

$$\mathbf{u}_{\text{ctrl}}(t) := {}^o\mathbf{u}_k^* [t_k, t_k + \delta] \cdot \frac{D(t)}{D_k^*}. \quad (9.6)$$

The state estimator in Figure 9.1 is needed so that the dynamic model in the real-time optimization block knows the current state of the biogas plant. In practice the state \mathbf{x} is estimated by the state estimator given in Chapter 8. Using this control scheme the given setpoint is robustly controlled and the setpoint itself is set to guarantee stable and optimal control.

This control structure is used in all experiments, with the restriction that in all but the last experiment (Section 9.3.6) a perfect state estimator is used leading to the simplified structure visualized in Figure 9.2.

As process control the very simple approach of Antonelli et al. (2003) is used. It just

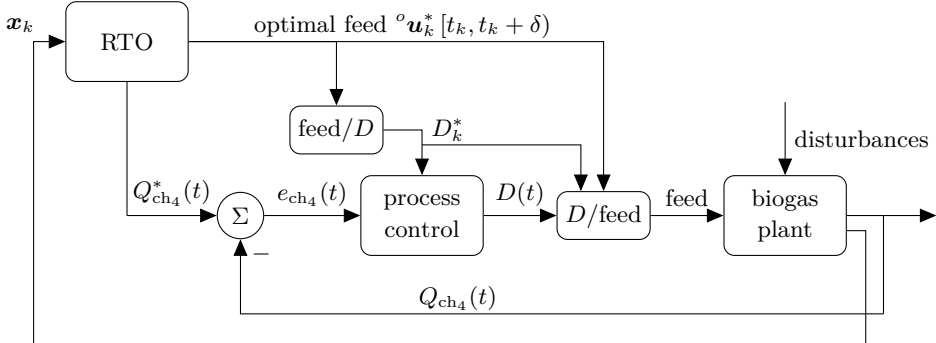


Figure 9.2: Real-Time Substrate Feed Optimization without State Estimator.

consists out of the one equation ($k_{\text{ch}_4} > 0$):

$$D'(t) = k_{\text{ch}_4} \cdot (Q_{\text{ch}_4}(t) - Q_{\text{ch}_4}^*(t)) \cdot (D(t) - D_{\max,k}) \cdot (D(t) - D_{\min,k}) \quad (9.7)$$

Here, the boundaries $D_{\min,k}$ and $D_{\max,k}$ are set according to ($\Delta D \geq 0 \frac{1}{d}$)

$$D_{\min,k} = D_k^* - \Delta D \quad \text{and} \quad D_{\max,k} = D_k^* + \Delta D \quad (9.8)$$

with the optimal dilution rate D_k^* determined by the real-time optimization, see eq. (9.5).

As this control has some limitations, in this thesis an extension is developed as follows. The factor k_{ch_4} of the original approach in eq. (9.7) is made dependent on the time derivative of the control error $e_{\text{ch}_4}(t)$. In the new approach k_{ch_4} must be replaced by the term given in equation (9.9), $k_{\text{ch}_4}, k_{\text{ch}_4,\text{rel}} > 0$.

$$k_{\text{ch}_4} + k_{\text{ch}_4,\text{rel}} \cdot [\min(e_{\text{ch}_4}(t), 0) \cdot \min(e'_{\text{ch}_4}(t), 0) + \max(e_{\text{ch}_4}(t), 0) \cdot \max(e'_{\text{ch}_4}(t), 0)] \quad (9.9)$$

Using this extension the original factor k_{ch_4} is increased if the signs of the control error $e_{\text{ch}_4}(t)$ and its derivative $e'_{\text{ch}_4}(t)$ are the same. Both signs are the same if the control error is negative and decreasing or positive and increasing, respectively. Both situations are not favorable, so that k_{ch_4} is increased to in-/decrease the dilution rate D faster. On the one hand this is advantageous, but on the other hand using the derivative of the control error $e'_{\text{ch}_4}(t)$ makes the control numerically more difficult. Furthermore, the derivative of the control error in reality can be rather noisy. Unfortunately, using this control in the Simulink® model of the modeled biogas plant did not work out because of numerical problems. Therefore, this control could not yet be tested at the simulation model. Nevertheless, it is planned to use it in the future to control the feed of a pilot-scale biogas plant and compare it with its original control by Antonelli et al. (2003).

9.3 Performance Experiments

In this section the results obtained in the four performance experiments

- Experiment I: Steady-state optimal feed (Section 9.3.3)
- Experiment II: Change of substrate mixture (Section 9.3.4)
- Experiment III: Setpoint control (Section 9.3.5)
- Experiment IV: State estimator (Section 9.3.6)

are presented and discussed. All four performance experiments are performed on three different computers. They are:

- Computer 1 (PC 1): Intel® Core™ i7-4770 CPU @ 3.40 GHz, 16.0 GB RAM, Windows 8, 64 bit
- Computer 2 (PC 2): Intel® Core™ i5-750 CPU @ 2.67 GHz, 4.0 GB RAM, Windows 7, 64 bit
- Computer 3 (PC 3): Intel® Core™2 Quad Q6600 CPU @ 2.40 GHz, 4.0 GB RAM, Windows 7, 64 bit

The obtained results are compared based on the fitness J_{1D} (7.70), one-dimensional stage cost F_{1D} (7.71), the hypervolume indicator I_H (Def. 3.1), the R2 (9.10) and Δ_p (9.13) indicator. The R2 indicator is defined in equation (9.10) (Trautmann et al., 2013).

$$R2 := \frac{1}{\text{card}(\mathcal{Q})} \sum_{\boldsymbol{\lambda} \in \mathcal{Q}} \min_{\boldsymbol{\varphi} \in \mathcal{PF}^*} \left\{ \max_{i_o=1, \dots, n_o} \{ \lambda_{i_o} \cdot (\varphi_{i_o} - i_{i_o}) \} \right\} \quad (9.10)$$

The R2 indicator of the Pareto front \mathcal{PF}^* with elements $\boldsymbol{\varphi} := (\varphi_1, \dots, \varphi_{n_o})^T \in \mathcal{PF}^*$ given in eq. (9.10) depends on the ideal point $\mathbf{i} := (i_1, \dots, i_{n_o})^T \in \mathbb{R}^{n_o}$ and weight vectors $\boldsymbol{\lambda} := (\lambda_1, \dots, \lambda_{n_o})^T \in \mathcal{Q}$ taken out of the set of weight vectors $\mathcal{Q} \subset \mathbb{R}^{n_o}$. In total 512 weight vectors $\boldsymbol{\lambda}$, $\|\boldsymbol{\lambda}\|_1 = 1$, are drawn from a normal distribution with mean 0.5 and standard deviation 0.2, bound between 0 and 1 and then each component λ_{i_o} is scaled by the corresponding weight ϖ_{i_o} (see eq. (2.19)). The normal distribution is favored over the uniform one, to concentrate more on the central points in the Pareto front that are much more likely to be chosen by the decision maker. The weights ϖ_{i_o} are set to $\varpi_1 = 0.125$ and $\varpi_2 = 1$.

The Δ_p indicator of an approximation set $\mathcal{A} \in \mathbb{R}^{n_o}$ for the Pareto front \mathcal{PF}^* is defined as in Schütze et al. (2012) using slightly modified versions of the generational distance GD_p (9.11) and inverted generational distance IGD_p (9.12) indicators, $p \in \mathbb{N}$.

$$GD_p(\mathcal{A}) := \left(\frac{1}{\text{card}(\mathcal{A})} \cdot \sum_{\mathbf{a}_A \in \mathcal{A}} \left(\inf_{\boldsymbol{\varphi} \in \mathcal{PF}^*} \|\mathbf{a}_A - \boldsymbol{\varphi}\|_2 \right)^p \right)^{\frac{1}{p}} \quad (9.11)$$

$$\text{IGD}_p(\mathcal{A}) := \left(\frac{1}{\text{card}(\mathcal{PF}^*)} \cdot \sum_{\varphi \in \mathcal{PF}^*} \left(\inf_{\mathbf{a}_{\mathcal{A}} \in \mathcal{A}} \|\mathbf{a}_{\mathcal{A}} - \varphi\|_2 \right)^p \right)^{\frac{1}{p}} \quad (9.12)$$

The Δ_p indicator is then given in eq. (9.13) (Schütze et al., 2012).

$$\Delta_p(\mathcal{A}) := \max(\text{GD}_p, \text{IGD}_p) \quad (9.13)$$

Here, $p = 1$ is selected, thus Δ_1 of the set \mathcal{A} is calculated. As the true Pareto front \mathcal{PF}^* often is not known, the Δ_p indicator must often be calculated against an optimal Pareto front approximation. Here, the one visualized in Figure 9.5 is used, see Section 9.3.3.2.

9.3.1 Implementation of Optimization Methods

To solve the minimization problem in eq. (9.1) three different optimization methods are evaluated in these experiments. The one most often used is the multi-objective method SMS-EGO. It is compared against the methods SMS-EMOA (see Section 3.1.1) and CMA-ES (Hansen, 2006). All algorithms are implemented in MATLAB®. The latter two methods (SMS-EMOA by Fabian Kretzschmar and Tobias Wagner and CMA-ES by Nikolaus Hansen) are freely available for download^{1,2}, whereas Tobias Wagner is greatly acknowledged for giving me the opportunity to use his MATLAB® implementation of SMS-EGO.

Both multi-objective optimization methods are configured (changed) so that they use the Pareto optimal set of the previous run at time t_{k-1} as initial points of the current run k . More precisely, for SMS-EMOA the complete previous population is used as initial population (not only the Pareto optimal set). For SMS-EGO at least five by Latin hypercube sampling (LHS) (Jin et al., 2005) selected individuals are used, the remaining initial points are taken out of the previous population starting with the Pareto optimal individuals. Furthermore, the optimal parameters of the previous DACE model are used as initial parameters for the DACE model used in the next run.

In the used CMA-ES implementation the previous population can not be used directly as initial population. Here, the best ever solution from the previous run $k-1$ is used to calculate the new population for the k th run.

9.3.1.1 Choice of Optimization Methods

The chosen optimization algorithms are all derivative-free and global methods. The question is why these methods are chosen and whether also algorithms could be chosen that do not possess these two properties.

¹<http://ls11-www.cs.uni-dortmund.de/rudolph/hypervolume/start>

²https://www.lri.fr/~hansen/cmaes_inmatlab.html

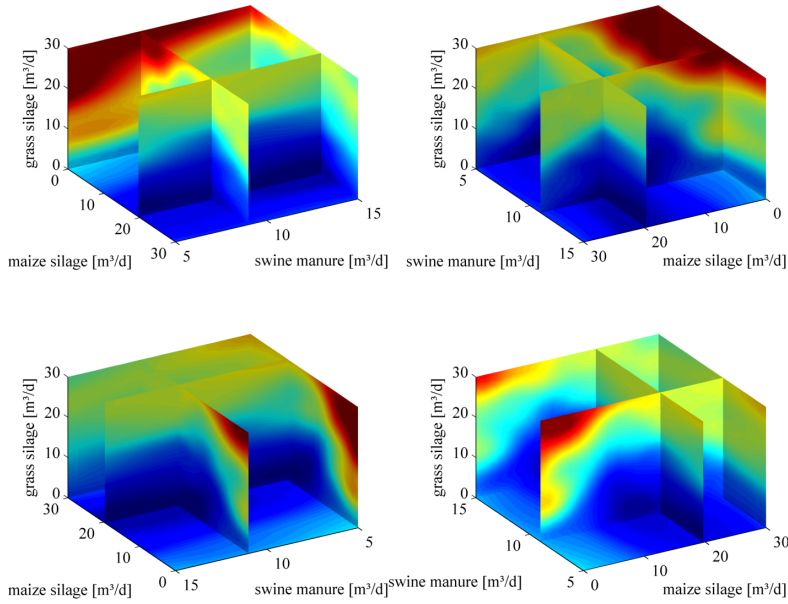


Figure 9.3: Landscape of one-dimensional steady-state stage cost F_{1D} . Each plot is created out of data taken from 1040 simulations, each simulation ran with a constant substrate feed taken from an equidistant distributed grid of substrate feeds. The interpolation of the data points is performed using a Kriging model.

As the objective function used here is quite complex, to determine the gradient of it with respect to the optimization variables analytically would be very difficult or even impossible. As the objective function contains some hard constraints it will not be possible to find a derivative for all components of the objective function. Therefore, derivative-free algorithms have a clear advantage here, because they do not need to know the gradient of the objective function.

Global optimization methods are used when the objective function possesses a lot of local optima. As local optimization algorithms easily get stuck in such local minima they are not suited for that kind of optimization problems. To get an idea whether the objective function used here has local optima the one-dimensional steady-state stage cost F_{1D} is plotted over the three substrates, which are used later during optimization. The results are depicted in Figure 9.3. It can be seen that the landscape is quite nonlinear but here there are not that many local minima. Therefore, it might be possible to also use derivative-free local optimization methods and obtain good results. An example could be to use the downhill simplex method by Nelder and Mead (1965). Therefore, as fourth optimization method MATLAB®'s fminsearchbnd algorithm is used that implements the simplex method of Lagarias et al. (1998).

Table 9.1: Miscalibrated values of substrate dependent ADM1 parameters to emulate plant-model mismatch. To be compared with Table 7.7, whose values are given here in brackets.

Substrate	k_{dis}	$k_{m,c4}$	$k_{m,\text{pro}}$	$k_{m,\text{ac}}$	$k_{m,h2}$
maize silage	0.1 (0.14)	20 (20)	4.0 (3.8)	5.0 (4.8)	35.0 (35.9)
swine manure	0.25 (0.27)	20 (20)	3.6 (3.8)	7.0 (6.8)	36.9 (36.1)
grass silage	0.09 (0.04)	20 (20)	7.7 (8)	4.6 (4.9)	36.1 (35.6)

9.3.2 Real World Simulation

To make the experiments as realistic as possible in some tests the model to be controlled is changed a little bit. In total, three changes are applied. First, to account for plant-model mismatch the ADM1 parameters calibrated in Section 7.5 are set to slightly different values, see Table 9.1. As second change the three parameters TS_{IN} , VS_{IN} and pH_{IN} of the substrates are made noisy as can be seen in Figure 9.4. Last, noise and drift are added to some measured variables, see the following list, using the sensor implementation of Rieger et al. (2003).

- sensor Q_{gas} : noise $\mathcal{N}\left(0 \frac{\text{m}^3}{\text{d}}, 32.5 \frac{\text{m}^3}{\text{d}}\right)$, drift of $0.5 \frac{\text{m}^3}{\text{d}}$, re-calibration after each 365 d
- sensor r_{ch_4} : noise $\mathcal{N}(0 \%, 0.5 \%)$, drift of 0.05 %, re-calibration after each 31 d
- sensor r_{co_2} : noise $\mathcal{N}(0 \%, 0.5 \%)$, drift of 0.05 %, re-calibration after each 31 d
- sensor pH: noise $\mathcal{N}(0, 0.07)$, drift of 0.01, re-calibration after each 14 d
- sensor Q_{IN} : noise $\mathcal{N}\left(0 \frac{\text{m}^3}{\text{d}}, 0.25 \frac{\text{m}^3}{\text{d}}\right)$, drift of $0.0 \frac{\text{m}^3}{\text{d}}$, re-calibration after each 365 d

Using these changes it is expected to create more realistic tests, so that the controller is optimally prepared for real world applications. Further realism could be added as in (Rosen et al., 2008). A process disturbance caused by fluctuations in the digester temperature is not modeled. The reason is that the stoichiometry of the implemented ADM1 is not temperature dependent yet. For a temperature dependent AD model see (Donoso-Bravo et al., 2013).

9.3.3 Experiment I: Steady-State Optimal Feed

In the first set of tests the biogas plant is in a stationary environment. The task is to find the optimal substrate feed for a steady-state operation which in the long run has the best performance. Therefore, in experiment I the following questions are tackled in different simulation studies:

1. Does MONMPC find the true Pareto front of the stage cost \mathbf{F} at steady state?
2. How large is the basin of attraction of the found Pareto front?
3. Is the closed loop control stable?
4. Can the results be repeated?

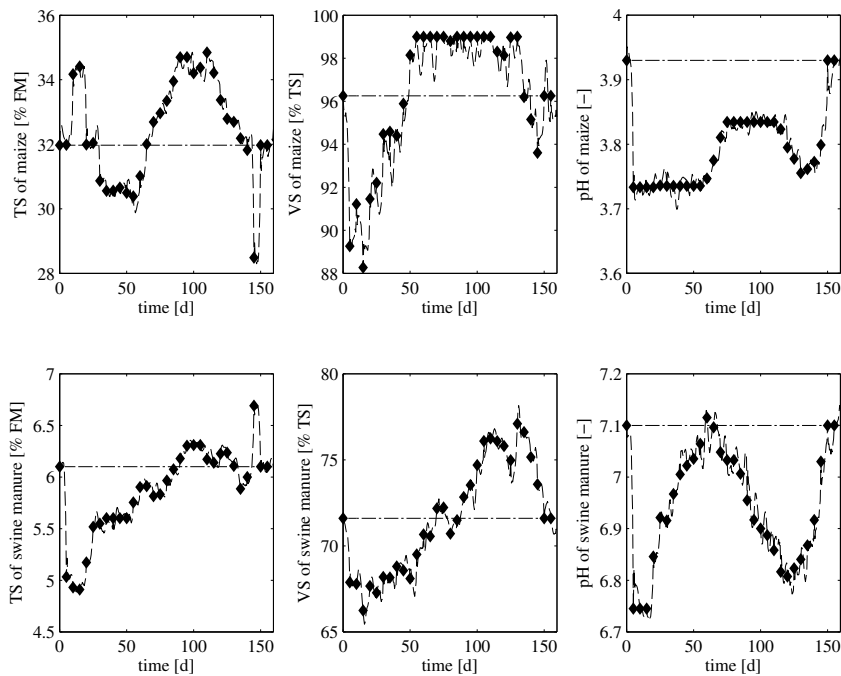


Figure 9.4: Noisy parameters TS_{IN} , VS_{IN} and pH_{IN} of the substrates maize silage and swine manure. The horizontal dash-dotted line in each plot visualizes the nominal value of the parameter used in the ideal world simulations. The diamonds show when offline analysis were done of the parameters, which is in a five day interval. The dashed, noisy curve shows the online measured values. The noise is drawn from a zero-mean normal distribution with 2 % error amplitude for TS_{IN} and VS_{IN} and 1 % for pH_{IN} .

9.3.3.1 Setup

Using simulation these questions cannot be answered conclusively. By designing well suited tests the questions can only be answered for the obtained results.

The first question is particularly difficult to answer. In the following the Pareto front of the stage cost \mathbf{F} at steady state is called steady-state Pareto front. Here, we search for the Pareto front of the stage cost \mathbf{F} and not of the objective function \mathbf{J} because we are only interested in the performance of a steady-state operation and not in the costs needed to get there. To determine the steady-state Pareto front, the only possible approach seems to be to compare the results obtained by the MONMPC with results gained by other multi-objective optimization methods which are applied in an open loop fashion, see eq. (9.14). In the optimization problem $t_{end} = 750$ d is seen as a long

enough simulation duration so that a steady state is reached.

$$\begin{aligned} \mathcal{P}\mathcal{F}_F^* := \min_{\underline{\mathbf{u}} \in \mathcal{U}_{\mathcal{F}}} \mathbf{F}({}^o\mathbf{x}(t_{\text{end}}), \underline{\mathbf{u}}) \\ \text{subject to } {}^o\mathbf{x}'(\tau) = \mathbf{f}({}^o\mathbf{x}(\tau), {}^o\mathbf{u}(0), \mathbf{0}), \quad {}^o\mathbf{x}(0) = \mathbf{x}(0), \\ {}^o\mathbf{x}(\tau) \in \mathcal{X}, \quad \forall \tau \in [0, t_{\text{end}}], \\ {}^o\mathbf{u} : [0, t_{\text{end}}] \rightarrow \mathcal{F}_{\mathcal{U}}(\underline{\mathbf{u}}), \quad s_c = 1. \end{aligned} \quad (9.14)$$

To study the second question the MONMPC is started at four different initial substrate feeds (see Table 9.2) to test whether the steady-state Pareto front is the same for all tests. Based on the obtained steady-state Pareto front, it can be concluded whether the corresponding substrate feed did or did not belong to the basin of attraction of the true steady-state Pareto front.

Stability of the closed loop is once investigated without noise, to test whether the control keeps the feed constant once the optimal steady state was found. This is to test whether the control is stationary. Furthermore, all experiments are repeated with measurement noise, drift and disturbances added to the controlled simulation model to examine the stability of the control towards such disturbances acting on the process.

Table 9.2: Initial substrate feeds and lower/upper boundaries (**LB**, **UB**) for substrates. The feeds of test I.A and I.C are moderate. The one of test I.B is very low and the one of test I.D is very high.

component	Test I.A	Test I.B	Test I.C	Test I.D	LB	UB	unit
Q_{maize}	15	5	40	85	0	30	m^3/d
Q_{manure}	10	5	30	85	5	15	m^3/d
Q_{grass}	2	0	10	45	0	30	m^3/d

To answer the last question some tests are repeated to get an estimate of the scattering in the results. This also applies to all other experiments performed further below in the other sections 9.3.4 - 9.3.6.

The effect of different parameters and configurations on the answers of above questions is investigated as well. They are:

- Optimization methods: Multi-objective as well as single-objective
- Algorithm parameters: Objective function \mathbf{J} evaluations $n_{\text{eval}} \in \mathbb{N}$ and initial population size $n_{\text{pop}} \in \mathbb{N}$
- Control parameters: Control horizon T_c , prediction horizon T_p and control sampling time δ

To avoid a combinatorial explosion not all parameters are changed at the same time. The parameter sets for all tests in experiment I are given in Table 9.3. All parameter sets are performed once for each initial substrate feed I.A to I.D. Therefore, the ID of a test in experiment I could be I.A5 or I.B2. In the first six tests in Table 9.3 the control

parameters prediction T_p and control horizon T_c are studied. As in experiment I the focus is on the steady-state solution the main emphasis is put here on the prediction horizon T_p (test I.1 until I.5) and only in test I.6 the control horizon T_c is changed. In all tests the control sampling time δ is set to the control horizon T_c , so that the substrate feed is only changed once over the control horizon ($s_c = 1$, see eq. (2.9)). The MATLAB® implementation in principle allows to choose $s_c > 1$ but as this increases the complexity of the optimization problem this option is not studied here. For more information about the implementation of this option and performance investigations see the Master's thesis of Venkatesan (2012). In tests I.7 to I.10 the effect of the number of simulations in each iteration n_{eval} is validated for the method SMS-EGO. In tests I.11 until I.14 and I.15 until I.18 two other optimization methods are evaluated. They are the multi-objective method SMS-EMOA and the single-objective method CMA-ES (see Section 9.3.1). Finally, in tests I.19 to I.21 the simplex method (fminsearchbnd) is used.

Table 9.3: Parameter sets for all tests in experiment I.

test no.	T_p [d]	T_c [d]	δ [d]	n_{pop}	n_{eval}	method
1	50	10	10	32	50	SMS-EGO
2	100	10	10	32	50	SMS-EGO
3	150	10	10	32	50	SMS-EGO
4	200	10	10	32	50	SMS-EGO
5	300	10	10	32	50	SMS-EGO
6	200	5	5	32	50	SMS-EGO
7	150	10	10	32	40	SMS-EGO
8	150	10	10	32	60	SMS-EGO
9	200	10	10	32	40	SMS-EGO
10	200	10	10	32	60	SMS-EGO
11	150	10	10	20	60	SMS-EMOA
12	150	10	10	25	75	SMS-EMOA
13	150	10	10	20	80	SMS-EMOA
14	150	10	10	30	90	SMS-EMOA
15	150	10	10	10	30	CMA-ES
16	150	10	10	15	45	CMA-ES
17	150	10	10	20	60	CMA-ES
18	150	10	10	20	80	CMA-ES
19	150	10	10	-	30	fminsearchbnd
20	150	10	10	-	40	fminsearchbnd
21	150	10	10	-	50	fminsearchbnd

The simulated control duration for all tests is kept constant and set to 150 days. This

should be enough time to find the optimal substrate feed and to maintain the feed at the optimum so that stationarity and stability can be examined.

As initial state vector $\mathbf{x}(t_0)$ the steady state corresponding to the initial substrate feed (see Table 9.2) is chosen. An exception is test I.D, because there the initial feed leads to the washout state (all biomass is washed out and therefore no biogas is produced anymore). So tests I.D are started in a transient state that is very close to a point of no return.

9.3.3.2 Results

Do we find the true steady-state Pareto front? From a practical point of view this question can be answered with yes. In Figure 9.5 the steady-state Pareto front resulting out of all performed tests in experiment I together with two extensive open loop optimization runs (SMS-EGO with $n_{\text{eval}} = 750$ and $n_{\text{eval}} = 900$, respectively) is shown. To make the MONMPC test results comparable to the results of the two optimization runs the steady-state Pareto front is determined by predicting the final Pareto optimal set of each MONMPC test for 600 days. As the simulated control duration of each test is 150 d, the total prediction horizon is 750 d and therefore equal to the prediction horizon of the two optimization tests, see eq. (9.14). In Figure 9.5 it can be seen that almost all simulation results are very close to the obtained steady-state Pareto front. However, looking at the performance of the MONMPC tests with respect to different parameters some differences can be observed, which are pointed out in the following.

In Figure 9.6 results for the tests I.A and I.C and in Figure 9.7 results for the tests I.B and I.D with respect to the prediction horizon T_p are visualized. The tests A/C and B/D are separated in two figures, because a different behavior can be observed for both groups. The lower boundaries (for the hypervolume indicator I_H upper boundary) of the plots are set to the optimal values gotten from the optimal Pareto front approximation shown in Figure 9.5. In the left plot of both figures the one-dimensional stage cost F_{1D} (see eq. (7.71)), obtained at the end of the 750 d long prediction, is shown. Note, that the obtained one-dimensional steady-state stage cost F_{1D} is the one the control really selects based on the information 150 d + T_p and not the one the control would select if it knows to which steady states all feeds in the final Pareto optimal set would lead (information: 750 d). Thus, the one-dimensional steady-state stage cost F_{1D} is not just the optimal one-dimensional criterion of the steady-state Pareto front. In both Figures 9.6 and 9.7 it can be seen that the one-dimensional steady-state stage cost F_{1D} improves with an increasing prediction horizon T_p , but only until a value for T_p of about 200 d. This seems about right, because the ones with a shorter prediction horizon are not foresighted enough and the ones with a larger T_p do not focus enough on the present situation. In the left plot of Figure 9.7 the disadvantage of a control

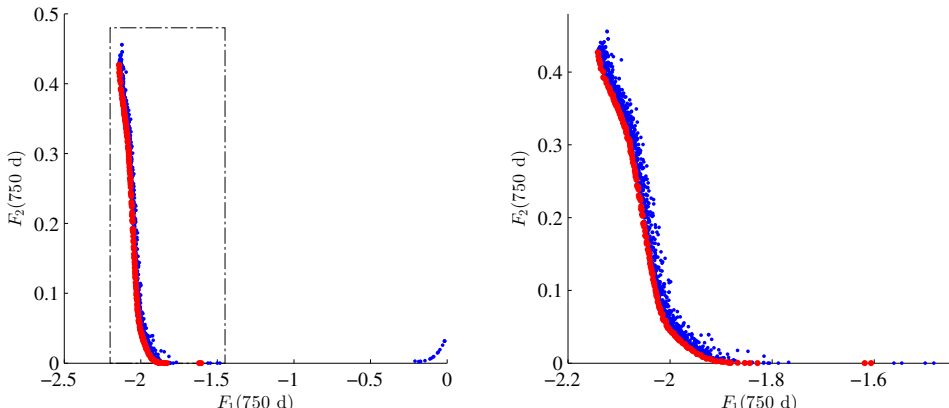


Figure 9.5: Optimal steady-state Pareto front approximation resulting out of all tests performed in experiment I. The blue dots belong to all experiments. The little bit larger red dots belong to the Pareto front of the set of all blue dots. Be aware that the steady-state Pareto front is not equal to the Pareto front of the final iteration of an MONMPC test. The first one is created out of the steady-state stage cost $\mathbf{F}(750 \text{ d})$, whereas the latter one out of the objective function \mathbf{J} evaluated at steady state: $\mathbf{J}(150 \text{ d} + T_p)$. The right plot is a zoom of the rectangular area in the left plot.

with a high prediction horizon T_p can be seen at the example of initial feed I.D. There, the biogas plant model crashes for $T_p = 300 \text{ d}$ (test I.D5), because the control chooses a feed that is successful only in the long run. This feed works inside the optimization problem, but due to numerical inaccuracies it does not work when it is applied to the model (or the real biogas plant)³. A crash of a biogas plant can easily be detected by a drop of pH value and methane production, see Figure 9.12.

This behavior of a biogas plant is also the reason why a dynamic model is used inside the RTO scheme and not a static model. As a static model does not consider the current state of the plant it will suggest feeds that will only be successful in the long run but that lead to a failure of the biogas plant before. Using a static model for prediction it is very likely that almost all tests in experiment I.D would have failed. For the other three experiments I.A to I.C a static model might be sufficient.

In the middle left part of Figures 9.6 and 9.7 the hypervolume indicator I_H (Def. 3.1) of both experiment pairs A/C and B/D is shown. In Figure 9.6 the hypervolume indicator I_H is quite large, independent of the prediction horizon T_p . In Figure 9.7 it can be observed, that the hypervolume indicator I_H increases with an increasing prediction horizon T_p with the only exception of test I.D5, see the previous discussion. This was to be expected, because the initial feeds A/C are quite near the optimal substrate feed where as to find the trajectory from the initial feeds B/D to the optimal one is much

³The optimization algorithm is not robust, see (Beyer and Sendhoff, 2006, Kruisselbrink, 2012) for robust optimization.

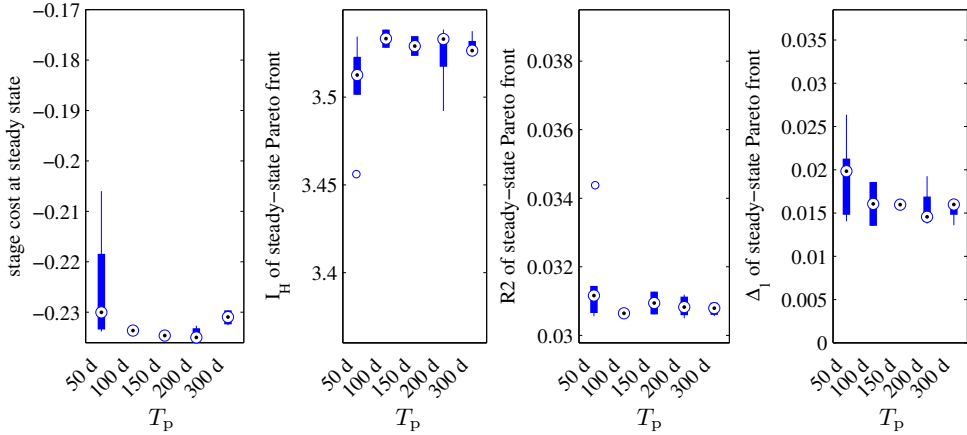


Figure 9.6: Dependency of the test results A/C on the prediction horizon T_p for the method SMS-EGO. Data from tests I.A1 until I.A5 and I.C1 until I.C5 are used. Therefore, the control horizon $T_c = 10$ d and the number of simulations $n_{\text{eval}} = 50$ are constant. Left: One-dimensional steady-state stage cost F_{1D} at day 750. Middle left: Hypervolume indicator I_H of the steady-state Pareto front. Middle right: R^2 indicator of the steady-state Pareto front. Right: Δ_1 indicator of the steady-state Pareto front.

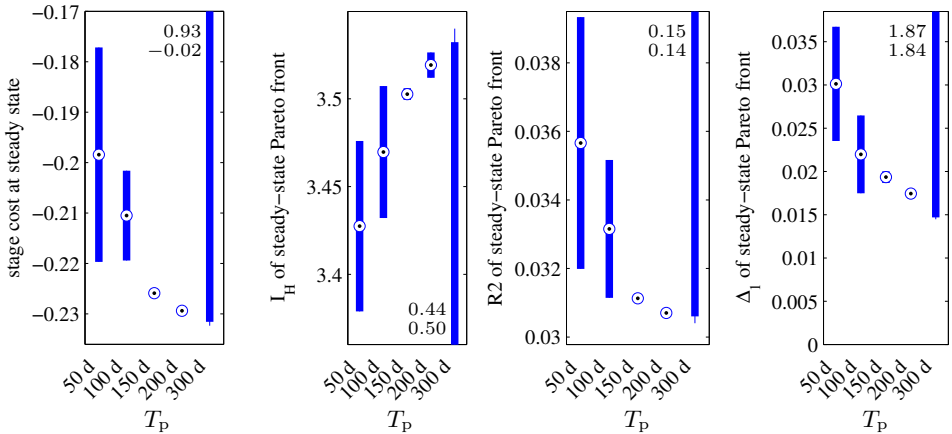


Figure 9.7: Dependency of the test results B/D on the prediction horizon T_p for the method SMS-EGO. This is the equivalent to Figure 9.6 for the tests I.B and I.D. Both tests I.D5, which is repeated once, lead to very poor results, which are outside the visualized region ($T_p = 300$ d).

harder and therefore more dependent on a proper choice of the prediction horizon T_p . The same is about true for the trends of the R^2 and Δ_1 indicator, shown in both Figures 9.6 and 9.7 middle right and right, respectively.

The comparison of the results for the optimization methods in Figure 9.8, based on the one-dimensional steady-state stage cost F_{1D} (left), shows that SMS-EGO performs significantly better than SMS-EMOA. This is in contrast to the values of F_{1D} in

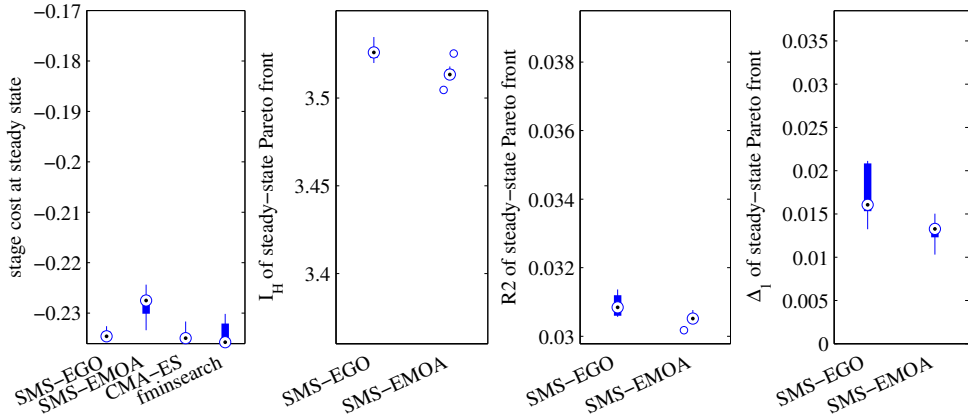


Figure 9.8: Dependency of the test results A/C on the optimization method. Data from tests I.A3, I.A7, I.A8 and I.A11 until I.A21 as well as I.C3, I.C7, I.C8 and I.C11 until I.C21 are used. In these plots prediction horizon $T_p = 150$ d and control horizon $T_c = 10$ d. Left: One-dimensional steady-state stage cost F_{1D} at day 750. Middle left: Hypervolume indicator I_H of the steady-state Pareto front. Middle right: R2 indicator of the steady-state Pareto front. Right: Δ_1 indicator of the steady-state Pareto front.

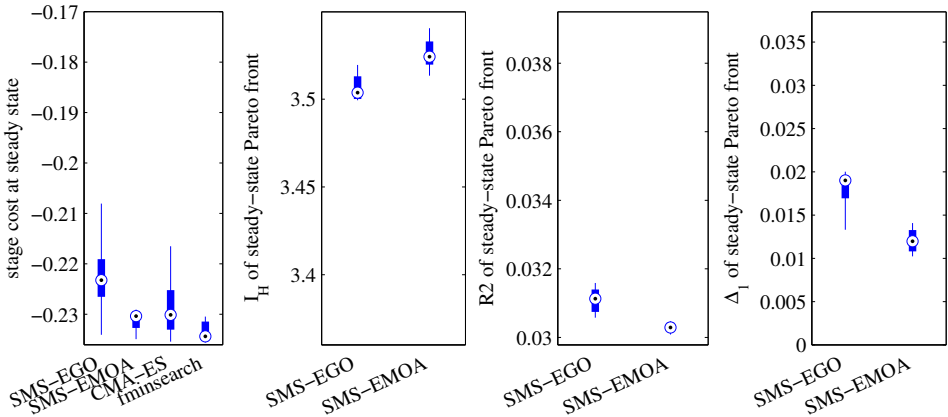


Figure 9.9: Dependency of the test results B/D on the optimization method. This is the equivalent to Figure 9.8 for the tests I.B and I.D. Test I.B20 (fminsearch) failed and therefore is not visualized in the plot.

Figure 9.9, where SMS-EMOA is clearly superior to SMS-EGO. With respect to the hypervolume indicator I_H , R2 and Δ_1 indicator, SMS-EMOA yields better results than SMS-EGO in five of six cases for all four categories A until D.

The number of simulations n_{eval} performed in SMS-EMOA and CMA-ES are chosen so that the total runtime of one test approximately lasts the same amount of time as a test using SMS-EGO does. About 77 % of all tests used to compare the optimization methods in experiment I (49 of 64 tests) are performed on computer 1 (see Section

9.3). There, the median of the runtime of a test using SMS-EGO as method lasts 16.9 h and for SMS-EMOA the median runtime is 15.6 h. With a median of 20.6 h the tests using CMA-ES last a little bit longer, but CMA-ES yields better one-dimensional steady-state stage cost F_{1D} results at least for tests A/C, see Figure 9.8. Surprisingly, the simplex method (fminsearch) with a median runtime of 16.9 h offers the best results. It seems to be that the objective function in this configuration does not have many local optima so that the locally converging simplex method provides such good results. Nevertheless, it cannot be guaranteed that the simplex method finds the global optimum if the configuration of the objective function is changed. This is why the simplex method is used out of competition and therefore is not further investigated in the following experiments. However, the simplex method can be used as a dual method or “polisher” to improve optimization results found by a global optimization method such as CMA-ES.

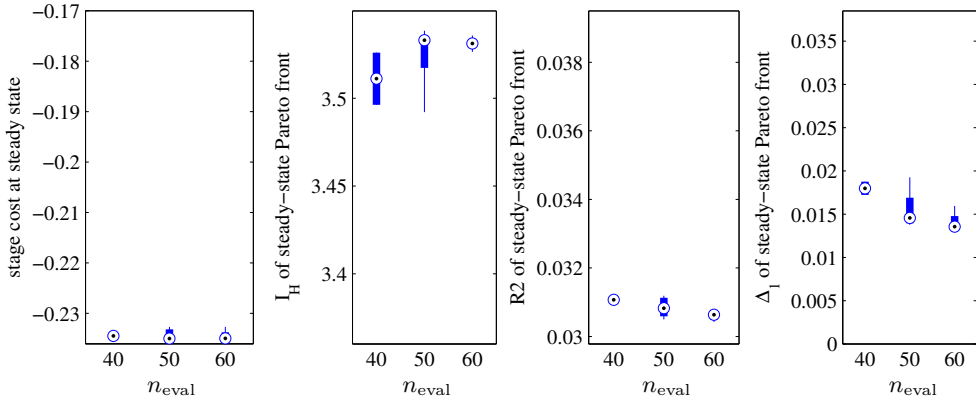


Figure 9.10: Dependency of the test results A/C on the number of simulations n_{eval} . Data from tests I.A4, I.A9 and I.A10 as well as I.C4, I.C9 and I.C10 are used, thus $T_p = 200$ d. Left: One-dimensional steady-state stage cost F_{1D} at day 750. Middle left: Hypervolume indicator I_H of the steady-state Pareto front. Middle right: R^2 indicator of the steady-state Pareto front. Right: Δ_1 indicator of the steady-state Pareto front.

For the number of simulations n_{eval} in each iteration no clear trend can be seen in both Figures 9.10 and 9.11 for the one-dimensional steady-state stage cost F_{1D} . It seems that for a good steady-state solution enough simulations ($150 \text{ d}/\delta \cdot n_{\text{eval}}$) are performed for all selected number of simulations n_{eval} . The quality of the obtained Pareto front, measured by the three performance measures I_H , R^2 and Δ_1 , appears to increase with the number of objective function evaluations, at least in five of six cases (the trend of the hypervolume indicator in Figure 9.10 is not counted).

The control horizon (test I.4 vs. test I.6, $T_c = 10$ d vs. $T_c = 5$ d) has not such a large influence on the steady-state solution. The fact that in test I.6 due to the control

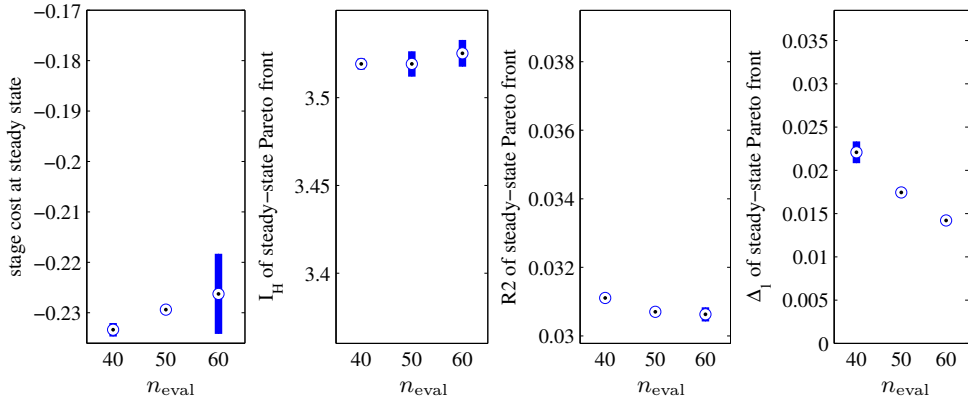


Figure 9.11: Dependency of the test results B/D on the number of simulations n_{eval} . This is the equivalent to Figure 9.10 for the tests I.B and I.D.

horizon twice as many simulations are performed as in test I.4 makes the results of test I.6 most of the time a little bit better than the ones of test I.4. Nevertheless, it can be expected that the influence of the control horizon in the setpoint experiment III is more apparent, see Section 9.3.5.

Size of the basin of attraction of the true steady-state Pareto front? Based on the optimal Pareto front approximation seen in Figure 9.5 it can be concluded that all selected initial feeds I.A to I.D (see Table 9.2) belong to the basin of attraction of the true steady-state Pareto front. This result is quite remarkable because the chosen initial feeds are taken from a quite large range of values. Dependent on the control parameters it can happen that a Pareto front approximation is obtained that is not as good as the true one. But in general it is possible to find the true steady-state Pareto front from each initial state.

If it is possible to reach the steady-state Pareto front from almost every initial state it means that the steady-state solution does not depend on the feed trajectory leading to the steady-state. In other words the steady-state solution only depends on the final substrate feed and not on the previous feed values. This means that using NMPC we will not find more optima as we can find using open loop optimization. At least the obtained results indicate that this observation could be true.

Stability of the closed loop? To test whether the control is stationary in Figure 9.13 the absolute change of the total substrate feed over the simulated control duration is shown. It can be seen that all controls are stationary. Only a very few controls change the feed after the 100th simulated day.

Note that in all tests above a perfectly known plant was assumed with no plant-model mismatch, measurement noise or drift. Here, the first five tests for experiments I.B and

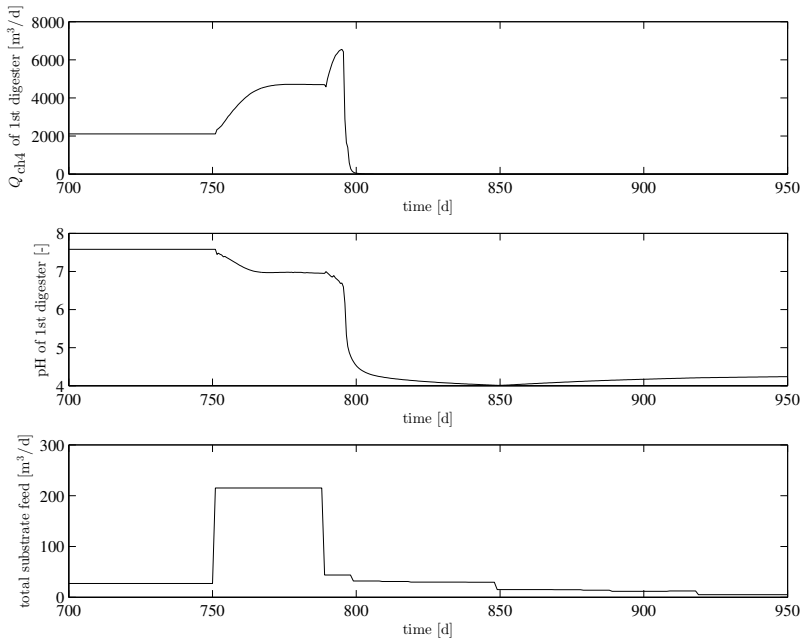


Figure 9.12: Simulation results for test I.D5. At hand of the methane production Q_{ch_4} and the pH value of the 1st digester one can see, that the digester fails. The total substrate feed in the lowest plot is the sum of the volumetric flow rate of the three fed substrates maize silage, swine manure and grass silage.

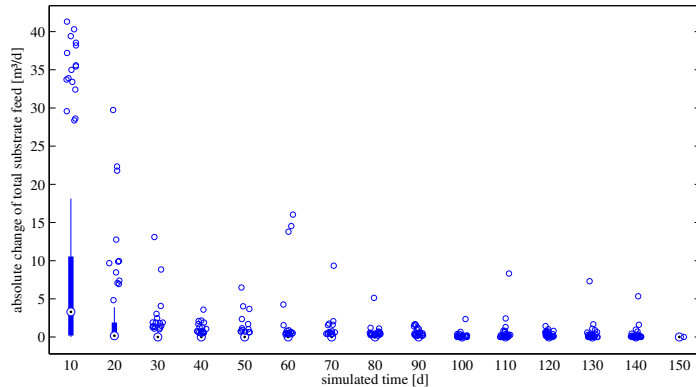


Figure 9.13: Absolute change of total substrate feed over the simulated control duration. The data of all tests in experiment I for the ideal model is used. It can be seen that all controls are stationary.

I.D (Table 9.3) are repeated with a not perfectly known controlled model (see Section 9.3.2). The results are depicted in Figure 9.14 in the same format as they are visualized in Figure 9.7 for the ideal world results.

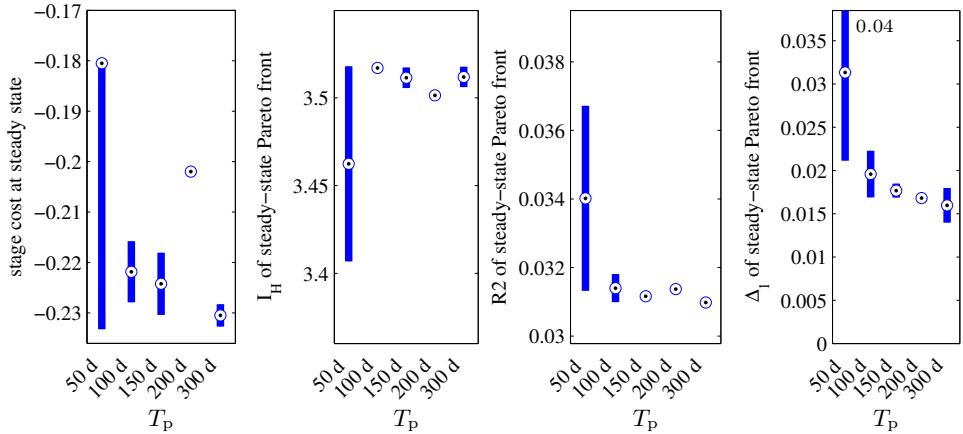


Figure 9.14: Dependency of the test results B/D on the prediction horizon T_p for the method SMS-EGO. This is the equivalent to Figure 9.7, but this time in a noisy environment created in Section 9.3.2. Solving the ADM1 in a non-stationary environment is numerically difficult. Because of that test I.B4 failed three times and therefore is not displayed. Left: One-dimensional steady-state stage cost F_{1D} at day 750. Middle left: Hypervolume indicator I_H of the steady-state Pareto front. Middle right: R2 indicator of the steady-state Pareto front. Right: Δ_1 indicator of the steady-state Pareto front. The Δ_1 indicator for test I.D1 is short outside the visualized region ($T_p = 50$ d).

The initial feeds I.B and I.D are very far away from the optimal feed (see Table 9.2). Therefore, it is not unexpected that the steady-state results in a noisy environment for both initial feeds are different to the results in the ideal world. By comparing Figures 9.7 and 9.14 it can be seen that the results are not that different. With respect to the one-dimensional steady-state stage cost F_{1D} only test I.D4 ($T_p = 200$ d) yields a considerable different result. The trend of the hypervolume indicator of the steady-state Pareto front looks different. Here indeed test I.D2 ($T_p = 100$ d) and again test I.D4 ($T_p = 200$ d) have different results. The trends of the R2 and Δ_1 indicator are very much alike, this is especially true for the Δ_1 indicator. In conclusion one can say that the RTO is quite robust against noise and plant-model mismatch. Be aware that the plant-model mismatch is still there at steady state whereas the noise is not.

Can the results be repeated? For experiment I in total 16 tests are repeated once and three tests are repeated twice. The median of the absolute values of the variation of the steady-state stage cost $F_{1D}(750$ d) in those repetitions is 0.0004. In comparison, the absolute median variation of the steady-state stage cost $F_{1D}(750$ d) in all tests of experiment I is 0.0024. For the hypervolume indicator (R2, Δ_1 indicator) these numbers are for the repetitions 0.0030 (0.0001, 0.0009) and 0.0095 (0.0003, 0.0027) for all tests. Based on these numbers, the variation in the repetitions can be seen as reasonably small compared to the total variation of the four measures. Therefore, the obtained

results seem to be repeatable.

Optimal feeds and parameter sets In Figure 9.15 the optimal, with respect to the fitness J_{1D} , substrate feeds taken out of the final approximation of the Pareto optimal set are shown. All feeds qualify for the manure bonus (see Section 7.3.2), it also can be seen that all substrate mixtures contain a little more manure than would be required for the bonus. In the upper left view it can be observed that all feeds almost lie on one line. When maize silage is decreased, grass silage is increased.

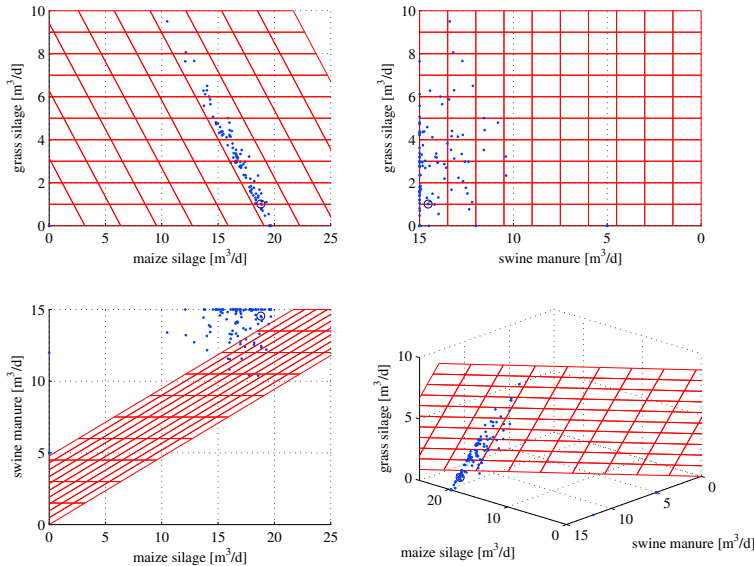


Figure 9.15: With respect to fitness J_{1D} optimal substrate feeds of the final approximation of the Pareto optimal set obtained in experiment I. The feeds are visualized in three views. Top left: Front view, top right: Left view, bottom left: Top view and bottom right: 3D view. The red plane divides the feeds in those which qualify for the manure bonus (see Section 7.3.2) and those who do not. The optimal feed, with respect to the one-dimensional steady-state stage cost F_{1D} , is emphasized by a circle.

With respect to the one-dimensional steady-state stage cost F_{1D} the best performing test in experiment I is test I.A21 (fminsearch) with a value of F_{1D} (750 d) ≈ -0.2361 . The corresponding optimal substrate mixture contains out of $18.79 \frac{m^3}{d}$ maize silage, $14.54 \frac{m^3}{d}$ swine manure and $1.01 \frac{m^3}{d}$ grass silage, which is also visualized in Figure 9.15 by a circle. The absolute best value ever obtained for the one-dimensional steady-state stage cost is F_{1D} (750 d) ≈ -0.2363 . It was found in an optimization run. The corresponding feed is $18.73 \frac{m^3}{d}$ maize silage, $14.99 \frac{m^3}{d}$ swine manure and $0.97 \frac{m^3}{d}$ grass silage. Thus, both feeds are almost exactly the same.

Among the three global optimization methods the best test is I.A16 (CMA-ES) with a

value of F_{1D} (750 d) ≈ -0.2359 . The corresponding optimal substrate mixture contains out of 19.68 $\frac{m^3}{d}$ maize silage, 15.00 $\frac{m^3}{d}$ swine manure and 0.00 $\frac{m^3}{d}$ grass silage.

The best value for the hypervolume indicator I_H is obtained in test I.B12 with a value of $I_H \approx 3.5405$. The best test for the other two indicators R2 and Δ_1 is I.D12. Their values are $R2 \approx 0.0301$ and $\Delta_1 \approx 0.0102$. In both tests SMS-EMOA is used as optimization method. It is interesting to see that the best steady-state Pareto front approximations are found when starting at the most difficult initial substrate feeds I.B and especially I.D.

The strength of the multi-objective optimization methods are that they return a set of optimal solutions from which the decision maker can pick a solution. But, if the applied solution is always chosen by predefined weights a single-objective method such as CMA-ES may yield better results. The problem of the used multi-objective methods is that they rather try to approximate the complete Pareto front, thus also its extremes, and do not concentrate their search in the region where the single-objective weighted criterion is optimized. Thus, the strength of the multi-objective solutions is only exploited well when based on the given Pareto front it is decided which solution is picked and not beforehand.

9.3.4 Experiment II: Change of Substrate Mixture

A sudden change in the substrate mixture of a biogas plant can often result in a transient decrease in performance (e.g. leaving a setpoint) or even lead to process instabilities or failure. Using predictive control such an adjustment of the fed substrates can be made smoothly and thus above mentioned disadvantages can be avoided. Such a scenario is investigated in this second experiment, where the substrate feed has to be changed because the substrate maize silage will be used up during the simulated control duration. Despite the change of the substrate mixture the control has to carry on tracking a given methane setpoint $Q_{ch_4,ext}^*(t)$. Furthermore, the new substrate mixture should also be optimal for the biogas plant given the limited amount of substrates available.

9.3.4.1 Setup

In a first test it will be evaluated what happens if the depletion of maize silage is not taken into account during prediction. This should be the worst case scenario. Then tests are done where the decreasing amount of maize silage in the silo is used as a further information during prediction. This is implemented by changing the upper boundary UB_{i_u} for the i_u th substrate so that the amount given by the upper boundary could be fed for the complete duration of some future horizon. The length of this future horizon is difficult to determine. If it is set to the prediction horizon the fed amount of the limited substrate will be very low if the prediction horizon is long. An optimal solution

for the horizon could not be determined in this thesis so it is set by experience to $\frac{T_p}{4}$, but at least to a value of 14 d. To avoid that shortly before the substrate is depleted only very small amounts of the substrate are fed the corresponding upper boundary UB_{i_u} is limited to a minimal value of $2 \frac{m^3}{d}$.

The prediction horizon T_p is the only control parameter which is evaluated in this experiment, using values 50 d, 100 d and 150 d. All tests are started with the optimal substrate feed found in test I.A16, which is $Q_{\text{maize}} \approx 19.68 \frac{m^3}{d}$, $Q_{\text{manure}} = 15.00 \frac{m^3}{d}$ and $Q_{\text{grass}} = 0.00 \frac{m^3}{d}$. The assumed amount of maize silage in the silo at the start of the simulation is 1000 t. The other two substrates swine manure and grass silage are not finite in time.

The simulated control duration is set to 300 days and the control is started at day 20. At day 160 the maize silage silo is refilled, so that the control has the task to return to the optimal substrate feed where it started from.

In this experiment the two best controller configurations obtained in experiment I are used, except of the different value for the prediction horizon T_p . They are the configuration I.12 using SMS-EMOA and I.16 using the method CMA-ES, see Table 9.3.

In order that during the simulated control duration the methane setpoint $Q_{\text{ch}_4,\text{ext}}^*(t)$ is hold, the objective function J is extended by a setpoint term. This term is used in experiment III as well and is described there, see Section 9.3.5. In this experiment a constant CH₄ setpoint is used with a value of $Q_{\text{ch}_4,\text{ext}}^*(t) = 2797.5 \frac{m^3}{d}$. This amount of methane is produced with the initial feed all tests are started from.

9.3.4.2 Results

In Figure 9.16 the obtained results for configuration I.16 and $T_p = 150$ d with and without including the available amount of maize silage in the silo are compared.

In Figure 9.16 it can be seen that the “hard” control, which changes the feed in a moment, tracks the methane setpoint very poorly during the transition. The reasons are the fast change of the feed but also the delayed switch to the usage of grass silage. The reason is, that once the setpoint error is larger than an upper boundary the fitness value is cut-off by the Tukey’s biweight function (see eq. (9.16)). Therefore, a reasonable control error and a huge one are rated the same. The reason is that the control should be able to leave a setpoint if it is beneficial for the biogas plant. As a high amount of grass silage leads to an increase of ammonia the control prefers to loose the setpoint for a while and only later (at day 110) changes the feeding regime to a higher amount of grass silage.

At the time maize silage is available again (day 160), the “smooth” control immediately changes back to a by maize silage dominated feed. This comes with a little overshoot of methane production. Furthermore, it can be observed that both controls do not

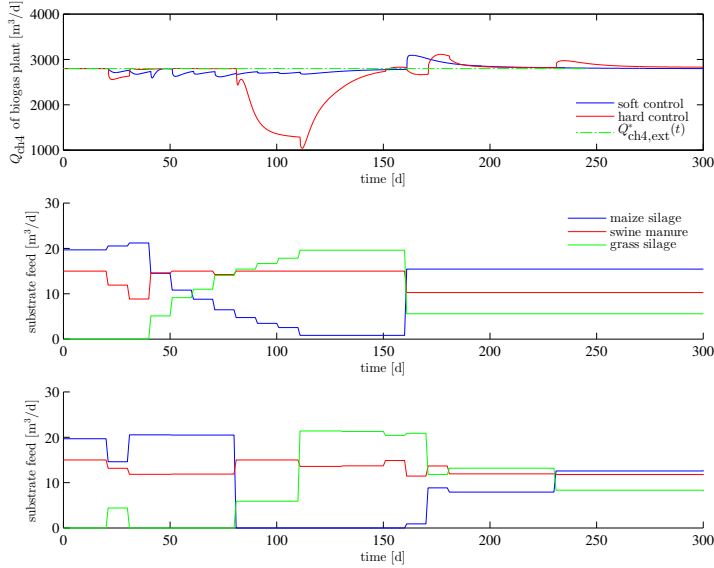


Figure 9.16: Comparison of controls with and without inclusion of the available amount of maize silage in the silo during prediction for configuration I.16 and $T_p = 150$ d. Top: Methane production of the biogas plant and methane setpoint $Q^*_{\text{ch}4,\text{ext}}(t)$. Middle: Substrate feed of the control with prediction of the available feed stock (“soft” control). Bottom: Substrate feed of the control without prediction of the available feed stock (“hard” control).

return to the substrate mix they started from, resulting in a worse one-dimensional steady-state stage cost F_{1D} compared to the one at initial state as can be seen in Figure 9.18 below.

In Figure 9.17 the same presentation as in Figure 9.16 is shown. Again configuration I.16 is used, but this time with a prediction horizon of $T_p = 50$ d. Here, the hard control is not that much worse than the soft control by just looking at the control error $e_{\text{ch}4,\text{ext}}(t)$ (see eq. (9.15)). The reason is that the first one is better and the latter one is worse than the ones for $T_p = 150$ d shown in Figure 9.16. For both controls the final substrate feed is almost the same as the initial one. Therefore, for this configuration the control almost returns to the optimal feed it started from.

In the top row of Figure 9.18 the obtained fitness values at the end of the simulated control duration J_{1D} (300 d) is shown. It can be seen that the fitness value for the soft control is most of the time worse than the one of the hard control. This was not expected but can be explained as follows. With the change to a grass silage dominated feed the ammonia, VFA and VFA/TA contents in the digesters increase. All three influence the fitness value negatively (the fitness value increases). As changing the feed leads to loosing the methane setpoint for a short while it is not beneficial for the soft control to leave the setpoint improving the fitness on a longer term. Only when the

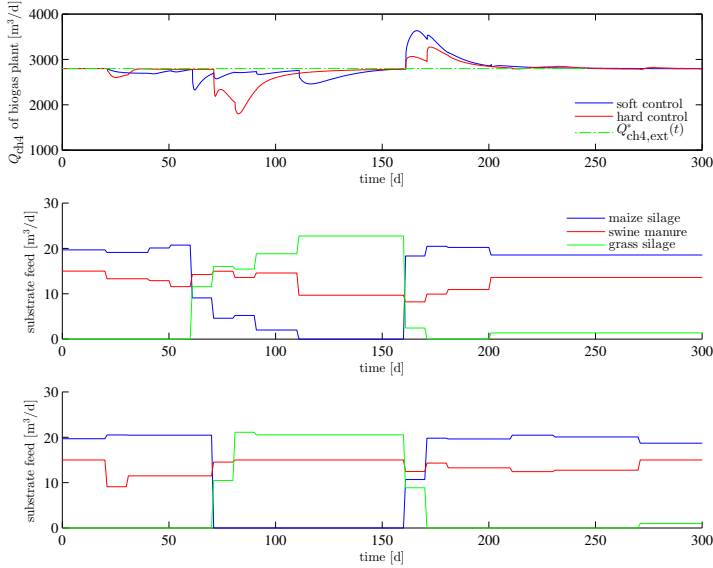


Figure 9.17: Comparison of controls with and without inclusion of the available amount of maize silage in the silo during prediction for configuration I.16 and $T_p = 50$ d. Top: Methane production of the biogas plant and methane setpoint $Q^*_{ch4,ext}(t)$. Middle: Substrate feed of the control with prediction of the available feed stock (“soft” control). Bottom: Substrate feed of the control without prediction of the available feed stock (“hard” control).

setpoint is already lost (hard control) the control has the freedom to leave the setpoint even more, because the fitness value corresponding to the control error is cut-off (see above).

In the middle row of Figure 9.18 the one-dimensional steady-state stage cost F_{1D} (500 d) is shown. Here again, the soft control is worse than the hard control. This is due to the fact that the final substrate feed of the hard control is most often better than the one of the soft control.

For SMS-EMOA the reason for this is that the soft control does not change the feed at day 160 at all. Therefore, maize silage is kept at $0 \frac{m^3}{d}$. In Figure 9.19 the reason for that behavior can be observed. There, the populations shortly before and at the time maize silage is available again (day 160) are plotted for configuration I.12 with $T_p = 150$ d. It can be observed that the solution candidates of the soft control are only located at the currently optimal feed and nowhere else. The versatility in feeds for the hard control is much higher. This is because the soft control sets the amount for maize silage at an earlier stage to $0 \frac{m^3}{d}$ as does the hard control. Therefore, the versatility in solutions is lost over the last number of iterations. This urged population is the reason why at day 160 SMS-EMOA cannot generate new and different solutions because the population does not allow space for exploration. Here, it can be seen that initializing

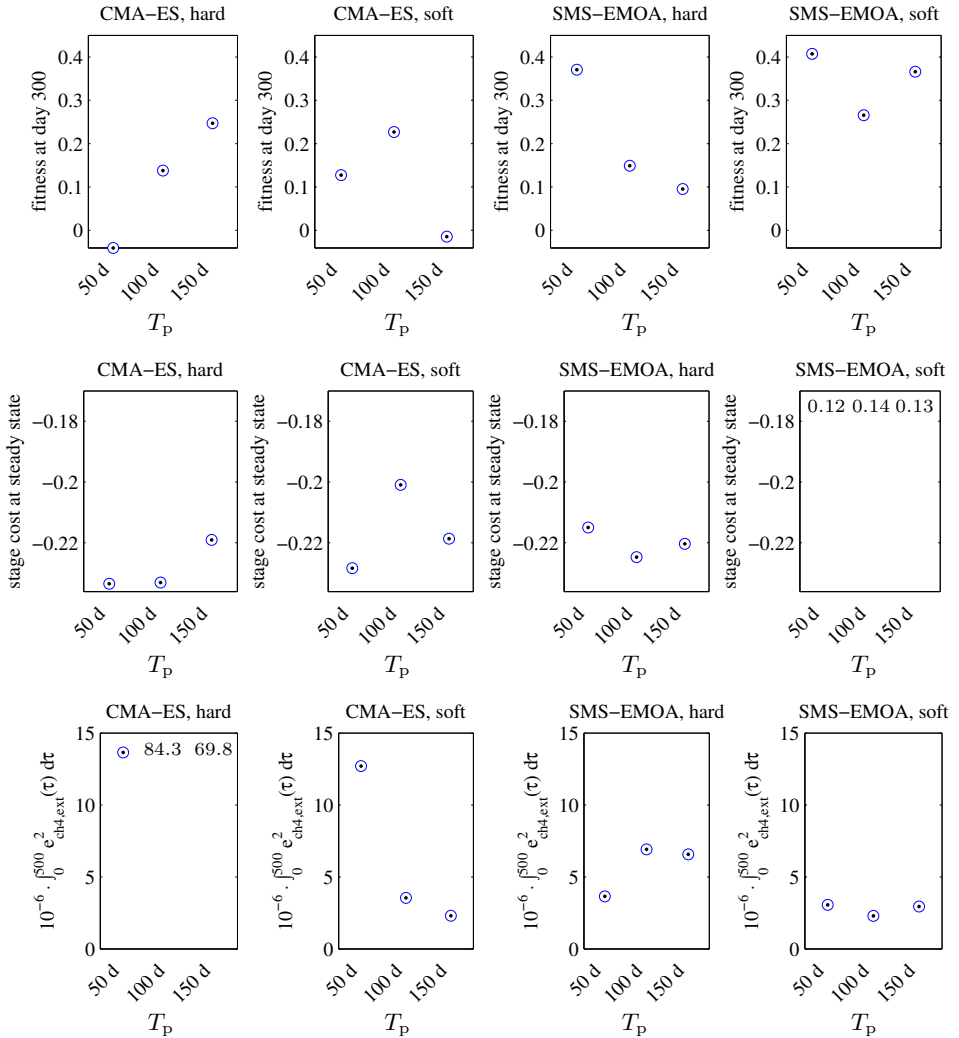


Figure 9.18: Obtained results for fitness at the end of the simulated control duration (J_{1D} (300 d), top row), one-dimensional steady-state stage cost (F_{1D} (500 d), middle row) and the integral of the squared control error over 500 days: $10^{-6} \cdot \int_0^{500} e_{ch4,ext}^2(\tau) d\tau$, bottom row. The figure compares the two optimization methods CMA-ES (config. I.16) and SMS-EMOA (config. I.12) as well as the inclusion of the feed stock during prediction (soft) and not (hard). The steady-state stage cost results for SMS-EMOA (soft) are out of the visualized region. This is also true for the tracking error obtained with CMA-ES (hard) for $T_p = 100$ d and $T_p = 150$ d.

SMS-EMOA only with the last population without any randomly generated solution candidates is a bad strategy (see Section 9.3.1). By replacing some solution candidates in the initial population by randomly (or LHS) selected candidates it can be expected that much better results are obtained. This is not done here to avoid that all tests

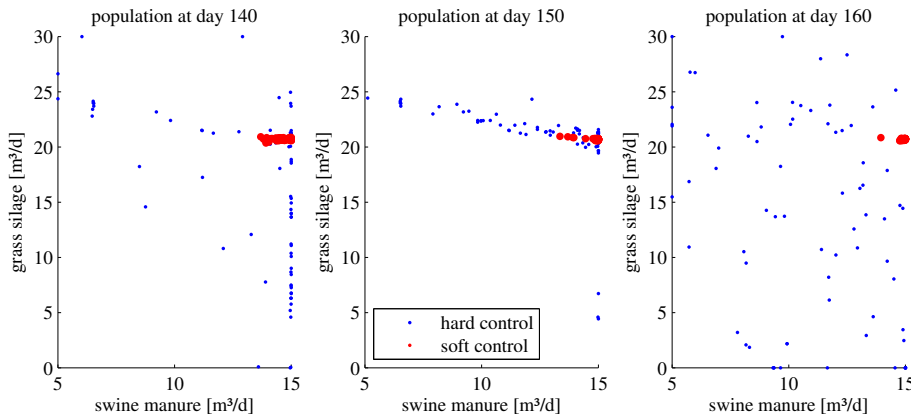


Figure 9.19: Comparison of the final populations of individuals from day 140 to day 160 (from left to right) for configuration I.12 (SMS-EMOA) with $T_p = 150$ d. The red dots for the soft control are plotted a little bit larger so that they can be located easier. It can be seen that the versatility of the solution candidates of the hard control is much higher compared with the soft control.

performed so far have to be repeated.

For CMA-ES the reason that the one-dimensional steady-state stage cost for the soft control is worse compared to the one for the hard control might be that at day 160 the soft control tracks the setpoint a little bit more accurate and therefore has more difficulty to leave it for a longer time.

In the bottom row of Figure 9.18 the integral of the squared control error over 500 days, $10^{-6} \cdot \int_0^{500} e_{\text{ch}_4,\text{ext}}^2(\tau) d\tau$, is shown. It can be seen that the soft control always yields better setpoint tracking results. For CMA-ES the hard control is very bad for $T_p = 100$ d and $T_p = 150$ d as could also be seen in Figure 9.16 above.

In this experiment no tests in the noisy environment are performed. The reason is that all tests in this experiment are computationally very expensive and performing them in the noisy environment would blast the performance of the available PCs.

The winning configuration of this experiment is the soft implementation of I.16 with $T_p = 150$ d. Thus, it is exactly configuration I.16 from Table 9.3 that was already the winner in experiment I.

Especially the soft control using configuration I.12 (SMS-EMOA) is a complete disappointment. At least the hard controls using SMS-EMOA for $T_p = 100$ d and $T_p = 150$ d yield somehow satisfying results.

9.3.5 Experiment III: Setpoint Control

In this third experiment the real-time optimization scheme is used as setpoint tracking control. In the tests performed here, the control variable is the volumetric flow rate of methane $Q_{\text{ch}_4}(t)$ which has to follow a given methane setpoint $Q_{\text{ch}_4,\text{ext}}^*(t)$. Therefore,

the objective function \mathbf{J} in Section 7.3.4 is extended by a term measuring the control error $e_{\text{ch}_4,\text{ext}}(t)$, defined in eq. (9.15).

$$e_{\text{ch}_4,\text{ext}}(t) := Q_{\text{ch}_4,\text{ext}}^*(t) - Q_{\text{ch}_4}(t) \quad (9.15)$$

More precisely the second component of the stage cost function F_2 given in eq. (7.66) is extended by the control error $e_{\text{ch}_4,\text{ext}}(t)$ by introducing a further constraint. This additional constraint is modeled as

$$\text{constraint}_{n_c+1}(\tau) := \rho_{\text{Ty}}(\zeta \cdot e_{\text{ch}_4,\text{ext}}^2(\tau)) \quad (9.16)$$

with Tukey's biweight function ρ_{Ty} (7.69) and a weight $\zeta \in \mathbb{R}^+$. The weight ζ is used to scale the squared control error $e_{\text{ch}_4,\text{ext}}^2(\tau)$ to the sensitive domain of Tukey's biweight function ρ_{Ty} .

Note the difference between the control error $e_{\text{ch}_4}(t)$ and the “external” control error $e_{\text{ch}_4,\text{ext}}(t)$. The first one is minimized by the process control and the latter one by the NMPC.

9.3.5.1 Setup

The setpoint trajectory $Q_{\text{ch}_4,\text{ext}}^*(t)$ used in the tests is characterized by two 100 d long constant periods and only two steps over the complete scenario (see Figure 9.20). The special property of the trajectory is that the setpoint at the start and the end of the scenario are the same and the setpoint in between is very bad for the biogas plant. Based on this trajectory the ability of the control to find and maintain a steady-state solution for a given setpoint and to find it again at a later point will be studied. To prove that the control is intelligent, it is investigated with the bad setpoint how the control behaves, because it may not just follow the setpoint. Furthermore, dynamics, oscillation, overshooting and action on the manipulated variable can be investigated in this experiment.

In the tests only the dependency of the results on the prediction horizon T_p is studied. As prediction horizon the four values $T_p = 10$ d, $T_p = 25$ d, $T_p = 75$ d and $T_p = 100$ d are chosen. The simulated control duration is set to 250 days. For all other parameters (optimization method and number of simulations) the two best configurations obtained in experiment I are used (Section 9.3.3). They are configuration I.12 with SMS-EMOA and I.16 with CMA-ES as optimization methods, see Table 9.3.

An important aspect for setpoint tracking is the performance of the control in a noisy and erroneous environment. Therefore, all tests are first performed in a perfect environment and then repeated in an environment where measurements are noisy, drifting and error-prone, a plant-model mismatch exists and substrate parameters are not exactly known (see Section 9.3.2). As the simulation studies with the real world model are computational very expensive the simulated control duration is reduced to

150 days. As setpoint a constant value of $Q_{\text{ch4,ext}}^*(t) = 2750 \frac{\text{m}^3}{\text{d}}$ is used, which is the same value as the previous setpoint trajectory has at the start and in the end. Next to the prediction horizon, here also the control horizon for the best configurations is changed once to $T_c = 5 \text{ d}$ for comparison.

9.3.5.2 Results

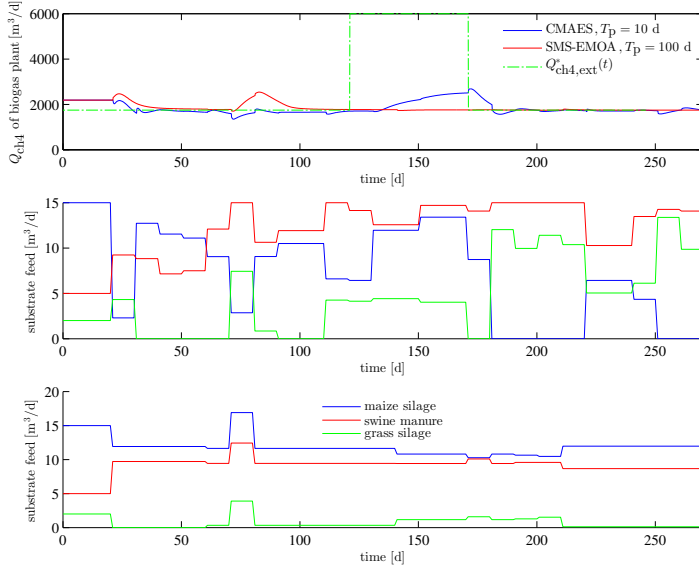


Figure 9.20: Setpoint control for ideal model: Comparison of two tests using configuration I.16 with $T_p = 10 \text{ d}$ and configuration I.12 with $T_p = 100 \text{ d}$. Top: Methane production of the biogas plant with setpoint $Q_{\text{ch4,ext}}^*(t)$. Middle: Substrate feed of the control with CMA-ES and $T_p = 10 \text{ d}$. Bottom: Substrate feed of the control with SMS-EMOA and $T_p = 100 \text{ d}$.

In Figure 9.20 simulation results for the setpoint tracking tests for the ideal simulation model are shown. Two controls, each with a different value for the prediction horizon, are compared. They are the best and worst performing controls in these tests. The controls are started at day 20 with an initial feed of $15 \frac{\text{m}^3}{\text{d}}$ maize silage, $5 \frac{\text{m}^3}{\text{d}}$ swine manure and $2 \frac{\text{m}^3}{\text{d}}$ grass silage. It can be seen that both controls converge to the setpoint, which the control with the larger prediction horizon tracks more accurately and much more stable. Because of the large bump in the setpoint between day 120 and day 170 both controls only slightly leave the previous setpoint for some time. This behavior is desired, because the setpoint of $6000 \frac{\text{m}^3}{\text{d}}$ is not beneficial for the biogas plant. In contrast to the control with $T_p = 100 \text{ d}$ the one with the short prediction horizon fails to find a stationary substrate feed. Furthermore, the final feed for $T_p = 10 \text{ d}$ is totally different to the nearly optimal one obtained for $T_p = 100 \text{ d}$. The latter substrate feed is

almost as good as the best one found in the tests below which can be seen as reference values (see Figure 9.23). With respect to the one-dimensional steady-state stage cost the difference between both optimal solutions is only 0.0034. Therefore, one can say that the control is able to find the optimal substrate feed while tracking a setpoint. But this wanted behavior is highly dependent on the prediction horizon as can be seen in Figure 9.21.

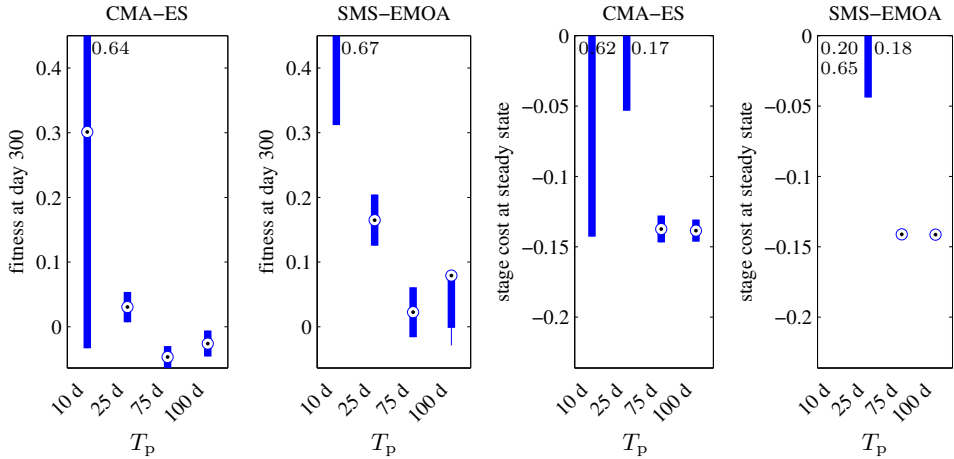


Figure 9.21: Setpoint control for ideal model: Results for fitness at the end of the simulated control duration (J_{1D} (300 d), left) and one-dimensional steady-state stage cost (F_{1D} (500 d), right). Comparison of configurations I.12 and I.16 for different values of the prediction horizon T_p . The tests with $T_p = 10$ d and $T_p = 25$ d yield very bad results and therefore are partly not visualized. All tests are repeated once, one test (SMS-EMOA, $T_p = 100$ d) is repeated twice.

In Figure 9.21 all results yield in experiment III for the setpoint shown in Figure 9.20 above and with the ideal model are shown. The fitness at the end of the simulated control duration (J_{1D} (300 d)) and the one-dimensional steady-state stage cost (F_{1D} (500 d)) are visualized and compared with respect to the chosen prediction horizon T_p and optimization method. Both, fitness and steady-state stage cost in general improve with an increasing prediction horizon. There is no best configuration. However, the CMA-ES based configurations most of the time yield better fitness values and the one for $T_p = 75$ d is pretty good.

To evaluate the control's performance in a noisy environment the next test results are obtained applying the control at the real world model. As explained in the setup above a constant setpoint is used here, as can be seen in the top plot of Fig. 9.22. For comparison the same tests are also evaluated at the ideal model.

In Figure 9.22 two tests using the same configuration (I.12 with $T_p = 100$ d) are compared. In the first test the control is applied to the ideal model and in the latter

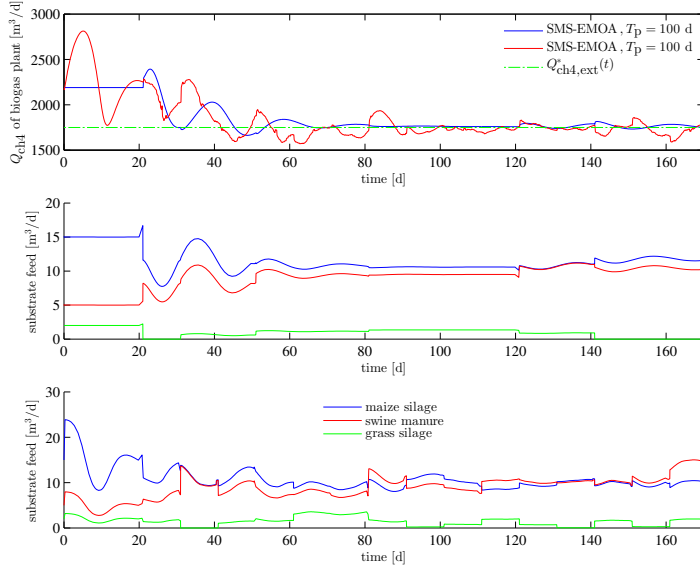


Figure 9.22: Setpoint control for real world model: Comparison of two tests using configuration I.12 with $T_p = 100$ d, one is evaluated at the ideal and the other at the real world model. Top: Methane production of the biogas plant with setpoint $Q_{\text{ch}4,\text{ext}}^*(t)$. In blue the CH₄ production of the ideal and in red the one of the real world model is visualized. Middle: Substrate feed of the control applied to the ideal model. Bottom: Substrate feed of the control applied to the real world model.

test the control is applied to the real world model. Using the ideal model the control tracks the setpoint very well finding a stationary feed at the end (see the top and middle plot in Figure 9.22). Applied to the real world model the control is able to track the setpoint without an offset. This is due to the used process control. The NMPC itself is not able to control the plant offset-free. However, it seems that the process control is not fast enough to compensate all disturbances immediately. It is apparent that the process control in the beginning between day 0 and day 20 produces a high over- and undershoot to get to the initial setpoint. This is very unfortunate and one of the weaknesses of the used process control. The extension of the process control proposed in Section 9.2 does not have this disadvantage. It reduces the overshoot by 77 %, results are not visualized here. Note, that an overshoot of the process control is not punished harder as an undershoot. However, as in reality an overshoot could mean that the additionally produced biogas must be burned in a torch an overshoot in this case would be inferior to an undershoot. Using a model-based process control instead of Antonelli et al. (2003) better results might be expected. Nevertheless, Antonelli et al. (2003) has the advantage of its simplicity and therefore it is used here.

The final substrate mixture found for the real world model is almost the same as is

found for the ideal model. This can also be seen at the one-dimensional steady-state stage cost which is visualized in Figure 9.23 among others.

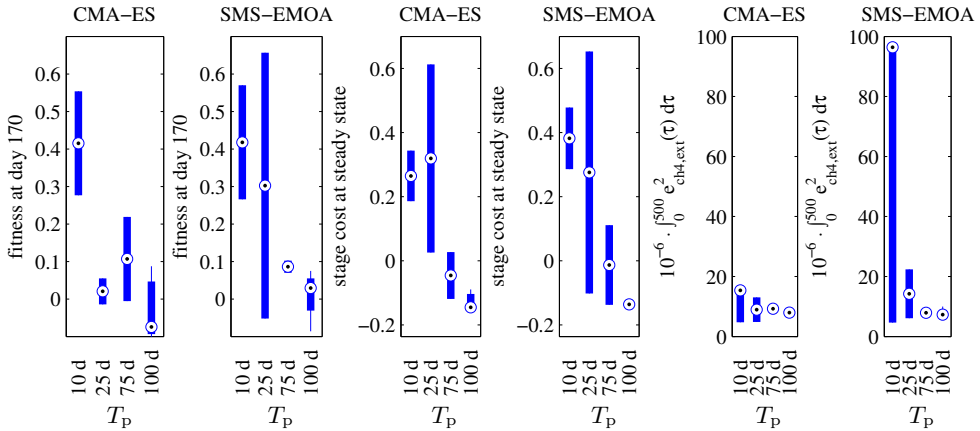


Figure 9.23: Setpoint control for ideal and real world model: Results for fitness at the end of the simulated control duration (J_{1D} (170 d), left), one-dimensional steady-state stage cost (F_{1D} (500 d), middle) and the integral of the squared control error over 500 days: $10^{-6} \cdot \int_0^{500} e_{\text{ch}_4,\text{ext}}^2(\tau) d\tau$, right. Comparison of configurations I.12 and I.16 for different values of the prediction horizon T_p .

In Figure 9.23 all results obtained for the constant setpoint are visualized. Both for the ideal and real world model together. It can be seen that for some configurations the achieved results for both models are quite different but for some they are almost the same. Here the focus is on the configurations leading to different results.

The configuration I.12 (SMS-EMOA) with $T_p = 10$ d yields very bad results. This is especially true for the integral over the squared control error $e_{\text{ch}_4,\text{ext}}$ while controlling the real world model (see most right plot in Figure 9.23). The reason for this huge control error is that at the end of the simulated control duration at day 170 the control for some reason leaves the setpoint. After 500 days this rather small deviation from the setpoint has summed up to this large value. The reason why the control leaves the setpoint at that time is that due to the badly chosen feed ammonia increases so that it affects the fitness value negatively. This lets the control change its feed leading to the setpoint deviation which is kept until the end after the control is switched off at day 170.

Using SMS-EMOA with $T_p = 25$ d different results for the substrate feed are obtained. This leads to the totally different results for the fitness value and steady-state stage cost. The same is true for configuration I.16 (CMA-ES) with $T_p = 25$ d. But here, this only affects the one-dimensional steady-state stage cost.

One can say that the smaller the prediction horizon the larger are the deviations of the real world simulation results from their ideal counterparts. Below a prediction horizon

of $T_p = 100$ d no satisfying results are obtained. But, for $T_p = 100$ d the simulation results for the real world model are almost the same as for the ideal model.

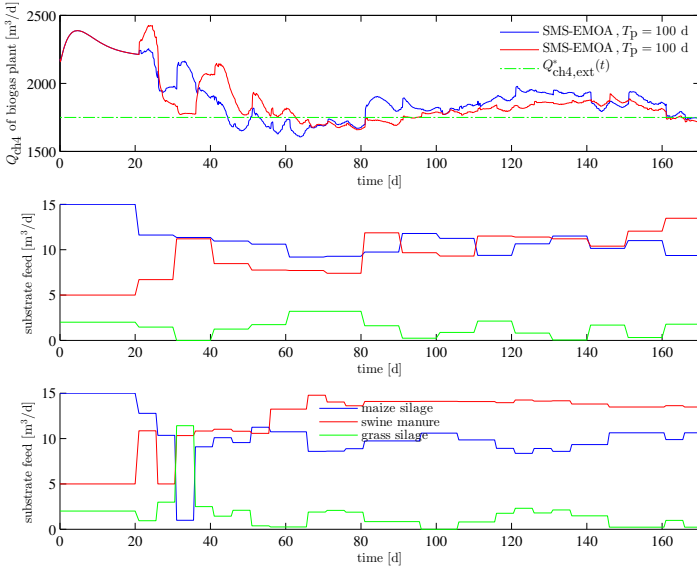


Figure 9.24: Setpoint control for real world model: Comparison of two tests using configuration I.12 with $T_p = 100$ d, $T_c = 10$ d and $T_c = 5$ d, respectively. Top: Methane production of the biogas plant with setpoint $Q_{\text{ch}4,\text{ext}}^*(t)$. In blue the CH_4 production of the control with $T_c = 10$ d and in red the one with $T_c = 5$ d is visualized. Middle: Substrate feed of the control with $T_c = 10$ d. Bottom: Substrate feed of the control with $T_c = 5$ d.

In a last test the value for the control horizon is set to $T_c = 5$ d instead of the value of $T_c = 10$ d used in the previous tests. The test results for configuration I.12 with $T_p = 100$ d for both control horizon values can be seen in Figure 9.24. It can be observed that the RTO with $T_c = 5$ d tracks the given setpoint $Q_{\text{ch}4,\text{ext}}^*(t)$ a little bit more accurately. In the tests the process control is switched off, to only see the performance of the NMPC. That the NMPC with $T_c = 5$ d has a better tracking performance could be expected, because the offline analysis of the substrate feeds are done in a five day interval (see Figure 9.4) so that the expected methane production can be predicted more accurately. However, if the process control is switched on it in general is able to adapt the feed so that the difference in results for both controls will be marginal. Because feed analysis is expensive the usage of a higher rate of analyses and a shorter control horizon in some cases might not be economically reasonable.

9.3.6 Experiment IV: State Estimator

In the last experiment which is presented in this section those tests yielding the best results in the above three experiments (Sections 9.3.3 - 9.3.5) are repeated. The only

difference is that this time the state estimator developed in Chapter 8 is used instead of the ideal state estimator used before. Thus, the control loop sketched in Figure 9.1 is utilized instead of the one in Figure 9.2 which is used in the other experiments. In this section is studied whether the corresponding tests yield approximately the same results. In contrast to the ideal state estimator the real estimator does not assume that the complete state vector of the ADM1 can be measured. Instead, the estimates of the real estimator are only based on a few measured process values (for details see Chapter 8). Therefore, if in this experiment satisfying results are obtained the control in principle will be ready to be used in practice.

As time and resources are limited not all tests are repeated. Only those tests are repeated that achieved best results in the previous experiments. They are:

- Experiment I: Configuration I.16: CMA-ES, $T_p = 150$ d.
- Experiment II: Configuration I.16: CMA-ES, $T_p = 150$ d, soft control.
- Experiment III: Configuration I.16: CMA-ES, $T_p = 75$ d for 1st setpoint and CMA-ES, $T_p = 100$ d for 2nd setpoint.

Similar results were already published in Gaida et al. (2012a) in the course of this thesis.

9.3.6.1 Setup

As the used state estimator just returns a class label for each state vector component \hat{x}_{i_x} based on the input variables, the real value for each component is in between a lower and upper boundary defined by the previously in Section 8.2 applied splitting of the state vector components into $C = 10$ classes. Remember that the state estimation problem is solved as a classification task (see Section 4.1). Instead of using the center values in between these lower and upper boundaries (named $\mathbf{lb}_x \in \mathbb{R}^{n_x}$ and $\mathbf{ub}_x \in \mathbb{R}^{n_x}$, respectively) that state vector as current state estimate is used, whose maximum norm of its derivative is minimal. Thus, the current state estimate $\hat{\mathbf{x}}_k$ is defined as:

$$\hat{\mathbf{x}}_k := \arg \min_{\mathbf{lb}_x \leq \mathbf{x} \leq \mathbf{ub}_x} |\mathbf{f}(\mathbf{x}, {}^o\mathbf{u}_k^*(t_k - \delta))|_\infty \quad (9.17)$$

In eq. (9.17) is searched for a steady-state solution by varying the states \mathbf{x} inside the allowed range $\mathbf{lb}_x \leq \mathbf{x} \leq \mathbf{ub}_x$. Thus, using this definition the chance should be increased that simulations of the RTO starting at $\hat{\mathbf{x}}_k$ converge to a steady-state solution respectively converge at all. This optimization problem is solved using CMA-ES with a population size of 25 and four generations.

For the setup details to each experiment please consult Section 9.3.3 to Section 9.3.5.

9.3.6.2 Results: Experiment I

In Figure 9.25 optimization results for the tests I.A16 until I.D16 are shown once using the ideal and once using the real state estimator. As with CMA-ES a single-objective

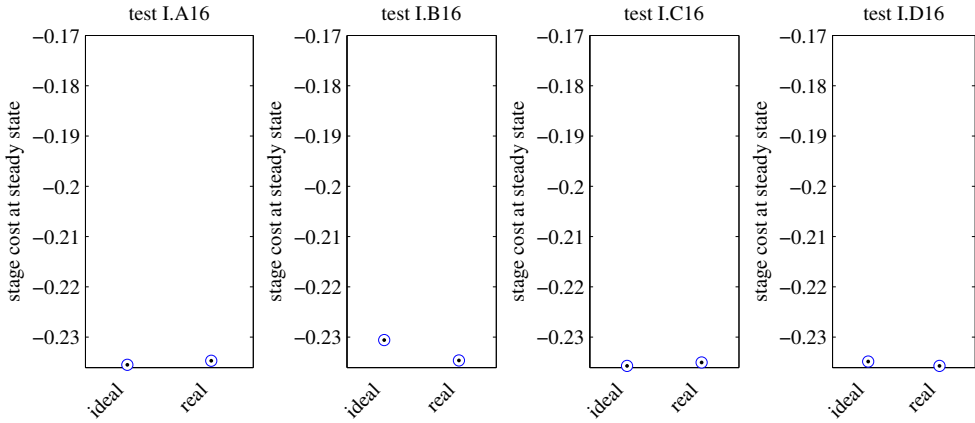


Figure 9.25: Experiment I: Test results of configurations I.A16 - I.D16 for the control using the ideal vs. the real state estimator. As in configuration I.16 the method CMA-ES is used only the one-dimensional steady-state stage cost F_{1D} at day 750 is visualized. All four tests I.A16 - I.D16 using the ideal state estimator are repeated once.

optimization method is used only the one-dimensional steady-state stage cost F_{1D} is shown. It can be seen that the obtained results for the one-dimensional steady-state stage cost are very similar and almost independent of the choice of the estimator. Therefore, it can be concluded that using the real state estimator steady states are found that are as good as the ones found with the ideal estimator.

9.3.6.3 Results: Experiment II

In Figure 9.26 simulation results for the best configuration from experiment II are presented. This is configuration I.16 as the soft implementation. In the top row the simulated methane production and the given methane setpoint $Q_{\text{ch}_4,\text{ext}}^*(t)$ are shown. In the middle row the fed substrates of the control with the ideal estimator and in the bottom row the ones proposed by the control with the real estimator are visualized. It can be seen that the results using the real state estimator are very bad. The reason is that the control has trouble to track the given setpoint. As the initial state estimate is not very accurate only at the end of the prediction horizon the setpoint might be achieved if the correct feed is chosen. Therefore, actually good feeds are evaluated badly. Furthermore, the state estimator is only calibrated for an amount of grass silage between $0 \frac{\text{m}^3}{\text{d}}$ and $5 \frac{\text{m}^3}{\text{d}}$, see Table 8.2. So, in case the control would suffice to feed high amounts of grass silage as it would be required, the state estimates might be unpredictably inaccurate. At least the feed at the end of the test is very close to the optimal one, where the test was started from.

To make setpoint tracking work, the way how the control error is included in the objective function must be revised. Once the setpoint is lost, in the current implementation

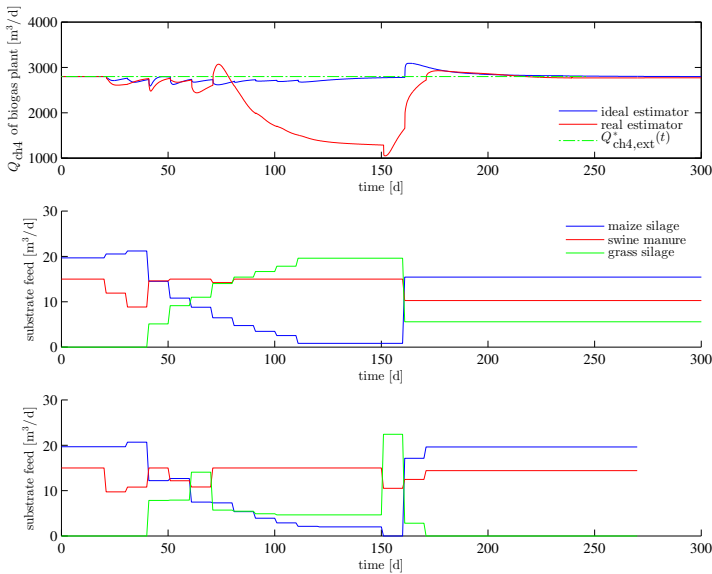


Figure 9.26: Experiment II: Comparison of controls with ideal vs. real state estimator for “soft” control configuration I.16 and $T_p = 150$ d. Top: Methane production of the biogas plant and methane setpoint $Q_{\text{ch}_4,\text{ext}}(t)$. Middle: Substrate feed of the control with ideal state estimator. Bottom: Substrate feed of the control with real state estimator. The test using the real state estimator was terminated after 270 days because of exhausted resources on the computer.

a very large and a small control error are evaluated the same. This leads to very large deviations from the setpoint as it can be seen in Figure 9.26.

Table 9.4: Results of control using ideal and real state estimator for configuration I.16 with $T_p = 150$ d in experiment II.

state estimator	J_{1D} (300 d)	F_{1D} (500 d)	$10^{-6} \cdot \int_0^{500} e_{\text{ch}_4,\text{ext}}^2(\tau) d\tau$
ideal	-0.015	-0.219	2.31
real	0.202	-0.218	136.71

Table 9.4 compares the obtained results visualized in Figure 9.26 by means of three performance measures. Based on these it can also be easily observed that the performance of the test using the real state estimator is far worse than the one using the ideal state estimator.

9.3.6.4 Results: Experiment III

In Figure 9.27 the achieved control trajectories for the 1st setpoint using the ideal model are shown. The figure compares the results obtained with the real and ideal

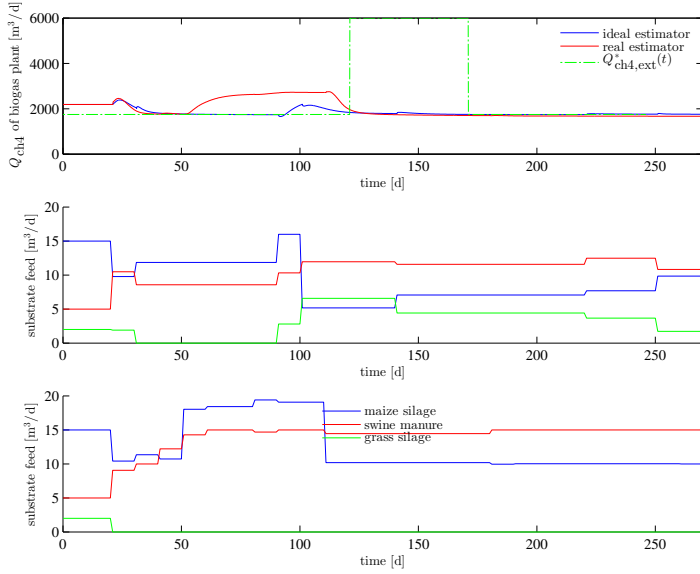


Figure 9.27: Experiment III: Setpoint control for ideal model and 1st setpoint: Comparison of two tests with ideal and with real state estimator using configuration I.16 with $T_p = 75$ d. Top: Methane production of the biogas plant with setpoint $Q^*_{\text{ch}4,\text{ext}}(t)$. Middle: Substrate feed of the control with ideal state estimator. Bottom: Substrate feed of the control with real state estimator.

state estimator. Although there is a small difference between both simulation results, using the real state estimator the setpoint is tracked accurately enough.

In Figure 9.28 the control results for the 2nd setpoint at the ideal model are shown. The trajectories obtained using the ideal and real state estimator are compared. It can be seen that the control using the real state estimator does not track the setpoint as accurately as the other, but the control error is quite small. The difference in the obtained feed mixtures is also only marginal.

Figure 9.29 visualizes the results obtained for the 2nd setpoint at the real-world model. Due to the noisy model the setpoint is not tracked exactly. As the simulations starting at the real state estimate, at the start of the simulations are very inaccurate the predicted biogas production of the RTO at the start is very unreliable. Therefore, using the real state estimator the process control is not used, because the setpoint trajectory generated by the RTO would be unpredictably inaccurate.

In Figure 9.30 simulation results for the setpoint experiment using the real and ideal state estimator are shown. In the two plots on the left side of the figure results of the first setpoint (see Figure 9.27) are visualized. The remaining three plots on the right side present the results for the second setpoint (see Figure 9.28).

For the 1st setpoint the results using the real state estimator are not that good as

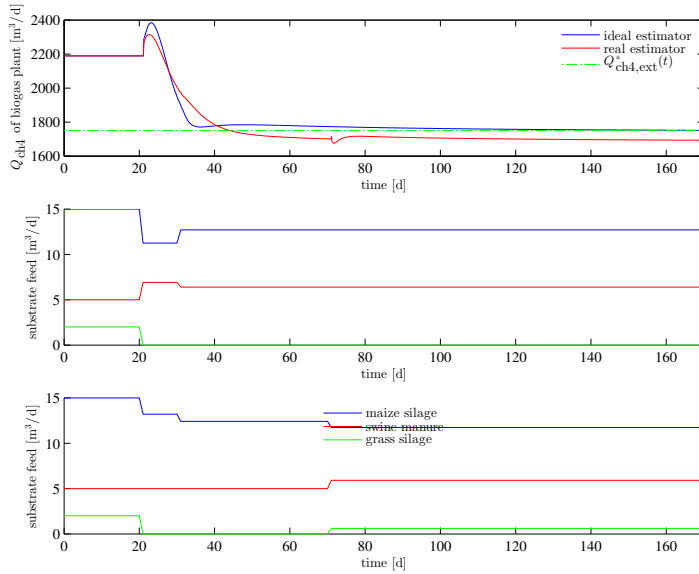


Figure 9.28: Experiment III: Setpoint control for ideal model and 2nd setpoint: Comparison of two tests with ideal and with real state estimator using configuration I.16 with $T_p = 100$ d. Top: Methane production of the biogas plant with setpoint $Q_{\text{ch4},\text{ext}}^*(t)$. Middle: Substrate feed of the control with ideal state estimator. Bottom: Substrate feed of the control with real state estimator.

the ones using the ideal state estimator. The reason is that the setpoint is not tracked accurately which increases both fitness and stage cost values. For the 2nd setpoint the deterioration of both values is introduced because the methane content of the produced biogas is below 50 %. This is a hard boundary defined in the objective function.

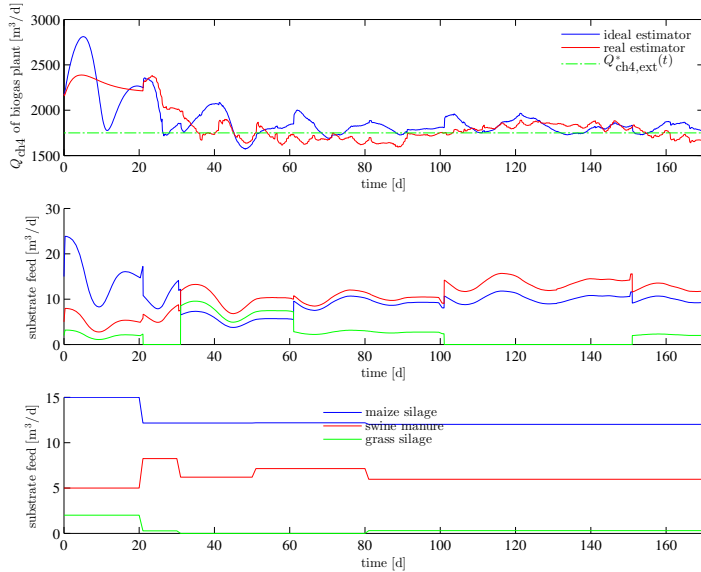


Figure 9.29: Experiment III: Setpoint control for real-world model and 2nd setpoint: Comparison of two tests with ideal and with real state estimator using configuration I.16 with $T_p = 100$ d. Top: Methane production of the biogas plant with setpoint $Q_{\text{ch4},\text{ext}}^*(t)$. Middle: Substrate feed of the control with ideal state estimator. Bottom: Substrate feed of the control with real state estimator.

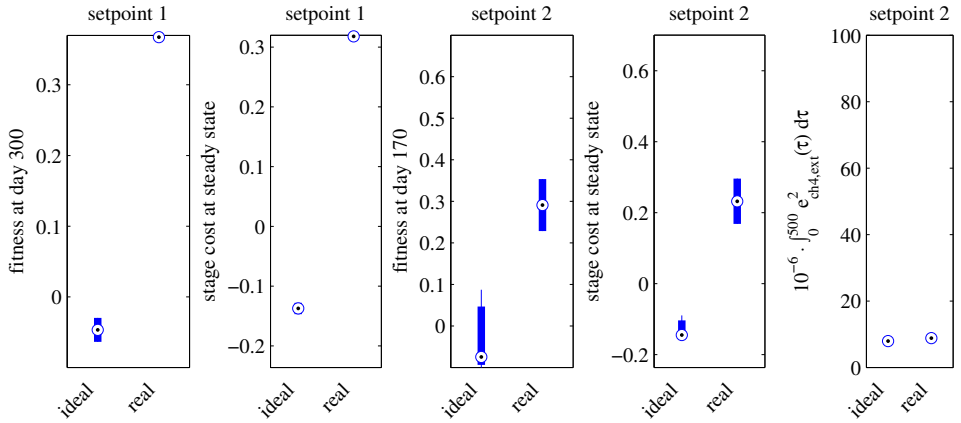


Figure 9.30: Setpoint control for ideal and real-world model using real and ideal state estimator. 1st setpoint: Results for fitness at the end of the simulated control duration (J_{1D} (300 d), left), one-dimensional steady-state stage cost (F_{1D} (500 d), middle left). 2nd setpoint: Results for fitness at the end of the simulated control duration (J_{1D} (300 d), middle), one-dimensional steady-state stage cost (F_{1D} (500 d), middle right) and the integral of the squared control error over 500 days: $10^{-6} \cdot \int_0^{500} e_{\text{ch4},\text{ext}}^2(\tau) d\tau$, right.

9.4 Summary and Discussion

The real-time optimization scheme in principle is able to find the optimal substrate feed with respect to a multi-objective objective function. The tests in experiment I revealed that the basin of attraction of the control is quite large and the optimal feed is kept once it is found. Under changing availability of substrates the predicting behavior of the control helps to change the substrate feed smoothly and to avoid a temporary deterioration of performance (see experiment II). As setpoint control a minimal prediction horizon of $T_p = 100$ d is needed as was observed in experiment III. This can also be said in general. A prediction horizon between 100 and 200 days can be suggested in general for all performed experiments.

Using the real instead of the ideal state estimator introduces some difficulties. Although the steady-state results are almost the same more dynamic scenarios such as changing the substrate feed or a setpoint tracking task are more challenging. With the used state estimator it is not yet possible to change the substrate feed without a loss in plant efficiency. Setpoint tracking is not that accurate but is possible. However, if more measurements are included in the state estimator, improved results will most certainly be observed.

In the following subsections 9.4.1 - 9.4.6 six extensions of the developed RTO control scheme are discussed. They are:

- Providing balancing energy for secondary and tertiary control.
- Parameter estimation and re-calibration of the process model and state estimator.
- Extension of the control scheme by a supervised expert system.
- Use of models to extend the process control.
- Increasing the speed of the RTO scheme.
- Implementation of simulation model and process control in different units.

9.4.1 Providing Balancing Energy for Secondary and Tertiary Control

Since the amendment of the Renewable Energy Sources Act in 2012 biogas plants in Germany may be used to provide balancing energy for secondary and tertiary control. Nowadays, with the high amount of renewable electrical energy production, the energy market is deregulated. In this market the price for electrical energy is volatile and its prediction is very valuable (cf. Che and Wang (2010), Esfahani (2011)). In Figure 9.31 an exemplary curve of block prices for electrical energy taken from the EPEX SPOT market is shown. When a biogas plant is participating in this market it must be able to start up or bring down its energy production within five (secondary) or fifteen minutes (tertiary), respectively⁴. As a biogas plant is a very slow system such fast responses are

⁴<http://www.next-kraftwerke.de/wissen/regelenergie>
<http://www.next-kraftwerke.de/energie-blog/praequalifikation-regelenergiemarkt>

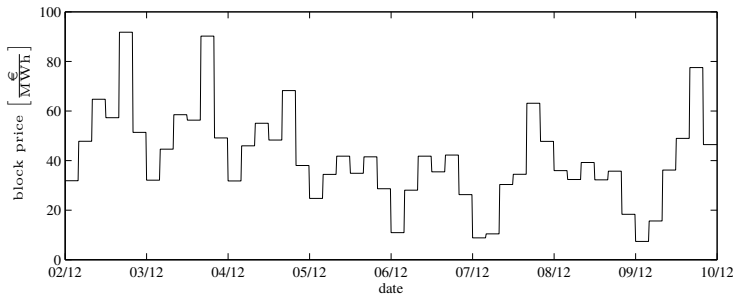


Figure 9.31: Block prices for electrical energy at the EPEX SPOT auction between 02/12/2013 and 09/12/2013.

only possible when the biogas plant has a gas storage unit. Here, an optimal control has the task to always keep the volume in the gas storage half-full so that the biogas plant can provide positive as well as negative balancing energy in the same amount. To predict the gas volume in the storage unit a model-based predictive control can use the predicted biogas production and the requested energy profile over the prediction horizon. To keep the gas storage unit at a minimal installation size a good prediction as well as an accurate setpoint tracking control is needed. As a minimum the gas volume should be able to store the produced biogas for a few hours at maximal biogas production.

As already written in the summary of Chapter 7 a gas storage unit is not yet implemented in the biogas plant model. Therefore, such a setpoint tracking problem unfortunately could not yet be simulated in this thesis.

9.4.2 Parameter Estimation and Re-Calibration of the Process Model and State Estimator

The problem with modeling of biogas plants is that after some time there will be a mismatch between model predictions and real plant behavior. There are numerous reasons that could lead to this situation. Examples are:

- Adaptation of anaerobic bacteria to (inhibiting) conditions in the digester.
- Insufficient calibration of model parameters (that are only locally valid).
- Drift in online measurement devices such as gas analyzer, pH and TS sensor.
- Change of substrate characteristics that are not measured, e.g. inclusion of toxic substances.
- Digester and substrate probes used for calibration are far from representative for the complete digester content or substrate storage.
- Unmodeled processes happening on the biogas plant such as some biochemical processes or process disturbances.

The questions are how to detect whether the model and the process are drifting apart and what is the reason for that. The first question is way easier to answer.

There are at least two methods to detect a deterioration of process model predictions. The first idea is to compare the simulated state vector of the last iteration ${}^o\boldsymbol{x}(t_{k-1} + \delta)$ with the predicted state vector of the current iteration $\hat{\boldsymbol{x}}_k$ on a moving horizon. If the sum of the deviation of both “predictions” ${}^o\boldsymbol{x}(t_{k-1} + \delta) - \hat{\boldsymbol{x}}_k$ over some horizon exceeds an upper boundary a drift between predictions of the process model and the real process behavior is very likely. The only problem of this approach is that both predictions are based on the same model. Therefore, in a worst case scenario, it is possible that a drift maybe remains undetected.

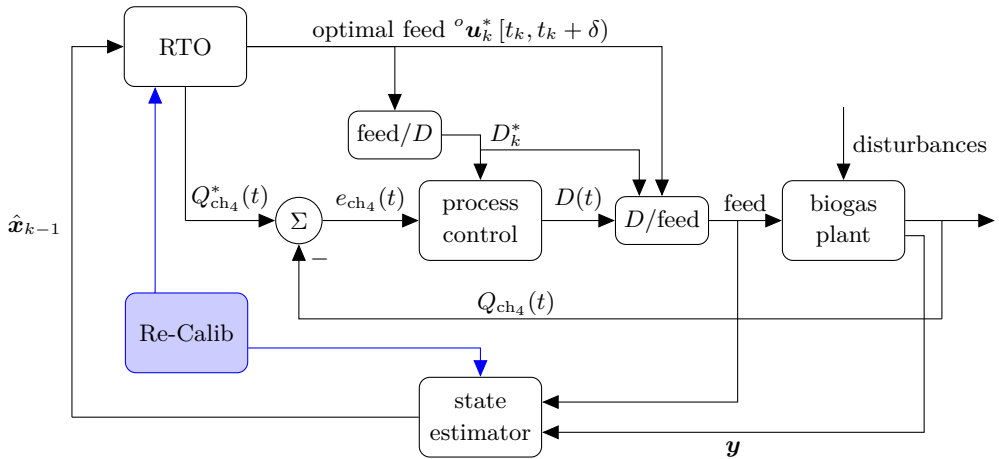


Figure 9.32: Real-Time Substrate Feed Optimization with a Re-Calibration Module. This figure is equal to Figure 9.1 with the only change that here a module to re-calibrate the process model and the state estimator is integrated. The new module is colored in blue.

The second idea is based on the fact that the control error $e_{ch_4}(t)$ must be minimal and at the same time the optimal feed ${}^o\boldsymbol{u}_k^* [t_k, t_k + \delta]$ and the really applied feed $\boldsymbol{u}_{ctrl}(t)$ (see eq. (9.6)) will be approximately the same if the model is perfect. The error between both feeds shall be denoted by $\Delta\boldsymbol{u}_{ctrl}(t) := \boldsymbol{u}_{ctrl}(t) - {}^o\boldsymbol{u}_k^* [t_k, t_k + \delta]$. By observing the weighted sum of both error terms over a moving window

$$\int_{t_k - N_{ctrl} \cdot \delta}^{t_k} \Delta\boldsymbol{u}_{ctrl}^T(\tau) \cdot \boldsymbol{Q}_{ctrl} \cdot \Delta\boldsymbol{u}_{ctrl}(\tau) + e_{ch_4}^2(\tau) d\tau > \epsilon_{ctrl}$$

it can be identified whether there is a deviation between model prediction and plant behavior. There, \boldsymbol{Q}_{ctrl} is a weighting matrix, $\epsilon_{ctrl} \in \mathbb{R}^+$ is an upper boundary and $N_{ctrl} \in \mathbb{N}$ defines the length of the moving window.

To answer the second question from above - what is the reason for the deviation of model predictions? - is very difficult. The reason is that there are many possible reasons

for this deviation as is listed above. By regular re-calibration of the online measurement devices their drift can at least be limited so that one item of the list above can be solved. A drift in methane concentration measurement could be detected by a static model calculating the biomethane potential of the substrate feed or by reverse calculation using the produced electrical energy assuming a constant electrical degree of efficiency of the CHPs and a drift free measurement of biogas production.

If, in case of a plant-model mismatch, model parameters should be re-calibrated the question arises whether they can be estimated reliably given available online and offline measurements of the plant. The field dealing with this kind of question is called practical identifiability analysis (Brun et al., 2001, Dochain and Vanrolleghem, 2001, Raue et al., 2009, 2011). To the author's knowledge such a practical identifiability analysis has not yet been performed for the ADM1. As on full-scale biogas plants there are only a few online or frequently measured values, practical identifiability of most ADM1 parameters will be rather difficult. The reason is also that most full-scale biogas plants are operated at steady state and therefore kinetic parameters cannot be determined. With a shift of biogas plant operation to demand-oriented operation this might change in the future. If a model mismatch is detected a re-calibration module could be implemented as is sketched in Figure 9.32.

9.4.3 Extension of the Control Scheme by a Supervised Expert System

Due to the complexity of the anaerobic digestion process also the most detailed model is always only a very scarce approximation of reality. As a failure in biogas plant operation can be very expensive one should not trust the RTO suggested feeds blindly. As optimal operation often also means risky operation in special situations the suggested feeds must be used with care. Therefore, a scheme as sketched in Figure 9.33 is suggested.

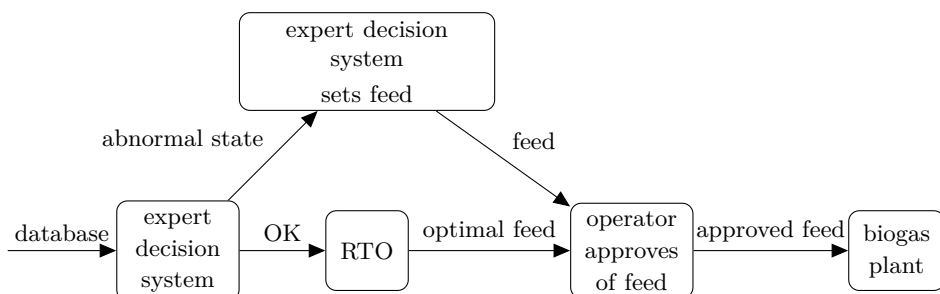


Figure 9.33: Expert decision system and operator are important parts of the closed-loop feed control.

In Figure 9.33 an expert system superimposes the RTO scheme and in special situations may overrule it. The expert system could be a rule-based system that analyses in which

state the biogas plant is in and based on that it decides whether the state is normal or abnormal. If the state is normal the RTO may propose its optimal substrate feed. If the state is abnormal then the expert system suggests a feed that is maybe more safe. The rules in the expert system could be defined by the biogas plant's operator using his valuable expert knowledge. The state detection of the expert system is based on the available data in the database and explicitly also can use measurements that can not be used in a mechanistic simulation model yet. This means that the state also may contain variables that can not be modeled yet. The final decision of the expert system might be implemented using fuzzy logic.

No matter which system suggests the feed it is always recommendable that the operator always has to approve (release) the feed before it is fed to the biogas plant, see Fig. 9.33.

9.4.4 Use of Models to Extend the Process Control

The process control Antonelli et al. (2003) that is used in the RTO control scheme above is not model-based. The literature review in Chapter 6 revealed that many process controls do exist that could be used instead of Antonelli et al. (2003). In the following some ideas are collected that could be worth investigating to improve the process control.

To use a MPC as process control using the linearized ADM1 would be a straight forward extension of the RTO scheme. As the state of the ADM1 is already estimated by the state estimation method the state estimate for the MPC comes for free. As nowadays it is no problem any more to solve a convex optimization problem online, to develop such a process control could be worth a try. The interested reader is referred to the following literature for a quick start: Kauder et al. (2007), Benhalla et al. (2010), Smets et al. (2003).

Instead of using the linearized ADM1 one could also use the singular thresholding method to create a linear model (Qin and Badgwell, 2003).

9.4.5 Increasing the Speed of the RTO Scheme

The time to solve the nonlinear optimization problem at each control sampling time is quite long and needs a lot of resources. Therefore, to shorten this time is of great interest. The time consuming part in the optimization problem is the evaluation of the objective function \mathbf{J} because it triggers a simulation of the biogas plant model. By using approximations of the complex model these times can severely be reduced. This approach is also followed by the method SMS-EGO (see Section 3.2) using a DACE model. This DACE model is learned on the fly using simulation results of the expensive model. An extension of this idea would be to use the methods of Co-Kriging (Forrester

et al., 2007). There, also simpler models can be used to train the DACE model and by that improve the quality of the resulting DACE model.

Static models are examples of such simpler models. Two ideas are presented in the following.

The first idea is to use a state dependent static model. Based on the current state and constant substrate feed of the plant it predicts its steady state solution. As noted in subsection 9.3.3.2 above most of the time the steady state of a biogas plant does not depend on its initial state but only on the substrate feed. Therefore, this model most of the time would be a usual static one and only for some special regions of the state space it would be state dependent. Such a model could be created as a “black-box” model which is trained beforehand by simulations with the complex simulation model. The second idea would be to use a mechanistic static model. Based on the biomethane potential (Angelidaki et al., 2009) of a substrate its potential for energy production can be estimated. Furthermore, given the purchasing cost of a substrate an economic gain can be calculated. Using this, the economic gain of a substrate mixture can be obtained. This is a very gross approximation of the complex model but it is a very simple and fast one. This approach is currently investigated by my colleague Martin Zaefferer at Cologne University of Applied Sciences.

9.4.6 Implementation of Simulation Model and Process Control in Different Units

Using the biogas plant model and the process control in the same Simulink® model causes numerical difficulties for the ODE solver to simulate the model. Therefore, separating both components in two different Simulink® models might be an option. Communication and synchronization of both might be possible using OPC (formerly: OLE for process control⁵).

⁵<http://www.opcconnect.com/>

Chapter 10

Conclusion

In this thesis a real-time substrate feed optimization scheme for biogas plants has been developed. The biogas market in Germany is highly dependent upon the government legislation which defines the profit that can be earned from the power market. As biogas plant operation is only economically feasible with a proper remuneration for the produced energy, their optimal operation is of highest importance. One aspect of optimization is the dynamic control of the substrate feed depending on the market situation and the fluctuating feed composition, when organic waste is the dominating source of energy. With optimal substrate feed control, biogas plants can be operated efficiently whilst maintaining stability. Therefore, this thesis is seen as a contribution to operate biogas plants more efficiently and with increased flexibility to make their economical operation feasible in the near future.

This chapter is divided in two parts. In Section 10.1 the main results of this thesis are summarized. An outlook on future work is given in Section 10.2.

10.1 Summary

Dynamic, multi-objective real-time optimization, as it is implemented in this thesis, consists out of four components. They are:

- Multi-Objective Nonlinear Model Predictive Control (MONMPC)
- Multi-Objective Optimization Algorithm
- State Estimation Method
- Dynamic Process Model

To optimally control the substrate feed of a full-scale biogas plant, all four components have to be developed and implemented. In the following the main results are summarized for all four parts.

Multi-Objective Nonlinear Model Predictive Control (MONMPC) As biogas plants are highly nonlinear and very slow systems, NMPC is considered to be a

reasonable approach to develop an optimal feed control. Furthermore, biogas plant operation has a multi-objective nature. On the one hand it has to be operated economically but on the other hand there is a higher level of risk present when operating at the most economical operation point. At that point the biogas production process may collapse and therefore it must be ensured that a safety margin is maintained at all times. To fulfill these requirements, a multi-objective NMPC is developed and applied. In numerous simulation and optimization experiments it has been shown that this approach is able to optimize the substrate feed in various situations. For steady-state operation it is able to find the optimal Pareto front from various different initial states. Furthermore, changes to the substrate mixture can be made smoothly as a result of the predictions additionally, setpoint control can also be performed. This approach is completely flexible with respect to the objective function so that priorities in the function can easily be altered or new objectives can be introduced. As the RTO scheme is developed as a two-layer system, the control is able to robustly track a setpoint even when there are uncertainties in the model. Model inaccuracies only lead to non-optimal substrate feeds generated by the RTO. Therefore, the MONMPC is seen as a successful approach to optimally control the substrate feed of biogas plants.

Multi-Objective Optimization Algorithm Because of the flexibility of the MONMPC with respect to the objective function, optimization algorithms must be used that will also find the global optimum, in case of non-linearities and local optima. Therefore, three global optimization algorithms are used. One local optimization algorithm is also used for comparative purposes. To allow the usage of surrogate model assisted algorithms such as SMS-EGO, the constraints in the objective function are implemented as soft constraints. This is done by plugging them into Tukey's biweight function, ensuring that the boundaries are smoothly limited. All utilized methods can be used out of the box. Elaborate configuration is possible but not needed if one accepts that the used configuration may not be optimal for the given problem. Using the standard configurations, all algorithms find very good solutions. For practical purposes, further fine tuning is not useful because the dynamic process model used by the algorithms is only a very rough approximation of reality, hence there is no guarantee that the global optimum in practice offers any improvement over the solutions found by the algorithms.

State Estimation Method To predict the future plant behavior, the MONMPC needs to know the current process state of the biogas plant. As the state vector is defined by the process model, its number of dimensions is highly affected by the complexity of the model. As the developed process model is based on the ADM1, each digester in the model is represented by a 37 dimensional state vector. To estimate it, an approach

is developed that uses current and past input and output values of the biogas plant. The knowledge of the correlation between input, output and process state values comes from the dynamic process model. This knowledge is saved in a machine learning method which has previously learned the correlations using extensive simulation results from the model. Using the Random Forests machine learning method, it was found that the process state can be estimated with sufficient accuracy.

Dynamic Process Model The dynamic process model uses the Anaerobic Digestion Model No. 1 to model the anaerobic digestion process. Furthermore, it contains algorithms that calculate the production and consumption of electrical and thermal energy on the plant, and it also contains models that determine the stability as well as the degradation performance of the plant. In total a very complex model for biogas plants is created. The individual components of the model are mostly taken from other publications, but the composition of these elements, selected here, has not been used until now.

The developed real-time optimization scheme has often been used to optimize chemical plant operation. However, it has not yet had been given control of the substrate feed for a biogas plant. The main reasons for this gap are believed to be:

- Difficulties in calibrating the dynamic process model at full-scale biogas plants.
- Necessity of state and input estimation for full-scale biogas plants.

Difficulties in calibrating the dynamic process model at full-scale biogas plants. Instrumentation on full-scale biogas plants often is very scarce, cf. Kujawski and Steinmetz (2009). Furthermore, it is not possible to operate these plants solely for the purpose of obtaining data to allow accurate calibration of model parameters. Both of these challenges make it very difficult to calibrate model parameters to a high degree of accuracy. However, to use the most complex mechanistic model is always better than to use simple mechanistic models, or to use black-box models. The latter suffer even more from the lack of data, and the simple models may be easier to calibrate, however do not deliver as much information as the complex ones. The predictions produced by the complex model are only very rough approximations of reality, however when the performance is compared to that of a model without these approximations, the more complex model performs favorably. Therefore, the problem remains that complex models as they are presented here cannot properly be calibrated for full-scale biogas plants, however, this may not hinder their use.

Necessity of state and input estimation for full-scale biogas plants. On agricultural biogas plants, often the parameters for the individual substrates are almost constant. This is not the case on waste digesting biogas plants, where the substrates contain mixtures of many different raw materials whose compositions constantly change. Therefore, at waste digesting plants, an input estimation scheme is needed to use a model-based control. In this thesis only tests for an agricultural biogas plant were performed. However, to control a waste treatment biogas plant with the proposed control structure would be much more challenging. For this scenario, online measurement devices designed for input characterization and input estimation would be required to characterize the input properly.

10.2 Outlook

There are a lot of possibilities to build upon this work and to investigate new areas of research. This section discusses some of the areas that are believed to be of particular interest to the biogas community.

Dynamic control for energy production on demand. The use of biogas plants to produce energy on demand will be intensified in the future. Therefore, biogas plants need to be controlled dynamically. This scenario was not tested in this thesis because the process model did not contain a gas storage tank. Nevertheless, it will be very important to enhance the model to include this feature and then to study whether the control system can also be used for dynamic energy production.

Moving horizon estimation for state, input and parameter estimation. With moving horizon estimation, another estimation method can be used to estimate the state of the biogas plant. In this thesis, MHE is only applied to a very simple model in Section 4.4. Use of MHE to estimate the process state of the ADM1 would be very interesting. It would also be of interest to test the suitability of MHE for input and parameter estimation.

Decreasing the runtime of RTO. To solve the optimization problem stated by the NMPC takes a substantial amount of time. It is believed that there is scope to decrease the runtime. Approaches such as multiple shooting or using Co-Kriging models in the optimization process are two candidates that could be used.

Extension of the process model. The accuracy of the solutions generated by the MONMPC approach are limited by the quality of the model. Thus, extending the process model so that it is more realistic will result in an increase in the quality of the

solutions. One such possible extension is the gas storage tank. A further substantial extension could be the incorporation of ecological considerations so that the object function is also capable of reflecting ecological issues. Further thoughts on this area are given in Section 7.6.

Improvement of process control. For process control, the relatively simple approach of Antonelli et al. (2003) is used. The use of a MPC instead would be a relatively straight forward approach, see also Section 9.4.

Using the benefits of multi-objective optimization. So far the computed Pareto optimal set is not fully used in each NMPC iteration. This is because the weighting factors that choose the optimal feed out of the Pareto optimal set are defined a priori. The weighting factors should be set after the Pareto optimal set is obtained to completely exploit the advantages of the multi-objective optimization algorithms.

Robust optimization. At present, the calculated optimum is not analyzed for stability against disturbances or noise in model or feed parameters. Robust optimization selects a solution that assumes the worst case disturbances. Frequently, the optimal operating points for biogas plants are near the stability boundary, thus it is important to analyze the operating point's robustness against noise. Therefore, the biogas plant model is an interesting application for robust optimization.

Application on a real biogas plant. In this thesis, it was not possible to apply the developed control system on a real biogas plant. It should be applied to both agricultural as well as waste digesters to take into account the future developments in anaerobic digestion. This will allow the determination of the usefulness of the proposed concept in reality.

Bibliography

- C.-A. Aceves-Lara, E. Latrille, and J.-P. Steyer. Optimal control of hydrogen production in a continuous anaerobic fermentation bioreactor. *Int J Hydrogen Energ*, 35(19):10710–10718, Oct. 2010. doi: 10.1016/j.ijhydene.2010.02.110.
- V. Adetola and M. Guay. Integration of real-time optimization and model predictive control. *Journal of Process Control*, 20(2):125–133, 2010.
- Agentschap NL. www.b-i-o.nl, 2013.
- E. Aguilar-Garnica, D. Dochain, V. Alcaraz-González, A. K. Dramé, and V. González-Álvarez. COD and VFA's control in a two-phase anaerobic digestion process. *Computer Applications in Biotechnology*, 10(1):67–72, June 2007. doi: 10.3182/20070604-3-MX-2914.00013.
- E. Aguilar-Garnica, D. Dochain, V. Alcaraz-González, and V. González-Álvarez. A multivariable control scheme in a two-stage anaerobic digestion system described by partial differential equations. *Journal of Process Control*, 19(8):1324–1332, Sept. 2009. doi: 10.1016/j.jprocont.2009.04.003.
- B. K. Ahring, M. Sandberg, and I. Angelidaki. Volatile fatty acids as indicators of process imbalance in anaerobic digestors. *Applied Microbiology and Biotechnology*, 43(3):559–565, July 1995. doi: 10.1007/BF00218466.
- E. Alba and C. Cotta. Evolutionary Algorithms. In S. Olariu and A. Y. Zomaya, editors, *Handbook of Bioinspired Algorithms and Applications*, chapter 1, pages 3–19. Taylor & Francis, 2006.
- V. Alcaraz-González and V. González-Álvarez. Robust Nonlinear Observers for Bioprocesses: Application to Wastewater Treatment. *Lecture Notes in Control and Information Sciences - Selected Topics in Dynamics and Control of Chemical and Biological Processes*, 361:119–164, 2007.
- V. Alcaraz-González, A. Maloum, J. Harmand, A. Rapaport, J. Steyer, V. González-Álvarez, and C. Pelayo-Ortiz. Robust interval-based SISO and SIMO regulation for a class of highly uncertain bioreactors: Application to the anaerobic digestion. In *Proceedings of the 39th IEEE Conference on Decision and Control (Cat. No.00CH37187)*, volume 5, pages 4532–4537. IEEE, 2000. doi: 10.1109/CDC.2001.914625.
- V. Alcaraz-González, J. Harmand, A. Rapaport, J. Steyer, V. González-Álvarez, and C. Pelayo-Ortiz. Robust interval-based SISO regulation under maximum uncertainty conditions in an anaerobic digester. In *Proceeding of the 2001 IEEE International Symposium on Intelligent Control (ISIC '01)*, pages 240–245. IEEE, 2001. doi: 10.1109/ISIC.2001.971515.
- V. Alcaraz-González, J. Harmand, A. Rapaport, J. P. Steyer, V. González-Álvarez, and C. Pelayo-Ortiz. Robust interval-based regulation for anaerobic digestion processes. *Water Science and Technology*, 52(1-2):449–56, Jan. 2005.

- V. Alcaraz-González, R. H. López-Bañuelos, J.-P. Steyer, H. O. Méndez-Acosta, V. González-Álvarez, and C. Pelayo-Ortiz. Interval-Based Diagnosis of Biological Systems - a Powerful Tool for Highly Uncertain Anaerobic Digestion Processes. *CLEAN - Soil, Air, Water*, 40(9):941–949, Sept. 2012. doi: 10.1002/clen.201100721.
- A. Alessandri, M. Baglietto, and G. Battistelli. Moving-horizon state estimation for nonlinear discrete-time systems: New stability results and approximation schemes. *Automatica*, 44(7):1753–1765, July 2008. doi: 10.1016/j.automatica.2007.11.020.
- A. Alessandri, M. Baglietto, G. Battistelli, and V. Zavala. Advances in moving horizon estimation for nonlinear systems. In *49th IEEE Conference on Decision and Control (CDC)*, pages 5681–5688, Atlanta, Dec. 2010. IEEE. doi: 10.1109/CDC.2010.5718126.
- A. Alessandri, M. Baglietto, G. Battistelli, and M. Gaggero. Moving-horizon state estimation for nonlinear systems using neural networks. *IEEE Trans Neural Netw.*, 22(5):768–80, May 2011. doi: 10.1109/TNN.2011.2116803.
- J. Alferes and I. Irizar. Combination of extremum-seeking algorithms with effective hydraulic handling of equalization tanks to control anaerobic digesters. *Water Sci Technol*, 61(11):2825–34, Jan. 2010. doi: 10.2166/wst.2010.093.
- J. Alferes, J. L. García-Heras, E. Roca, C. García, and I. Irizar. Integration of equalisation tanks within control strategies for anaerobic reactors. Validation based on ADM1 simulations. *Water Sci Technol*, 57(5):747–52, Jan. 2008. doi: 10.2166/wst.2008.104.
- J. Alvarez-Ramirez, R. Femat, O. Monroy, and F. Cuervo. An adaptive control strategy for anaerobic digester. In *Proceeding of the 1996 IEEE International Conference on Control Applications*, pages 1019–1024. IEEE, 1996. doi: 10.1109/CCA.1996.559055.
- J. Alvarez-Ramirez, M. Meraz, O. Monroy, and A. Velasco. Feedback control design for an anaerobic digestion process. *J Chem Technol Biot*, 77(6):725–734, June 2002. doi: 10.1002/jctb.609.
- R. M. B. Alves, C. A. O. Nascimento, E. C. Biscaia, L. A. Alvarez, and D. Odloak. Robust integration of real time optimization with linear model predictive control. *Computers & Chemical Engineering*, 34(12):1937–1944, 2010.
- J. F. Andrews. A Dynamic Model of the Anaerobic Digestion Process. In *Proceedings of the 23rd Industrial Waste Conference*, pages 285–310, 1968.
- J. F. Andrews. Dynamic models and control strategies for wastewater treatment processes. *Water Res*, 8(5):261–289, May 1974. doi: 10.1016/0043-1354(74)90090-6.
- I. Angelidaki, M. Alves, D. Bolzonella, L. Borzacconi, J. L. Campos, a. J. Guwy, S. Kalyuzhnyi, P. Jenicek, and J. B. van Lier. Defining the biomethane potential (BMP) of solid organic wastes and energy crops: a proposed protocol for batch assays. *Water Sci Technol*, 59(5):927–34, Jan. 2009. doi: 10.2166/wst.2009.040.
- F. Angulo, G. Olivari, and A. Rincon. Control of an anaerobic upflow fixed bed bioreactor. In *2007 Mediterranean Conference on Control & Automation*, pages 1–6, Athens, June 2007. IEEE. doi: 10.1109/MED.2007.4433758.
- R. Antonelli, J. Harmand, J. Steyer, and A. Astolfi. Output feedback regulation of an anaerobic digestion process. In *Proceedings of the 2002 American Control Conference (IEEE Cat. No.CH37301)*, volume 5, pages 4062–4067. American Automatic Control Council, 2002. doi: 10.1109/ACC.2002.1024565.

- R. Antonelli, J. Harmand, J.-P. Steyer, and A. Astolfi. Set-point regulation of an anaerobic digestion process with bounded output feedback. *IEEE T Contr Syst T*, 11(4):495–504, July 2003. doi: 10.1109/TCST.2003.813376.
- L. Appels, J. Baeyens, J. Degrève, and R. Dewil. Principles and potential of the anaerobic digestion of waste-activated sludge. *Progress in Energy and Combustion Science*, 34(6):755–781, Dec. 2008. doi: 10.1016/j.pecs.2008.06.002.
- S. Astals, M. Esteban-Gutiérrez, T. Fernández-Arévalo, E. Aymerich, J. L. García-Heras, and J. Mata-Alvarez. Anaerobic digestion of seven different sewage sludges: A biodegradability and modelling study. *Water research*, 47(16):6033–43, Oct. 2013. doi: 10.1016/j.watres.2013.07.019.
- P. Axaopoulos, P. Panagakis, A. Tsavdaris, and D. Georgakakis. Simulation and experimental performance of a solar-heated anaerobic digester. *Solar Energy*, 70(2):155–164, Jan. 2001. doi: 10.1016/S0038-092X(00)00130-4.
- M. W. Barnett and J. F. Andrews. Expert System for Anaerobic Digestion Process Operation. *Journal of Environmental Engineering*, 118(6):949–963, Nov. 1992. doi: 10.1061/(ASCE)0733-9372(1992)118:6(949).
- G. Bastin and D. Dochain. *On-line Estimation and Adaptive Control of Bioreactors (Process Measurement and Control, 1)*. Elsevier Science, Amsterdam, 1990.
- D. J. Batstone and J.-P. Steyer. Use of modelling to evaluate best control practice for winery-type wastewaters. *Water Sci Technol*, 56(2):147, July 2007. doi: 10.2166/wst.2007.483.
- D. J. Batstone, J. Keller, I. Angelidaki, S. V. Kalyuzhnyi, S. G. Pavlostathis, A. Rozzi, W. T. M. Sanders, H. Siegrist, and V. a. Vavilin. The IWA Anaerobic Digestion Model No 1 (ADM1). *Water Sci Technol*, 45(10):65–73, Jan. 2002a.
- D. J. Batstone, J. Keller, I. Angelidaki, S. V. Kalyuzhnyi, S. G. Pavlostathis, A. Rozzi, W. T. M. Sanders, H. Siegrist, and V. A. Vavilin. *Anaerobic Digestion Model No.1 (ADM1)*. IWA Publishing, 1st edition, 2002b.
- D. J. Batstone, K. V. Gernaey, and J. P. Steyer. Instrumentation and Control in Anaerobic Digestion. In *2nd IWA Leading-Edge Conference on Water and Wastewater Treatment Technologie*, pages 173–182, London, 2004. IWA Publishing.
- D. J. Batstone, S. Tait, and D. Starrenburg. Estimation of hydrolysis parameters in full-scale anaerobic digesters. *Biotechnol Bioeng*, 102(5):1513–20, Apr. 2009. doi: 10.1002/bit.22163.
- A. Bemporad and D. Muñoz de la Peña. Multiobjective model predictive control. *Automatica*, 45(12):2823–2830, Dec. 2009. doi: 10.1016/j.automatica.2009.09.032.
- A. Benhalla, M. Houssou, and M. Charif. Linearization of the full activated sludge model No 1 for interaction analysis. *Bioproc Biosyst Eng*, 33(6):759–71, Aug. 2010. doi: 10.1007/s00449-009-0404-z.
- J. M. Berg, J. L. Tymoczko, and L. Stryer. *Stryer Biochemie (German Edition)*. Springer Spektrum, 6th edition, 2007.
- M. Berglund and P. l. Börjesson. Assessment of energy performance in the life-cycle of biogas production. *Biomass and Bioenergy*, 30(3):254–266, Mar. 2006. doi: 10.1016/j.biombioe.2005.11.011.

- O. Bernard, Z. Hadj-Sadok, and D. Dochain. Software sensors to monitor the dynamics of microbial communities: application to anaerobic digestion. *Acta biotheoretica*, 48(3-4):197–205, Dec. 2000.
- O. Bernard, Z. Hadj-Sadok, D. Dochain, A. Genovesi, and J. P. Steyer. Dynamical model development and parameter identification for an anaerobic wastewater treatment process. *Biotechnol Bioeng*, 75(4):424–38, Nov. 2001a.
- O. Bernard, M. Polit, Z. Hadj-Sadok, M. Pengov, D. Dochain, M. Estaben, and P. Labat. Advanced monitoring and control of anaerobic wastewater treatment plants: software sensors and controllers for an anaerobic digester. *Water Sci Technol*, 43(7):175–82, Jan. 2001b.
- S. Besgen. *Energie- und Stoffumsetzung in Biogasanlagen*. Dissertation, Rheinische Friedrich-Wilhelm-Universität Bonn, 2005.
- N. Beume, B. Naujoks, and M. Emmerich. SMS-EMOA: Multiobjective selection based on dominated hypervolume. *European Journal of Operational Research*, 181(3):1653–1669, Sept. 2007. doi: 10.1016/j.ejor.2006.08.008.
- N. Beume, B. Naujoks, and G. Rudolph. SMS-EMOA - Effektive evolutionäre Mehrziel-optimierung (SMS-EMOA - Effective Evolutionary Multiobjective Optimization). *at - Automatisierungstechnik*, 56(7):357–364, July 2008. doi: 10.1524/auto.2008.0715.
- H.-G. Beyer and B. Sendhoff. Evolution Strategies for Robust Optimization. In *2006 IEEE International Conference on Evolutionary Computation*, pages 1346–1353, Vancouver, BC, 2006. IEEE. doi: 10.1109/CEC.2006.1688465.
- L. T. Biegler. Solution of dynamic optimization problems by successive quadratic programming and orthogonal collocation. 1984.
- W. Bischofsberger, N. Dichtl, K.-H. R. Carl, and F. Seyfried. *Anaerobtechnik*. Springer-Verlag, Berlin/Heidelberg, 2005. doi: 10.1007/b137857.
- L. Björnsson, M. Murto, and B. Mattiasson. Evaluation of parameters for monitoring an anaerobic co-digestion process. *Appl Microbiol Biot*, 54(6):844–9, Dec. 2000.
- BMU. Gesetz für den Vorrang Erneuerbarer Energien (Erneuerbare-Energien-Gesetz - EEG), 2009.
- BMU. Renewable Energy Sources Act - EEG, 2012a.
- BMU. *Messmethodensammlung Biogas*. DBFZ, Leipzig, 1st edition, 2012b.
- K. Boe. *Online monitoring and control of the biogas process*. Ph.d., Technical University of Denmark, 2006.
- K. Boe and I. Angelidaki. Pilot-scale application of an online VFA sensor for monitoring and control of a manure digester. *Water Sci Technol*, 66(11):2496–503, Jan. 2012. doi: 10.2166/wst.2012.498.
- K. Boe, J.-P. Steyer, and I. Angelidaki. Monitoring and control of the biogas process based on propionate concentration using online VFA measurement. *Water Sci Technol*, 57(5):661–6, Jan. 2008. doi: 10.2166/wst.2008.046.
- K. Boe, D. J. Batstone, J.-P. Steyer, and I. Angelidaki. State indicators for monitoring the anaerobic digestion process. *Water research*, 44(20):5973–80, Dec. 2010. doi: 10.1016/j.watres.2010.07.043.

- A. Boscolo, C. Mangiaciacci, F. Drius, F. Rongione, P. Pavan, and F. Cecchi. Fuzzy control of an anaerobic digester for the treatment of the organic fraction of municipal solid waste (MSW). *Water Sci Technol*, 27(2):57–68, Mar. 1993.
- S. Boyd and L. Vandenberghe. *Convex optimization*. Cambridge University Press, Cambridge, 2004.
- L. Breiman. Random forests. *Machine learning*, 45(1):5–32, 2001. doi: 10.1023/A:1010933404324.
- R. S. Brito, H. Pinheiro, F. Ferreira, J. S. Matos, and N. Lourenço. In situ UV-Vis spectroscopy to estimate COD and TSS in wastewater drainage systems. *Urban Water Journal*, pages 1–13, June 2013. doi: 10.1080/1573062X.2013.783087.
- R. Brun, P. Reichert, and H. R. Künsch. Practical identifiability analysis of large environmental simulation models. *Water Resources Research*, 37(4):1015–1030, Apr. 2001. doi: 10.1029/2000WR900350.
- J. Busch, P. Kühl, and J. Schlöder. State estimation for large-scale wastewater treatment plants. *Advanced Control of Chemical Processes*, 7(1):596–601, July 2009. doi: 10.3182/20090712-4-TR-2008.00096.
- J. Busch, D. Elixmann, P. Kühl, C. Gerkens, J. P. Schlöder, H. G. Bock, and W. Marquardt. State estimation for large-scale wastewater treatment plants. *Water research*, 47(13):4774–87, Sept. 2013. doi: 10.1016/j.watres.2013.04.007.
- S. Carlos-Hernandez, J. F. Beteau, and E. N. Sanchez. Intelligent control strategy for an anaerobic fluidized bed reactor. In P. Michel, editor, *Computer Applications in Biotechnology*, volume 1, pages 73–78, Cancun, Mexico, June 2007. doi: 10.3182/20070604-3-MX-2914.00014.
- S. Carlos-Hernandez, E. Sanchez, and J. Béteau. Fuzzy observers for anaerobic WWTP: Development and implementation. *Control Engineering Practice*, 17(6):690–702, June 2009. doi: 10.1016/j.conengprac.2008.11.008.
- S. Carlos-Hernandez, E. Sanchez, and J. Beteau. Fuzzy Control Strategy for an Anaerobic Wastewater Treatment Process. *Chem Biochem Eng Q*, 24(2):235–245, 2010a.
- S. Carlos-Hernandez, E. Sanchez, and J. Bueno. Neurofuzzy Control Strategy for an Abattoir Wastewater Treatment Process. In J. R. Banga, P. Bogaerts, J. V. Impe, D. Dochain, and I. Smets, editors, *11th International Symposium on Computer Applications in Biotechnology*, number Cab, pages 84–89, Leuven, Belgium, 2010b.
- E. Carrasco. Rule-based diagnosis and supervision of a pilot-scale wastewater treatment plant using fuzzy logic techniques. *Expert Systems with Applications*, 22(1):11–20, Jan. 2002. doi: 10.1016/S0957-4174(01)00045-8.
- M. Castellano, G. Ruiz-Filippi, W. González, E. Roca, and J. Lema. Selection of variables using factorial discriminant analysis for the state identification of an anaerobic UASB-UAF hybrid pilot plant, fed with winery effluents. *Water Sci Technol*, 56(2):139, July 2007. doi: 10.2166/wst.2007.482.
- Centraal Bureau voor de Statistiek. Hernieuwbare energie in Nederland 2012. Technical report, Centraal Bureau voor de Statistiek, Den Haag/Heerlen, 2013.
- A. Chamroo, I. Simeonov, C. Vasseur, and N. Christov. On the Piecewise Continuous Control of Methane Fermentation Processes. *Studies in Informatics and Control*, 17(2):181–188, 2008.

- J. Che and J. Wang. Short-term electricity prices forecasting based on support vector regression and Auto-regressive integrated moving average modeling. *Energy Conversion and Management*, 51(10):1911–1917, 2010.
- Y. Chen, J. J. Cheng, and K. S. Creamer. Inhibition of anaerobic digestion process: a review. *Bioresource technology*, 99(10):4044–64, July 2008. doi: 10.1016/j.biortech.2007.01.057.
- F. Cherubini and A. H. Strømman. Life cycle assessment of bioenergy systems: state of the art and future challenges. *Bioresource technology*, 102(2):437–51, Jan. 2011. doi: 10.1016/j.biortech.2010.08.010.
- H.-H. Chou, J.-S. Huang, S.-K. Chen, and M.-C. Lee. Process kinetics of an expanded granular sludge bed reactor treating sulfate-containing wastewater. *Chemical Engineering Journal*, 170(1):233–240, May 2011. doi: 10.1016/j.cej.2011.03.061.
- D. Chynoweth, S. Svoronos, G. Lyberatos, J. Harmand, P. Pullammanappallil, J. Owens, and J. Peck. Real-time expert system control of anaerobic digestion. *Water Science and Technology*, 30(12):21–29, Dec. 1994.
- C. A. Coello Coello. Evolutionary multi-objective optimization: basic concepts and some applications in pattern recognition. *Lecture Notes in Computer Science - Pattern Recognition*, 6718:22–33, 2011. doi: 10.1007/978-3-642-21587-2__3.
- A. I. Comport, E. Marchand, M. Pressigout, and F. Chaumette. Real-time markerless tracking for augmented reality: the virtual visual servoing framework. *IEEE T Vis Comput Gr*, 12(4):615–28, 2006. doi: 10.1109/TVCG.2006.78.
- R. Cord-Ruwisch, T. I. Mercz, C. Y. Hoh, and G. E. Strong. Dissolved hydrogen concentration as an on-line control parameter for the automated operation and optimization of anaerobic digesters. *Biotechnol Bioeng*, 56(6):626–34, Dec. 1997. doi: 10.1002/(SICI)1097-0290(19971220)56:6<626::AID-BIT5>3.0.CO;2-P.
- D. J. Costello, P. L. Lee, and P. F. Greenfield. Control of anaerobic digesters using Generic Model Control. *Bioprocess Engineering*, 4(3):119–122, Apr. 1989. doi: 10.1007/BF00369760.
- D. D. Cox and S. John. SDO : A Statistical Method for Global Optimization. *Multidisciplinary design optimization*, 2:315–329, 1997.
- A. Criminisi, J. Shotton, and E. Konukoglu. Decision Forests for Classification, Regression, Density Estimation, Manifold Learning and Semi-Supervised Learning. Technical report, Microsoft Research, 2011.
- A. Custódio, M. Emmerich, and J. Madeira. Recent Developments in Derivative-Free Multiobjective Optimisation. *Computational Technology Reviews*, 5:1–30, Sept. 2012. doi: 10.4203/ctr.5.1.
- M. L. Darby, M. Nikolaou, J. Jones, and D. Nicholson. RTO: An overview and assessment of current practice. *Journal of Process Control*, 21(6):874–884, July 2011. doi: 10.1016/j.jprocont.2011.03.009.
- C. L. Davey, H. M. Davey, D. B. Kell, and R. W. Todd. Introduction to the dielectric estimation of cellular biomass in real time, with special emphasis on measurements at high volume fractions. *Analytica Chimica Acta*, 279(1):155–161, July 1993. doi: 10.1016/0003-2670(93)85078-X.

- G. De Souza, D. Odloak, and A. C. Zanin. Real time optimization (RTO) with model predictive control (MPC). *Computers & Chemical Engineering*, 34(12):1999–2006, Dec. 2010. doi: 10.1016/j.compchemeng.2010.07.001.
- K. Deb, A. Pratap, S. Agarwal, and T. Meyarivan. A fast and elitist multiobjective genetic algorithm: NSGA-II. *IEEE Trans Evolut Comput*, 6(2):182–197, Apr. 2002. doi: 10.1109/4235.996017.
- K. Deb, M. Mohan, and S. Mishra. A fast multi-objective evolutionary algorithm for finding well-spread pareto-optimal solutions. Technical report, Indian Institute of Technology, Kanpur, 2003.
- M. Denac, K. Griffin, P. Lee, and P. Greenfield. Selection of controlled variables for a high rate anaerobic reactor. *Environmental Technology Letters*, 9(10):1029–1040, Oct. 1988. doi: 10.1080/09593338809384666.
- M. Denac, P. Lee, R. Newell, and P. Greenfield. Automatic control of effluent quality from a high-rate anaerobic treatment system. *Water Research*, 24(5):583–586, May 1990. doi: 10.1016/0043-1354(90)90190-H.
- M. Denil, D. Matheson, and N. de Freitas. Consistency of Online Random Forests. In *30th International Conference on Machine Learning*, page 21, Atlanta, 2013.
- R. Dewil, J. Lauwers, L. Appels, G. Gins, J. Degrève, and J. F. Van Impe. Anaerobic Digestion of Biomass and Waste: Current Trends in Mathematical Modeling. In B. Sergio, editor, *Proceedings of the 18th IFAC World Congress*, number 1969, pages 5024–5033, Aug. 2011. doi: 10.3182/20110828-6-IT-1002.03208.
- M. Diehl, R. Findeisen, S. Schwarzkopf, I. Uslu, F. Allgöwer, H. G. Bock, E.-D. Gilles, and J. P. Schlöder. An Efficient Algorithm for Nonlinear Model Predictive Control of Large-Scale Systems Part I: Description of the Method (Ein effizienter Algorithmus für die nichtlineare prädiktive Regelung großer Systeme Teil I: Methodenbeschreibung). *at - Automatisierungstechnik*, 50(12_2002):557, Dec. 2002. doi: 10.1524/auto.2002.50.12.557.
- M. Diehl, R. Findeisen, S. Schwarzkopf, I. Uslu, F. Allgöwer, H. G. Bock, E.-D. Gilles, and J. P. Schlöder. Ein effizienter Algorithmus für die nichtlineare prädiktive Regelung großer Systeme Teil II: Experimentelle Erprobung an einer Destillationskolonne (An Efficient Algorithm for Nonlinear Model Predictive Control of Large-Scale Systems Part II: Experimental. *at - Automatisierungstechnik*, 51 (1-2003):22–29, Jan. 2003. doi: 10.1524/auto.51.1.22.18879.
- M. Diehl, H. Bock, H. Diedam, and P. Wieber. Fast direct multiple shooting algorithms for optimal robot control. *Fast Motions in Biomechanics and Robotics*, 340:65–93, 2006a. doi: 10.1007/978-3-540-36119-0\4.
- M. Diehl, P. Kühl, H. Bock, and J. Schlöder. Combined nonlinear model predictive control and moving horizon estimation for a copolymerization process. *Comput Aided Chem Eng*, 21:1527–1532, 2006b. doi: 10.1016/S1570-7946(06)80264-6.
- M. Diehl, P. Kühl, H. G. Bock, and J. P. Schlöder. Schnelle Algorithmen für die Zustands- und Parameterschätzung auf bewegten Horizonten (Fast Algorithms for State and Parameter Estimation on Moving Horizons). *at - Automatisierungstechnik*, 54(12):602–613, Dec. 2006c. doi: 10.1524/auto.2006.54.12.602.
- N. Dimitrova and M. Krastanov. Nonlinear adaptive control of a model of an uncertain fermentation process. *Int J Robust Nonlin*, 20(9):1001–1009, 2009. doi: 10.1002/rnc.1503.

- DIN. DIN 38404-4 - Bestimmung der Temperatur (determination of temperature). Technical Report 0004, Deutsches Institut für Normung e.V., Berlin, 1976.
- DIN. DIN 38406-5 - Bestimmung des Ammonium-Stickstoffs (E5) (determination of ammonia-nitrogen). Technical report, Deutsches Institut für Normung e.V., 1983.
- DIN. DIN 51857 - Berechnung von Brennwert, Heizwert, Dichte, relativer Dichte und Wobbeindex von Gasen und Gasgemischen (Calculation of calorific value, density, relative density and Wobbe index of pure gases and gas mixtures). Technical Report 0009, Deutsches Institut für Normung e.V., 1997.
- DIN. DIN EN 12176 - Bestimmung des pH-Wertes (Determination of pH-value). Technical Report 2306, Deutsches Institut für Normung e.V., Berlin, 1998.
- DIN. DIN EN 12880 - Bestimmung des Trockenrückstandes und des Wassergehalts (Determination of dry residue and water content). Technical Report 2306, Deutsches Institut für Normung e.V., 2001a.
- DIN. DIN EN 12879 - Bestimmung des Glühverlustes der Trockenmasse (Determination of the loss on ignition of dry mass). Technical Report 2306, Deutsches Institut für Normung e.V., 2001b.
- DIN. DIN ISO 15705 - Bestimmung des chemischen Sauerstoffbedarfs (Determination of the chemical oxygen demand index). Technical Report 2212, Deutsches Institut für Normung e.V., 2003.
- DIN. DIN 38409-7 - Bestimmung der Säure- und Basekapazität (Determination of acid and base capacity). Technical report, Deutsches Institut für Normung e.V., Berlin, 2005.
- D. Dochain and G. Bastin. Stable adaptive controllers for waste treatment by anaerobic digestion. *Environ Technol Lett*, 6(12):584–593, Dec. 1985. doi: 10.1080/0959338509384379.
- D. Dochain and M. Perrier. Control design for nonlinear wastewater treatment processes. *Water Science & Technology*, 28(11-12):283–293, Mar. 1993.
- D. Dochain and P. Vanrolleghem. *Dynamical Modelling and Estimation in Wastewater Treatment Processes*. IWA Publishing, Cornwall, UK, 1 edition, 2001.
- D. Dochain, M. Perrier, and A. Pauss. Adaptive control of the hydrogen concentration in anaerobic digestion. *Ind Eng Chem Res*, 30(1):129–136, Jan. 1991. doi: 10.1021/ie00049a020.
- A. Donoso-Bravo, J. Mailier, C. Martin, J. Rodríguez, C. A. Aceves-Lara, and A. Vande Wouwer. Model selection, identification and validation in anaerobic digestion: a review. *Water Res*, 45(17):5347–64, Nov. 2011. doi: 10.1016/j.watres.2011.08.059.
- A. Donoso-Bravo, W. M. K. R. T. W. Bandara, H. Satoh, and G. Ruiz-Filippi. Explicit temperature-based model for anaerobic digestion: application in domestic wastewater treatment in a UASB reactor. *Bioresource technology*, 133:437–42, Apr. 2013. doi: 10.1016/j.biortech.2013.01.174.
- R. O. Duda, P. E. Hart, and D. G. Stork. *Pattern Classification (2nd Edition)*. Wiley-Interscience, 2000.
- F. Ehlinger, Y. Escoffier, J. Couderc, J. Leyris, and R. Moletta. Development of an automatic control system for monitoring an anaerobic fluidized-bed. *Water science and technology*, 29(10-11):289–295, May 1994.

- M. Ellis and P. D. Christofides. Integrating dynamic economic optimization and model predictive control for optimal operation of nonlinear process systems. *Control Engineering Practice*, 22:242–251, Jan. 2014. doi: 10.1016/j.conengprac.2013.02.016.
- C. Emmanouilides and L. Petrou. Identification and control of anaerobic digesters using adaptive, on-line trained neural networks. *Computers & Chemical Engineering*, 21(1):113–143, Sept. 1996. doi: 10.1016/0098-1354(95)00244-8.
- M. Emmerich, N. Beume, and B. Naujoks. An EMO algorithm using the hypervolume measure as selection criterion. *Lecture Notes in Computer Science - Evolutionary Multi-Criterion Optimization*, 3410:62–76, 2005. doi: 10.1007/978-3-540-31880-4__5.
- M. Emmerich, K. Giannakoglou, and B. Naujoks. Single- and multiobjective evolutionary optimization assisted by Gaussian random field metamodels. *IEEE T Evolut Comput*, 10(4):421–439, Aug. 2006. doi: 10.1109/TEVC.2005.859463.
- S. Engell. Feedback control for optimal process operation. *Journal of Process Control*, 17(3):203–219, Mar. 2007. doi: 10.1016/j.jprocont.2006.10.011.
- M. Esfahani. Neuro-fuzzy approach for short-term electricity price forecasting developed MATLAB-based software. *Fuzzy Information and Engineering*, 3(4):339–350, Dec. 2011. doi: 10.1007/s12543-011-0089-2.
- M. Estaben, M. Polit, and J. Steyer. Fuzzy control for an anaerobic digester. *Control Eng Pract*, 5(9):1303–1310, Sept. 1997. doi: 10.1016/S0967-0661(97)84369-9.
- Eurostat. Share of energy from renewable sources, 2013.
- H. Feitkenhauer, S. J. Von, and U. Meyer. On-line titration of volatile fatty acids for the process control of anaerobic digestion plants. *Water Res*, 36(1):212–8, Jan. 2002.
- A. P. Ferreira, L. M. Vieira, J. P. Cardoso, and J. C. Menezes. Evaluation of a new annular capacitance probe for biomass monitoring in industrial pilot-scale fermentations. *J Biotechnol*, 116(4):403–9, Apr. 2005. doi: 10.1016/j.jbiotec.2004.12.006.
- R. Findeisen, L. Imsland, F. Allgöwer, and B. A. Foss. State and Output Feedback Nonlinear Model Predictive Control: An Overview. *European Journal of Control*, 9(2-3):190–206, June 2003. doi: 10.3166/ejc.9.190-206.
- M. Fleischer. The measure of Pareto optima applications to multi-objective metaheuristics. *Lecture Notes in Computer Science - Evolutionary Multi-Criterion Optimization*, 2632:519–533, 2003. doi: 10.1007/3-540-36970-8__37.
- P. Fleming and R. Purshouse. Evolutionary algorithms in control systems engineering: a survey. *Control Eng Pract*, 10(11):1223–1241, Nov. 2002. doi: 10.1016/S0967-0661(02)00081-3.
- J. Flores, B. Arcay, and J. Arias. An intelligent system for distributed control of an anaerobic wastewater treatment process. *Engineering Applications of Artificial Intelligence*, 13(4):485–494, Aug. 2000a. doi: 10.1016/S0952-1976(00)00015-4.
- J. Flores, B. Arcay, and J. Dafonte. Knowledge-based system for telecontrol of anaerobic wastewater treatment plants. *Expert Systems*, 17(2):71–80, May 2000b. doi: 10.1111/1468-0394.00129.
- R. A. Flores-Estrella, G. Quiroz, H. O. Méndez-Acosta, and A. R. Femat. Hinfty control of anaerobic digester for winery industry wastewater treatment. *Ind Eng Chem Res*, page 130127193624002, Jan. 2013. doi: 10.1021/ie302233t.

- A. Flores-Tlacuahuac, P. Morales, and M. Rivera-Toledo. Multiobjective Nonlinear Model Predictive Control of a Class of Chemical Reactors. *Ind Eng Chem Res*, 51(17):5891–5899, May 2012. doi: 10.1021/ie201742e.
- FNR. Mediathek FNR, 2013.
- A. I. Forrester, A. Sóbester, and A. J. Keane. Multi-fidelity optimization via surrogate modelling. *Proceedings of the Royal Society A: Mathematical, Physical and Engineering Sciences*, 463(2088):3251–3269, Dec. 2007. doi: 10.1098/rspa.2007.1900.
- L. Fortuna, S. Graziani, A. Rizzo, and M. G. Xibilia. *Soft sensors for monitoring and control of industrial processes*. Springer-Verlag, London, 2007.
- M. Franke, A. Weger, and M. Faulstich. Prozessregelung von Vergärungsanlagen mit Hilfe des Parameters Wasserstoff. In *Güldzower Fachgespräche: Band 27 Messen, Steuern, Regeln bei der Biogaserzeugung*, number Fkz 22016200, pages 121–145, Güldzow, 2008. FNR.
- D. Gaida, C. Wolf, T. Bäck, and M. Bongards. Nonlinear model predictive substrate feed control of biogas plants. In *2012 20th Mediterranean Conference on Control & Automation (MED)*, pages 652–657, Barcelona, July 2012a. IEEE. doi: 10.1109/MED.2012.6265712.
- D. Gaida, C. Wolf, C. Meyer, A. Stuhlsatz, J. Lippel, T. Bäck, M. Bongards, and S. McLoone. State estimation for anaerobic digesters using the ADM1. *Water Sci Technol*, 66(5):1088–95, Jan. 2012b. doi: 10.2166/wst.2012.286.
- C. Garcia, F. Molina, E. Roca, and J. M. Lema. Fuzzy-Based Control of an Anaerobic Reactor Treating Wastewaters Containing Ethanol and Carbohydrates. *Ind Eng Chem Res*, 46(21):6707–6715, Oct. 2007. doi: 10.1021/ie0617001.
- C. García-Diézquez, F. Molina, and E. Roca. Multi-objective cascade controller for an anaerobic digester. *Process Biochemistry*, 46(4):900–909, Apr. 2011. doi: 10.1016/j.procbio.2010.12.015.
- P. García-Sandoval, V. González-Álvarez, and B. Castillo-Toledo. Control of a bioreactor with sampled delayed measurement. In *10th International IFAC Symposium on Computer Applications in Biotechnology*, volume 1, pages 315–320, Cancún, Mexico, 2007. IFAC.
- H. N. Gavala, I. Angelidaki, and B. K. Ahring. Kinetics and modeling of anaerobic digestion process. *Adv Biochem Eng Biot*, 81:57–93, Jan. 2003.
- K. G. Gebremedhin, B. Wu, C. Gooch, P. Wright, and S. Inglis. Heat Transfer Model for Plug Flow Anaerobic Digesters. *Transactions of ASAE*, 48(2):777–785, 2005.
- T. Gehring, K. Koch, H. Horn, and M. Wichern. Einsatz von mathematischen Prozessmodellen zur Optimierung des anaeroben Abbauprozesses (Application of mathematical models for optimization of the anaerobic digestion process). In S. Köhler, editor, *Bornimer Agrartechnische Berichte Heft 68*, volume 1, pages 96–113, Potsdam-Bornim, 2009. ATB.
- M. H. Gerardi. *The Microbiology of Anaerobic Digesters*. Wiley-Interscience, Hoboken, NJ, USA, 2003.
- M. Gerber. *Ganzheitliche stoffliche und energetische Modellierung des Biogasbildungssprozesses*. Dissertation, Ruhr-Universität Bochum, 2009.

- M. Gerber and R. Span. An analysis of available mathematical models for anaerobic digestion of organic substances for production of biogas. In *IGU Research Conference*, Paris, 2008.
- R. Girault, P. Rousseau, J. P. Steyer, N. Bernet, and F. Béline. Combination of batch experiments with continuous reactor data for ADM1 calibration: application to anaerobic digestion of pig slurry. *Water Sci Technol*, 63(11):2575–82, Jan. 2011.
- S. Graef and J. Andrews. Stability and control of anaerobic digestion. *Journal (Water Pollution Control Federation)*, 46(4):666–683, 1974.
- S. P. Graef. *Dynamics and control strategies for the anaerobic digestion*. Dissertation, Clemson University, 1972.
- M. Grepmeier. *Experimentelle Untersuchungen an einer zweistufigen fuzzy-geregelten anaeroben Abwasserreinigungsanlage mit neuartigem Festbettmaterial*. Doktor-ingenieur, TU Munich, 2002.
- M. S. Grewal and A. P. Andrews. *Kalman Filtering: Theory and Practice Using MATLAB*, volume 5. John Wiley & Sons, Inc., Hoboken, NJ, USA, 3rd edition, Aug. 2008. doi: 10.1002/9780470377819.
- F. Grognard and O. Bernard. Stability analysis of a wastewater treatment plant with saturated control. *Water Science and Technology*, 53(1):149–57, Jan. 2006.
- W. Gujer and A. J. B. Zehnder. Conversion Processes in Anaerobic Digestion. *Water Sci Technol*, 15(8-9):127–167, 1983.
- K. J. Gurubel, E. N. Sanchez, S. Carlos-Hernandez, and F. Ornelas-Tellez. PSO hybrid intelligent inverse optimal control for an anaerobic process. In *2013 IEEE Congress on Evolutionary Computation*, pages 876–883. IEEE, June 2013. doi: 10.1109/CEC.2013.6557660.
- A. Guwy, F. Hawkes, S. Wilcox, and D. Hawkes. Neural network and on-off control of bicarbonate alkalinity in a fluidised-bed anaerobic digester. *Water Research*, 31(8): 2019–2025, Aug. 1997. doi: 10.1016/S0043-1354(97)00016-X.
- N. Hansen. The CMA evolution strategy: a comparing review. *Towards a new evolutionary computation*, 192(2006):75–102, 2006. doi: 10.1007/3-540-32494-1__4.
- J. Harmand, A. G. Manh, and J. P. Steyer. Identification and disturbance accommodating control of a fluidized bed anaerobic digester. *Bioprocess Engineering*, 23(2):0177–0185, Aug. 2000. doi: 10.1007/s004499900147.
- J. Harmon, P. Pullamanapallil, G. Lyberatos, S. Svoronos, and D. Chynoweth. Stabilization of a Continuous Glucose-Fed Anaerobic Digester via Feed Rate Control. In *American Control Conference*, pages 2156–2160, 1990.
- J. Harmon, S. Svoronos, G. Lyberatos, and D. Chynoweth. Adaptive temperature optimization of continuous anaerobic digesters. *Biomass and Bioenergy*, 5(3-4): 279–288, Jan. 1993. doi: 10.1016/0961-9534(93)90077-H.
- E. L. Haseltine and J. B. Rawlings. Critical Evaluation of Extended Kalman Filtering and Moving-Horizon Estimation. *Ind Eng Chem*, 44(8):2451–2460, Apr. 2005. doi: 10.1021/ie0343081.
- E. Heinzel, I. J. Dunn, and G. B. Ryhiner. Modeling and control for anaerobic wastewater treatment. *Bioprocess Design and Control*, 48(Advances in Biochemical Engineering/Biotechnology):79–114, 1993. doi: 10.1007/BFb0007193.

- M. Henze and P. Harremoës. Anaerobic Treatment of Wastewater in Fixed Film Reactors - A Literature Review. *Water Sci Technol*, 15(8-9):1–101, Feb. 1983.
- M. Henze, W. Gujer, T. Mino, and M. C. M. van Loosdrecht. *Activated Sludge Models ASM1, ASM2, ASM2d and ASM3*. IWA Publishing, London, 2000.
- R. F. Hickey, W.-M. Wu, M. C. Veiga, and R. Jones. Start-Up, Operation, Monitoring and Control of High-Rate Anaerobic Treatment Systems. *Water Sci Technol*, 24(8):207–255, Mar. 1991.
- N. Hilgert, J. Harmand, J.-P. Steyer, and J.-P. Vila. Nonparametric identification and adaptive control of an anaerobic fluidized bed digester. *Control Engineering Practice*, 8(4):367–376, Apr. 2000. doi: 10.1016/S0967-0661(99)00165-3.
- D. Hill, S. Cobb, and J. Bolte. Using volatile fatty acid relationships to predict anaerobic digester failure. *Trans. ASAE; (United States)*, 30(2):496–501, Jan. 1987.
- G. E. Hinton, S. Osindero, and Y.-W. Teh. A fast learning algorithm for deep belief nets. *Neural comput*, 18(7):1527–54, July 2006. doi: 10.1162/neco.2006.18.7.1527.
- J. B. Holm-Nielsen, T. Al Seadi, and P. Oleskowicz-Popiel. The future of anaerobic digestion and biogas utilization. *Bioresour Technol*, 100(22):5478–84, Nov. 2009. doi: 10.1016/j.biortech.2008.12.046.
- P. Holubar, L. Zani, M. Hager, W. Fröschl, Z. Radak, and R. Braun. Advanced controlling of anaerobic digestion by means of hierarchical neural networks. *Water research*, 36(10):2582–8, May 2002.
- P. Holubar, L. Zani, M. Hager, W. Fröschl, Z. Radak, and R. Braun. Start-up and recovery of a biogas-reactor using a hierarchical neural network-based control tool. *J Chem Technol Biot*, 78(8):847–854, Aug. 2003. doi: 10.1002/jctb.854.
- R. Huang, L. T. Biegler, and S. C. Patwardhan. Fast Offset-Free Nonlinear Model Predictive Control Based on Moving Horizon Estimation. *Industrial & Engineering Chemistry Research*, 49(17):7882–7890, Sept. 2010. doi: 10.1021/ie901945y.
- O. Ince, F. G. Babuna, B. Kasapgil, and G. K. Anderson. Experimental Determination of the Inert Soluble COD Fraction of a Brewery Wastewater under Anaerobic Conditions. *Environ Technol*, 19(4):437–442, Apr. 1998. doi: 10.1080/09593331908616700.
- J. Iza, E. Colleran, J. M Paris, and W.-M. Wu. International Workshop on Anaerobic Treatment Technology for Municipal and Industrial Wastewaters: Summary Paper. *Water Science & Technology*, 24(8):1–16, Mar. 1991.
- A. Jaiantilal. randomforest-matlab - Random Forest (Regression, Classification and Clustering) implementation for MATLAB (and Standalone), 2010.
- E. A. Jáuregui-Medina, V. Alcaraz-González, H. O. Méndez-Acosta, and V. González-Alvarez. Observer-based input estimation in continuous anaerobic wastewater treatment processes. *Water Sci Technol*, 60(3):805–12, Jan. 2009. doi: 10.2166/wst.2009.354.
- H.-S. Jeong, C.-W. Suh, J.-L. Lim, S.-H. Lee, and H.-S. Shin. Analysis and application of ADM1 for anaerobic methane production. *Bioprocess and biosystems engineering*, 27(2):81–9, Apr. 2005. doi: 10.1007/s00449-004-0370-4.

- U. Jeppsson, M.-N. Pons, I. Nopens, J. Alex, J. B. Copp, K. V. Gernaey, C. Rosen, J.-P. Steyer, and P. A. Vanrolleghem. Benchmark simulation model no 2: general protocol and exploratory case studies. *Water Sci Technol*, 56(8):67–78, Jan. 2007. doi: 10.2166/wst.2007.604.
- R. Jin, W. Chen, and A. Sudjianto. An efficient algorithm for constructing optimal design of computer experiments. *Journal of Statistical Planning and Inference*, 134(1):268–287, Sept. 2005. doi: 10.1016/j.jspi.2004.02.014.
- T. Johansen. Introduction to Nonlinear Model Predictive Control and Moving Horizon Estimation. In *Selected Topics on Constrained and Nonlinear Control*, number 1, chapter 5, pages 1–53. 2011.
- K. A. Johnson, A. D. Wheatley, and C. J. Fell. An application of an adaptive control algorithm for the anaerobic treatment of industrial effluent. *Process safety and environmental protection*, 73(3):203–211, 1995.
- D. Jones, M. Schonlau, and W. Welch. Efficient global optimization of expensive black-box functions. *Journal of Global optimization*, 13(4):455–492, 1998. doi: 10.1023/A:1008306431147.
- R. Jones, J. MacGregor, K. Murphy, and E. Hall. Towards a Useful Dynamic Model of the Anaerobic Wastewater Treatment Process: A Practical Illustration of Process Identification. *Water Sci Technol*, 25(7):61–71, Mar. 1992.
- R. M. Jones, J. F. Macgregor, and K. L. Murphy. State estimation in wastewater engineering: Application to an anaerobic process. *Environ Monit Assess*, 13(2-3):271–282, Nov. 1989. doi: 10.1007/BF00394233.
- P. Karlson, D. Doenecke, J. Koolman, G. Fuchs, and W. Gerok. *Karlsons Biochemie und Pathologie [Hardcover]*. Thieme Georg Verlag, 15th edition, 2005.
- J. Kauder, N. Boes, C. Pasel, and J.-D. Herbell. Combining Models ADM1 and ASM2d in a Sequencing Batch Reactor Simulation. *Chemical Engineering & Technology*, 30(8):1100–1112, Aug. 2007. doi: 10.1002/ceat.200700045.
- R. Kleerebezem and M. C. M. Van Loosdrecht. Waste characterization for implementation in ADM1. *Water Sci Technol*, 54(4):167–74, Jan. 2006.
- J. Knowles. ParEGO: a hybrid algorithm with on-line landscape approximation for expensive multiobjective optimization problems. *IEEE Transactions on Evolutionary Computation*, 10(1):50–66, Feb. 2006. doi: 10.1109/TEVC.2005.851274.
- J. Knowles, D. Corne, and M. Fleischer. Bounded archiving using the lebesgue measure. In *The 2003 Congress on Evolutionary Computation, 2003. CEC '03.*, volume 4, pages 2490–2497. Ieee, 2003. doi: 10.1109/CEC.2003.1299401.
- K. Koch. *Verfahrenstechnische Untersuchungen und mathematische Modellierung der Prozesse bei der Vergärung von Grassilage*. Dissertation, Technische Universität München, 2010.
- K. Koch, M. Wichern, M. Lübken, and H. Horn. Mono fermentation of grass silage by means of loop reactors. *Bioresource technology*, 100(23):5934–40, Dec. 2009. doi: 10.1016/j.biortech.2009.06.020.
- K. Koch, M. Lübken, T. Gehring, M. Wichern, and H. Horn. Biogas from grass silage - Measurements and modeling with ADM1. *Bioresource technology*, 101(21):8158–65, Nov. 2010. doi: 10.1016/j.biortech.2010.06.009.

- T. Kottas, Y. Boutalis, V. Diamantis, O. Kosmidou, and A. Aivasidis. A Fuzzy Cognitive Network Based Control Scheme for An Anaerobic Digestion Process. In *14th Mediterranean Conference on Control and Automation*, pages 1–7. IEEE, June 2006. doi: 10.1109/MED.2006.328850.
- C. Kravaris and G. Savoglidis. Tracking the singular arc of a continuous bioreactor using sliding mode control. *Journal of the Franklin Institute*, 349(4):1583–1601, May 2012. doi: 10.1016/j.jfranklin.2011.06.011.
- J. W. Kruisselbrink. *Evolution Strategies for Robust Optimization*. Phd, Universiteit Leiden, 2012.
- O. Kujawski and H. Steinmetz. Development of instrumentation systems as a base for control of digestion process stability in full-scale agricultural and industrial biogas plants. *Water Sci Technol*, 60(8):2055–63, Jan. 2009. doi: 10.2166/wst.2009.531.
- J. C. Lagarias, J. A. Reeds, M. H. Wright, and P. E. Wright. Convergence Properties of the Nelder–Mead Simplex Method in Low Dimensions. *SIAM Journal on Optimization*, 9(1):112–147, Jan. 1998. doi: 10.1137/S1052623496303470.
- G. Langergraber, N. Fleischmann, F. Hofstaedter, and A. Weingartner. Monitoring of a paper mill wastewater treatment plant using UV/VIS spectroscopy. *Water Sci Technol*, 49(1):9–14, Jan. 2004.
- J. Lauwers, L. Appels, I. P. Thompson, J. Degrève, J. F. Van Impe, and R. Dewil. Mathematical modelling of anaerobic digestion of biomass and waste: Power and limitations. *Progress in Energy and Combustion Science*, 39(4):383–402, 2013.
- M.-Y. Lee, C.-W. Suh, Y.-T. Ahn, and H.-S. Shin. Variation of ADM1 by using temperature-phased anaerobic digestion (TPAD) operation. *Bioresource technology*, 100(11):2816–22, June 2009. doi: 10.1016/j.biortech.2008.12.025.
- G. Lettinga, A. F. M. van Velsen, S. W. Hobma, W. de Zeeuw, and A. Klapwijk. Use of the upflow sludge blanket (USB) reactor concept for biological wastewater treatment, especially for anaerobic treatment. *Biotechnology and Bioengineering*, 22(4):699–734, Apr. 1980. doi: 10.1002/bit.260220402.
- H. Lindorfer, R. Braun, and R. Kirchmayr. Self-heating of anaerobic digesters using energy crops. *Water Sci Technol*, 53(8):159–66, Jan. 2006.
- J. Liu, G. Olsson, and B. Mattiasson. Monitoring and control of an anaerobic upflow fixed-bed reactor for high-loading-rate operation and rejection of disturbances. *Biotechnology and bioengineering*, 87(1):43–53, July 2004a. doi: 10.1002/bit.20088.
- J. Liu, G. Olsson, and B. Mattiasson. Control of an anaerobic reactor towards maximum biogas production. *Water Sci Technol*, 50(11):189–98, Jan. 2004b.
- J. Liu, G. Olsson, and B. Mattiasson. Extremum-seeking with variable gain control for intensifying biogas production in anaerobic fermentation. *Water Sci Technol*, 53(4-5):35–44, Jan. 2006.
- Y. Liu, H.-L. Xu, S.-F. Yang, and J.-H. Tay. Mechanisms and models for anaerobic granulation in upflow anaerobic sludge blanket reactor. *Water Res*, 37(3):661–73, Feb. 2003.
- M. Lübken. *Mathematical modeling of anaerobic digestion processes*. Dissertation, Technische Universität München, 2009.

- M. Lübken, M. Wichern, F. Bischof, S. Prechtl, and H. Horn. Development of an empirical mathematical model for describing and optimizing the hygiene potential of a thermophilic anaerobic bioreactor treating faeces. *Water Sci Technol*, 55(7):95, Apr. 2007a. doi: 10.2166/wst.2007.132.
- M. Lübken, M. Wichern, M. Schlattmann, A. Gronauer, and H. Horn. Modelling the energy balance of an anaerobic digester fed with cattle manure and renewable energy crops. *Water Res*, 41(18):4085–96, Oct. 2007b. doi: 10.1016/j.watres.2007.05.061.
- M. Lübken, T. Gehring, and M. Wichern. Microbiological fermentation of lignocellulosic biomass: current state and prospects of mathematical modeling. *Applied microbiology and biotechnology*, 85(6):1643–52, Feb. 2010. doi: 10.1007/s00253-009-2365-1.
- M. Madsen, J. B. Holm-Nielsen, and K. H. Esbensen. Monitoring of anaerobic digestion processes: A review perspective. *Renewable and Sustainable Energy Reviews*, 15(6):3141–3155, Aug. 2011. doi: 10.1016/j.rser.2011.04.026.
- U. Maeder, F. Borrelli, and M. Morari. Linear offset-free Model Predictive Control. *Automatica*, 45(10):2214–2222, 2009.
- L. Mailleret and O. Bernard. A simple robust controller to stabilise an anaerobic digestion process. In *Proceedings of the 8th Conference on Computer Applications in Biotechnology*, pages 213–218, 2001.
- L. Mailleret, O. Bernard, and J. P. Steyer. Robust regulation of anaerobic digestion processes. *Water Science and Technology*, 48(6):87–94, Jan. 2003.
- L. Mailleret, O. Bernard, and J.-P. Steyer. Nonlinear adaptive control for bioreactors with unknown kinetics. *Automatica*, 40(8):1379–1385, Aug. 2004. doi: 10.1016/j.automatica.2004.01.030.
- U. Marchaim and C. Krause. Propionic to acetic acid ratios in overloaded anaerobic digestion. *Bioresource Technol*, 43(3):195–203, Jan. 1993. doi: 10.1016/0960-8524(93)90031-6.
- N. Marcos, M. Guay, and D. Dochain. Output feedback adaptive extremum seeking control of a continuous stirred tank bioreactor with Monod's kinetics. *Journal of Process Control*, 14(7):807–818, Oct. 2004a. doi: 10.1016/j.jprocont.2003.12.002.
- N. Marcos, M. Guay, D. Dochain, and T. Zhang. Adaptive extremum-seeking control of a continuous stirred tank bioreactor with Haldane's Kinetics. *Journal of Process Control*, 14(3):317–328, Apr. 2004b. doi: 10.1016/S0959-1524(03)00070-2.
- S. Marsili-Libelli and S. Beni. Shock load modelling in the anaerobic digestion process. *Ecol Modell*, 84(1-3):215–232, Jan. 1996. doi: 10.1016/0304-3800(94)00125-1.
- S. Marsili-Libelli and A. Müller. Adaptive fuzzy pattern recognition in the anaerobic digestion process. *Pattern Recognition Letters*, 17(6):651–659, May 1996. doi: 10.1016/0167-8655(96)00030-X.
- A. Martinez-Sibaja, R. Posada-Gomez, A. Alvarado-Lassman, and A. Sebastia-Cortes. Cascade Fuzzy Logic Controller for an Anaerobic Digester. In *Electronics, Robotics and Automotive Mechanics Conference (CERMA 2007)*, pages 395–399, Morelos, Sept. 2007. IEEE. doi: 10.1109/CERMA.2007.4367719.
- D. Mayne, J. Rawlings, C. Rao, and P. Scokaert. Constrained model predictive control: Stability and optimality. *Automatica*, 36(6):789–814, June 2000. doi: 10.1016/S0005-1098(99)00214-9.

- P. McKendry. Energy production from biomass (part 1): overview of biomass. *Bioresource Technol.*, 83(1):37–46, May 2002. doi: 10.1016/S0960-8524(01)00118-3.
- H. Méndez-Acosta, D. Campos-Delgado, and R. Femat. Intelligent control of an anaerobic digester: fuzzy-based gain scheduling for a geometrical approach. In *Proceedings of the 2003 IEEE International Symposium on Intelligent Control ISIC-03*, pages 298–303. IEEE, 2003. doi: 10.1109/ISIC.2003.1254650.
- H. Méndez-Acosta, D. Campos-Delgado, R. Femat, and V. González-Alvarez. A robust feedforward/feedback control for an anaerobic digester. *Comput. Chem. Eng.*, 29(7):1613–1623, June 2005. doi: 10.1016/j.compchemeng.2005.01.005.
- H. Méndez-Acosta, B. Palacios-Ruiz, J. Steyer, V. Alcaraz-González, E. Latrille, and V. González-Alvarez. Nonlinear approach for the VFA regulation in an anaerobic digester. In P. Michel, editor, *10th International IFAC Symposium on Computer Applications in Biotechnology*, volume 1, pages 79–84, June 2007a. doi: 10.3182/20070604-3-MX-2914.00015.
- H. Méndez-Acosta, B. Palacios-Ruiz, V. Alcaraz-González, V. González-Álvarez, and J. García-Sandoval. A robust control scheme to improve the stability of anaerobic digestion processes. *Journal of Process Control*, 20(4):375–383, Apr. 2010. doi: 10.1016/j.jprocont.2010.01.006.
- H. O. Méndez-Acosta, R. Femat, and D. U. Campos-Delgado. Improving the Performance on the Chemical Oxygen Demand Regulation in Anaerobic Digestion. *Ind Eng Chem Res*, 43(1):95–104, Jan. 2004. doi: 10.1021/ie030298c.
- H. O. Méndez-Acosta, J. P. Steyer, R. Femat, and V. González-Alvarez. Robust Nonlinear Control of a Pilot-Scale Anaerobic Digester. *Lect Notes Contr Inf*, 361/2007:165–199, 2007b. doi: 10.1007/978-3-540-73188-7__6.
- H. O. Méndez-Acosta, B. Palacios-Ruiz, V. Alcaraz-González, J.-P. Steyer, V. González-Álvarez, and E. Latrille. Robust Control of Volatile Fatty Acids in Anaerobic Digestion Processes. *Ind Eng Chem Res*, 47(20):7715–7720, Oct. 2008. doi: 10.1021/ie800256e.
- H. O. Méndez-Acosta, J. P. García-Sandoval, V. González-Álvarez, V. Alcaraz-González, and J. A. Jáuregui-Jáuregui. Regulation of the organic pollution level in anaerobic digesters by using off-line COD measurements. *Bioresource Technol*, 102(17):7666–72, Sept. 2011. doi: 10.1016/j.biortech.2011.05.053.
- J. Mockus, V. Tiesis, and A. Zilinskas. The application of Bayesian methods for seeking the extremum. *Towards Global Optimization*, 2:117–129, 1978.
- R. Moletta, Y. Escoffier, F. Ehlinger, J. Coudert, and J. Leyris. On-line automatic control system for monitoring an anaerobic fluidized-bed reactor: response to organic overload. *Water Sci Technol*, 30(12):11–20, Dec. 1994.
- F. Molina, M. Castellano, C. García, E. Roca, and J. M. Lema. Selection of variables for on-line monitoring, diagnosis, and control of anaerobic digestion processes. *Water Science and Technology*, 60(3):615–22, Jan. 2009. doi: 10.2166/wst.2009.379.
- O. Monroy, J. Alvarez-Ramirez, F. Cuervo, and R. Femat. An Adaptive Strategy To Control Anaerobic Digesters for Wastewater Treatment. *Industrial & Engineering Chemistry Research*, 35(10):3442–3446, Jan. 1996. doi: 10.1021/ie960238p.

- J. L. Montiel-Escobar, V. Alcaraz-González, H. O. Méndez-Acosta, and V. González-Álvarez. ADM1-Based Robust Interval Observer for Anaerobic Digestion Processes. *CLEAN - Soil, Air, Water*, 40(9):933–940, Sept. 2012. doi: 10.1002/clen.201100718.
- M. Morari and J. H. Lee. Model predictive control: past, present and future. *Comput. Chem. Eng.*, 23(4-5):667–682, May 1999. doi: 10.1016/S0098-1354(98)00301-9.
- M. Morari and U. Maeder. Nonlinear offset-free model predictive control. *Automatica*, 48(9):2059–2067, 2012.
- E. Morel, B. Tartakovsky, S. Guiot, and M. Perrier. Design of a multi-model observer-based estimator for anaerobic reactor monitoring. *Comput. Chem. Eng.*, 31(2):78–85, Dec. 2006a. doi: 10.1016/j.compchemeng.2006.05.003.
- E. Morel, B. Tartakovsky, S. R. Guiot, and M. Perrier. ADM1 application for tuning and performance analysis of a multi-model observer-based estimator. *Water Sci Technol*, 54(4):93–100, Jan. 2006b.
- S. Mu, Y. Zeng, and P. Wu. Multivariable control of anaerobic reactor by using external recirculation and bypass ratio. *Journal of Chemical Technology & Biotechnology*, 83(6):892–903, June 2008. doi: 10.1002/jctb.1888.
- S. J. Mu, Y. Zeng, B. Tartakovsky, and P. Wu. Simulation and Control of an Upflow Anaerobic Sludge Blanket (UASB) Reactor Using an ADM1-Based Distributed Parameter Model. *Ind Eng Chem Res*, 46(5):1519–1526, Feb. 2007. doi: 10.1021/ie0608531.
- A. Müller, S. Marsili-Libelli, A. Aivasidis, T. Lloyd, S. Kröner, and C. Wandrey. Fuzzy control of disturbances in a wastewater treatment process. *Water Research*, 31(12):3157–3167, Dec. 1997. doi: 10.1016/S0043-1354(97)00215-7.
- E. Murnleitner. *State Detection and Feedback Control of the Anaerobic Wastewater Treatment Using Fuzzy Logic*. Dissertation, Technische Universität München, 2001.
- E. Murnleitner, T. M. Becker, and A. Delgado. State detection and control of overloads in the anaerobic wastewater treatment using fuzzy logic. *Water Res*, 36(1):201–11, Jan. 2002.
- V. Nallathambi Gunaseelan. Anaerobic digestion of biomass for methane production: A review. *Biomass and Bioenergy*, 13(1-2):83–114, Jan. 1997. doi: 10.1016/S0961-9534(97)00020-2.
- J. A. Nelder and R. Mead. A Simplex Method for Function Minimization. *The Computer Journal*, 7(4):308–313, Jan. 1965. doi: 10.1093/comjnl/7.4.308.
- A. M. Nielsen, H. Spanjers, and E. I. P. Volcke. Calculating pH in pig manure taking into account ionic strength. *Water Sci Technol*, 57(11):1785–90, Jan. 2008. doi: 10.2166/wst.2008.099.
- OBSERV'ER. The state of renewable energies in europe - 12th EurObserv'ER Report. Technical Report 0, OBSERV'ER, Paris, 2012.
- M. Oigurek and J. Alex. Überlegungen zur Modellierung mit dem ADM1. In *ifak Workshop: Steuerung, Regelung und Simulation von Biogasanlagen*, Leipzig, 2013. ifak e.V.
- G. Olsson, M. K. Nielsen, and Z. Yuan. *Instrumentation, Control and Automation in Wastewater Systems (Scientific & Technical Report)*. IWA Publishing, 2007.

- A. Ordace, C. Ionescu, T. P. Vannecke, E. I. P. Volcke, I. Nasu, and R. De Keyser. Predictive control of anaerobic digestion of wastewater sludge: a feasibility study. In *Proceedings of the 16th International Conference on System Theory, Control and Computing*, Sinaia, Romania, 2012.
- H. E. Osman. Online random forests based on CorrFS and CorrBE. In *2008 IEEE Computer Society Conference on Computer Vision and Pattern Recognition Workshops*, pages 1–7, Anchorage, AK, June 2008. IEEE. doi: 10.1109/CVPRW.2008.4563065.
- T. Patterson, S. Esteves, R. Dinsdale, and A. Guwy. Life cycle assessment of biogas infrastructure options on a regional scale. *Bioresource technology*, 102(15):7313–23, Aug. 2011. doi: 10.1016/j.biortech.2011.04.063.
- M. Perrier and D. Dochain. Evaluation of control strategies for anaerobic digestion processes. *International Journal of Adaptive Control and Signal Processing*, 7(4):309–321, July 1993. doi: 10.1002/acs.4480070408.
- E. Petre, D. Selisteanu, and D. Sendrescu. On adaptive control of an anaerobic digestion bioprocess. In *7th WSEAS International Conference on Systems Theory and Scientific Computation*, pages 7–12, Athè, 2007.
- E. Petre, D. Selisteanu, and D. Sendrescu. Adaptive and robust-adaptive control strategies for anaerobic wastewater treatment bioprocesses. *Chemical Engineering Journal*, 217:363–378, Feb. 2013. doi: 10.1016/j.cej.2012.11.129.
- P. F. Pind, I. Angelidaki, B. K. Ahring, K. Stamatelatou, and G. Lyberatos. Monitoring and control of anaerobic reactors. *Adv Biochem Eng Biot*, 82:135–82, Jan. 2003.
- R. Plank. *Wärmeaustauscher (Handbuch der Kältetechnik Band 6)*. Springer, 1st edition, 1988.
- M. F. Podruzny and L. van den Berg. Development of a computer control system for anaerobic methane-producing reactors. *Biotechnology and bioengineering*, 26(4):392–3, Apr. 1984. doi: 10.1002/bit.260260419.
- M. Polihronakis, L. Petrou, and A. Deligiannis. Parameter adaptive control techniques for anaerobic digesters - real-life experiments. *Computers & Chemical Engineering*, 17(12):1167–1179, Dec. 1993. doi: 10.1016/0098-1354(93)80097-7.
- M. Polit, A. Genovesi, and B. Claudet. Fuzzy logic observers for a biological wastewater treatment process. *Appl Numer Math*, 39(2):173–180, Nov. 2001. doi: 10.1016/S0168-9274(01)00098-8.
- A. Polster. *Anwendung des erweiterten KALMAN-Filters zur Zustandsbeobachtung in Biogasanlagen (Application of the extended Kalman filter for state estimation in biogas plants)*. Dissertation, Technische Universität Dresden (Dresden University of Technology), 2009.
- W. Ponweiser, T. Wagner, D. Biermann, and M. Vincze. Multiobjective Optimization on a Limited Budget of Evaluations Using Model-Assisted S-Metric Selection. *Lecture Notes in Computer Science - Parallel Problem Solving from Nature*, 5199:784–794, 2008. doi: 10.1007/978-3-540-87700-4__78.
- W. Pretorius. pH-controlled feed-on-demand for high-rate anaerobic systems. *Water Science and Technology*, 30(8):1–8, Oct. 1994.

- A. Puñal, J. Rodríguez, A. Franco, E. F. Carrasco, E. Roca, and J. M. Lema. Advanced monitoring and control of anaerobic wastewater treatment plants: diagnosis and supervision by a fuzzy-based expert system. *Water Sci Technol*, 43(7):191–8, Jan. 2001.
- A. Puñal, J. Rodríguez, E. F. Carrasco, E. Roca, and J. M. Lema. Expert system for the on-line diagnosis of anaerobic wastewater treatment plants. *Water Sci Technol*, 45(10):195–200, Jan. 2002.
- A. Puñal, L. Palazzotto, J. C. Bouvier, T. Conte, and J. P. Steyer. Automatic control of volatile fatty acids in anaerobic digestion using a fuzzy logic based approach. *Water Science and Technology*, 48(6):103–10, Jan. 2003.
- P. Pullammanappallil, J. Harmon, D. P. Chynoweth, G. Lyberatos, and S. A. Svoronos. Avoiding digester imbalance through real-time expert system control of dilution rate. *Appl Biochem Biotech*, 28-29(1):33–42, Mar. 1991. doi: 10.1007/BF02922587.
- P. C. Pullammanappallil, S. A. Svoronos, D. P. Chynoweth, and G. Lyberatos. Expert system for control of anaerobic digesters. *Biotechnol Bioeng*, 58(1):13–22, Apr. 1998.
- P. C. Pullammanappallil, D. P. Chynoweth, G. Lyberatos, and S. A. Svoronos. Stable performance of anaerobic digestion in the presence of a high concentration of propionic acid. *Bioresource technology*, 78(2):165–9, June 2001.
- S. Qin and T. A. Badgwell. A survey of industrial model predictive control technology. *Control Eng Pract*, 11(7):733–764, July 2003. doi: 10.1016/S0967-0661(02)00186-7.
- J. Rajesh Banu and S. Kaliappan. Treatment of tannery wastewater using hybrid upflow anaerobic sludge blanket reactor. *Journal of Environmental Engineering and Science*, 6(4):415–421, July 2007. doi: 10.1139/s06-063.
- A. Ramakrishnan and R. Y. Surampalli. Performance of anaerobic hybrid reactors for the treatment of complex phenolic wastewaters with biogas recirculation. *Bioresource technology*, 129C(null):26–32, Nov. 2012. doi: 10.1016/j.biortech.2012.11.035.
- C. Rao, J. Rawlings, and D. Mayne. Constrained state estimation for nonlinear discrete-time systems: stability and moving horizon approximations. *IEEE Trans Automat Contr*, 48(2):246–258, Feb. 2003. doi: 10.1109/TAC.2002.808470.
- C. V. Rao. *Moving horizon strategies for the constrained monitoring and control of nonlinear discrete-time systems*. Doctor of philosophy, University of Wisconsin-Madison, 2000.
- A. Rapaport and J. Harmand. Robust regulation of a class of partially observed nonlinear continuous bioreactors. *Journal of Process Control*, 12(2):291–302, Feb. 2002. doi: 10.1016/S0959-1524(01)00029-4.
- A. Raue, C. Kreutz, T. Maiwald, J. Bachmann, M. Schilling, U. Klingmüller, and J. Timmer. Structural and practical identifiability analysis of partially observed dynamical models by exploiting the profile likelihood. *Bioinformatics (Oxford, England)*, 25(15):1923–9, Aug. 2009. doi: 10.1093/bioinformatics/btp358.
- A. Raue, C. Kreutz, T. Maiwald, U. Klingmuller, and J. Timmer. Addressing parameter identifiability by model-based experimentation. *IET systems biology*, 5(2):120–30, Mar. 2011. doi: 10.1049/iet-syb.2010.0061.
- J. B. Rawlings and B. R. Bakshi. Particle filtering and moving horizon estimation. *Comput. Chem. Eng.*, 30(10-12):1529–1541, Sept. 2006. doi: 10.1016/j.compchemeng.2006.05.031.

- K. Reif, S. Günther, E. Yaz, and R. Unbehauen. Stochastic stability of the discrete-time extended Kalman filter. *IEEE Trans Automat Contr*, 44(4):714–728, Apr. 1999. doi: 10.1109/9.754809.
- K. Reif, S. Günther, E. Yaz, and R. Unbehauen. Stochastic stability of the continuous-time extended Kalman filter. *IEE Proceedings - Control Theory and Applications*, 147(1):45–52, Jan. 2000. doi: 10.1049/ip-cta:20000125.
- P. Renard, D. Dochain, G. Bastin, H. Naveau, and E. J. Nyns. Adaptive control of anaerobic digestion processes - a pilot-scale application. *Biotechnology and bioengineering*, 31(4):287–94, Mar. 1988. doi: 10.1002/bit.260310402.
- P. Renard, V. Van Breusegem, M. T. Nguyen, H. Naveau, and E. J. Nyns. Implementation of an adaptive controller for the startup and steady-state running of a biomethanation process operated in the CSTR mode. *Biotechnology and bioengineering*, 38(8):805–12, Oct. 1991. doi: 10.1002/bit.260380802.
- L. Rieger, J. Alex, S. Winkler, M. Boehler, M. Thomann, and H. Siegrist. Progress in sensor technology - progress in process control? Part 1: sensor property investigation and classification. *Water Sci Technol*, 47(2):103–12, Jan. 2003.
- A. Rincon, F. Angulo, and G. Olivari. Control of an anaerobic digester through normal form of fold bifurcation. *J Process Contr*, 19(8):1355–1367, Sept. 2009. doi: 10.1016/j.jprocont.2009.04.006.
- A. Rincón, C. Erazo, and F. Angulo. A robust adaptive controller for an anaerobic digester with saturated input: Guarantees for the boundedness and convergence properties. *J Process Contr*, 22(9):1785–1792, Oct. 2012. doi: 10.1016/j.jprocont.2012.07.014.
- A. Rodriguez, G. Quiroz, J. de Leon, and R. Femat. State and parameter estimation of an anaerobic digester model. In *2011 IEEE International Conference on Automation Science and Engineering*, pages 690–695. IEEE, Aug. 2011. doi: 10.1109/CASE.2011.6042484.
- J. Rodríguez, G. Ruiz, F. Molina, E. Roca, and J. Lema. A hydrogen-based variable-gain controller for anaerobic digestion processes. *Water Science & Technology*, 54(2):57–62, July 2006. doi: 10.2166/wst.2006.486.
- M. Romli, P. Greenfield, and P. Lee. Effect of recycle on a two-phase high-rate anaerobic wastewater treatment system. *Water Research*, 28(2):475–482, Feb. 1994. doi: 10.1016/0043-1354(94)90285-2.
- C. Rosen, U. Jeppsson, L. Rieger, and P. A. Vanrolleghem. Adding realism to simulated sensors and actuators. *Water Sci Technol*, 57(3):337–44, Jan. 2008. doi: 10.2166/wst.2008.130.
- A. Rozzi. Modelling and control of anaerobic digestion processes. *Transactions of the Institute of Measurement and Control*, 6(3):153–159, July 1984. doi: 10.1177/014233128400600306.
- A. Rozzi, A. Di Pinto, and A. Brunetti. Anaerobic process control by bicarbonate monitoring. *Environmental Technology Letters*, 6(12):594–601, Dec. 1985. doi: 10.1080/09593338509384380.
- G. Ryhiner, I. Dunn, E. Heinze, and S. Rohani. Adaptive on-line optimal control of bioreactors: application to anaerobic degradation. *Journal of Biotechnology*, 22(1-2):89–105, Jan. 1992. doi: 10.1016/0168-1656(92)90134-U.

- G. B. Ryhiner, E. Heinzel, and I. J. Dunn. Modeling and simulation of anaerobic wastewater treatment and its application to control design: Case whey. *Biotechnology Progress*, 9(3):332–343, May 1993. doi: 10.1021/bp00021a013.
- A. Saffari, C. Leistner, J. Santner, M. Godec, and H. Bischof. On-line Random Forests. In *2009 IEEE 12th International Conference on Computer Vision Workshops, ICCV Workshops*, pages 1393–1400. IEEE, Sept. 2009. doi: 10.1109/ICCVW.2009.5457447.
- V. Saravanan and T. R. Sreekrishnan. Modelling anaerobic biofilm reactors—a review. *J Environ Manage*, 81(1):1–18, Oct. 2006. doi: 10.1016/j.jenvman.2005.10.002.
- M. Sbarciog and A. Vande Wouwer. Some Considerations About Control of Multi-species Anaerobic Digestion Systems. In *7th Vienna International Conference on Mathematical Modelling (MATHMOD)*, 2012.
- M. Sbarciog, M. Loccoufier, and A. Vande Wouwer. On the Optimization of Biogas Production in Anaerobic Digestion Systems. In *18th IFAC World Congress*, pages 7150–7155, Milano, 2011.
- M. Sbarciog, M. Loccoufier, and A. Vande Wouwer. An optimizing start-up strategy for a bio-methanator. *Bioproc Biosyst Eng*, 35(4):565–78, May 2012a. doi: 10.1007/s00449-011-0629-5.
- M. Sbarciog, J. A. Moreno, and A. Vande Wouwer. A Biogas-Based Switching Control Policy for Anaerobic Digestion Systems. In K. Vinay, editor, *Advanced Control of Chemical Processes*, volume 8, pages 603–608, Furama Riverfront, Singapore, July 2012b. doi: 10.3182/20120710-4-SG-2026.00056.
- P. Scherer, S. Ergun, and O. Schmidt. Entwicklung einer Fuzzy-Logik-Regelung für eine Hochdurchsatz-Biogasanlage: "Telefermentation" zwischen Hamburg und Nordhausen. In *Güldzower Fachgespräche: Band 27 Messen, Steuern, Regeln bei der Biogaserzeugung*, pages 146–171, Güldzow, 2008. FNR.
- P. Scherer, K. Lehmann, O. Schmidt, and B. Demirel. Application of a fuzzy logic control system for continuous anaerobic digestion of low buffered, acidic energy crops as mono-substrate. *Biotechnol Bioeng*, 102(3):736–48, Feb. 2009. doi: 10.1002/bit.22108.
- M. Schlegel, K. Stockmann, T. Binder, and W. Marquardt. Dynamic optimization using adaptive control vector parameterization. *Comput. Chem. Eng.*, 29(8):1731–1751, 2005.
- M. A. Schoen, D. Sperl, M. Gadermaier, M. Goberna, I. Franke-Whittle, H. Insam, J. Ablinger, and B. Wett. Population dynamics at digester overload conditions. *Bioresource Technol*, 100(23):5648–55, Dec. 2009. doi: 10.1016/j.biortech.2009.06.033.
- A. Schuldt and R. Dinse. Übungen zur Tierernährung im Rahmen des Moduls "Tierernährung und Futtermittekunde" (B-PM15), 2010.
- O. Schütze, X. Esquivel, A. Lara, and C. A. C. Coello. Using the Averaged Hausdorff Distance as a Performance Measure in Evolutionary Multiobjective Optimization. *IEEE T Evolut Comput*, 16(4):504–522, Aug. 2012. doi: 10.1109/TEVC.2011.2161872.
- L. Seghezzo, G. Zeeman, J. B. van Lier, H. Hamelers, and G. Lettinga. A review: The anaerobic treatment of sewage in UASB and EGSB reactors. *Bioresource Technology*, 65(3):175–190, Sept. 1998. doi: 10.1016/S0960-8524(98)00046-7.

- J. Seok. Hybrid adaptive optimal control of anaerobic fluidized bed bioreactor for the de-icing waste treatment. *Journal of Biotechnology*, 102(2):165–175, Apr. 2003. doi: 10.1016/S0168-1656(03)00018-X.
- S. Shen, G. C. Premier, A. Guwy, and R. Dinsdale. Bifurcation and stability analysis of an anaerobic digestion model. *Nonlinear Dyn*, 48(4):391–408, Aug. 2006. doi: 10.1007/s11071-006-9093-1.
- H. Siegrist, D. Vogt, J. L. Garcia-Heras, and W. Gujer. Mathematical model for meso- and thermophilic anaerobic sewage sludge digestion. *Environmental science & technology*, 36(5):1113–23, Mar. 2002. doi: 10.1021/es010139p.
- I. Simeonov. Modelling and control of anaerobic digestion of organic waste. *Chem Biochem Eng Q*, 8(2):45–52, 1994.
- I. Simeonov and I. Queinnec. Linearizing control of the anaerobic digestion with addition of acetate (control of the anaerobic digestion). *Control Engineering Practice*, 14(7):799–810, July 2006. doi: 10.1016/j.conengprac.2005.04.011.
- I. Simeonov and S. Stoyanov. Modelling and Dynamic Compensator Control of the Anaerobic Digestion of Organic Wastes. *Chem Biochem Eng Q*, 17(4):285–292, 2003.
- I. Simeonov and S. Stoyanov. Modelling and Extremum Seeking Control of a Cascade of Two Anaerobic Bioreactors. *International Journal Bioautomation*, 15(1):13–24, 2011.
- I. Simeonov, N. Noykova, and M. Gyllenberg. Identification and Extremum Seeking Control of the Anaerobic Digestion of Organic Wastes. *Cybernetics and Information technologies*, 7(2):73–84, 2007.
- D. Simon. *Optimal State Estimation: Kalman, H Infinity, and Nonlinear Approaches*. Wiley-Interscience, 2006.
- I. V. Skiadas, H. N. Gavala, J. E. Schmidt, and B. K. Ahring. Anaerobic granular sludge and biofilm reactors. *Adv Biochem Eng Biot*, 82:35–67, Jan. 2003.
- I. Y. Smets, J. V. Haegebaert, R. Carrette, and J. F. Van Impe. Linearization of the activated sludge model ASM1 for fast and reliable predictions. *Water research*, 37(8):1831–51, Apr. 2003. doi: 10.1016/S0043-1354(02)00580-8.
- H. Spanjers and J. van Lier. Instrumentation in anaerobic treatment: research and practice. *Water Sci Technol*, 53(4-5):63–76, Mar. 2006. doi: 10.2166/wst.2006.111.
- K. Stamatelatou, G. Lyberatos, C. Tsiligiannis, S. Pavlou, P. Pullammanappallil, and S. A. Svoronos. Optimal and suboptimal control of anaerobic digesters. *Environ Model Assess*, 2(4):355–363, 1997. doi: 10.1023/A:1019034032664.
- Statistics Netherlands. Renewable energy in the Netherlands 2011. Technical report, Centraal Bureau voor de Statistiek, The Hague/Heerlen, 2012.
- J. P. Steyer, D. Rolland, J. C. Bouvier, and R. Moletta. Hybrid fuzzy neural network for diagnosis — application to the anaerobic treatment of wine distillery wastewater in a fluidized bed reactor. *Water Sci Technol*, 36(6-7):209–217, 1997. doi: 10.1016/S0273-1223(97)00525-8.
- J.-P. Steyer, P. Buffière, D. Rolland, and R. Moletta. Advanced control of anaerobic digestion processes through disturbances monitoring. *Water Research*, 33(9):2059–2068, June 1999. doi: 10.1016/S0043-1354(98)00430-8.

- J. P. Steyer, O. Bernard, D. Batstone, and I. Angelidaki. Lessons learnt from 15 years of ICA in anaerobic digesters. *Water Sci Technol*, 53(4-5):25–33, Mar. 2006. doi: 10.2166/wst.2006.107.
- S. Strömberg, M. O. Posselt, and J. Liu. Computer simulation of control strategies for optimal anaerobic digestion. *Water Sci Technol*, 67(3):594–603, Jan. 2012. doi: 10.2166/wst.2012.603.
- A. Stuhlsatz, J. Lippel, and T. Zielke. Discriminative feature extraction with Deep Neural Networks. In *The 2010 International Joint Conference on Neural Networks (IJCNN)*, volume 0, pages 1–8, Barcelona, July 2010a. IEEE. doi: 10.1109/IJCNN.2010.5596329.
- A. Stuhlsatz, J. Lippel, and T. Zielke. Feature Extraction for Simple Classification. In *2010 20th International Conference on Pattern Recognition*, number x, pages 1525–1528, Istanbul, Aug. 2010b. IEEE. doi: 10.1109/ICPR.2010.377.
- A. Stuhlsatz, J. Lippel, and T. Zielke. Feature Extraction With Deep Neural Networks by a Generalized Discriminant Analysis. *IEEE Transactions on Neural Networks and Learning Systems*, 23(4):596–608, Apr. 2012. doi: 10.1109/TNNLS.2012.2183645.
- H. O. Tabrizi, G. Amoabediny, B. Moshiri, A. Adhami, M. P. H. Abbas, and E. Imenipour. Sliding mode control of an anaerobic upflow fixed bed bioreactor. *J Biotechnol*, 150(null):227–228, Nov. 2010. doi: 10.1016/j.jbiotec.2010.09.065.
- B. Tartakovsky, E. Morel, J. P. Steyer, and S. R. Guiot. Application of a variable structure model in observation and control of an anaerobic digestor. *Biotechnology progress*, 18(4):898–903, 2002. doi: 10.1021/bp010142c.
- B. Tartakovsky, E. Morel, and S. R. Guiot. Application of a VSM-Based Process Control to a Bench-Scale Anaerobic Digestor. *Industrial & Engineering Chemistry Research*, 44(1):106–113, Jan. 2005. doi: 10.1021/ie030799y.
- D. Theilliol, J.-C. Ponsart, J. Harmand, C. Join, and P. Gras. On-line estimation of unmeasured inputs for anaerobic wastewater treatment processes. *Control Eng Pract*, 11(9):1007–1019, Sept. 2003. doi: 10.1016/S0967-0661(02)00230-7.
- X. Tian, P. Wang, D. Huang, and S. Chen. Offset-free multistep nonlinear model predictive control under plant-model mismatch. *International Journal of Adaptive Control and Signal Processing*, pages n/a–n/a, Nov. 2012. doi: 10.1002/acs.2367.
- P. A. Tipler and G. Mosca. *Physik: für Wissenschaftler und Ingenieure (German Edition)*. Spektrum Akademischer Verlag, 2nd edition, 2007.
- M. C. Tomei, C. M. Braguglia, G. Cento, and G. Mininni. Modeling of Anaerobic Digestion of Sludge. *Critical Reviews in Environmental Science and Technology*, 39(12):1003–1051, Nov. 2009. doi: 10.1080/10643380801977818.
- H. Trautmann, T. Wagner, and D. Brockhoff. R2-EMOA : Focused Multiobjective Search Using R2-Indicator-Based Selection. In *Learning and Intelligent Optimization Conference*, 2013.
- R. Tschepeetzki and M. Ogurek. SIMBA, 2010.
- M. Türk. Rohrleitungstransport von Flüssigmist - Druckverlustberechnung, Stoffdaten, Tabellen, Programmbeschreibung. Technical report, Institut für Agrartechnik Bornim e.V., Potsdam, 1994.

- D. Urrego-Patarroyo, E. Sanchez, S. Carlos-Hernandez, and J. F. Beteau. Recurrent Neural Networks Biomass Observer for Anaerobic Processes. In *2008 IEEE International Symposium on Intelligent Control*, pages 183–188. IEEE, Sept. 2008. doi: 10.1109/ISIC.2008.4635946.
- J. J. Valera García, V. Gómez Garay, E. Irigoyen Gordo, F. Artaza Fano, and M. Larrea Sukia. Intelligent Multi-Objective Nonlinear Model Predictive Control (iMO-NMPC): Towards the 'on-line' optimization of highly complex control problems. *Expert Syst Appl*, 39(7):6527–6540, June 2012. doi: 10.1016/j.eswa.2011.12.052.
- P. J. Van Soest, J. B. Robertson, and B. A. Lewis. Methods for dietary fiber, neutral detergent fiber, and nonstarch polysaccharides in relation to animal nutrition. *J Dairy Sci*, 74(10):3583–97, Oct. 1991. doi: 10.3168/jds.S0022-0302(91)78551-2.
- VDI. *VDI 4630 - Vergärung organischer Stoffe*. Verein deutscher Ingenieure, Düsseldorf, april 2006 edition, 2006.
- V. D. L. U.-u. F. VDLUFA. *Methodenbuch. Band III. Die chemische Untersuchung von Futtermitteln*. VDLUFA-Verlag, Darmstadt, inkl. 4. e edition, 1997.
- A. K. Venkatesan. *Optimization of Substrate Feed in a Biogas Plant Using Non-linear Model Predictive Control*. Master thesis, Cologne University of Applied Sciences, 2012.
- J. von Sachs, U. Meyer, P. Rys, and H. Feitkenhauer. New approach to control the methanogenic reactor of a two-phase anaerobic digestion system. *Water research*, 37(5):973–82, Mar. 2003.
- E. Voß, D. Weichgrebe, and K.-H. Rosenwinkel. FOS/TAC: Herleitung, Methodik, Anwendung und Aussagekraft. In *Internationale Wissenschaftstagung Biogas Science 2009 Band 3*, pages 675–682, Freising, 2009. Bayerische Landesanstalt für Landwirtschaft.
- C. Waewsak, A. Nopharatana, and P. Chaiprasert. Neural-fuzzy control system application for monitoring process response and control of anaerobic hybrid reactor in wastewater treatment and biogas production. *Journal of Environmental Sciences*, 22(12):1883–1890, Dec. 2010. doi: 10.1016/S1001-0742(09)60334-X.
- T. Wagner and H. Trautmann. Integration of Preferences in Hypervolume-Based Multiobjective Evolutionary Algorithms by Means of Desirability Functions. *IEEE T Evolut Comput*, 14(5):688–701, Oct. 2010. doi: 10.1109/TEVC.2010.2058119.
- T. Wagner, N. Beume, and B. Naujoks. Pareto-, aggregation-, and indicator-based methods in many-objective optimization. *Lecture Notes in Computer Science - Evolutionary Multi-Criterion Optimization*, 4403(September):742–756, 2007. doi: 10.1007/978-3-540-70928-2__56.
- T. Wagner, M. Emmerich, A. Deutz, and W. Ponweiser. On expected-improvement criteria for model-based multi-objective optimization. *Lecture Notes in Computer Science - Parallel Problem Solving from Nature - PPSN XI*, 6238:718–727, 2010. doi: 10.1007/978-3-642-15844-5__72.
- H. Wang, B. Kalchev, Y. Tian, I. Simeonov, N. Christov, and C. Vasseur. Composed Adaptive Control for a second-order nonlinear model of a biotechnological process. In *2011 19th Mediterranean Conference on Control & Automation (MED)*, pages 1140–1143, Corfu, June 2011. IEEE. doi: 10.1109/MED.2011.5983138.

- H. Wang, B. Kalchev, Y. Tian, I. Simeonov, and N. Christov. Modelling and Composed Recursive Model Free Control for the Anaerobic Digestion Process. *Advances in Intelligent Control Systems and Computer Science - Advances in Intelligent Systems and Computing*, 187:265–278, 2013. doi: 10.1007/978-3-642-32548-9\19.
- P. Weiland. Biomass Digestion in Agriculture: A Successful Pathway for the Energy Production and Waste Treatment in Germany. *Engineering in Life Sciences*, 6(3): 302–309, June 2006. doi: 10.1002/elsc.200620128.
- P. Weiland. Biogas production: current state and perspectives. *Applied microbiology and biotechnology*, 85(4):849–60, Jan. 2010. doi: 10.1007/s00253-009-2246-7.
- F. Weißbach and C. Strubelt. Die Korrektur des Trockensubstanzgehaltes von Grassilagen als Substrat für Biogasanlagen. *Landtechnik*, 63(4):210–212, 2008a.
- F. Weißbach and C. Strubelt. Die Korrektur des Trockensubstanzgehaltes von Maissilagen als Substrat für Biogasanlagen. *Landtechnik*, 63(2):2–4, 2008b.
- F. Weißbach and C. Strubelt. Die Korrektur des Trockensubstanzgehaltes von Zuckerrübensilagen als Substrat für Biogasanlagen. *Landtechnik*, 63(6):354–356, 2008c.
- A. Wenzel. Evolutionary Algorithm Application for Parameter Estimation of the Anaerobic Digestion Model No. 1. In *2008 IEEE International Conference on Computational Cybernetics*, number 1, pages 101–105. IEEE, Nov. 2008. doi: 10.1109/ICCCYB.2008.4721387.
- B. Wett, A. Eladawy, and M. Ogurek. Description of nitrogen incorporation and release in ADM1. *Water Sci Technol*, 54(4):67–76, Jan. 2006.
- T. Whitmore, D. Lloyd, G. Jones, and T. Williams. Hydrogen-dependent control of the continuous anaerobic digestion process. *Applied Microbiology and Biotechnology*, 26(4):383–388, July 1987. doi: 10.1007/BF00256675.
- T. N. Whitmore and D. Lloyd. Mass spectrometric control of the thermophilic anaerobic digestion process based on levels of dissolved hydrogen. *Biotechnology Letters*, 8(3):203–208, Mar. 1986. doi: 10.1007/BF01029381.
- M. Wichern, M. Lübken, K. Koch, T. Gehring, H. Horn, K. Fischer, M. Schlattmann, and A. Gronauer. Eignung des Anaerobic Digestion Model No. 1 (ADM 1) zur Prozesssteuerung landwirtschaftlicher Biogasanlagen. In *Gültower Fachgespräche: Band 27 Messen, Steuern, Regeln bei der Biogaserzeugung*, pages 172–194, Gültow, 2007. FNR.
- M. Wichern, M. Lübken, H. Horn, M. Schlattmann, and A. Gronauer. Investigations and mathematical simulation on decentralized anaerobic treatment of agricultural substrate from livestock farming. *Water Sci Technol*, 58(1):67–72, Jan. 2008. doi: 10.2166/wst.2008.332.
- M. Wichern, T. Gehring, K. Fischer, D. Andrade, M. Lübken, K. Koch, A. Gronauer, and H. Horn. Monofermentation of grass silage under mesophilic conditions: measurements and mathematical modeling with ADM 1. *Bioresource technology*, 100(4):1675–81, Feb. 2009. doi: 10.1016/j.biortech.2008.09.030.
- J. Wiese and R. König. From a black-box to a glass-box system: the attempt towards a plant-wide automation concept for full-scale biogas plants. *Water Sci Technol*, 60 (2):321–7, Jan. 2009. doi: 10.2166/wst.2009.337.

- S. Wilcox, D. Hawkes, F. Hawkes, and A. Guwy. A neural network, based on bicarbonate monitoring, to control anaerobic digestion. *Water Research*, 29(6):1465–1470, June 1995. doi: 10.1016/0043-1354(94)00314-W.
- C. Wolf. *Simulation, optimization and instrumentation of agricultural biogas plants*. Doctoral dissertation, NUI Maynooth, 2013.
- C. Wolf, S. McLoone, and M. Bongards. Biogas Plant Control and Optimization Using Computational Intelligence Methods (Biogasanlagenregelung und -optimierung mit Computational Intelligence Methoden). *at - Automatisierungstechnik*, 57(12):638–649, Dec. 2009. doi: 10.1524/auto.2009.0809.
- A. Wolfsberger. *Modelling and Control of the Anaerobic Digestion of Energy Crops*. Dissertation, Universität für Bodenkultur, 2008.
- B. Wu and E. L. Bibeau. Development of 3-D anaerobic digester heat transfer model for cold weather applications. *Transactions of the ASABE*, 49(3):749–757, 2006.
- L. Würth, R. Hannemann, and W. Marquardt. A two-layer architecture for economically optimal process control and operation. *Journal of Process Control*, 21(3):311–321, Mar. 2011. doi: 10.1016/j.jprocont.2010.12.008.
- S. Yordanova, R. Petrova, and V. Mladenov. Neuro-Fuzzy Control for Anaerobic Wastewater Treatment. *WSEAS Transactions on Systems*, 2(3):724–729, 2004.
- U. Zaher, R. Li, U. Jeppsson, J.-P. Steyer, and S. Chen. GISCOD: general integrated solid waste co-digestion model. *Water research*, 43(10):2717–27, June 2009. doi: 10.1016/j.watres.2009.03.018.
- U. E.-S. Zaher. *Modelling and Monitoring the Anaerobic Digestion Process in view of Optimisation and smooth Operation of WWTP's*. PhD thesis, Universiteit Gent, 2005.
- H. Zhou, H. Li, and F. Wang. Anaerobic digestion of different organic wastes for biogas production and its operational control performed by the modified ADM1. *J Environ Sci Heal A*, 47(1):84–92, Jan. 2012. doi: 10.1080/10934529.2012.629585.
- J. Ziegenhirt, T. Bartz-Beielstein, O. Flasch, W. Konen, and M. Zaefferer. Optimization of biogas production with computational intelligence a comparative study. In *IEEE Congress on Evolutionary Computation*, pages 1–8. IEEE, July 2010. doi: 10.1109/CEC.2010.5586509.
- E. Zitzler and L. Thiele. Multiobjective optimization using evolutionary algorithms—A comparative case study. *Lecture Notes in Computer Science - Parallel Problem Solving from Nature—PPSN V*, 1498(September):292–301, 1998. doi: 10.1007/BFb0056872.
- E. Zitzler, M. Laumanns, and L. Thiele. SPEA2: Improving the strength Pareto evolutionary algorithm. Technical report, 2001.
- E. Zitzler, L. Thiele, M. Laumanns, C. Fonseca, and V. da Fonseca. Performance assessment of multiobjective optimizers: an analysis and review. *IEEE T Evolut Comput*, 7(2):117–132, Apr. 2003. doi: 10.1109/TEVC.2003.810758.

Appendix A

Anaerobic Digestion Model (Simple)

In the following the anaerobic digestion model, used in Section 4.4 to compare different state estimation schemes, is presented. It is the implementation used in Shen et al. (2006). The state equations are given in equation (A.1). The state, output and input variables are explained in Table 4.1 and all model parameters in Table A.1.

$$\begin{aligned}
 S'(t) &= D \cdot (S_i(t) - S(t)) - f_a(S(t), S_i(t)) \cdot X_a(t) \cdot Y_a \\
 X'_a(t) &= [f_a(S(t), S_i(t)) - D_a] \cdot X_a(t) \\
 V'_a(t) &= -D \cdot V_a(t) + f_a(S(t), S_i(t)) \cdot X_a(t) \cdot y_{vf}^a - \\
 &\quad - f_m((H_a \circ V_a)(t)) \cdot X_m(t) \cdot Y_m \\
 X'_m(t) &= [f_m((H_a \circ V_a)(t)) - D_m] \cdot X_m(t) \\
 C'(t) &= -D \cdot C(t) + f_a(S(t), S_i(t)) \cdot X_a(t) \cdot y_{co_2}^a + \\
 &\quad + f_m((H_a \circ V_a)(t)) \cdot X_m(t) \cdot y_{co_2}^m - k_{la} \cdot (C(t) - k_h \cdot P_c(t)) \\
 P'_c(t) &= k_g \cdot [k_{la} \cdot (1 - P_c(t)) \cdot (C(t) - k_h \cdot P_c(t)) - \\
 &\quad - r_g \cdot P_c(t) \cdot f_m((H_a \circ V_a)(t)) \cdot X_m(t) \cdot y_{ch4}^m]
 \end{aligned} \tag{A.1}$$

The model outputs are produced methane Q_{ch_4} and carbon dioxide Q_{co_2} as well as the pH value of the reactor. The output equations are given in eq. (A.2).

$$\begin{aligned}
 Q_{ch_4}(t) &= k_g \cdot r_g \cdot f_m((H_a \circ V_a)(t)) \cdot X_m(t) \cdot y_{ch4}^m \\
 Q_{co_2}(t) &= k_g \cdot k_{la} \cdot (C(t) - k_h \cdot P_c(t)) \\
 pH(t) &= -\log_{10}(c(H^+(t)))
 \end{aligned} \tag{A.2}$$

Further variables of the model are given in equation (A.3).

$$\begin{aligned}
 Y_a &:= y_{vf}^a + y_{co_2}^a + \frac{1}{y_s^a} & Y_m &:= y_{ch4}^m + y_{co_2}^m + \frac{1}{y_s^m} \\
 D_a &:= \chi \cdot D + k_{da} & D_m &:= \chi \cdot D + k_{dm} \\
 k_g &:= \frac{S_v \cdot V_{liq}}{C_{co_2} \cdot V_{gas}} & r_g &:= \frac{C_{co_2}}{C_{ch4}}
 \end{aligned} \tag{A.3}$$

The growth rate of the acidogenic bacterial population is modeled by f_a and the one for the methanogenic population by f_m , both are given in equation (A.4).

$$\begin{aligned} f_a(S(t), S_i(t)) &= \frac{\mu_{\max}^a \cdot S(t)}{k_{sa} + S(t)} \cdot \frac{k_{sa} + S_i(t)}{S_i(t)} \\ f_m((H_a \circ V_a)(t)) &= \frac{\mu_{\max}^m \cdot (H_a \circ V_a)(t)}{(H_a \circ V_a)(t) + k_{sm} + \frac{((H_a \circ V_a)(t))^2}{k_{im}}} \end{aligned} \quad (\text{A.4})$$

The undissociated fraction of the acetic acid concentration V_a is symbolized by H_a and given in equation (A.5). The needed hydrogen cation concentration $c(H^+(t))$ is governed by the cubic equation in (A.6).

$$H_a(V_a(t)) := (H_a \circ V_a)(t) := \frac{V_a(t) \cdot c(H^+(t))}{k_a + c(H^+(t))} \quad (\text{A.5})$$

$$\begin{aligned} (c(H^+(t)))^3 + (k_a + B_{ic}(t)) \cdot (c(H^+(t)))^2 - \\ - [k_a \cdot (V_a(t) - B_{ic}(t)) + k_w + k_h \cdot k_{co_2} \cdot P_c(t)] \cdot c(H^+(t)) = \\ = k_a \cdot (k_w + k_h \cdot k_{co_2} \cdot P_c(t)) \end{aligned} \quad (\text{A.6})$$

Table A.1: Model parameters as in Shen et al. (2006).

Parameter	Value	Unit	Description
$\mu_{\text{max}}^{\text{a}}$	0.5033	h^{-1}	Maximum growth rate of acidogenic bacteria
k_{sa}	238.1	mg/l	Acidogenic bacteria half-velocity
k_{da}	$3.1e^{-2}$	h^{-1}	Acidogenic bacteria decay rate
$\mu_{\text{max}}^{\text{m}}$	$2.27e^{-3}$	h^{-1}	Maximum growth rate of methanogenic bacteria
k_{sm}	$1.45e^{-2}$	mg/l	Methanogenic bacteria half-velocity
k_{im}	35.47	mg/l	Methanogenic bacteria inhibition concentration
k_{dm}	$8e^{-4}$	h^{-1}	Methanogenic bacteria decay rate
y_s^{a}	0.688	—	Yield coefficient (substrate to acidogenic bacteria)
y_{vf}^{a}	0.6427	—	Yield coefficient (substrate to acetic acid)
$y_{\text{co}_2}^{\text{a}}$	0.5	—	Yield coefficient (substrate to CO_2)
y_s^{m}	3.27	—	Yield coefficient (acetic acid to methanogenic bacteria)
$y_{\text{ch}_4}^{\text{m}}$	20.732	—	Yield coefficient (acetic acid to CH_4)
$y_{\text{co}_2}^{\text{m}}$	5.174	—	Yield coefficient (acetic acid to CO_2)
k_w	$1e^{-14}$	—	Water dissociation constant
k_{co_2}	$4.5e^{-7}$	—	Carbonic acid dissociation constant
k_h	$1.08e^3$	—	Henry's law constant
k_a	$1.85e^{-5}$	—	Weak acid dissociation constant
k_{la}	6.832	—	CO_2 mass transfer rate coefficient
S_v	22.4	—	Avogadro's constant
C_{co_2}	$4.4e4$	—	mole to mg/l conversion constant for CO_2
C_{ch_4}	$1.6e4$	—	mole to mg/l conversion constant for CH_4
χ	0.01667	—	Liquid/solid dilution rate ratio
D	0.042	h^{-1}	Dilution rate
V_{liq}	30	l	Liquid phase volume
V_{gas}	5	l	Gas phase volume
P_t	1	atm	Total pressure in the gas phase

Appendix B

Biogas Toolbox in MATLAB®

In this thesis detailed simulation models of biogas plants play a key role. In MATLAB®, more precisely in Simulink®, simulation models can be created quite easily. Therefore, MATLAB® was used as a platform to develop a general model for biogas plants, as well as all other components developed in this thesis, such as the state estimators and the NMPC.

The key idea of the developed MATLAB® toolbox is to treat algorithms for optimization and control and biogas simulation models separately. The advantage is that all algorithms can be easily applied to different tasks and different biogas plant models as well. The result is a collection of 16 different MATLAB® toolboxes, each with its own purpose. Seven of these toolboxes have something to do with biogas and three toolboxes form the foundation of each of the other toolboxes and have no own use. The remaining six toolboxes have each their special purpose and can be used independently of the others. Their purposes for example are data analysis, file-I/O, machine learning or optimization. The following list gives an overview.

- `biogas_blocks`: Simulink® blocks to create complex models of biogas plants.
- `biogas_calibration`: Framework to automatically calibrate the ADM1 parameters of a biogas plant model.
- `biogas_control`: Contains the algorithms of the NMPC for optimal feed control of biogas plants.
- `biogas_gui`: GUIs to create and define the simulation model, feeds, boundaries, etc.
- `biogas_ml`: Framework to use machine learning methods in biogas applications.
- `biogas_optimization`: Framework to use optimization methods in biogas applications.
- `biogas_scripts`: Collection of useful functions in biogas applications.
- `data_tool`: Collection of functions for data preparation and visualization.
- `doc_tool`: Creates the online documentation of all functions in the other tool-

boxes.

- gecoc_tool_def: Needed for all toolboxes.
- io_tool: Collection of functions for file-I/O.
- ml_tool: Collection of functions that belong to the family of machine learning.
- numerics_tool: Contains classes and functions to perform some numerical mathematics.
- optimization_tool: Collection of optimization methods.
- script_collection: Collection of functions that are generally useful.
- setup_tool: Provides a general installation method that is used by all other toolboxes.

The separation of methods and models requires general algorithms and methods, but also the models must somehow be general. As prerequisite all models have to be designed following the same guidelines, which are facilitated by using well-developed graphical user interfaces (GUIs) implemented in the toolbox. With these GUIs the user can e.g. specify the setup of the plant, like the number and properties of the fermenters as well as those for the cogeneration units available on the plant. Furthermore, physical and chemical characteristics of the substrate feed can be specified (see Figure B.1), which makes detailed simulations of various substrate mixtures possible. The toolbox then uses this information to semi-automatically generate a Simulink® model of the specified biogas plant, which by default satisfies the needed guidelines (see Figure 7.6). This developed model then can be used to learn the state estimator in Chapter 8 or as prediction model inside the control application in Chapter 9.

To improve the speed of the simulations parts of the algorithms are implemented in C#. The implemented classes are included in MATLAB® by importing them as DLLs. Upon request the complete MATLAB® toolbox is given to the interested user licensed under the GNU General Public Licence¹.

¹<http://www.gnu.org/copyleft/gpl.html>

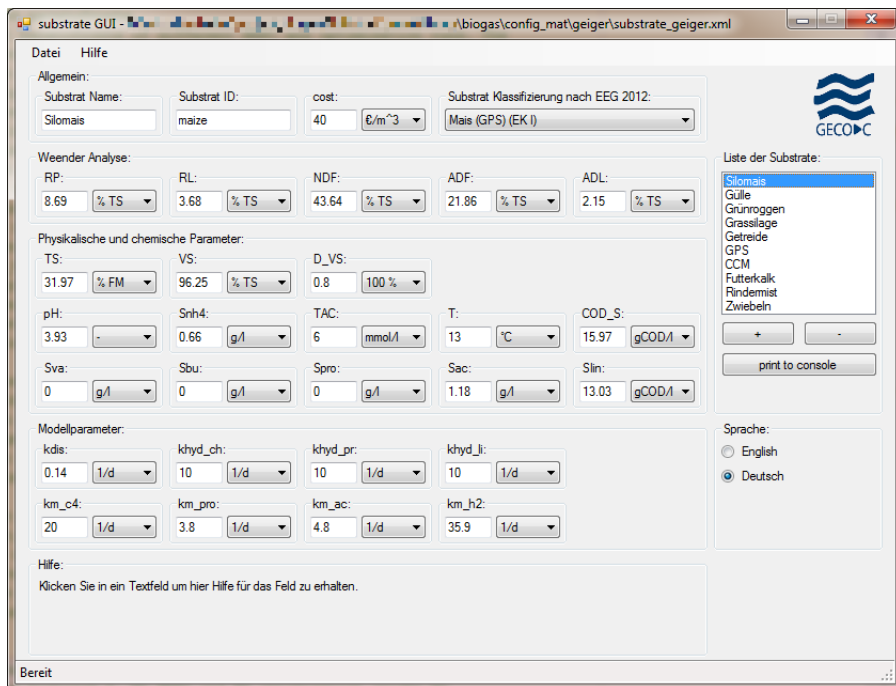


Figure B.1: GUI to define chemical and physical parameters of the substrate feed.

Appendix C

ADM1: Petersen Matrix and Model Parameters

On the following pages the parameters and variables of the ADM1, introduced in Section 7.1, are given. The ADM1 is modeled as a system of ordinary differential equations. The system equation is given in eq. (7.1) and is repeated here for convenience.

$${}^o\boldsymbol{x}_{AD}'(\tau) = \mathbf{D}_u(\tau) \cdot {}^o\boldsymbol{u}_{AD}(\tau) - \mathbf{D}_x(\tau) \cdot {}^o\boldsymbol{x}_{AD}(\tau) + \mathbf{V}({}^o\boldsymbol{x}_{AD})^T \cdot \boldsymbol{\rho}({}^o\boldsymbol{x}_{AD}) \quad (C.1)$$

The input \mathbf{D}_u and state transition matrix \mathbf{D}_x are given in eq. (C.2). There, $\mathbf{1}_{33} \in \mathbb{N}_0^{33 \times 33}$ is the 33 dimensional identity matrix and $\mathbf{0}_{n \times m}$ is the $n \times m$ dimensional zero matrix, $n, m \in \mathbb{N}_0$.

$$\begin{aligned} \mathbf{D}_u(\tau) &:= \begin{pmatrix} D(\tau) \cdot \mathbf{1}_{33} & \mathbf{0}_{33 \times 1} \\ \mathbf{0}_{4 \times 33} & \mathbf{0}_{4 \times 1} \end{pmatrix} \in \mathbb{R}^{37 \times 34} & D(\tau) &:= \frac{{}^o u_{AD,34}(\tau)}{V_{liq}} \stackrel{(7.2)}{=} \frac{Q_{IN}}{V_{liq}} \\ \mathbf{D}_x(\tau) &:= \begin{pmatrix} D(\tau) \cdot \mathbf{1}_{33} & \mathbf{0}_{33 \times 4} \\ \mathbf{0}_{4 \times 33} & \mathbf{0}_{4 \times 4} \end{pmatrix} \in \mathbb{R}^{37 \times 37} \end{aligned} \quad (C.2)$$

The stoichiometric matrix $\mathbf{V} : \mathbb{R}^{37} \rightarrow \mathbb{R}^{29 \times 37}$ and the vector of process rates $\boldsymbol{\rho} : \mathbb{R}^{37} \rightarrow \mathbb{R}^{29}$ are given in the Petersen matrix (Henze et al., 2000) form, see Tables C.1 and C.2. The matrix layout is $[\mathbf{V} | \boldsymbol{\rho}]$. The process rate vector $\boldsymbol{\rho}$ is shown in eq. (C.3). All variables and parameters of the ADM1 are given in eqs. (C.4) - (C.6) and Table C.3, respectively. The implementation and all values are adapted from Tschepeetzki and Ogurek (2010).

Table C.1: ADM1 Petersen Matrix: Part I

Table C.2: ADM1 Petersen Matrix: Part II

Component →	<i>i</i>	15	16	17	18	19	20	21	22	23	24	25	26	27	28	29	30	31	32	33	34	35	36	37	process rate	
<i>j</i> Process ↓		X_{pr}	X_{ll}	X_{su}	X_{aa}	X_{fa}	X_{c4}	X_{pro}	X_{ac}	X_{b2}	X_1	X_p	S_{cat}^+	S_{an}^-	S_{va}^-	S_{bu}^-	S_{pro}^-	S_{hco3}^-	S_{nh3}	p_{iSh2}	p_{iSch4}	p_{iSco2}	p_{total}	ρ_j		
1 Disintegration		$f_{pr,Xc}$	$f_{ll,Xc}$										$f_{xi,Xc}$	$f_{xp,Xc}$											ρ_1	
2 Hydrolysis of X_{aa}																									ρ_2	
3 Hydrolysis of X_{pr}																									ρ_3	
4 Hydrolysis of lipids																									ρ_4	
5 Uptake of sugars			Y_{su}	Y_{aa}																					ρ_5	
6 Uptake of S_{aa}					Y_{fa}																				ρ_6	
7 Uptake of LCFAs						Y_{c4}																			ρ_7	
8 Uptake of valerate							Y_{c4}																		ρ_8	
9 Uptake of butyrate								Y_{pro}																	ρ_9	
10 Uptake of propionate									Y_{ac}																ρ_{10}	
11 Uptake of acetate										Y_{b2}															ρ_{11}	
12 Uptake of hydrogen																										ρ_{12}
13 Decay of X_{su}		$f_{pr,xb}$	$f_{ll,xb}$																							ρ_{13}
14 Decay of X_{aa}		$f_{pr,xb}$	$f_{ll,xb}$																							ρ_{14}
15 Decay of X_{fa}		$f_{pr,xb}$	$f_{ll,xb}$																							ρ_{15}
16 Decay of X_{c4}		$f_{pr,xb}$	$f_{ll,xb}$																							ρ_{16}
17 Decay of X_{pro}		$f_{pr,xb}$	$f_{ll,xb}$																							ρ_{17}
18 Decay of X_{ac}		$f_{pr,xb}$	$f_{ll,xb}$																							ρ_{18}
19 Decay of X_{b2}		$f_{pr,xb}$	$f_{ll,xb}$																							ρ_{19}
20 S_{hco3}/S_{va}^- equil.																										ρ_{20}
21 S_{hco3}/S_{an}^- equil.																										ρ_{21}
22 S_{hco3}/S_{pro}^- equil.																										ρ_{22}
23 S_{hco3}/S_{ac}^- equil.																										ρ_{23}
24 S_{hco3}/S_{hco3}^- equil.																										ρ_{24}
25 S_{nh3}/S_{nh3}^- equil.																										ρ_{25}
26 part. pressure S_{n2}																		$R \cdot T$	$\frac{R \cdot T}{16}$						ρ_{26}	
27 part. pressure S_{ch4}																		$R \cdot T$	$\frac{R \cdot T}{64}$						ρ_{27}	
28 part. pressure S_{co2}																				$R \cdot T$	$R \cdot T$				ρ_{28}	
29 total part. pressure																		$\frac{p_{iSh2}}{p_{total}}$	$\frac{p_{iSch4}}{p_{total}}$	$\frac{p_{iSco2}}{p_{total}}$						ρ_{29}

Process rate vector ρ :

$$\rho := \begin{pmatrix} k_{\text{dis}} \cdot X_c \\ k_{\text{hyd,ch}} \cdot X_{\text{ch}} \cdot \frac{1}{1 + \left(\frac{\text{TS}}{K_{\text{hyd}}} \right)^n_{\text{hyd}}} \\ k_{\text{hyd,pr}} \cdot X_{\text{pr}} \cdot \frac{1}{1 + \left(\frac{\text{TS}}{K_{\text{hyd}}} \right)^n_{\text{hyd}}} \\ k_{\text{hyd,li}} \cdot X_{\text{li}} \cdot \frac{1}{1 + \left(\frac{\text{TS}}{K_{\text{hyd}}} \right)^n_{\text{hyd}}} \\ \frac{k_{m,su} \cdot S_{su}}{K_{S,su} + S_{su}} \cdot X_{\text{su}} \cdot I_1 \\ \frac{k_{m,aa} \cdot S_{aa}}{K_{S,aa} + S_{aa}} \cdot X_{\text{aa}} \cdot I_1 \\ \frac{k_{m,fa} \cdot S_{fa}}{K_{S,fa} + S_{fa}} \cdot X_{\text{fa}} \cdot I_1 \cdot I_{H2,fa} \\ \frac{k_{m,c4} \cdot S_{va}}{K_{S,c4} + S_{va}} \cdot X_{c4} \cdot \frac{S_{va}}{S_{va} + S_{bu}} \cdot I_1 \cdot I_{H2,c4} \\ \frac{k_{m,c4} \cdot S_{bu}}{K_{S,c4} + S_{bu}} \cdot X_{c4} \cdot \frac{S_{bu}}{S_{va} + S_{bu}} \cdot I_1 \cdot I_{H2,c4} \\ \frac{k_{m,pro} \cdot S_{pro}}{K_{S,pro} + S_{pro}} \cdot X_{\text{pro}} \cdot I_1 \cdot I_{H2,pro} \\ \frac{k_{m,ac} \cdot S_{ac}}{K_{S,ac} + S_{ac}} \cdot X_{\text{ac}} \cdot I_{\text{in}} \cdot I_{\text{NH3}} \cdot I_{\text{pH,ac}} \\ \frac{k_{m,h2} \cdot S_{h2}}{K_{S,h2} + S_{h2}} \cdot X_{h2} \cdot I_{\text{in}} \cdot I_{\text{pH,h2}} \\ k_{\text{dec,su}} \cdot X_{\text{su}} \\ k_{\text{dec,aa}} \cdot X_{\text{aa}} \\ k_{\text{dec,fa}} \cdot X_{\text{fa}} \\ k_{\text{dec,c4}} \cdot X_{c4} \\ k_{\text{dec,pro}} \cdot X_{\text{pro}} \\ k_{\text{dec,ac}} \cdot X_{\text{ac}} \\ k_{\text{dec,h2}} \cdot X_{h2} \\ k_{A/Bva} \cdot \left(S_{va}^- \cdot c(H^+) - K_{a,va} \cdot S_{hva} \right) \\ k_{A/Bbu} \cdot \left(S_{bu}^- \cdot c(H^+) - K_{a,bu} \cdot S_{hbu} \right) \\ k_{A/Bpro} \cdot \left(S_{pro}^- \cdot c(H^+) - K_{a,pro} \cdot S_{hpro} \right) \\ k_{A/Bac} \cdot \left(S_{ac}^- \cdot c(H^+) - K_{a,ac} \cdot S_{hac} \right) \\ k_{A/Bco2} \cdot \left(S_{hco3}^- \cdot c(H^+) - K_{a,co2} \cdot S_{co2} \right) \\ k_{A/Bin} \cdot \left(S_{nh3}^- \cdot c(H^+) - K_{a,in} \cdot S_{nh4}^+ \right) \\ k_L a_{h2} \cdot \left(S_{h2} - p_{Sh2} \cdot \frac{16}{R \cdot T \cdot K_{H,h2}} \right) \cdot \frac{V_{liq}}{V_{gas}} \\ k_L a_{ch4} \cdot \left(S_{ch4} - p_{Sch4} \cdot \frac{64}{R \cdot T \cdot K_{H,ch4}} \right) \cdot \frac{V_{liq}}{V_{gas}} \\ k_L a_{co2} \cdot \left(S_{co2} - p_{ScO2} \cdot \frac{1}{R \cdot T \cdot K_{H,co2}} \right) \cdot \frac{V_{liq}}{V_{gas}} \\ k_p \cdot (p_{\text{total}} - p_{\text{ext}}) \cdot \frac{V_{liq}}{V_{gas}} \end{pmatrix} \quad (\text{C.3})$$

$$\begin{aligned}
f_{xi,Xc} &:= 1 - f_{si,Xc} - f_{ch,Xc} - f_{pr,Xc} - f_{li,Xc} - f_{xp,Xc} \\
f_{co2,Xc} &:= C_{Xc} - f_{si,Xc} \cdot C_{SI} - f_{ch,Xc} \cdot C_{Xch} - f_{pr,Xc} \cdot C_{Xpr} - f_{li,Xc} \cdot C_{Xli} - f_{xi,Xc} \cdot C_{XI} - f_{xp,Xc} \cdot C_{Xp} \\
f_{co2,Xli} &:= C_{Xli} - f_{fa,li} \cdot C_{fa} - (1 - f_{fa,li}) \cdot C_{Xch} \\
f_{ac,su} &:= 1 - f_{h2,su} - f_{bu,su} - f_{pro,su} \\
f_{co2,su} &:= C_{Xch} - (f_{bu,su} \cdot C_{bu} + f_{pro,su} \cdot C_{pro} + f_{ac,su} \cdot C_{ac}) \cdot (1 - Y_{su}) - Y_{su} \cdot C_{xb} \\
f_{ac,aa} &:= 1 - f_{h2,aa} - f_{va,aa} - f_{bu,aa} - f_{pro,aa} \\
f_{co2,aa} &:= C_{Xpr} - (f_{va,aa} \cdot C_{va} + f_{bu,aa} \cdot C_{bu} + f_{pro,aa} \cdot C_{pro} + f_{ac,aa} \cdot C_{ac}) \cdot (1 - Y_{aa}) - Y_{aa} \cdot C_{xb} \\
f_{ac,fa} &:= 1 - f_{h2,fa} \\
f_{co2,fa} &:= C_{fa} - f_{ac,fa} \cdot C_{ac} \cdot (1 - Y_{fa}) - Y_{fa} \cdot C_{xb} \\
f_{ac,va} &:= 1 - f_{pro,va} - f_{h2,va} \\
f_{co2,va} &:= C_{va} - (f_{pro,va} \cdot C_{pro} + f_{ac,va} \cdot C_{ac}) \cdot (1 - Y_{c4}) - Y_{c4} \cdot C_{xb} \\
f_{ac,bu} &:= 1 - f_{h2,bu} \\
f_{co2,bu} &:= C_{bu} - f_{ac,bu} \cdot C_{ac} \cdot (1 - Y_{c4}) - Y_{c4} \cdot C_{xb} \\
f_{ac,pro} &:= 1 - f_{h2,pro} \\
f_{co2,pro} &:= C_{pro} - (1 - Y_{pro}) \cdot f_{ac,pro} \cdot C_{ac} - Y_{pro} \cdot C_{xb} \\
f_{co2,ac} &:= C_{ac} - (1 - Y_{ac}) \cdot C_{ch4} - Y_{ac} \cdot C_{xb} \\
f_{co2,h2} &:= -(1 - Y_{h2}) \cdot C_{ch4} - Y_{h2} \cdot C_{xb}
\end{aligned} \tag{C.4}$$

Inhibition functions:

$$\begin{aligned}
I_1 &:= I_{in} \cdot I_{pH,a} & I_{in} &:= \frac{S_{nh4}^+ + S_{nh3}}{S_{nh4}^+ + S_{nh3} + K_{s,in}} & I_{NH3} &:= \frac{K_{1,NH3}}{K_{1,NH3} + S_{nh3}} \\
I_{H2,fa} &:= \frac{K_{1,H2,fa}}{K_{1,H2,fa} + S_{h2}} & I_{H2,c4} &:= \frac{K_{1,H2,c4}}{K_{1,H2,c4} + S_{h2}} & I_{H2,pro} &:= \frac{K_{1,H2,pro}}{K_{1,H2,pro} + S_{h2}} \\
K_{1,H,a} &:= 10^{-\frac{1}{2}(pH_{UL,a} + pH_{LL,a})} & K_{1,H,b2} &:= 10^{-\frac{1}{2}(pH_{UL,b2} + pH_{LL,b2})} & K_{1,H,ac} &:= 10^{-\frac{1}{2}(pH_{UL,ac} + pH_{LL,ac})} \\
I_{pH,a} &:= \frac{K_{1,H,a}^2}{c(H^+)^2 + K_{1,H,a}^2} & I_{pH,b2} &:= \frac{K_{1,H,b2}^3}{c(H^+)^3 + K_{1,H,b2}^3} & I_{pH,ac} &:= \frac{K_{1,H,ac}^3}{c(H^+)^3 + K_{1,H,ac}^3}
\end{aligned} \tag{C.5}$$

$$\begin{aligned}
f_{ch,xb} &:= \frac{f_{ch,Xc}}{f_{ch,Xc} + f_{pr,Xc} + f_{li,Xc}} \cdot (1 - f_P) \\
f_{pr,xb} &:= \frac{f_{pr,Xc}}{f_{ch,Xc} + f_{pr,Xc} + f_{li,Xc}} \cdot (1 - f_P) \\
f_{li,xb} &:= \frac{f_{li,Xc}}{f_{ch,Xc} + f_{pr,Xc} + f_{li,Xc}} \cdot (1 - f_P) \\
f_{sin,xb} &:= N_{xb} - f_P \cdot N_{Xp} - f_{pr,xb} \cdot N_{aa} \\
f_{co2,xb} &:= C_{xb} - f_P \cdot C_{Xp} - f_{ch,xb} \cdot C_{Xch} - f_{pr,xb} \cdot C_{Xpr} - f_{li,xb} \cdot C_{Xli} \\
Q_{gas} &:= k_p \cdot \frac{P_{total} - P_{ext}}{R \cdot T \cdot 44.643} \cdot V_{liq}
\end{aligned} \tag{C.6}$$

Table C.3: ADM1 parameter values as in Tschepeetzki and Ogurek (2010).

Parameter	Value	Unit	Description
N_i	0.06/14	mol/g _{COD}	nitrogen content of inerts
N_{aa}	0.098/14	mol/g _{COD}	nitrogen content of amino acids and proteins
N_{sb}	0.08/14	mol/g _{COD}	nitrogen content of biomass
N_{X_p}	0.06/14	mol/g _{COD}	nitrogen content of X_p
C_{X_c}, C_{X_p}	0.03	mol/g _{COD}	carbon content of composites (X_p)
C_{Si}, C_{Xi}	0.03	mol/g _{COD}	carbon content of soluble (particulate) inerts
C_{Xch}	0.0313	mol/g _{COD}	carbon content of carbohydrates
C_{Xpr}	0.03	mol/g _{COD}	carbon content of proteins
C_{Xli}	0.022	mol/g _{COD}	carbon content of lipids
C_{fa}	0.0217	mol/g _{COD}	carbon content of LCFA
C_{va}	0.024	mol/g _{COD}	carbon content of valerate
C_{bu}	0.025	mol/g _{COD}	carbon content of butyrate
C_{pro}	0.0268	mol/g _{COD}	carbon content of propionate
C_{ac}	0.0313	mol/g _{COD}	carbon content of acetate
C_{ch4}	0.0156	mol/g _{COD}	carbon content of methane
C_{sb}	0.0313	mol/g _{COD}	carbon content of biomass
Y_{su}	0.1	g _{COD} /g _{COD}	yield uptake of sugars
Y_{aa}	0.08	g _{COD} /g _{COD}	yield uptake of amino acids
Y_{fa}, Y_{c4}, Y_{bu}	0.06	g _{COD} /g _{COD}	yield uptake of LCFA (butyrate and valerate, hydrogen)
Y_{pro}	0.04	g _{COD} /g _{COD}	yield uptake of propionate
Y_{ac}	0.05	g _{COD} /g _{COD}	yield uptake of acetate
$f_{fa,li}$	0.95	g _{COD} /g _{COD}	fatty acids from lipids
$f_{j2,su}$	0.19	g _{COD} /g _{COD}	hydrogen from sugars
$f_{j2,aa}$	0.13	g _{COD} /g _{COD}	butyrate from sugars
$f_{j2,eu}$	0.27	g _{COD} /g _{COD}	propionate from sugars
$f_{j2,aa}$	0.06	g _{COD} /g _{COD}	hydrogen from amino acids
$f_{va,aa}$	0.23	g _{COD} /g _{COD}	valerate from amino acids
$f_{bu,aa}$	0.26	g _{COD} /g _{COD}	butyrate from amino acids
$f_{pro,aa}$	0.05	g _{COD} /g _{COD}	propionate from amino acids
$f_{j2,fa}$	0.3	g _{COD} /g _{COD}	hydrogen from LCFA
$f_{j2,va}$	0.15	g _{COD} /g _{COD}	hydrogen from valerate
$f_{pro,va}$	0.54	g _{COD} /g _{COD}	propionate from valerate
$f_{j2,bu}$	0.2	g _{COD} /g _{COD}	hydrogen from butyrate
$f_{j2,pro}$	0.43	g _{COD} /g _{COD}	hydrogen from propionate
f_p	0.08	100 %	fraction of biomass leading to particulate products
$K_{N,IN}$	$1 \cdot 10^{-4}$	mol/l	half saturation coefficient of inorganic nitrogen
$K_{s,su}$	0.5	g _{COD} /l	half saturation coefficient of sugars
$K_{s,aa}$	0.3	g _{COD} /l	half saturation coefficient of amino acids
$K_{s,fa}$	0.4	g _{COD} /l	half saturation coefficient of LCFA
$K_{s,c4}$	0.2	g _{COD} /l	half saturation coefficient of valerate and butyrate
$K_{s,pro}$	0.1	g _{COD} /l	half saturation coefficient of propionate
$K_{s,ac}$	0.15	g _{COD} /l	half saturation coefficient of acetate
$K_{H,h2}$	$7 \cdot 10^{-6}$	g _{COD} /l	half saturation coefficient of hydrogen
$k_{m,su}$	30	1/d	max. uptake rate of sugars
$k_{m,aa}$	50	1/d	max. uptake rate of amino acids
$k_{m,fa}$	6	1/d	max. uptake rate of LCFA
$K_{1,H2,fa}$	$5 \cdot 10^{-6}$	g _{COD} /l	hydrogen inhibition constant for LCFA uptake
$K_{1,H2,c4}$	$1 \cdot 10^{-5}$	g _{COD} /l	hydrogen inhibition constant for valerate and butyrate uptake
$K_{1,H2,pro}$	$3.5 \cdot 10^{-6}$	g _{COD} /l	hydrogen inhibition constant for propionate uptake
$K_{1,NH3}$	0.0018	mol/l	free ammonia inhibition constant for acetate uptake
$p_{H_{UL,a}}, p_{H_{LL,a}}$	5.5, 4	—	upper (lower) pH limit for p_5 to p_{10}
$p_{H_{UL,b2}}, p_{H_{LL,b2}}$	7, 6	—	upper (lower) pH limit for p_{11}
$k_{dec,aa}, k_{dec,aa}$	0.02	1/d	decay rate of X_{su}, X_{aa}
$k_{dec,fa}, k_{dec,c4}$	0.02	1/d	decay rate of X_{fa}, X_{c4}
$k_{dec,pro}, k_{dec,ac}$	0.02	1/d	decay rate of X_{pro}, X_{ac}
$k_{dec,h2}$	0.02	1/d	decay rate of X_{h2}
$K_{a,va}$	$10^{-4.86}$	mol/l	acid-base equilibrium coefficient of valerate
$K_{a,bu}$	$10^{-4.82}$	mol/l	acid-base equilibrium coefficient of butyrate
$K_{a,pro}$	$10^{-4.88}$	mol/l	acid-base equilibrium coefficient of propionate
$K_{a,ac}$	$10^{-4.76}$	mol/l	acid-base equilibrium coefficient of acetate
$K_{a,co2}$	$4.94 \cdot 10^{-7}$	mol/l	acid-base equilibrium coefficient of carbon dioxide
$K_{a,am}$	$1.11 \cdot 10^{-9}$	mol/l	acid-base equilibrium coefficient of ammonia
$k_{A/Bva}, k_{A/Bbu}, k_{A/Bpro}$	$1 \cdot 10^8$	kmol/d	acid-base kinetic parameter (valerate, butyrate, propionate)
$k_{A/Bac}, k_{A/Bco2}, k_{A/Bin}$	$1 \cdot 10^8$	kmol/d	acid-base kinetic parameter (acetate, carbon dioxide, ammonia)
$k_{L,a2}, k_{L,ac4}, k_{L,ac2}$	200	1/d	gas-liquid transfer coefficient of hydrogen (methane, carbon dioxide)
$K_{H,co2}$	$1 / (0.0271 \cdot R \cdot [T])$	mol / (bar · m ³)	Henry constant of carbon dioxide, $[T] \stackrel{!}{=} K$
$K_{H,ch4}$	$1 / (0.00116 \cdot R \cdot [T])$	mol / (bar · m ³)	Henry constant of methane, $[T] \stackrel{!}{=} K$
$K_{H,h2}$	$1 / (7.38 \cdot 10^{-4} \cdot R \cdot [T])$	mol / (bar · m ³)	Henry constant of hydrogen, $[T] \stackrel{!}{=} K$
K_{hyd}	2.5	% _{FM}	inhibition constant of hydrolysis
n_{hyd}	2.3	100 %	inhibition index of hydrolysis
R	$8.31399 \cdot 10^{-2}$	m ³ · bar / (kmol · K)	gas constant
p_{ext}	$1.04 - 0.0084147 \cdot \exp(0.054 \cdot [T])$	bar	external pressure, $[T] \stackrel{!}{=} {}^\circ C$
k_p	10000	m ³ / (m ³ · d)	proportional control constant for gas balance

Appendix D

Symbols and Abbreviations

General Symbols		
Symbol	Description	Ref.
$\mathbf{1}_n$	$n \in \mathbb{N}_0$ dimensional identity matrix	C
$\mathbf{0}_{n \times m}$	$n \times m$ dimensional zero matrix, $n, m \in \mathbb{N}_0$	C
$t \in \mathbb{R}_0^+$	continuous time, can be real and simulated	2
$\tau \in \mathbb{R}_0^+$	some time	2
d	differential	
$\delta_D(x) = \begin{cases} \infty & \text{if } x = 0 \\ 0 & \text{if } x \neq 0 \end{cases}, \quad \int_{-\infty}^{\infty} \delta_D(x) dx = 1$	Dirac delta “function” (distribution)	2
$\delta_{\alpha\beta} = \begin{cases} 0 & \text{if } \alpha \neq \beta \\ 1 & \text{if } \alpha = \beta \end{cases}$	Kronecker delta	4.2
$E\langle x \rangle$	expectation value of the process x	2
$\mathbb{N}_0 := \{0, 1, 2, \dots\}$	set of natural numbers	
$\mathbb{N} := \{1, 2, 3, \dots\}$	set of natural numbers without zero	
\mathbb{R}	set of real numbers	
$\mathbb{R}^+ : t > 0$	set of positive real numbers	
$\mathbb{R}_0^+ : t \geq 0$	set of positive real numbers including 0	

System Definition (Biogas Plant)

Symbol	Description	Ref.
$n_x \in \mathbb{N}_0$	number of states of the real-world system	2
$i_x \in \{1, \dots, n_x\}$	iterator for the number of states of the real-world system	2
$\mathcal{X}_{i_x} \subseteq \mathbb{R}$	vector space of the i_x th state of the real-world system	2
$x_{i_x} : \mathbb{R}^+ \rightarrow \mathcal{X}_{i_x}$	i_x th state of the real-world system	2
$\mathcal{X} := (\mathcal{X}_{i_x})^{n_x} := \mathcal{X}_1 \times \dots \times \mathcal{X}_{n_x}$	n_x dimensional state space of the real-world system	2
$\mathbf{x} := (x_1, \dots, x_{i_x}, \dots, x_{n_x})^T$	state vector of the real-world system	2
$n_u \in \mathbb{N}_0$	number of inputs of the real-world system	2
$i_u \in \{1, \dots, n_u\}$	iterator for the number of inputs of the real-world system	2
$\mathcal{U}_{i_u} \subseteq \mathbb{R}$	vector space of the i_u th input of the real-world system	2
$u_{i_u} : \mathbb{R}^+ \rightarrow \mathcal{U}_{i_u}$	i_u th input of the real-world system	2
$\mathcal{U} := (\mathcal{U}_{i_u})^{n_u} := \mathcal{U}_1 \times \dots \times \mathcal{U}_{n_u}$	n_u dimensional input space of the real-world system	2
$\mathbf{u} := (u_1, \dots, u_{i_u}, \dots, u_{n_u})^T$	input vector of the real-world system	2
${}^o\mathbf{x} : \mathbb{R}^+ \rightarrow \mathcal{X}$	open loop predicted state of the real-world system	(2.1)
${}^o\mathbf{x} := ({}^o x_1, \dots, {}^o x_{i_x}, \dots, {}^o x_{n_x})^T$	open loop predicted state of the real-world system	(2.1)
$\mathbf{f} : \mathcal{X} \times \mathcal{U} \times \mathbb{R}^{n_\omega} \rightarrow \mathcal{T}\mathcal{X}$	model of the real-world system	(2.1)
$\mathcal{T}\mathcal{X} \subseteq \mathbb{R}^{n_x}$	tangential state space of the real-world system	2
$\boldsymbol{\omega} : \mathbb{R}^+ \rightarrow \mathbb{R}^{n_\omega}, n_\omega \in \mathbb{N}_0$	n_ω dimensional process noise of the model \mathbf{f}	2
$\boldsymbol{\Psi}_\omega \in \mathbb{R}^{n_\omega \times n_\omega}$	covariance matrix of process noise	2
$\omega(t) \sim \mathcal{N}(\mathbf{0}, \boldsymbol{\Psi}_\omega),$	normal distribution, zero-mean, white and uncorrelated	2
$E \langle \omega(t) \cdot \omega^T(\tau) \rangle = \boldsymbol{\Psi}_\omega \cdot \delta_D(t - \tau)$	process noise	2
$\sigma_{\omega_{i_u}} \in \mathbb{R}^+$	standard deviation of the i_u th process noise ω_{i_u}	4.4.3
$n_y \in \mathbb{N}_0$	number of outputs of the real-world system	4
$i_y \in \{1, \dots, n_y\}$	iterator for the number of outputs of the real-world system	4
$\mathcal{Y}_{i_y} \subseteq \mathbb{R}$	vector space of the i_y th output of the real-world system	4
$y_{i_y} : \mathbb{R}^+ \rightarrow \mathcal{Y}_{i_y}$	i_y th output of the real-world system	4
$\mathcal{Y} := (\mathcal{Y}_{i_y})^{n_y} := \mathcal{Y}_1 \times \dots \times \mathcal{Y}_{n_y}$	n_y dimensional output space of the real-world system	4
$\mathbf{y} := (y_1, \dots, y_{i_y}, \dots, y_{n_y})^T$	output vector of the real-world system	4
$\sigma_{v_{i_y}} \in \mathbb{R}^+$	standard deviation of the i_y th measurement noise v_{i_y}	4.4.3

Model Predictive Control		
Symbol	Description	Ref.
$n_o \in \mathbb{N}_0$	number of objectives	(2.2)
$i_o \in \{1, \dots, n_o\}$	iterator for the number of objectives	(2.3)
$\tilde{\mathcal{J}} : \mathcal{X} \times \mathcal{U} \rightarrow \mathbb{R}^{n_o}$	n_o dimensional objective function for continuous input	(2.2)
$\tilde{\mathcal{J}} := (\tilde{\mathcal{J}}_1, \dots, \tilde{\mathcal{J}}_{n_o})^T$, $\tilde{\mathcal{J}}_{i_o} : \mathcal{X} \times \mathcal{U} \rightarrow \mathbb{R}$	n_o dimensional objective function for continuous input	(2.3)
$\mathbf{u}^* : \mathbb{R}^+ \rightarrow \mathcal{U}$	optimal input function for the real-world system	(2.5)
$T_p \in \mathbb{R}^+$	prediction horizon	2.1
$T_c \in \mathbb{R}^+$	control horizon	2.1
$\delta \in \mathbb{R}^+$	control sampling time	2.1
$t_k := k \cdot \delta$, $k = 0, 1, 2, \dots$	discrete time t_k , control sampling instant k	(2.6)
${}^o\mathbf{u} : [t_k, t_k + T_p] \rightarrow \mathcal{U}$	open loop input applied to the model f	(2.7)
${}^o\mathbf{u} := ({}^o u_1, \dots, {}^o u_{i_u}, \dots, {}^o u_{n_u})^T$	open loop input applied to the model f	(2.7)
${}^o\mathbf{u}_k^* : [t_k, t_k + T_p] \rightarrow \mathcal{U}$	optimal open loop input applied to the model f	(2.7)
$s_c := \frac{T_c}{\delta} \in \mathbb{N}_0$	number of steps of the piecewise constant input over the control horizon T_c	2.1
$\mathbf{u}_{i_u} := (u_{i_u,1}, \dots, u_{i_u,s_c})^T \in (\mathcal{U}_{i_u})^{s_c}$	vector of $i = 1, \dots, s_c$ amplitudes $u_{i_u,i} \in \mathcal{U}_{i_u}$	(2.9)
$\mathcal{U}_{\mathcal{F}} := (\mathcal{U}_1)^{s_c} \times \dots \times (\mathcal{U}_{i_u})^{s_c} \times \dots \times (\mathcal{U}_{n_u})^{s_c}$	input space for piecewise constant input, this is the feasible region	(2.10)
$\mathbf{u} := (\mathbf{u}_1^T, \dots, \mathbf{u}_{i_u}^T, \dots, \mathbf{u}_{n_u}^T)^T \in \mathcal{U}_{\mathcal{F}}$	vector of optimization variables	(2.10)
$n_v := s_c \cdot n_u \in \mathbb{N}_0$	number of optimization variables	2.1
$i_v \in \{1, \dots, n_v\}$	iterator for the number of optimization variables	2.1
$f_{\mathcal{U}} : \mathcal{U}_{\mathcal{F}} \rightarrow \mathcal{U}$,	transformation from vector of decision variables to piecewise constant input	(2.11)
${}^o\mathbf{u} : [t_k, t_k + T_p] \rightarrow f_{\mathcal{U}}(\mathbf{u})$	multi-objective function for piecewise constant input	(2.13)
$\mathcal{J} : \mathcal{X} \times \mathcal{U}_{\mathcal{F}} \rightarrow \mathbb{R}^{n_o}$	multi-objective function for piecewise constant input	(2.13)
$\tilde{\mathcal{J}}({}^o\mathbf{x}(\tau), {}^o\mathbf{u}(\tau)) = \tilde{\mathcal{J}}({}^o\mathbf{x}(\tau), f_{\mathcal{U}}(\mathbf{u}))$ =: $\mathcal{J}({}^o\mathbf{x}(\tau), \mathbf{u})$, $\forall \tau \in [t_k, t_k + T_p]$	multi-objective function for piecewise constant input	(2.13)
$\mathbf{J} := (J_1, \dots, J_{n_o})^T$,	multi-objective function for piecewise constant input	(2.13)
$J_{i_o} : \mathcal{X} \times \mathcal{U}_{\mathcal{F}} \rightarrow \mathbb{R}$	multi-objective function for piecewise constant input (omitting ${}^o\mathbf{x}$)	(2.16)
$J_{\mathbf{x}}(\mathbf{u}) := \mathcal{J}({}^o\mathbf{x}(\tau), \mathbf{u})$	multi-objective function for piecewise constant input (omitting ${}^o\mathbf{x}$)	(2.16)
$J_{\mathbf{x}} : \mathcal{U}_{\mathcal{F}} \rightarrow \mathbb{R}^{n_o}$,	multi-objective function for piecewise constant input (omitting ${}^o\mathbf{x}$)	(2.16)
$J_{\mathbf{x}, i_o} := (J_{\mathbf{x},1}, \dots, J_{\mathbf{x},n_o})^T$,	multi-objective function for piecewise constant input (omitting ${}^o\mathbf{x}$)	(2.16)
$\varpi_{i_o} \in (0, 1)$, $\sum_{i_o=1}^{n_o} \varpi_{i_o} = 1$	weighting factors in weighted sum of optimization criteria	(2.19)

Multi-Objective Optimization

Symbol	Description	Ref.
$\mathcal{P}^* : \{\underline{\mathbf{u}} \in \mathcal{U}_{\mathcal{F}} \mid \underline{\mathbf{u}} \text{ is Pareto optimal}\}$	Pareto optimal set	2.3
$\mathcal{PF}^* := \{\mathbf{J}_x(\underline{\mathbf{u}}) \in \mathbb{R}^{n_o} \mid \underline{\mathbf{u}} \in \mathcal{P}^*\}$	Pareto front	2.4
$Vol : \mathbb{R}^{n_o} \rightarrow \mathbb{R}$	Lebesgue measure for a n_o dimensional set	3.1
$r \in \mathbb{R}^{n_o}$	reference point used in definition of hypervolume indicator	3.1
$I_H : \mathbb{R}^{n_o} \rightarrow \mathbb{R}$	hypervolume indicator for a n_o dimensional set	3.1
$d_n(\phi, \mathcal{A}) := \text{card } \{\mathbf{a}_{\mathcal{A}} \in \mathcal{A} \mid \mathbf{a}_{\mathcal{A}} \prec \phi\}$	number of dominating points	(3.1)
$\Delta I_H(\mathbf{a}_{\mathcal{A}}, \mathcal{A}) := I_H(\mathcal{A}) - I_H(\mathcal{A} \setminus \{\mathbf{a}_{\mathcal{A}}\}), \mathbf{a}_{\mathcal{A}} \in \mathcal{A}, \mathcal{A} \subset \mathbb{R}^{n_o}$	contributing hypervolume	(3.2)
$\mathcal{D} \subset \mathbb{R}^{n_v}, \phi \in \mathcal{D}$	set of dominated individuals ϕ	3
$\mathcal{P} \subset \mathbb{R}^{n_v}$	population of an evolutionary algorithm	3
$\mu \in \mathbb{N}_0$	number of parents in an evolutionary algorithm	3
$\lambda \in \mathbb{N}_0$	number of offspring in an evolutionary algorithm	3
$\kappa = 0, 1, 2, \dots$	iterator of an evolutionary algorithm	3

State Estimation: Part I

Symbol	Description	Ref.
$\mathbf{h} : \mathcal{X} \times \mathbb{R}^{n_v} \rightarrow \mathcal{Y}$	measurement function	(4.1)
$\mathbf{v} : \mathbb{R}^+ \rightarrow \mathbb{R}^{n_v}, n_v \in \mathbb{N}_0$	n_v dimensional measurement noise of the model \mathbf{h}	(4.1)
$\Psi_{\mathbf{v}} \in \mathbb{R}^{n_v \times n_v}$	covariance matrix of measurement noise	(4.1)
$\mathbf{v}(t) \sim \mathcal{N}(\mathbf{0}, \Psi_{\mathbf{v}}),$ $E \langle \mathbf{v}(t) \cdot \mathbf{v}^T(\tau) \rangle = \Psi_{\mathbf{v}} \cdot \delta_D(t - \tau)$	normal distribution, zero-mean, white and uncorrelated measurement noise	(4.1)
$\delta_u \in \mathbb{R}^+$	sampling time for input values	(4.2)
$\delta_y \in \mathbb{R}^+$	sampling time for output (measurement) values	(4.2)
$N_{\delta_u} := \frac{\delta}{\delta_u} \in \mathbb{N}_0$	ratio of sampling times δ/δ_u	(4.2)
$N_{\delta_y} := \frac{\delta}{\delta_y} \in \mathbb{N}_0$	ratio of sampling times δ/δ_y	(4.2)
$\mathbf{F}_E : \mathcal{Y}^{N_{\delta_y} \cdot t_k} \times \mathcal{U}^{N_{\delta_u} \cdot t_k} \rightarrow \mathcal{X}$	state calculation function	4.1
$\mathcal{Y}^{N_{\delta_y} \cdot t_k} := \{\mathbf{y}(0), \mathbf{y}(\delta_y), \dots, \mathbf{y}(\delta), \mathbf{y}(\delta + \delta_y), \dots, \mathbf{y}(t_k)\}$	set of measurements until t_k	(4.3)
$\mathcal{U}^{N_{\delta_u} \cdot t_k} := \{\mathbf{u}(0), \mathbf{u}(\delta_u), \dots, \mathbf{u}(\delta), \mathbf{u}(\delta + \delta_u), \dots, \mathbf{u}(t_k)\}$	set of inputs until t_k	(4.4)
$\hat{\mathbf{x}}_{\mathbf{F}_E}(t_k) := \mathbf{F}_E(\mathbf{y}(0), \dots, \mathbf{y}(t_k), \mathbf{u}(0), \dots, \mathbf{u}(t_k))$	best state estimate using \mathbf{F}_E	(4.5)
$\tilde{\mathbf{F}}_E : \mathcal{Y}^{N_y+1} \times \mathcal{U}^{N_u+1} \rightarrow \mathcal{X}$	state estimation function, approximation of \mathbf{F}_E	4.1
$\hat{\mathbf{x}} : \mathbb{R}^+ \rightarrow \mathcal{X}$	state vector estimate	4
$N_u \in \mathbb{N}_0$	number of moving average filters for input	4.1
$N_y \in \mathbb{N}_0$	number of moving average filters for measurement (output)	4.1
$w_u \in \mathcal{W}_u \subset \mathbb{N}_0$	window size of moving average filters for input	4.1
$w_y \in \mathcal{W}_y \subset \mathbb{N}_0$	window size of moving average filters for measurement	4.1
$\Lambda_u : \mathcal{U}^{w_u} \rightarrow \mathcal{U}$	moving average filter for input	(4.6)
$\Lambda_y : \mathcal{Y}^{w_y} \rightarrow \mathcal{Y}$	moving average filter for output	(4.8)
$i_{\Lambda_u} \in \{1, \dots, N_u\}$	iterator for the number of moving average filter for input	4.1
$i_{\Lambda_y} \in \{1, \dots, N_y\}$	iterator for the number of moving average filter for output	4.1
$w_{u,i_{\Lambda_u}} \in \mathcal{W}_u \subset \mathbb{N}_0$	window size of i_{Λ_u} th moving average input filter	4.1
$w_{y,i_{\Lambda_y}} \in \mathcal{W}_y \subset \mathbb{N}_0$	window size of i_{Λ_y} th moving average measurement filter	4.1
$\bar{\mathbf{u}}_{i_{\Lambda_u}} : \mathbb{R}^+ \rightarrow \mathcal{U}$	moving average value of input	(4.7)
$\bar{\mathbf{y}}_{i_{\Lambda_y}} : \mathbb{R}^+ \rightarrow \mathcal{Y}$	moving average value of output	(4.9)
$D := n_y \cdot (N_y + 1) + n_u \cdot (N_u + 1)$	dimension of original feature space	(4.11)
$d \in \mathbb{N}_0$	dimension of projected feature space	4.1.1.1
$\mathbf{Y} \in \mathbb{R}^{N \times D}, N := k \cdot N_{\delta_y} + 1$	data of input and output values for state estimation	(4.11)
$\mathbf{Y}_T \in \mathbb{R}^{N_T \times D}, N_T < N$	training data of input and output values for state estimation	4.1.1
$\mathbf{Y}_V \in \mathbb{R}^{N_V \times D}, N_V := N - N_T$	validation data of input and output values for state estimation	4.1.1
$\mathbf{X} := (\mathbf{x}_{i_x}, \dots, \mathbf{x}_{n_x}) \in \mathbb{R}^{N \times n_x}$	data of state vector values for state estimation	(4.12)
$\mathbf{x}_{i_x} \in \mathbb{R}^N$	data of state vector $i_x = 1, \dots, n_x$ for state estimation	(4.12)
$C \in \mathbb{N}_0$	number of classes in the classification problem	4.1.1
$\vartheta_{i_x} \in \{1, \dots, C\}^N$	clustered data of state vector $\mathbf{X}_{i_x}, i_x = 1, \dots, n_x$	4.1.1

State Estimation: Part II (the methods)

Symbol	Description	Ref.
$\mathbf{A}_{\text{LDA}} \in \mathbb{R}^{d \times D}$	transformation matrix of linear discriminant analysis	4.1.1.1
$\mathbf{Z} := (\mathbf{z}_1, \dots, \mathbf{z}_{N_{\text{T}}}) \in \mathbb{R}^{d \times N_{\text{T}}}$	matrix of projected features of discriminant analysis	4.1.1.1
$\mathbf{S}_{\text{T}} \in \mathbb{R}^{D \times D}$	total scatter-matrix of linear discriminant analysis	(4.13)
$\mathbf{S}_{\text{B}} \in \mathbb{R}^{D \times D}$	between-class scatter-matrix of linear discriminant analysis	(4.13)
\mathcal{F}	function space of nonlinear GerDA transformations, defined by a DNN	4.1.1.2
$\mathbf{f}_{\text{GerDA}} : \mathbb{R}^D \rightarrow \mathbb{R}^d$, $\mathbf{f}_{\text{GerDA}} \in \mathcal{F}$	some nonlinear GerDA transformation	4.1.1.2
$\mathbf{f}_{\text{GerDA}}^* : \mathbb{R}^D \rightarrow \mathbb{R}^d$, $\mathbf{f}_{\text{GerDA}}^* \in \mathcal{F}$	optimal nonlinear GerDA transformation	4.1.1.2
\mathbf{W}, \mathbf{b}	weights and biases of GerDA	4.1.1.2
$t_j := j \cdot \delta_y$, $j = 0, 1, 2, \dots$	discrete time t_j , control sampling instant j	(4.14)
$\mathbf{X}_j := \mathbf{X}(t_j)$ and $\mathbf{x}_j := \mathbf{x}(t_j)$	simplified notation for any matrix $\mathbf{X}(t_j) \in \mathbb{R}^{m \times n}$ and vector $\mathbf{x}(t_j) \in \mathbb{R}^n$, $n, m \in \mathbb{N}$	4.2
$\mathbf{X}_k := \mathbf{X}(t_k)$ and $\mathbf{x}_k := \mathbf{x}(t_k)$	simplified notation for any matrix $\mathbf{X}(t_k) \in \mathbb{R}^{m \times n}$ and vector $\mathbf{x}(t_k) \in \mathbb{R}^n$, $n, m \in \mathbb{N}$	4.2
$\hat{\mathbf{x}}_j^- := \hat{\mathbf{x}}(t_j^-) \in \mathcal{X}$	a priori state estimate of Kalman filter at time t_j^-	4.2
$\hat{\mathbf{x}}_j^+ := \hat{\mathbf{x}}(t_j^+) \in \mathcal{X}$	a posteriori state estimate of Kalman filter at time t_j^+	4.2
$\mathbf{P}_j^- := E \left\langle (\mathbf{x}_j^- - \hat{\mathbf{x}}_j^-) \cdot (\mathbf{x}_j^- - \hat{\mathbf{x}}_j^-)^T \right\rangle$ $\mathbf{P}_j^- \in \mathbb{R}^{n_{\text{x}} \times n_{\text{x}}}$	a priori estimation error covariance matrix of Kalman filter at time t_j^-	(4.18)
$\mathbf{P}_j^+ := E \left\langle (\mathbf{x}_j^+ - \hat{\mathbf{x}}_j^+) \cdot (\mathbf{x}_j^+ - \hat{\mathbf{x}}_j^+)^T \right\rangle$ $\mathbf{P}_j^+ \in \mathbb{R}^{n_{\text{x}} \times n_{\text{x}}}$	a posteriori estimation error covariance matrix of Kalman filter at time t_j^+	(4.18)
$\mathbf{A}_j := \frac{\partial \mathbf{f}}{\partial \mathbf{x}}(\hat{\mathbf{x}}_{j-1}^+, \mathbf{u}(t_j), \mathbf{0}) \in \mathbb{R}^{n_{\text{x}} \times n_{\text{x}}}$	system matrix of linearized model of \mathbf{f}	(4.19)
$\mathbf{C}_j := \frac{\partial \mathbf{h}}{\partial \mathbf{x}}(\hat{\mathbf{x}}_{j-1}^+, \mathbf{0}) \in \mathbb{R}^{n_{\text{y}} \times n_{\text{x}}}$	measurement matrix of linearized model of \mathbf{h}	(4.19)
$\mathbf{E}_j := \frac{\partial \mathbf{f}}{\partial \omega}(\hat{\mathbf{x}}_{j-1}^+, \mathbf{u}(t_j), \mathbf{0}) \in \mathbb{R}^{n_{\text{x}} \times n_{\omega}}$	process noise matrix of linearized model of \mathbf{f}	(4.19)
$\mathbf{F}_j := \frac{\partial \mathbf{h}}{\partial \omega}(\hat{\mathbf{x}}_{j-1}^+, \mathbf{0}) \in \mathbb{R}^{n_{\text{y}} \times n_{\omega}}$	measurement noise matrix of linearized model of \mathbf{h}	(4.19)
$\mathbf{K}_j^* \in \mathbb{R}^{n_{\text{x}} \times n_{\text{y}}}$	optimal discrete Kalman matrix	(4.20)
$\mathbf{x}_o \in \mathcal{X}$	optimization variable (initial state) of MHE	4.3
$\mathbf{x}_o^* \in \mathcal{X}$	optimal value of optimization variable of MHE	4.3
$\delta_{\text{MHE}} := w_{\text{MHE}} \cdot \delta_y \in \mathbb{R}^+$	length of the moving horizon	(4.21)
$w_{\text{MHE}} \in \mathbb{N}$	unit-less length of the horizon, measured in units of δ_y	(4.21)
$\tilde{w}_{\text{MHE}} := \frac{1}{N_{\delta_y}} \cdot w_{\text{MHE}} \in \mathbb{N}$	unit-less length of the horizon, measured in units of δ	(4.22)
$\tilde{\mathbf{x}} : \mathbb{R}^+ \rightarrow \mathcal{X}$	initial state estimate in MHE	(4.23)
$\tilde{\mathbf{x}}_o := {}^o \mathbf{x}(t_{k+1} - \delta_{\text{MHE}}) \in \mathcal{X}$	simple version of initial state estimate in MHE	4.3
$\kappa_{\text{MHE}} \in \mathbb{R}^+$	weighting factor of MHE	(4.23)
$\mathbf{x}_{\text{LB}}, \mathbf{x}_{\text{UB}} \in \mathcal{X}$	lower, upper boundary for optimization variable in MHE	(4.23)
$\mathbf{x}_{i_{\text{x}}, [j_1, j_2]}$	vector of samples of state vector component i_{x}	(4.26)
$\mathbf{x}_{i_{\text{x}}, [k_1, k_2]}$	vector of samples of state vector component i_{x}	(4.27)
$e_{\hat{\mathbf{x}}, i_{\text{x}}} \in \mathbb{R}^+$	performance measure of i_{x} th estimated state vector component $\hat{\mathbf{x}}_{i_{\text{x}}}$	(4.28)
$e_{\hat{\mathbf{x}}} := \frac{1}{n_{\text{x}}} \cdot \sum_{i_{\text{x}}=1}^{n_{\text{x}}} e_{\hat{\mathbf{x}}, i_{\text{x}}} \in \mathbb{R}^+$	total performance measure of experiments in Section 4.4	(4.29)

Anaerobic Digestion

Symbol	Description	Ref.
ash	ash in substrate	7.2
COD _{total}	total chemical oxygen demand of a substrate	7.2.1
COD _{SX}	disintegrated particulate chemical oxygen demand of substrate	(7.9)
COD _X	particulate chemical oxygen demand of a substrate	7.2.1
COD _{filtrate}	total chemical oxygen demand in the filtrate of a substrate	7.2.1
$d = \frac{\text{NDF} - \text{VS}_{\text{IN}} \cdot (1 - D_{\text{VS}})}{\text{NDF} - \text{ADL}} \in [0, 1]$	degradable part of cellulose and hemicellulose	(7.11)
$D := \frac{Q_{\text{IN}}}{V_{\text{liq}}}$	dilution rate of digester	(5.6)
$\mathbf{D}_u : \mathbb{R}^+ \rightarrow \mathbb{R}^{37 \times 34}$	input and state transition matrix of ADM1	(7.1)
$\mathbf{D}_x : \mathbb{R}^+ \rightarrow \mathbb{R}^{37 \times 37}$	carbohydrates, proteins in non-disintegrated part of particulate COD	(7.11)
$f_{\text{ch}, \text{Xc}}, f_{\text{pr}, \text{Xc}}$	lipids, inerts in non-disintegrated part of particulate COD	(7.11)
$f_{\text{li}, \text{Xc}}, f_{\text{x}, \text{Xc}}$	inhibition function of ADM1	7.1
$I : \mathbb{R}^{37} \rightarrow [0, 1]$	process rate index of ADM1	7.1
$j \in \{1, \dots, 29\}$	bijective function	(7.5)
$js : \{2, 3, 4\} \rightarrow \{\text{ch, pr, li}\}$	hydrolysis rates for carbohydrates, protein and lipids	(7.5)
$k_{\text{hyd, ch}}, k_{\text{hyd, pr}}, k_{\text{hyd, li}}$	inhibition constant of hydrolysis	(7.5)
K_{hyd}	unit of the amount of substance, called mole	5.3.1
mol	molar mass	5.3.1
M	inhibition index of hydrolysis	(7.5)
n_{hyd}	cost of substrate	7.2
p_{IN}	pH of sludge in digester, of substrate	7.2
pH, pH _{IN}	volumetric flow rate of a material	(5.5)
$Q := \frac{dV}{dt}$	volumetric flow rate of a substrate	(5.5)
Q_{IN}	volumetric flow rate of sludge flowing into final storage tank	(5.5)
Q_{FST}	volumetric flow rates of biogas, hydrogen, methane and CO ₂	(7.3)
$Q_{\text{gas}}, Q_{\text{h}_2}, Q_{\text{ch}_4}, Q_{\text{co}_2}$	relative content of hydrogen, methane and carbon dioxide in biogas	(7.4)
$r_{\text{h}_2}, r_{\text{ch}_4}, r_{\text{co}_2}$	raw fiber, raw proteins and raw lipids of substrate	7.2
RF, RP and RL	temperature in digester, of substrate	5.3.8
T, T_{IN}	total alkalinity in digester, of substrate	7.2
TA, TAIN	theoretical oxygen demand of carbohydrates, proteins, lipids, lignin	7.2.1
ThOD _{ch} , ThOD _{pr} , ThOD _{li} , ThOD _l	weighted mean of ThOD of substrate feed, see eq. (7.6)	(7.6)
$\overline{\text{ThOD}}$	total solids of sludge in digester, of substrate	5.3.10
TS, TS _{IN}	input vector of ADM1	(7.2)
${}^\circ \mathbf{u}_{\text{AD}} : \mathbb{R}^+ \rightarrow \mathbb{R}^{34}$	stoichiometric matrix of ADM1	(7.1)
$\mathbf{V} : \mathbb{R}^{37} \rightarrow \mathbb{R}^{29 \times 37}$	volatile solids of sludge in digester, of substrate	5.3.11
VS, VS _{IN}	digester volume of liquid phase, of gas phase	(5.6)
$V_{\text{liq}}, V_{\text{gas}}$	ratio of volatile fatty acids (intermediate alkalinity) over TA	7.3.3.8
VFA/TA	state vector of ADM1	(7.2)
${}^\circ \mathbf{x}_{\text{AD}} : \mathbb{R}^+ \rightarrow \mathbb{R}^{37}$	process rates of ADM1	(7.1)
$\rho : \mathbb{R}^{37} \rightarrow \mathbb{R}^{29}$	density of substrate feed, of sludge in digester (eq. (7.20))	(7.6)
$\rho_{\text{IN}}, \rho_{\text{digester}}$		

Performance Indicators (Section 7.3, Part I)

Symbol	Description	Ref.
$A_{\text{ground}}, A_{\text{roof}}, A_{\text{wall}}$	surface area of ground, area and wall of cylindrical digester	(7.42)
$c_{\text{substrate}}$	specific heat capacity of a substrate	(7.39)
d_{dig}	diameter of digester	(7.40)
d_{mix}	diameter of agitator	(7.20)
d_{pipe}	diameter of a pipe	(7.31)
ΔE_j	thermal energy released due to microbial activity in reaction j	(7.43)
E_{plant}	total profit of produced electrical and thermal energy	(7.46)
g	gravitational acceleration	(7.30)
h_{dig}	wall height of digester	(7.40)
Δh_{geo}	geodetic head of a pump	(7.30)
h_{roof}	height of digester roof	(7.41)
$h_{v,h}$	higher heating value of produced biogas	(7.19)
$h_{v,h,h_2}, h_{v,h,\text{ch}_4}, h_{v,h,\text{co}_2}$	higher heating values of biogas components H_2 , CH_4 and CO_2	(7.19)
$k_{\text{ground}}, k_{\text{roof}}, k_{\text{wall}}$	heat transfer coefficient of digester ground, roof and wall	(7.42)
k_{pipe}	pipe roughness	(7.34)
K_c	consistency coefficient to calculate effective viscosity η_{eff}	(7.23)
l_{pipe}	transport distance of a pump	(7.30)
n_{mix}	rotation speed of agitator	(7.20)
n_{flow}	flow index to calculate effective viscosity η_{eff}	(7.24)
N_p	Newton (or power) number	(7.20)
p_{char}	specific energy value for typical solid supply unit	(7.38)
p_{el}	costs for consumed electrical energy	(7.46)
p_{th}	costs for produced thermal energy by heating	(7.46)
Δp_L	pressure loss in a pipe	(7.31)
$P_{\text{el}}, P_{\text{th}}$	produced electrical, thermal power of a CHP	(7.17)
$P_{\text{el,consume}}$	total consumed electrical energy per day	(7.44)
P_{mix}	mechanical power of agitator	(7.20)
P_{MIX}	electrical energy consumption of agitator	(7.28)
P_{diss}	dissipated power of agitator	(7.29)
$P_{\text{mic_heat}}$	thermal energy production due to microbial activity	(7.43)
P_{pump}	electrical energy consumption of liquid substrate and sludge transport	(7.30)
P_{solids}	electrical energy consumption of solids substrate transport	(7.38)
$P_{\text{substrate}}$	thermal power needed to heat substrates	(7.39)
ΔP_{th}	daily thermal energy balance of a biogas plant	(7.45)
r_{EEG}	remuneration of produced electrical energy	(7.46)
r_{th}	virtual or real revenue of produced thermal energy	(7.46)
Re	Reynolds number	(7.21)
Re_{pipe}	Reynolds number of a stream in a pipe	(7.33)
v_{pipe}	velocity of a medium in a pipe	(7.32)

Performance Indicators (Section 7.3, Part II)

Symbol	Description	Ref.
$F_{1D} := \sum_{i_o=1}^{n_o} \varpi_{i_o} \cdot F_{i_o}$	one-dimensional stage cost	(7.71)
$\mathbf{F} := (F_1, F_2)^T$	stage cost in NMPC objective function	(7.62)
$J_{1D} := \sum_{i_o=1}^{n_o} \varpi_{i_o} \cdot J_{i_o}$	fitness value	(7.70)
$\mathbf{T}_{\text{penalty}} := (T_{\text{penalty},1}, T_{\text{penalty},2})^T$	terminal cost (terminal penalty term) in NMPC objective function	(7.62)
α_T	temperature correction for effective viscosity η_{eff}	(7.25)
$\dot{\gamma}$	shear rate	(7.36)
η_{eff}	effective viscosity of sludge in digester	(7.22)
$\eta_{\text{eff,pipe}}$	effective viscosity of a medium in a pipe	(7.35)
$\eta_{\text{el}}, \eta_{\text{th}}$	electrical, thermal degree of efficiency of a CHP	(7.17)
η_{heat}	degree of efficiency of a heating	(7.45)
η_w	viscosity of water	(7.35)
$\kappa_{T,1}, \kappa_{T,2} \in \mathbb{R}^+$	weighting factor of terminal cost $T_{\text{penalty},1}, T_{\text{penalty},2}$	(7.64)
$\kappa_{i_c} \in \mathbb{R}^+$	weight of constraint $i_c = 1, \dots, n_c$ in stage cost component F_2	(7.66)
λ_{pipe}	pressure loss coefficient of a medium in a pipe	(7.34)
$\rho_{\text{Tu}} : \mathbb{R} \rightarrow \mathbb{R}^+$	Tukey biweight function	(7.69)
τ_{mix}	runtime of the stirrer	(7.28)
τ_{pipe}	shear stress	(7.37)

Abbreviations (A - G)

Abbreviation	Description	Ref.
ABP	agricultural biogas plant	6
AD	anaerobic digestion	5
ADF	acid detergent fiber	7.2
ADL	acid detergent lignin	7.2
ADM1	anaerobic digestion model no. 1	7.1
ADM1d	distributed anaerobic digestion model no. 1	6
AF	anaerobic filter	5.4.2
AFB	anaerobic fixed bed	5.4.2
AM1	anaerobic digestion model introduced by Bernard et al. (2001a)	6
ANN	artificial neural networks	6
ARMAX	autoregressive moving average model with exogenous inputs	6
BA	bicarbonate alkalinity	6
BSM2	benchmark simulation model no. 2 (for wastewater treatment)	6
CCM	corn-cob-mix	7.4
CH ₄	methane	5.1
CHP	combined heat and power plant	7
CMA-ES	covariance matrix adaptation evolution strategy	9.3.1
CO ₂	carbon dioxide	5.1
COD	chemical oxygen demand	5.3.3
CSTR	continuous stirred-tank reactor	5.4.1
CV	curriculum vitae	1
DACE	design and analysis of computer experiments	3.2
dB	decibel	4.4
DIN	German institute for standardization (deutsches Institut für Normung)	7.2
DLL	dynamic link library	B
DNN	deep neural network	4.1.1
EA	evolutionary algorithm	3.1.1
EEG	Renewable Energy Sources Act	7.3.2
EGSB	expanded granular sludge bed	5.4.2
EKF	extended Kalman filter	6
EN	European standards (europäische Normen)	7.2
EPEX SPOT	European power spot market	1
EPSAC	extended prediction self-adaptive control	6
EU	European Union	1
FBR	fluidized bed reactor	5.4.2
FM	fresh mass: mass of untreated material	5.3.5
HRT	hydraulic retention time of digester	5.3.6
GerDA	generalized discriminant analysis	4.1.1
GC	gas chromatography	7.2
GPS	whole crop silage (Ganzpflanzensilage)	7.4
GUI	graphical user interface	B

Abbreviations (H - Z)

Abbreviation	Description	Ref.
H ₂	hydrogen	5.1
HTML	hypertext markup language	B
I/O	input/output	B
ID	identifier	9.3
ISO	international organization for standardization	7.2
LCA	life cycle assessment	7.3.4
LCFA	long chain fatty acid	7.1.1
LDA	linear discriminant analysis	4.1.1
LHS	Latin hypercube sampling	9.3.1
LQT	linear quadratic tracking	6
MATLAB [®]	matrix laboratory	B
MCR	misclassification rate	8
MHE	moving horizon estimation	4.3
MONMPC	multi-objective nonlinear model predictive control	2
NDF	neutral detergent fiber	7.2
NfE	nitrogen free extract	7.2
NFC	non fiber carbohydrates	7.2
NMPC	nonlinear model predictive control	2
O ₂	oxygen	5.3.3
ODE	ordinary differential equation	7
OFMSW	organic fraction of municipal solid waste	1
OLR	organic loading rate of digester	5.3.7
P	proportional controller	6
PC	personal computer	9.3
PCA	principal component analysis	6
pCO ₂	partial pressure of CO ₂	6
PDE	partial differential equation	6.3
PI	proportional-integral controller	6
PID	proportional-integral-derivative controller	6
PLC	programmable logic controller	9.2
PSO	particle swarm optimization	6
RTO	real-time optimization	2
RMSE	root-mean-square error	4.4
SCFA	short chain fatty acid	7.2.1
SDE+	Renewable Energy Production Incentive Scheme	1
SMS-EGO	\mathcal{S} -metric selection-based efficient global optimization	3.2
SMS-EMOA	\mathcal{S} metric selection evolutionary multi-objective optimization algorithm	3.1.1
SRT	sludge retention time	5.3.6
ThOD	theoretical oxygen demand	5.3.9
TOC	total organic carbon	6
UASB	upflow anaerobic sludge blanket	5.4.2
UASB-AF	upflow anaerobic sludge blanket-anaerobic filter	5.4.2
UV/Vis	ultraviolet-visible	9.2
VFA	volatile fatty acids	7.3.3.8
VSM	variable structure model	6
WW	wastewater	6

Samenvatting (Dutch)

De doelstelling van de Europese Unie (EU) om tot het jaar 2020 20 % van het bruto energetisch eindverbruik met hernieuwbare energiebronnen te verzorgen, wekt een enorme behoefte aan onderzoek en ontwikkeling op het gebied van hernieuwbare energiebronnen. De productie van biogas door middel van anaerobe vergisting van biologisch afbreekbare materialen kan een bijdrage aan deze “Energiewende” leveren. Biogas kan voor stroom- en warmteproductie gebruikt worden, alsmede als opgewerkt groen gas in het aardgasnet geïnjecteerd of als biobrandstof ingezet worden. Als grondstoffen kunnen biologisch afbreekbare reststoffen, mest, gras, energiegewassen en andere dienen.

In Duitsland kwam het in de laatste jaren, gestimuleerd door de “Erneuerbare-Energien-Gesetz (EEG)”, tot een massale groei van het aantal agrarische biogasinstallaties. Deze gebruiken grotendeels mais, dat speciaal verbouwd moet worden voor de productie van energie in biogasinstallaties. Bij het gebruik van zulke waardevolle grondstoffen is het efficiënte gebruik daarvan erg belangrijk. Dat geldt zowel uit economisch, ecologisch als ook uit ethisch (“tank of bord”) gezichtspunt. Een efficiënt en gelijktijdig stabiel functioneren is uiteraard ook voor biogasinstallaties die afval vergisten heel belangrijk daar deze anders niet rendabel in bedrijf gehouden kunnen worden.

In dit proefschrift wordt een regelsysteem voor de automatische aanpassing van de toevoer van substraat voor biogasinstallaties ontwikkeld. De methode past de toevoer van substraat zo aan, dat zowel de economie van het bedrijf gemaximeerd wordt, als ook de stabiliteit van het functioneren van de vergisters in elke situatie gewaarborgd is. Voor de berekening en de voorspelling van het procesgedrag gebruikt de methode een gedetailleerd dynamisch simulatiemodel van de biogasinstallatie. Het procesmodel gebruikt het *Anaerobic Digestion Model No. 1* (ADM1) om de anaerobe vergisting te modelleren. Verder kunnen thermische en electrische energiestromen en ook de rentabiliteit van het biogas bedrijf gesimuleerd worden.

Het ontwikkelde regelsysteem is gerealiseerd als op een modelgebaseerde voorspellende regelaar en hoort tot de klasse van de real-time optimalisering. Aan de hand van het model berekent een optimalisatie algoritme de optimale toevoer van substraat voor de volgende tijdsperiode, welke dan op de echte installatie toegepast wordt. Doordat de optimalisatie op regelmatige tijdstippen steeds weer opnieuw gedaan wordt, kan een

optimale regeling van de toevoer van substraat voor de biogasinstallatie bereikt worden. Het gebruik van een dynamisch model vereist dat de toestand van de biogasinstallatie bij het begin van elke optimalisatiestap bekend is. Omdat deze voor het ontwikkelde model niet direct gemeten kan worden, moet de toestand door een toestandschatter bepaald worden.

De essentiële bijdragen van dit proefschrift zijn:

- De ontwikkeling van een algemeen, gedetailleerd, dynamisch simulatiemodel voor biogasinstallaties.
- De ontwikkeling van een regeling voor de toevoer van substraat voor biogasinstallaties op basis van real-time optimalisatie.
- De ontwikkeling van een toestandschatter voor het ADM1.
- De omzetting en het testen van alle componenten in omvangrijke simulatiestudies.

In talrijke simulatie- en optimalisatie-onderzoeken kon in dit proefschrift aangetoond worden, dat het ontwikkelde regelconcept voor de optimalisatie van de toevoer van substraat geëigend is. Het regelsysteem is in staat de optimale toevoer van substraat voor de stationaire exploitatie van de installatie te vinden. Bovendien kunnen substraataanpassingen uitgevoerd worden op grond van voorspelde waarden, waardoor verlies bij de biogasproductie verhinderd kan worden. Tenslotte is eveneens een setpoint regelaar realiseerbaar, die enerzijds het voorgegeven setpoint traject volgt en anderzijds de stabiliteit van de installatie waarborgt.

De volgende stap zal zijn, het regelsysteem in een echte installatie in te zetten om de capaciteit ervan in de praktijk te valideren. Het doel van het proefschrift was een substraatregelaar voor grootschalige biogasinstallaties te ontwikkelen, die eraan kan bijdragen dat biogas bedrijven in de toekomst onafhankelijk van een subsidie economisch in bedrijf gehouden kunnen worden.

Curriculum Vitae



Daniel Gaida was born on October 28th 1983 in Radevormwald, Germany. In 2003 he started to study Automation Systems at Cologne University of Applied Sciences where he received his BSc in 2006. Right after, he started to study Electrical Engineering and Information Technology at the University of Applied Sciences in Düsseldorf. Having obtained his MSc degree in 2009 he returned to Cologne University of Applied Sciences to work in the research group of prof. Michael Bongards called GECO►C. In 2009 he also started his PhD studies at Leiden University in the Natural Computing Group of prof. Thomas Bäck.

